

# Local Joint Flexibility

A study to modelling LJF into  
a beam model, for fatigue de-  
sign of a stinger

E. Wierenga





# Local Joint Flexibility

## A study to modelling LJF into a beam model, for fatigue design of a stinger

by

E. Wierenga

to obtain the degree of Master of Science  
**in Mechanical Engineering**  
at the Delft University of Technology,  
to be defended publicly on Monday September 6, 2021 at 10:00 AM

Student number: 4488962  
Report number: 2021.MME.8536  
Project duration: December 1, 2020 – September 6, 2021  
Thesis committee: Dr. ir. D.L. Schott, TU Delft, faculty 3mE, committee chair  
Dr. ir. X.L. Jiang, TU Delft, faculty 3mE, university supervisor  
Dr. M. Pavlović, TU Delft, faculty CiTG  
Dr. ir. N. Ermolaeva, Allseas Engineering B.V., company supervisor  
Dr. ir. Y. Yu, Allseas Engineering B.V., company supervisor

An electronic version of this thesis is available at <http://repository.tudelft.nl/>.



# Acknowledgement

This report contains the research conducted as part of the thesis to obtain the Master of Science in Mechanical Engineering at the Delft University of Technology. The project is performed in close collaboration with Allseas Engineering B.V., whom I would like to thank for providing this possibility and welcoming me in the company.

The thesis would not have been possible without the guidance and assistance of the members of the graduation committee. I would like to express my gratitude to: dr. ir. X.L. Jiang, dr. ir. N. Ermolaeva, dr. Y. Yu, dr. ir. D. L. Schott and dr. M. Pavlović. With their experience they provided me with valuable feedback, each from a different perspective.

During the project I spend most time at the office of Allseas Engineering B.V. I want to thank my colleagues, in special: Basem, Daan, Huijin, Joost, Koos, Leslie, Rudy and Steven for their support, interesting discussions, lunch walks, drinks after work, teaching me how to serve coffee, but above all, the good times in office.

The thesis fulfills the last part of the degree Master of Science and thereby marks the end of studies and life as a student. I want to thank my family for their unconditional support during all those years.

*E. Wierenga  
Delft, August 2021*



# Summary

Allseas Group S.A. is a Swiss based offshore contractor and global leader in offshore pipeline installation and subsea construction. Allseas uses several ships to lay pipelines following the S-lay method. In this configuration, pipelines are assembled horizontally on a vessel and guided into the water by a stinger frame, to reduce strain in the pipeline and prevent it from buckling. The stinger is a steel space frame structure made of tubular sections and mounted on the bow or stern of a vessel. The hydrodynamic loads make the stinger, especially the tubular joints, sensitive to fatigue damage. As part of the fatigue assessment, member loads on the tubular joints, as effect of the load-cases, are determined with a beam model.

A beam model is a simplified method of modelling structures. The results of a beam model are generally not as accurate as the results of a shell model. However, for complex geometries subjected to a high number of load-cases ( $\approx 10000$ ), a beam model is a more efficient method of modelling and computational times are strongly reduced. In a standard beam model, no attention is paid to modelling the joint itself. In the model, the beam element of the brace is extended from the surface of the chord to the centerline of the chord. This connection is also referred to as rigid. In reality, tubular joints possess considerable elastic flexibility through local deformation of the chord wall. In literature, this is also described as Local Joint Flexibility (LJF). It is suggested that a model accounting for LJF, leads possibly to the redistribution of the member-loads, with a reduction of the stresses in the joint as effect. For the determination of the ultimate strength of a joint, the influence of LJF is negligible, but in a fatigue assessment the influence can lead to considerable differences in predicted fatigue life. The main research question of this project states:

How can Local Joint Flexibility be modelled in a beam model of a stinger and what is the influence on the predicted fatigue life?

LJF is defined as the flexibility through local chord wall deformation caused by an external load. A brace can deform in three DOF (axial, out-of-plane bending, in-plane bending) as effect of three possible DOF unit-load (axial force, out-of-plane bending moment, in-plane bending moment), applied on the brace itself or adjacent braces. In other degrees the chord is subjected to shear loads for which the flexibility is assumed to be negligible. Until initial yielding joints show linear elastic behaviour, hence the flexibility can be described by a constant value.

Three methods to determine the LJF of a tubular joint are discussed in literature: physical experiments, Finite Element Analysis and parametric equations. Three methods to model the LJF in a beam model are discussed in literature: a spring element, a customized beam element, and via the global stiffness matrix. For this research, it is chosen to determine and model LJF with the most accurate method, in order to obtain reliable results. The LJF of tubular joints is determined with FEA and the LJF is modelled in the beam model via the global stiffness matrix.

Initially, a model which is able to determine the flexibilities of single-brace joints is developed. The numerical model is validated by comparing the results to 27 experiments of Fessler et al.[31]. Statistics show that the numerical model is able to determine the flexibilities of tubular joints, with a mean deviation of +3% with a SD of  $\pm 20\%$  to physically performed experiments in literature. The accuracy is compared to the accuracy of the brace extension element in the model without LJF. The flexibilities in a model without LJF have a mean deviation of  $-36\%$  to the experimentally determined flexibility, with a SD of  $\pm 74\%$ . Thus, it is proven, that the flexibilities according to the numerical model provide a more accurate representation of the LJF than the model without LJF. The numerical model is expanded to a multi-brace model. Because of a shortage of suitable data for the validation of the numerical model,

no additional validation for the multi-brace model is performed. The single-brace model validation in combination with the verification of the multi-brace model is considered as sufficient.

A methodology is presented to model the LJJ of a tubular joint into a beam model in Simcenter FEMAP. The brace extension element, used in a model without LJJ, is replaced by a GENEL. The GENEL is an element, which allows inserting stiffnesses and flexibilities between nodes, directly in the global stiffness matrix in the Simcenter NASTRAN solver. Because the flexibilities are inserted in the global coordinate system, several transformations and rotations are performed. Because the insertion of the flexibilities is a purely mathematical operation, no validation is performed. In the verification, it is observed that the flexibilities are presented without deviation in the beam model.

A numerical test-case is performed to investigate the influence of modelling LJJ on the predicted fatigue life of the braces in the stinger. In order to determine the influence, two models are considered, one model with LJJ and another without LJJ. The fatigue assessment is performed for seven joints. Because modelling LJJ in one brace has appeared to affect surrounding braces, LJJ is modelled in the seven joints of interest and all surrounding joints. The influence of LJJ has appeared to be strongly load-case dependent. Therefore, the total accumulated damage in the hot spots of the braces as effect of exposure to 16 load-cases for three hours each is calculated. The accumulated fatigue damage in the most affected hot spot of each brace as effect of exposure to the sixteen load-cases for three hours each, according to a model with and without LJJ, is compared. The accumulated fatigue damage in the most affected hot spots has changed with factor 0.29 up to factor 2.88 as effect of LJJ. The change in predicted fatigue life as effect of modelling LJJ, is equal to factor 0.35 up to 3.45. These values are not expected to be the maximum and minimum values, in exceptional cases these values can be exceeded. However, because the fatigue assessment is performed over sixteen load-cases in total, the values are considered as a reliable prediction of the influence of modelling LJJ in the joints of the stinger. No large alterations of the most critical brace or most affected hot spot within the brace, as effect of modelling LJJ are observed. Thus, modelling LJJ would not lead to a different fatigue monitoring. In the test-case modelling LJJ has been beneficial for the four most critically damaged braces. The braces endure an increase of predicted fatigue life of factor 1.17 up to 2.00. Thus, modelling LJJ does not only provide a more accurate predicted fatigue life but additionally can help to improve the predicted fatigue life.

# Summary (in Dutch)

Allseas Group S.A. is een in Zwitserland gevestigde offshore aannemer en marktleider in offshore pijp-leggen en sub-zee constructie. Allseas gebruikt verschillende schepen om pijpleidingen volgens de S-lay methode te leggen. In deze configuratie worden pijpleidingen horizontaal op het vaartuig geassembleerd. Om hoge spanningen en knik te voorkomen wordt de pijpleiding met een stinger te water gelaten. De stinger is een stalen frame, gemaakt uit buisvormige secties, gemonteerd op de boeg of het achterstevan van een vaartuig. Door de hydrodynamische belasting is de stinger, in bijzonder de buisvormige verbindingen, gevoelig voor vermoeiing. Als onderdeel van de vermoeiing-berekeningen wordt door middel van een balken model de kracht op de buisvormige verbindingen, veroorzaakt door de verschillende belastingen, bepaald.

Een balken model is een versimpelde methode om constructies te modelleren. De uitkomst van een balken model is niet even nauwkeurig als een model van plaat element. Echter, voor complexe geometrieën belast met een groot aantal belastingen ( $\approx 10000$ ), is een balken model een efficiëntere methode van modelleren met minder benodigde rekentijd. In een standaard balken model wordt geen aandacht besteed aan het modelleren van de verbinding. In het model wordt de 'brace' verlengd van het oppervlak van de 'chord' tot de centrale lijn van de 'chord'. Deze verbinding wordt beschouwd als stijf. Echter, buisvormige verbindingen bezitten elastische flexibiliteit door lokale vervorming van de chord wand. In de wetenschap wordt hier ook naar gerefereerd als 'lokale verbindings flexibiliteit' (LJF). Er wordt gesuggereerd dat een model dat rekening houdt met LJF kan leiden tot een herverdeling van de krachten, met als gevolg een afname van de spanningen in de verbindingen. Voor de bepaling van de maximale spanningen in de verbinding wordt de invloed beschouwd als verwaarloosbaar, maar voor de vermoeiing berekening, kan het modelleren van flexibiliteit leiden tot aanzienlijke verschillen in verwachte vermoeiings levensduur. De onderzoeksvraag van dit project is geformuleerd als:

Hoe kan lokale verbindings flexibiliteit in een balken model van een stinger worden gemodelleerd en wat is de invloed op de voorspelde levensduur?

LJF is gedefinieerd als flexibiliteit door lokale vervorming van de chord wand, veroorzaakt door een externe belasting. Een brace kan in drie vrijheidsgraden vervormen (axiaal, uit het vlak buiging, in het vlak buiging), als gevolg van drie belastingen (axiale kracht, uit het vlak buigend moment, in het vlak buigend moment), op de brace. In andere vrijheidsgraden wordt de chord op afschuiving belast en vervormingen zijn aangenomen als verwaarloosbaar. Tot de elastische limiet hebben verbindingen een lineaire elasticiteit die met een constant getal kan worden beschreven. Verbindingen met meerdere braces bezitten gelijke flexibiliteit en daarnaast de flexibiliteit als gevolg van een belasting op een aanliggende brace.

Drie methoden om de LJF van een buisvormige verbinding te berekenen zijn beschreven in literatuur: Fysische experimenten, Eindige Elementen Analyse en parametrische vergelijkingen. Drie methoden om LJF in een balken model te modelleren zijn beschreven in literatuur: een veer element, een aangepast balk element en via de globale stijfheid matrix. Voor dit onderzoek is er gekozen voor de meest nauwkeurige methoden. Voor het bepalen van de LJF wordt gebruik gemaakt van eindige elementen analyse en LJF wordt gemodelleerd in de globale stijfheid matrix.

Allereerst is een model ontwikkeld voor het bepalen van de LJF van verbindingen met een enkele brace. Het numerieke model is gevalideerd door de resultaten te vergelijken met 27 experimenten van Fessler et al. [31]. Het numerieke model kan de flexibiliteit van de buisvormige verbindingen bepalen met een gemiddelde afwijking van +3% met een standaardafwijking van  $\pm 20\%$ . De nauwkeurigheid is vergeleken met de nauwkeurigheid van het verlengde brace element dat in het oude balken model

wordt gebruikt. De flexibiliteit in een model zonder LJF heeft een gemiddelde afwijking van  $-36\%$  en een standaard afwijking van  $\pm 74\%$  tot de experimenteel bepaalde flexibiliteit. Daarmee is bewezen dat de flexibiliteit volgens het numerieke model een nauwkeurigere representatie van de flexibiliteit is, dan de flexibiliteit in een model zonder LJF. Het numerieke model is uitgebreid naar een model geschikt voor verbindingen met meerdere braces. Door een tekort aan geschikte metingen voor de validatie is besloten om geen extra validatie voor het uitgebreide model uit te voeren. De validatie van het model voor verbindingen met een enkele brace, in combinatie met de verificatie van het model voor verbindingen met meerdere braces wordt beschouwd als voldoende.

Een methode is ontwikkeld om LJF van buisvormige verbindingen in een balken model in Simcenter FEMAP te modelleren. Het gedeelte van de balk, gelegen binnen het oppervlak van de chord, is vervangen voor een GENEL. Het GENEL is een element dat de mogelijkheid biedt om stijfheden of flexibiliteiten tussen twee knooppunten, direct in de globale stijfheid matrix in Simcenter NASTRAN te voegen. Voordat de flexibiliteiten in het globale coördinaten systeem worden ingevoegd, zijn verschillende transformaties en rotaties uitgevoerd. Omdat het modelleren van LJF een wiskundige handeling is, is geen validatie uitgevoerd. In de verificatie is aangetoond dat de flexibiliteiten in het balken model worden gemodelleerd zonder afwijking.

Een numerieke test is uitgevoerd om de invloed van het modelleren van LJF op de voorspelde vermoeiing levensduur van de verbindingen in de stinger te bepalen. Om de invloed te bepalen is gebruik gemaakt van twee modellen. Een model met LJF en een model zonder LJF. LJF is gemodelleerd in zeven verbindingen waarvan de vermoeiing berekening is uitgevoerd, en daarnaast in alle omringende verbindingen. Omdat de invloed van het modelleren van LJF sterk belasting afhankelijk is gebleken, is de totaal geaccumuleerde schade in de braces als gevolg van zestien belastingen voor drie uur ieder berekend. De geaccumuleerde vermoeiing schade in de kritische locaties van iedere brace in de stinger als gevolg van blootstelling aan zestien verschillende ladingen, voor drie uur elk, volgens een model met en zonder LJF, is vergeleken. De geaccumuleerde schade in de meest beschadigde locaties van de braces is veranderd met factor 0.29 tot factor 2.88 als gevolg van het modelleren van LJF. De verandering in voorspelde levensduur als gevolg van het modelleren van LJF is gelijk aan factor 0.35 tot factor 3.4. Deze waarden worden niet beschouwd als de absolute maximum en minimum waarden, maar worden beschouwd als een betrouwbare indicatie voor de invloed van het modelleren van LJF. Geen grote veranderingen in kritieke braces en/of meest beschadigde locaties in de braces zijn waargenomen als gevolg van het modeleren van LJF. In de numerieke test heeft het modeleren van LJF een voordelige werking ondervonden voor de meest kritische braces. De desbetreffende braces ondervinden een toename in voorspelde levensduur van factor 1.17 tot 2.00. Het modeleren van LJF leidt dus niet alleen tot een nauwkeurigere berekening, maar kan dus ook leiden tot een verbeterde levensduur.

# Contents

<b>Summary</b>	<b>v</b>
<b>Summary (in Dutch)</b>	<b>vii</b>
<b>List of Figures</b>	<b>xii</b>
<b>List of Tables</b>	<b>xvii</b>
<b>Symbols and Acronyms</b>	<b>xix</b>
<b>1 Introduction</b>	<b>1</b>
1.1 Background . . . . .	1
1.2 Problem definition . . . . .	2
1.3 Aim of the project . . . . .	5
1.4 Research questions . . . . .	5
1.5 Scientific contribution . . . . .	6
1.6 Scope . . . . .	6
1.7 Research outline . . . . .	7
<b>2 Literature review</b>	<b>9</b>
2.1 Introduction . . . . .	9
2.2 Geometries and flexibilities of tubular joints . . . . .	9
2.2.1 Joint geometry . . . . .	9
2.2.2 Single-brace joint flexibilities . . . . .	10
2.2.3 Multi-brace joint flexibilities . . . . .	14
2.3 Determination of LJF . . . . .	15
2.3.1 Physical measurements . . . . .	15
2.3.2 Finite Element Analysis . . . . .	16
2.3.3 Parametric equations . . . . .	17
2.4 Modelling of LJF . . . . .	20
2.4.1 Spring element . . . . .	20
2.4.2 Customized beam element . . . . .	20
2.4.3 Global stiffness matrix . . . . .	21
2.4.4 Expansion of methodologies to multi-brace elements . . . . .	23
2.5 Definition of orientation of flexibilities . . . . .	24
2.6 Conclusion . . . . .	26
<b>3 Determination of methodology</b>	<b>27</b>
3.1 Introduction . . . . .	27
3.2 Specification of joints in a stinger . . . . .	27
3.3 Determination of methodologies . . . . .	28
3.3.1 Approach . . . . .	28
3.3.2 Methodology to determine LJF . . . . .	28
3.3.3 Methodology to model LJF . . . . .	29
3.4 Conclusion . . . . .	29
<b>4 Development of method to determine the LJF of tubular joints</b>	<b>31</b>
4.1 Introduction . . . . .	31
4.2 Methodology single-brace numerical model . . . . .	31
4.2.1 General model overview . . . . .	31
4.2.2 FEA . . . . .	34
4.2.3 Calculation chord wall deformation . . . . .	38
4.2.4 Calculation flexibility matrix . . . . .	40

4.3	Verification single-brace numerical model . . . . .	41
4.3.1	Analysis of results and comparison to literature . . . . .	41
4.3.2	Mesh refinement . . . . .	43
4.3.3	Consistency of results . . . . .	43
4.4	Validation single-brace numerical model . . . . .	44
4.4.1	Data for comparison . . . . .	44
4.4.2	Analysis of results . . . . .	47
4.4.3	Accuracy of methodologies . . . . .	47
4.4.4	Discussion of reliability of experiments . . . . .	51
4.5	Methodology multi-brace numerical model . . . . .	53
4.5.1	General model overview . . . . .	53
4.5.2	FEA . . . . .	56
4.5.3	Calculation chord wall deformation . . . . .	56
4.5.4	Calculation flexibility matrix . . . . .	60
4.6	Verification multi-brace numerical model . . . . .	60
4.6.1	Analysis of results . . . . .	60
4.7	Validation multi-brace numerical model . . . . .	64
4.8	Conclusion . . . . .	64
<b>5</b>	<b>Development of a method to model LJF in a beam model</b>	<b>67</b>
5.1	Introduction . . . . .	67
5.2	Methodology . . . . .	67
5.2.1	Split matrix into sub-matrices . . . . .	69
5.2.2	Transformation from local-brace to local-chord coordinate system . . . . .	69
5.2.3	Transformation from three to six DOF . . . . .	70
5.2.4	Rotation from local chord to local joint coordinate system . . . . .	71
5.2.5	Merge sub-matrices . . . . .	72
5.2.6	Rotation from local joint to global coordinate system . . . . .	72
5.2.7	Insert global flexibility matrix in FEMAP . . . . .	74
5.3	Verification . . . . .	75
5.4	Validation . . . . .	77
5.5	Conclusion . . . . .	77
<b>6</b>	<b>Numerical test-case of model with LJF</b>	<b>85</b>
6.1	Introduction . . . . .	85
6.2	Numerical test-case setup . . . . .	86
6.2.1	Geometry and joints of interest . . . . .	86
6.2.2	Load-case . . . . .	87
6.3	Fatigue assessment . . . . .	87
6.3.1	Member-loads and nominal stresses . . . . .	88
6.3.2	Hot spot stress range . . . . .	88
6.3.3	Accumulated fatigue damage . . . . .	91
6.3.4	Predicted fatigue life . . . . .	93
6.4	Preliminary results . . . . .	94
6.4.1	Modelling LJF solely in a brace with underestimated flexibility . . . . .	94
6.4.2	Modelling LJF solely in a brace with overestimated flexibility . . . . .	97
6.4.3	Influence of different load-cases . . . . .	99
6.5	Results . . . . .	105
6.6	Discussion . . . . .	108
6.7	Conclusion . . . . .	108
<b>7</b>	<b>Conclusion</b>	<b>111</b>
7.1	Conclusion . . . . .	111
7.2	Recommendations . . . . .	113

<b>Bibliography</b>	<b>115</b>
<b>A Academic essay</b>	<b>119</b>
<b>B Mesh contours</b>	<b>129</b>
B.1 Single-brace model numerical model . . . . .	129
B.2 Multi-brace numerical model expansion . . . . .	132
<b>C Coordinate systems</b>	<b>133</b>
C.1 Global coordinate system . . . . .	133
C.2 Local joint coordinate system . . . . .	133
C.3 Local chord coordinate system . . . . .	133
C.4 Local brace coordinate system . . . . .	133
<b>D Results verification single-brace numerical model</b>	<b>135</b>
<b>E Results of validations of single-brace joint</b>	<b>137</b>
<b>F Plots of results of validations of single-brace joint</b>	<b>145</b>
<b>G Equations to calculate the non-dimensional flexibility of a joint</b>	<b>153</b>
G.1 Single-brace joint . . . . .	153
G.2 Multi-brace joint. . . . .	154
<b>H Parametric equations</b>	<b>155</b>
<b>I Plots of parametric equations</b>	<b>159</b>
<b>J Stress Concentration Factors</b>	<b>165</b>
<b>K Joint classification</b>	<b>171</b>
K.1 Examples of joint classifications 1 . . . . .	171
K.2 Examples of joint classifications 2 . . . . .	172
<b>L Results of implementation</b>	<b>173</b>
L.1 Member-loads . . . . .	173
L.2 Stress range and accumulated fatigue damage . . . . .	196
<b>M Chord wall displacements for single-brace model verification</b>	<b>219</b>
M.1 Chord wall displacements of joint 1 . . . . .	219
M.2 Chord wall displacements of joint 2 . . . . .	219
<b>N Flexibilities of braces in numerical test case</b>	<b>221</b>
<b>O Specification of joints in stinger CONFIDENTIAL</b>	<b>223</b>
O.1 Overview of geometry Solitaire stinger section 1 . . . . .	223
O.2 Geometrical parameters of joints Solitaire stinger section 1 . . . . .	224
<b>P Joint parameters CONFIDENTIAL</b>	<b>225</b>
P.1 Location of joints . . . . .	225
P.2 Specification of brace numbers . . . . .	226
P.3 Joint parameters . . . . .	226
<b>Q Numerical Model MATLAB Code CONFIDENTIAL</b>	<b>235</b>
Q.1 Generation and execution of FEA . . . . .	236
Q.2 Calculation of LJF matrix. . . . .	251
Q.3 Calculation of global Flexibility matrix . . . . .	253



# List of Figures

1.1	Visualisation of the S-lay pipeline configuration [27] . . . . .	1
1.2	The Solitaire with a retracted stinger . . . . .	2
1.3	Schematic overview of the fatigue assessment for tubular joints in a beam model . . . . .	3
1.4	Beam model of the Solitaire stinger . . . . .	4
1.5	Schematic presentation of the simplification made when modelling tubular joints with beam elements. In red: the brace extension element . . . . .	4
1.6	Comparison of deformations as effect of an axial force, according to a shell model (left) and beam model (right). . . . .	5
2.1	Schematic presentation of the dimensions of a tubular joint . . . . .	10
2.2	Deformations of a T-joint. From left to right: axial, in-plane bending and out-of-plane bending [6]. . . . .	11
2.3	The flexibilities of a single-brace joint, defined in the local brace coordinate system . . . . .	12
2.4	The typical load-displacement relationship of a T-joint [55] . . . . .	13
2.5	The flexibilities of a multi-brace joint, defined in the local brace coordinate system . . . . .	14
2.6	The test set-up used by Fessler et al. to measure the flexibilities of a tubular joint [31] . . . . .	16
2.7	The influence of $\beta_1$ on the dimensionless in-plane bending flexibility. . . . .	18
2.8	The influence of $\gamma$ on the dimensionless in-plane bending flexibility. . . . .	18
2.9	The influence of $\theta_1$ on the dimensionless in-plane bending flexibility. . . . .	19
2.10	The influence of $\tau$ on the dimensionless in-plane bending flexibility. . . . .	19
2.11	Schematic representation of the brace extension element (left) and the replaced LJF element (right) . . . . .	21
2.12	Different methods of modelling LJF of a single-brace joint. From left to right: spring element, customized beam element, global stiffness matrix . . . . .	21
2.13	Six unit-loads with corresponding reaction forces for the determination of the transformation matrix [6] . . . . .	22
2.14	Different methods of modelling LJF of a multi-brace joint. From left to right: spring element, customized beam element, global stiffness matrix . . . . .	24
2.15	Shell model, representing the chord wall deformations as effect of an axial force. . . . .	24
2.16	Comparison of the flexibilities of a single-brace joint, defined in different coordinate systems . . . . .	25
3.1	The Solitaire with highlighted stinger section 1 . . . . .	27
4.1	Schematic presentation of the numerical model. . . . .	32
4.2	The flexibilities of a single-brace joint defined in the local brace coordinate system . . . . .	33
4.3	SHELL281 element (ANSYS) [9]. . . . .	34
4.4	Schematic presentation of the location of the elements for mid-surface model (blue) and top-surface model (red). . . . .	35
4.5	Example of the applied mesh in the FEA . . . . .	36
4.6	Example of the applied boundary conditions . . . . .	37
4.7	Location, and direction of measured displacements $\kappa_{p,j}$ in points $p$ . . . . .	40
4.8	Chord wall displacements as effect of axial, out-of-plane and in-plane load-case. . . . .	40
4.9	The two joints for the verification of the single-brace model . . . . .	42
4.10	Example of the different mesh sizes, from left to right: coarse, fine and extra fine mesh . . . . .	44
4.11	Schematic presentation of the brace extension element (left) and a beam model with LJF element (right). . . . .	46
4.12	The in-plane bending LJF of the 27 joint geometries investigated by Fessler et al., according to: the experiment of Fessler et al., the numerical model and the flexibility of the brace extension element, presented under a variable $\beta$ . . . . .	48

4.13	The in-plane bending LJF of the 27 joint geometries investigated by Fessler et al., according to: the experiment of Fessler et al., the numerical model and the flexibility of the brace extension element, presented under a variable $\gamma$ . . . . .	49
4.14	The in-plane bending LJF of the 27 joint geometries investigated by Fessler et al., according to: the experiment of Fessler et al., the numerical model and the flexibility of the brace extension element, presented under a variable $\theta$ . . . . .	50
4.15	The flexibilities of a multi-brace joint defined in the local brace coordinate system . . . . .	54
4.16	Example of a multi-brace joint in the FEA . . . . .	56
4.17	Example of mesh contours after reduction of the contour width . . . . .	57
4.18	Example of a meshed joint after reduction of the contour width . . . . .	57
4.19	Example of displacements of a multi-brace DT-joint . . . . .	58
4.20	Example of displacements of a multi-brace K/TY-joint . . . . .	58
4.21	The four joints for the verification of the multi-brace model . . . . .	61
5.1	Schematic presentation of a global flexibility element. . . . .	67
5.2	Schematic overview of the calculation to model LJF in FEMAP . . . . .	68
5.3	The transformation of axial and out-of plane loads/deformations from local brace to local chord coordinate system. . . . .	70
5.4	The flexibilities defined in the local chord coordinate system . . . . .	71
5.5	Rotation from local chord coordinate system to local joint coordinate system. . . . .	72
5.6	Example of insertion of the GENEL in FEMAP for a single-brace joint . . . . .	75
5.7	Example of insertion of the GENEL in FEMAP for a multi-brace joint . . . . .	76
6.1	Beam model of stinger section 1 with LJF elements. . . . .	85
6.2	Overview of braces/joints of interest. . . . .	86
6.3	Definition of wave heading. . . . .	88
6.4	Schematic overview of the fatigue assessment for tubular joints in a beam model . . . . .	89
6.5	Orientation of the member loads according to DNV [23]. . . . .	90
6.6	Hot spot locations and superposition of stresses [23] . . . . .	90
6.7	S-N curve for tubular joints in air and in seawater with cathodic protection [23]. . . . .	92
6.8	The effects of load-case 6 on brace 1.3 . . . . .	95
6.9	The effects of load-case 6 on brace 6.1 . . . . .	96
6.10	The effects of load-case 4 on brace 1.4 . . . . .	98
6.11	The effects of load-case 4 on brace 1.3 . . . . .	99
6.12	The stress range in the hot spots of brace 1.3 as effect of the sixteen load-cases . . . . .	100
6.13	The accumulated fatigue damage in the hot spots of brace 1.3 as effect of the sixteen load-cases . . . . .	101
6.14	Comparison of total accumulated fatigue damage in hot spots as effect of exposure to 16 load-cases, according to a model without LJF and with LJF modelled solely in brace 1.3 . . . . .	102
6.15	Comparison of total accumulated fatigue damage in hot spots as effect of exposure to 16 load-cases, according to a model without LJF and with LJF modelled solely in brace 1.4 . . . . .	104
6.16	Comparison of total accumulated fatigue damage in hot spots as effect of exposure to 16 load-cases, according to a model without LJF and with LJF. . . . .	106
6.17	An overview of the braces in which LJF is modelled in the research of MSL Engineering Ltd. [45]. . . . .	109
B.1	The coordinate systems of the chord and brace [15] . . . . .	129
B.2	Unfolding of the chord surface [15] . . . . .	130
B.3	The chord intersection in the $Y'Z'$ plane [27] (a) and the mesh contours on the flattened chord surface, on the in- and outside of the intersection line (b). . . . .	131
B.4	An example of the mesh contours on the chord wall . . . . .	132
C.1	Schematic presentation of the coordinate systems . . . . .	134

F.1	The axial LJF of the 27 joint geometries investigated by Fessler et al., according to: the experiment of Fessler et al., the numerical model and the flexibility of the brace extension element, presented under a variable $\beta$ . . . . .	146
F.2	The axial LJF of the 27 joint geometries investigated by Fessler et al., according to: the experiment of Fessler et al., the numerical model and the flexibility of the brace extension element, presented under a variable $\gamma$ . . . . .	147
F.3	The axial LJF of the 27 joint geometries investigated by Fessler et al., according to: the experiment of Fessler et al., the numerical model and the flexibility of the brace extension element, presented under a variable $\theta$ . . . . .	148
F.4	The out-of-plane bending LJF of the 27 joint geometries investigated by Fessler et al., according to: the experiment of Fessler et al., the numerical model and the flexibility of the brace extension element, presented under a variable $\beta$ . . . . .	149
F.5	The out-of-plane bending LJF of the 27 joint geometries investigated by Fessler et al., according to: the experiment of Fessler et al., the numerical model and the flexibility of the brace extension element, presented under a variable $\gamma$ . . . . .	150
F.6	The out-of-plane bending LJF of the 27 joint geometries investigated by Fessler et al., according to: the experiment of Fessler et al., the numerical model and the flexibility of the brace extension element, presented under a variable $\theta$ . . . . .	151
I.1	The influence of $\beta_1$ on the dimensionless axial flexibility. . . . .	160
I.2	The influence of $\gamma$ on the dimensionless axial flexibility. . . . .	160
I.3	The influence of $\theta_1$ on the dimensionless axial flexibility. . . . .	161
I.4	The influence of $\tau$ on the dimensionless axial flexibility. . . . .	161
I.5	The influence of $\beta_1$ on the dimensionless out-of-plane bending flexibility. . . . .	162
I.6	The influence of $\gamma$ on the dimensionless out-of-plane bending flexibility. . . . .	162
I.7	The influence of $\theta_1$ on the dimensionless out-of-plane bending flexibility. . . . .	163
I.8	The influence of $\tau$ on the dimensionless out-of-plane bending flexibility. . . . .	163
K.1	Different classifications of a tubular joint [51] . . . . .	171
K.2	Examples of combinations of different joint classifications [23] . . . . .	172
L.1	Member loads on brace 1.1 . . . . .	174
L.2	Member loads on brace 1.2 . . . . .	175
L.3	Member loads on brace 1.3 . . . . .	176
L.4	Member loads on brace 1.4 . . . . .	177
L.5	Member loads on brace 2.1 . . . . .	178
L.6	Member loads on brace 2.2 . . . . .	179
L.7	Member loads on brace 2.3 . . . . .	180
L.8	Member loads on brace 2.4 . . . . .	181
L.9	Member loads on brace 3.1 . . . . .	182
L.10	Member loads on brace 3.2 . . . . .	183
L.11	Member loads on brace 3.3 . . . . .	184
L.12	Member loads on brace 3.4 . . . . .	185
L.13	Member loads on brace 3.5 . . . . .	186
L.14	Member loads on brace 4.1 . . . . .	187
L.15	Member loads on brace 4.2 . . . . .	188
L.16	Member loads on brace 4.3 . . . . .	189
L.17	Member loads on brace 4.4 . . . . .	190
L.18	Member loads on brace 4.5 . . . . .	191
L.19	Member loads on brace 5.1 . . . . .	192
L.20	Member loads on brace 5.2 . . . . .	193
L.21	Member loads on brace 6.1 . . . . .	194
L.22	Member loads on brace 7.1 . . . . .	195
L.23	Details of fatigue assessment brace 1.1 . . . . .	197
L.24	Details of fatigue assessment brace 1.2 . . . . .	198
L.25	Details of fatigue assessment brace 1.3 . . . . .	199
L.26	Details of fatigue assessment brace 1.4 . . . . .	200

L.27 Details of fatigue assessment brace 2.1 . . . . .	201
L.28 Details of fatigue assessment brace 2.2 . . . . .	202
L.29 Details of fatigue assessment brace 2.3 . . . . .	203
L.30 Details of fatigue assessment brace 2.4 . . . . .	204
L.31 Details of fatigue assessment brace 3.1 . . . . .	205
L.32 Details of fatigue assessment brace 3.2 . . . . .	206
L.33 Details of fatigue assessment brace 3.3 . . . . .	207
L.34 Details of fatigue assessment brace 3.4 . . . . .	208
L.35 Details of fatigue assessment brace 3.5 . . . . .	209
L.36 Details of fatigue assessment brace 4.1 . . . . .	210
L.37 Details of fatigue assessment brace 4.2 . . . . .	211
L.38 Details of fatigue assessment brace 4.3 . . . . .	212
L.39 Details of fatigue assessment brace 4.4 . . . . .	213
L.40 Details of fatigue assessment brace 4.5 . . . . .	214
L.41 Details of fatigue assessment brace 5.1 . . . . .	215
L.42 Details of fatigue assessment brace 5.2 . . . . .	216
L.43 Details of fatigue assessment brace 6.1 . . . . .	217
L.44 Details of fatigue assessment brace 7.1 . . . . .	218
O.1 Solitaire's stinger section 1 . . . . .	223
P.1 Solitaire's stinger section 1, with adapted joints. . . . .	225
P.2 Overview of numbering of braces/joints. . . . .	226

# List of Tables

2.1	Distinction between different joint classifications according to DNV-GL [23]	9
2.2	Element and software choices of authors investigating joint flexibility	16
2.3	List of publications of parametric equations	20
4.1	Overview of equations to calculate the chord wall deformations	39
4.2	Geometrical properties of test joints	42
4.3	Comparison between LJF of joint 1 according to the numerical model and parametric equation of Buitrago et al. [13]	43
4.4	Comparison between LJF of joint 2 according to the numerical model and parametric equation of Buitrago et al. [13]	43
4.5	Results of a course, fine and extra fine mesh	43
4.6	Test for verification of the model	44
4.7	The mean deviation and standard deviation of the deviation, of the LJF according to the methodology towards the experimentally determined LJF	52
4.8	Comparison of influence of deviations in joint dimension on calculated LJF.	53
4.9	Overview of equations to calculate the chord wall deformations of a multi-brace joint	59
4.10	Geometries of the four joints used for verification	62
4.11	The non-dimensional LJF matrices of the four joints presented in table 4.10, according to the numerical model	63
5.1	Comparison of local chord wall deformations joint 4 according to a model with shell elements, beam model with LJF and a beam model without LJF	77
5.2	Comparison of local chord wall deformations joint 3 according to a model with shell elements, beam model with LJF and a beam model without LJF	77
5.3	Comparison of deformations and displacements, as effect of an axial load on brace 2, according to a shell model, a beam model without LJF and a beam model with LJF.	78
5.4	Comparison of deformations and displacements, as effect of an out-of-plane bending moment on brace 2, according to a shell model, a beam model without LJF and a beam model with LJF.	79
5.5	Comparison of deformations and displacements, as effect of an in-plane bending moment on brace 2, according to a shell model, a beam model without LJF and a beam model with LJF.	80
5.6	Comparison of deformations and displacements, as effect of an axial load on brace 1, according to a shell model, a beam model without LJF and a beam model with LJF.	81
5.7	Comparison of deformations and displacements, as effect of an out-of-plane bending moment on brace 1, according to a shell model, a beam model without LJF and a beam model with LJF.	82
5.8	Comparison of deformations and displacements, as effect of an in-plane bending moment on brace 1, according to a shell model, a beam model without LJF and a beam model with LJF.	83
6.1	Overview of load-cases	87
6.2	Comparison of the diagonal flexibilities (non-dimensional) of brace 1.3 in a model with and without LJF	94
6.3	Comparison of the diagonal flexibilities of brace 1.4 in model with and without LJF	97
6.4	Comparison of critical fatigue damage according to a model with and without LJF	103
6.5	Comparison of critical fatigue damage according to a model with and without LJF	105
6.6	Comparison of critical fatigue damage according to a model with and without LJF	107

D.1	Results from verification single-brace numerical model . . . . .	136
E.1	Comparison of results from 31 measurements for axial flexibility. . . . .	138
E.2	Comparison of results from 31 measurements for out-of-plane bending flexibility. . . . .	140
E.3	Comparison of results from 31 measurements for in-plane bending flexibility. . . . .	142
M.1	Joint 1: Chord wall displacements $\kappa_{p,j}$ of point $p$ as effect of unit-load $P_j$ . . . . .	219
M.2	Joint 2: Chord wall displacements $\kappa_{p,j}$ of point $p$ as effect of unit-load $P_j$ . . . . .	219
N.1	The flexibilities of the 7 joints / 22 braces of interest, discussed in the numerical test case of chapter 6. . . . .	222
O.1	Geometrical properties of the joint categories in the stinger . . . . .	224
P.1	Parameters joint 1 . . . . .	227
P.2	Parameters joint 2 . . . . .	228
P.3	Parameters joint 3 . . . . .	229
P.4	Parameters joint 4 . . . . .	230
P.5	Parameters joint 5 . . . . .	231
P.6	Parameters joint 6 . . . . .	232
P.7	Parameters joint 7 . . . . .	233

# Symbols and Acronyms

## Symbols

### Latin

$A$	Cross surface area	$m^2$
$\underline{a}$	Vector representing the axis of rotation	-
$B$	Total number of (deforming) braces	-
$b$	Index for (deforming) brace number	-
$C$	Total number of (loaded) braces	-
$c$	Index for (loaded) brace number	-
$corr$	Correction for wall thickness within fatigue assessment	-
$D$	Accumulated fatigue damage	-
$D$	Chord (outer) diameter	$m$
$d$	Brace (outer) diameter	$m$
$E$	Young's modulus of elasticity	$MPa$
$e$	Gap length at chord centerline	$m$
$[F]$	Flexibility matrix	$\frac{m}{N}$ or $\frac{rad}{Nm}$ or $\frac{1}{N}$ or $\frac{rad}{N}$
$[F_{bc}]$	Flexibility sub-matrix for brace $b$ loaded by brace $c$	$\frac{m}{N}$ or $\frac{rad}{Nm}$ or $\frac{1}{N}$ or $\frac{rad}{N}$
$F_{AX}$	Axial force	$N$
$f_{ij}$	Flexibility in direction $i$ under load $j$	$\frac{m}{N}$ or $\frac{rad}{Nm}$ or $\frac{1}{N}$ or $\frac{rad}{N}$
$f_{ij}^*$	Non-dimensional flexibility in direction $i$ under load $j$	-
$g$	Gap length at chord surface	$m$
$I$	Second moment of area	$m^4$
$I$	Total number of displacement DOF	-
$i$	Index for displacement DOF	-
$J$	Total number of load DOF	-
$j$	Index for load DOF	-
$[K]$	Stiffness matrix	$\frac{N}{m}$ or $\frac{Nm}{rad}$ or $N$ or $\frac{N}{rad}$
$k$	Stiffness	$\frac{N}{m}$ or $\frac{Nm}{rad}$ or $N$ or $\frac{N}{rad}$
$k$	Thickness exponent applied within fatigue assessment	-
$L$	Chord length	$m$
$l$	Brace length	$m$
$l_e$	Element length	$m$
$[LJF]$	Local joint flexibility matrix	$\frac{m}{N}$ or $\frac{rad}{Nm}$ or $\frac{1}{N}$ or $\frac{rad}{N}$
$[LJF_{bc}]$	Local joint flexibility sub-matrix containing the 9 flexibilities from brace $b$ loaded by brace $c$	$\frac{m}{N}$ or $\frac{rad}{Nm}$

$[LJF^*]$	Non-dimensional local joint flexibility matrix	-
$M_{IPB}$	In-plane bending moment	$Nm$
$M_{OPB}$	Out-of-plane bending moment	$Nm$
$m$	Negative inverse of slope of S-N curve	-
$N$	Total number of samples	-
$N$	Predicted number of cycles to failure	-
$n$	Sample number	-
$n_0$	Number of cycles per load-case	-
$[P]$	Matrix containing the unit-loads	$N$ or $Nm$
$[P_c]$	Sub-matrix containing the unit-loads on brace $c$	$N$ or $Nm$
$P_C$	Vector containing constrained applied loads	$N$ or $Nm$
$P_F$	Vector containing free applied loads	$N$ or $Nm$
$P_j$	Unit-load in DOF $j$	$N$ or $Nm$
$p$	Index for points located at chord wall	-
$[Q_P]$	Matrix to transform from dimensional to non-dimensional loads	$N$ or $Nm$
$[Q_\Delta]$	Matrix to transform from dimensional to non-dimensional deformations	$m$ or -
$Q$	Probability of exceedence	-
$[R^{a \rightarrow b}]$	Rotation matrix for the rotation from coordinate system $a$ to coordinate system $b$	-
$R$	Chord (outer) radius	$m$
$r$	Brace (outer) radius	$m$
$[S]$	Transformation matrix connecting basic and initial degrees of freedom	-
$[T^{a \rightarrow b}]$	Transformation matrix for the transformation from system $a$ to system $b$	-
$T$	Chord wall thickness	$m$
$t$	Brace wall thickness	$m$
$t_{ref}$	reference thickness, 16 for tubular joints [23]	$mm$
$u$	Displacements	$mm$
$\underline{v}$	Vector representing the direction	
$v$	Value used for pivots of rigid DOF in flexibility matrix	$\frac{m}{N}$ or $\frac{rad}{Nm}$
$W$	Section modulus	$m^3$
$w$	Width of mesh cycle	$m$
$w_r$	Width reduction of mesh cycle	$m$
$X$	Coordinate in local chord coordinate system (Cartesian)	$m$
$x$	Coordinate in local brace coordinate system (Cartesian)	$m$
$Y$	Coordinate in local chord coordinate system (Cartesian)	$m$
$Y'$	Coordinate in local chord unfolded coordinate system (Cartesian)	$m$
$y$	Coordinate in local brace coordinate system (Cartesian)	$m$

$Z$	Coordinate in local chord coordinate system (Cartesian)	$m$
$Z'$	Coordinate in local chord unfolded coordinate system (Cartesian)	$m$
$z$	Coordinate in local brace coordinate system (Cartesian)	$m$

## Greek

$\alpha$	Geometrical joint parameter $\frac{2L}{D}$	-
$\alpha_b$	Geometrical joint parameter $\frac{2l}{d}$	-
$\beta$	Geometrical joint parameter $\frac{d}{D}$	-
$\Gamma(a, x)$	Gamma function $\int_x^\infty t^{a-1} \exp(-t) dt$	-
$\gamma(a, x)$	Incomplete gamma function $\int_0^\infty t^{a-1} \exp(-t) dt$	-
$\gamma$	Geometrical joint parameter $\frac{D}{2T}$	-
$\underline{\Delta}_i$	Vector containing the deformation in DOF $i$	$m$ or $rad$
$\underline{\Delta}_C$	Vector containing the constrained deformations $i$	$m$ or $rad$
$\underline{\Delta}_F$	Vector containing the free deformations $i$	$m$ or $rad$
$\Delta\sigma$	Hot spot stress range	$MPa$
$\delta_{ij}$	Deformation in DOF $i$ under load in DOF $j$	$m$ or $rad$
$\epsilon$	Geometrical joint parameter $\frac{e}{D}$	-
$\zeta$	Geometrical joint parameter $\frac{g}{D}$	-
$\theta$	In-plane brace angle	$^\circ$
$\kappa_{p,j,b}$	Chord wall displacement at point $p$ on brace $b$ under load case $j$ in the plane defined by chord and brace, in the direction perpendicular to the chord.	$m$
$\lambda_n$	Fraction of joint classification	-
$\mu$	Mean deviation	%
$\nu$	Poisson's ratio	-
$\pi$	Ratio of a circles circumference to its diameter = 3.14159	-
$\sigma$	Standard deviation	%
$\sigma_{rms}$	Root mean square deviation	-
$\sigma_n$	Hot spot stress	$MPa$
$\sigma_x$	Nominal stress due to axial force	$MPa$
$\sigma_{my}$	Nominal stress due to in-plane bending moment	$MPa$
$\sigma_{mz}$	Nominal stress due to out-f-plane bending moment	$MPa$
$\tau$	Geometrical joint parameter $\frac{t}{T}$	-
$\Phi$	Angle in cylindrical coordinate system from chord	$rad$
$\phi$	Angle in cylindrical coordinate system from brace	$rad$
$\psi$	Out-of-plane brace angle	$^\circ$
$\omega_n$	Deviation of sample number $n$	%

## Acronyms

ANSYS	ANalysis SYStems, Inc is an engineering analysis program from Ansys Inc.
APDL	ANSYS Parametric Design Language
AQWA	ANSYS software package for the determination of hydrodynamic interaction of vessels and structures
CHS	Circular Hollow Section
CS	Coordinate System
DOF	Degree(s) Of Freedom
FEMAP	Finite Element modelling And Post-processing, is an engineering analysis program from Siemens PLM Software
FJC	Field Joint Coating
FEA	Finite Element Analysis
LJF	Local Joint Flexibility
MATLAB	Programming language and numeric computing environment developed by MathWorks
NASTRAN	NASA STRucture ANalysis, is an engineering analysis program originally developed for NASA
NDT	Non Destructive Testing
SCF	Stress Concentration Factor
SD	Standard Deviation

# Introduction

## 1.1. Background

Allseas Group S.A. is a Swiss based offshore contractor and global leader in offshore pipeline installation and subsea construction. The company is founded in 1985 by owner and CEO Edward Heerema. Currently, Allseas employs over 4000 people worldwide and operates a fleet of specialized heavy-lift, pipelay and support vessels, designed and developed in-house. The innovation department responsible for the design and optimization of their vessels, equipment and processes is located in Delft, Eindhoven and Enschede. For public, Allseas is mostly known for their ship 'Pioneering Spirit', the largest construction vessel in the world. The vessel is designed to lift entire platform topsides of up to 48,000 Tons and thereby reducing the amount of work required for installation and decommissioning.

Allseas uses several ships to lay pipelines following the S-lay method. In this configuration, pipelines are assembled horizontally on a vessel and guided into the water by a stinger frame, to reduce strain in the pipeline and prevent it from buckling (figure 1.1). In the production line, also called 'firing line' pipe joints with a length of 12.2 meter, or 24.4 meter for vessels with a double joint production line, are welded together to a pipeline. Besides welding stations, the firing line is as well equipped with Non-Destructive Testing (NDT) and Field Joint Coating (FJC) stations. After completion of the connection of a new joint the vessel moves forward and a part of the pipeline is guided into the water. A tensioner is used to regulate the movement of the pipeline and keep it on-board. During this process, the vessel position is maintained by dynamic positioning or by anchoring.

The stinger is made of a steel space frame structure and mounted on the bow or stern on a vessel (figure 1.2). Usually, the stinger consists of multiple sections between which the relative angle can be changed in order to meet the pipelay radius requirement. This is important as the theoretical pipe

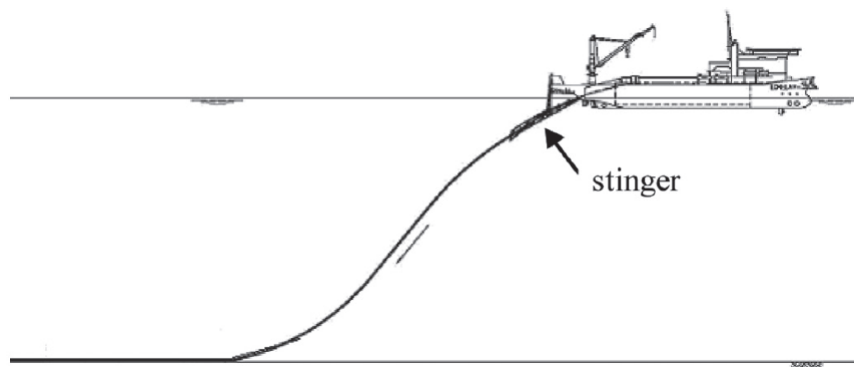


Figure 1.1: Visualisation of the S-lay pipeline configuration [27]



Figure 1.2: The Solitaire with a retracted stinger

bending strain is equal to the pipe radius divided by the stinger radius. Height adjustable roller-boxes are applied to tune the stinger radius and support the pipeline during pipe laying.

The stinger frame is made of tubular sections. In particular circular hollow sections are commonly used in offshore structures because of their good properties for resisting compression, tension, bending and torsion forces but as well as their low drag coefficients when being subjected to wind and wave loads. The stinger structure is made of upper and lower chords supported by horizontal, vertical and diagonal braces. The braces and chord are welded together in uni- and multi-planar joints.

The stinger is subjected to multiple loads. Primarily by its own dead weight and loads of the pipeline also called roller box loads. In addition, the stinger is subjected to vessel-induced accelerations due to waves and Morison drag due to wave current around the stinger. These loads are referred to as hydrodynamic loads. The hydrodynamic loads make the stinger, especially the tubular joints sensitive for fatigue.

Fatigue is defined as the weakening of a material through large amounts of cycles consisting of different stress levels. Due to the nature of the previously mentioned loads, fatigue assessment is important for the lifetime prediction of the stinger. A schematic overview of the fatigue assessment approach for tubular joints in a stinger, exposed to hydrodynamic loads, used by Allseas is shown in figure 1.3. First, the 'life matrix' of the ship is determined. The life matrix contains an estimation of the load-cases to which the stinger is subjected and the occurrence of subjection. With AQWA simulations, for every load-case, a set of six hydrodynamic sub-load-cases is determined. These sub-load-cases are later used to determine the minimum and maximum stress for each load-case. The sub-load-cases are applied in a beam model, in order to calculate the member forces on the tubular joints. An example of a beam model of a stinger is shown in figure 1.4. The beam member forces are used to calculate the hot spot stresses in the brace/chord intersection. The difference in stress among the six-sub-load-cases determines the hot spot stress range for every location. With the hot spot stress range, and the number of cycles the accumulated fatigue damage in the brace is calculated. The fatigue damage determines the predicted fatigue life.

## 1.2. Problem definition

A beam model is a simplified method of modelling structures. The results of a beam model are not as accurate as the results of a shell model. However, for complex geometries subjected to a high number of load-cases ( $\approx 10000$ ) a beam model is a more efficient method of modelling and computational times are strongly reduced.

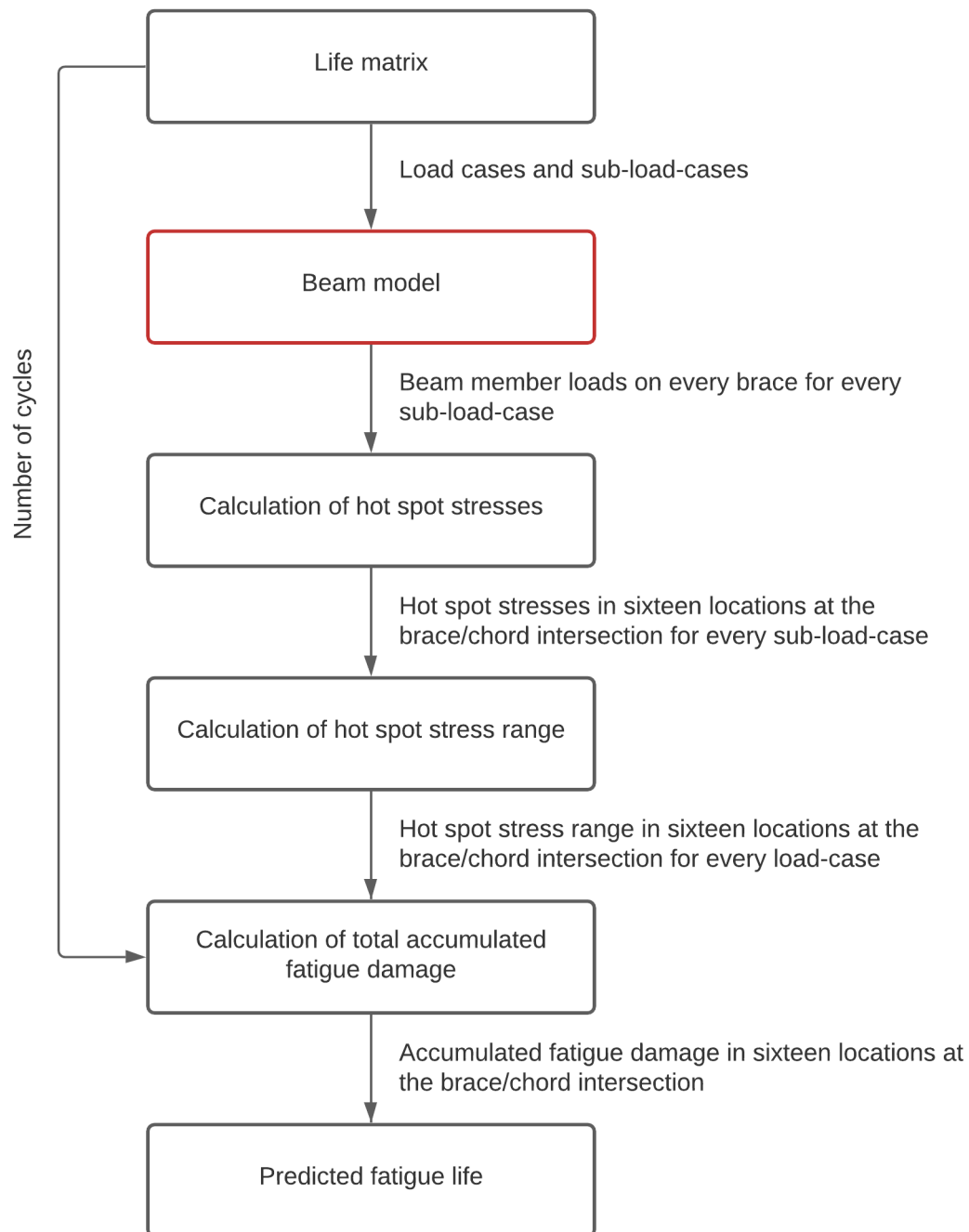


Figure 1.3: Schematic overview of the fatigue assessment for tubular joints in a beam model

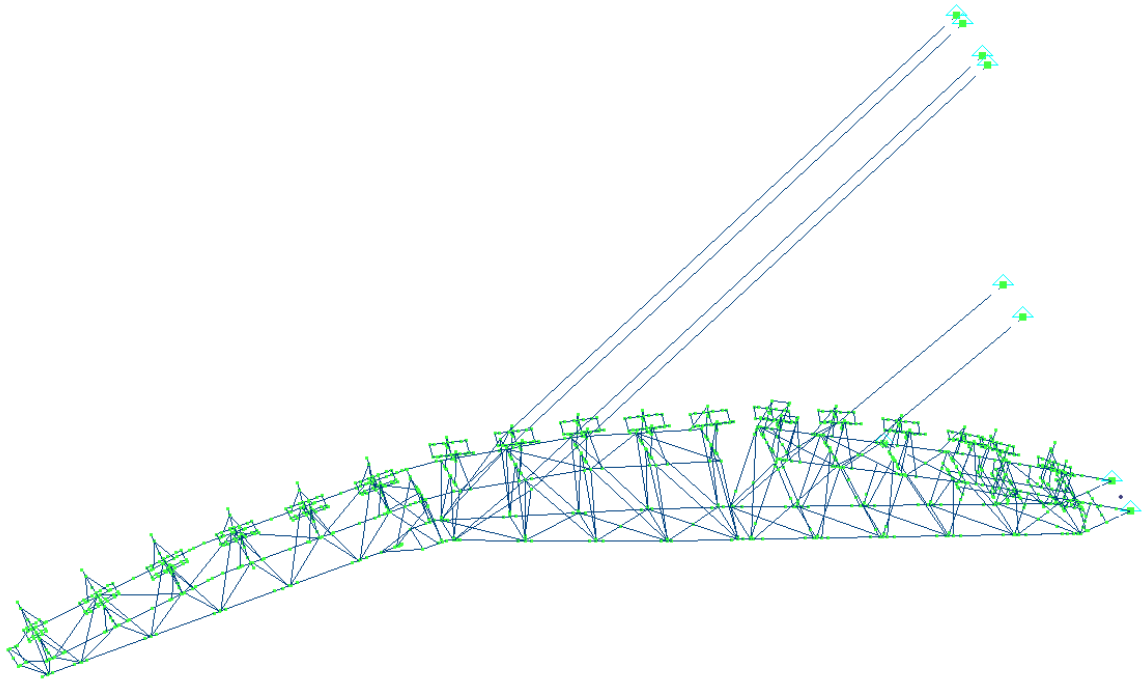


Figure 1.4: Beam model of the Solitaire stinger

In a standard beam model, no attention is paid to modelling the joint itself. In the model, the beam elements of the brace is extended from the surface of the chord to the centerline of the chord. This part of the brace is referred to as 'brace extension element' and is schematically presented in figure 1.5. The brace extension element is considered as rigid [18] [54] [31]. In reality, tubular joints possess considerable elastic flexibility through local deformation of the chord wall (figure 1.6). In literature, this is also described as Local Joint Flexibility (LJF).

MSL Engineering Ltd. [45]: "Structural engineering mechanics suggests that, in essence, representing the joints with finite linear elastic flexibility instead of no flexibility, would result in a reduction of acting loads at the joints, with a commensurate increase in member loads to maintain equilibrium".

A more accurate model taking LJF into account, leads to a redistribution of member-loads which can possibly lead to a reduction of the stresses in the joints [12]. For the determination of the ultimate

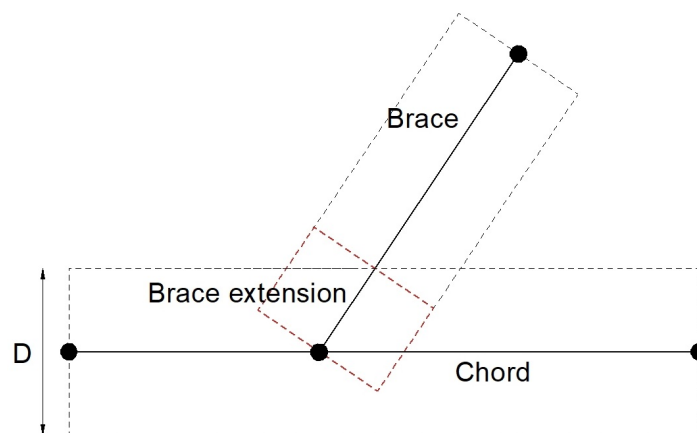


Figure 1.5: Schematic presentation of the simplification made when modelling tubular joints with beam elements. In red: the brace extension element

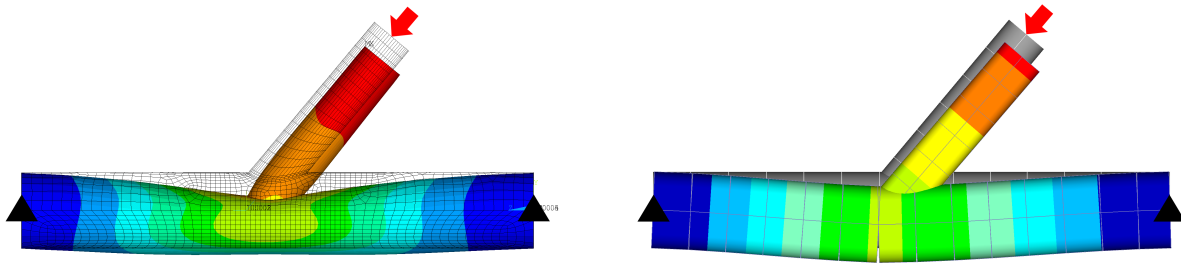


Figure 1.6: Comparison of deformations as effect of an axial force, according to a shell model (left) and beam model (right).

strength of a joint, the influence of LJF is negligible, but for fatigue assessment the influence can lead to considerable differences in predicted fatigue life. In a case study, performed by MSL Engineering Ltd. [45], it is observed that modelling LJF in an offshore steel jacket structure of a platform in the North Sea, led to an average increase in predicted fatigue life of respectively FACTOR 19.3, 9.2 and 8.0 for transverse-, longitudinal- and horizontal- frames. Worth to mention, but out of the scope of this assignment: the redistribution of forces leads to a reduction of buckling loads and to a change of the natural frequencies and mode shapes of tubular structures [17].

### 1.3. Aim of the project

This research concerns an exploratory character towards modelling LJF in a stinger and the influence of modelling LJF on the predicted fatigue life. The focus of the research is on the development, verification and validation of a methodology to account for LJF. When the model is finished a numerical test-case to investigate and estimate the influence of LJF on the predicted fatigue life needs to be performed.

To simulate LJF in a beam model, first the flexibilities of a tubular joint shall be determined. Therefore, the problem is divided into two sub-problems. Both problems are strongly related to each other, but are treated as two separate problems. The following distinction is made:

1. *Determination of LJF*: Measuring the flexibilities of a tubular joint.
2. *Modelling of LJF*: Simulating the flexibilities of a tubular joint in a beam model.

Research to possible methods to determine the local flexibility of tubular joints and to model this in a beam member model shall be conducted. Succeeding, the most suitable method for implementation in a stinger shall be determined and developed. In the last phase, through a numerical test-case the results of a model with and without LJF shall be compared, in order to determine the influence of modelling LJF on the predicted fatigue life. At the end of this project, a clear recommendation about the methodology for implementation and the influence on the predicted fatigue life shall be given.

### 1.4. Research questions

The main research question of this project states:

How can Local Joint Flexibility be modelled in a beam model of a stinger and what is the influence on the predicted fatigue life?

The main research question is supported by the following sub-questions:

1. What is Local Joint Flexibility and what flexibilities do tubular joints have?
2. What methodologies, to determine and model Local Joint Flexibility, are presented in literature?
3. What are the most suitable methodologies, to determine and model Local Joint Flexibility, in order to determine its influence?
4. How can the Local Joint Flexibility of joints in a stinger be determined, and with what accuracy? How can this method be verified and validated?
5. How can Local Joint Flexibility of joints in a stinger be modelled in a beam member model and with what accuracy? How can this method be verified and validated?
6. What is the influence, of accounting for Local Joint Flexibility in a beam model, on the predicted fatigue life of a stinger?

## 1.5. Scientific contribution

Multiple articles are published considering methods to determine and model the LJF of a tubular joint. Their methodologies are limited to a certain type of joint classification, and for flexibilities in specific DOF. No general approach for the calculation of flexibilities in every DOF, applicable to every single joint is available. Furthermore, large differences in approach and results among different authors are noticed (section 2.3 and 2.4). The differences raise questions about the accuracy of the presented methodologies. In this project, a new generally applicable method to determine and model the flexibilities of any non-overlapping joint is presented. The methodology is verified and validated.

The influence of modelling LJF on the predicted fatigue life of joints in a steel jacket structure is already investigated. It is unknown how these results are obtained and whether the same results can also be obtained for a stinger. Compared to a steel jacket structure, the joints of a stinger have a different classification and different geometric properties. The differences may influence the effectiveness of implementation, as well on the most suitable method to account for LJF in a beam model. No research is published considering the effect of modelling LJF on fatigue assessment of a stinger.

## 1.6. Scope

This research concerns an exploratory character to the effects of modelling LJF in a stinger. The focus of the research is on the development of a methodology which provides validated results and to explore the magnitude of the influence on the predicted fatigue life. The research is not focused on the development of a method which is accessible for implementation or to exactly define the relation between LJF and predicted fatigue. These questions are too complicated to answer within this research due to wide scenario of aspects which are involved. However, those questions could be a possible sequel of this research.

For the execution of this project, the full fatigue assessment of Allseas needs to be performed. The focus of this research is within modelling LJF in the beam model. Peripheral matters such as research towards the validity and accuracy of the fatigue assessment itself, simulations in AQWA or the trade-off between modelling the stinger with shell or beam elements is not part of this project.

The research is limited to the Solitaire stinger, one of the ships of Allseas. This stinger is considered as a representative geometry for the stingers operated within Allseas and therefore, will give representative results for all stingers. All joints of the stinger are built out of Circular Hollow Sections (CHS). Overlapped joints or joints reinforced with gussets are out of the scope of the project.

## 1.7. Research outline

In chapter 2, the flexibilities of a joint and the state-of-the-art methods to determine the LJF and model the LJF in a beam model are discussed. In chapter 3, the most suitable methodology for this project is determined. Therefore the joints in the stinger are investigated and the suitability of the different methodologies is evaluated. In chapter 4, the development of a method to determine the LJF is discussed. In chapter 5, the methodology applied to model LJF in a beam model is presented. In chapter 6, a simplified numerical test-case is performed to determine the influence of modelling LJF in a beam model. In chapter 7, the conclusion of the project is presented.



# 2

## Literature review

### 2.1. Introduction

A wide spectrum of articles, considering tubular joints and LJF is published in literature. In this chapter, the state of the art literature is briefly discussed. In section 2.2, the geometry and local flexibilities of a tubular joint are discussed. In section 2.3, the methodologies described in literature to determine the LJF of tubular joints are discussed. In section 2.4, the published methodologies to model LJF in a beam model are analysed. Literature conceives a dichotomy regarding the orientation of the flexible degrees of freedom. The difference between both orientations, is discussed in section 2.5. The conclusion is given in section 2.6. Where the sub-questions: “What is Local Joint Flexibility and what local flexibilities do tubular joints have?” and: “What methodologies to determine and model Local Joint Flexibility are presented in literature?” are answered.

### 2.2. Geometries and flexibilities of tubular joints

#### 2.2.1. Joint geometry

Tubular joints are distinguished in different classifications. A single-brace joint is classified as Y-joint. When the brace is located perpendicular to the chord ( $\theta = 90^\circ$ ) the joint is also referred to as T-joint. For joints with multiple braces the classification is beside geometry, load-case dependent as well. Joints in one common plane, also referred as single-plane joints, are classified into three joint types: Y-, X- and K-joints. Braces within  $\pm 15^\circ$  degree planes may be considered as being in a common plane. Classification is dependent on the axial force, perpendicular to the chord wall. Table 2.1 presents the distinction between different single-plane joints, made by DNV-GL [23]. Because joint classification is load dependent, a joint in a structure may have different classifications among different load-cases. Multi-brace joints are a combination of previously mentioned joint classifications. Examples of joint classifications are shown in appendix K.

Table 2.1: Distinction between different joint classifications according to DNV-GL [23]

Y-joint	The axial force in the brace is reacted as beam shear to the chord.
K-joint	The axial force in the brace is balanced to within 10% by forces in other braces in the same plane and on the same side of the joint.
X-joint	The axial force in the brace is carried through the chord to braces on the opposite side.

The dimensions of a joint are presented in figure 2.1. The geometry of tubular joints is often defined with dimensionless geometric parameters. These parameters make it easier to relate to the behaviour and properties of the joint. The size of the joint, is defined with chord diameter  $D$ .

$$\alpha = \frac{2L}{D} \quad (2.1)$$

$$\alpha_b = \frac{2l}{d} \quad (2.2)$$

$$\beta = \frac{d}{D} \quad (2.3)$$

$$\gamma = \frac{D}{2T} \quad (2.4)$$

$$\epsilon = \frac{e}{D} \quad (2.5)$$

$$\zeta = \frac{g}{D} \quad (2.6)$$

$$\tau = \frac{t}{T} \quad (2.7)$$

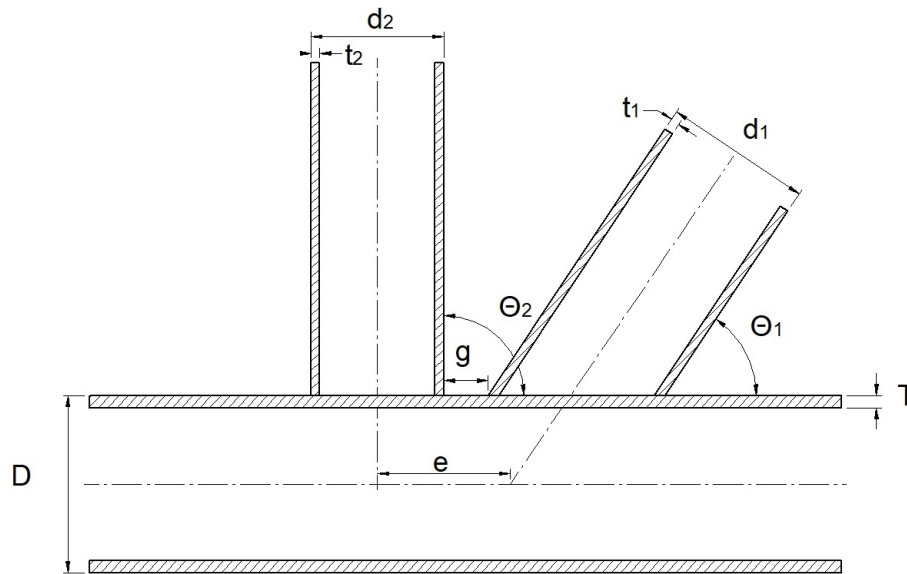


Figure 2.1: Schematic presentation of the dimensions of a tubular joint

### 2.2.2. Single-brace joint flexibilities

Flexibility  $f$  is defined as the deformation per unit-load. Also noted as:

$$f = \frac{\delta}{P} \quad (2.8)$$

Deformation  $\delta$ , may be a translation as well as a rotation and unit-load  $P$ , may be a force as well as a bending moment. Flexibility is the inverse of stiffness  $k$ . It follows that:

$$f = \frac{1}{k} \quad (2.9)$$

Local Joint Flexibility is defined as the local chord wall deformation as effect of an external load. The deformations appear due to bending of the chord wall, in the direction perpendicular to the chord axis. In the direction parallel to the chord axis, the joint is subjected to shear loads and therefore, the flexibility in this direction assumed to be negligible [6] [7] [13] [18] [36]. The physical impression of the three deformations is presented in figure 2.2.

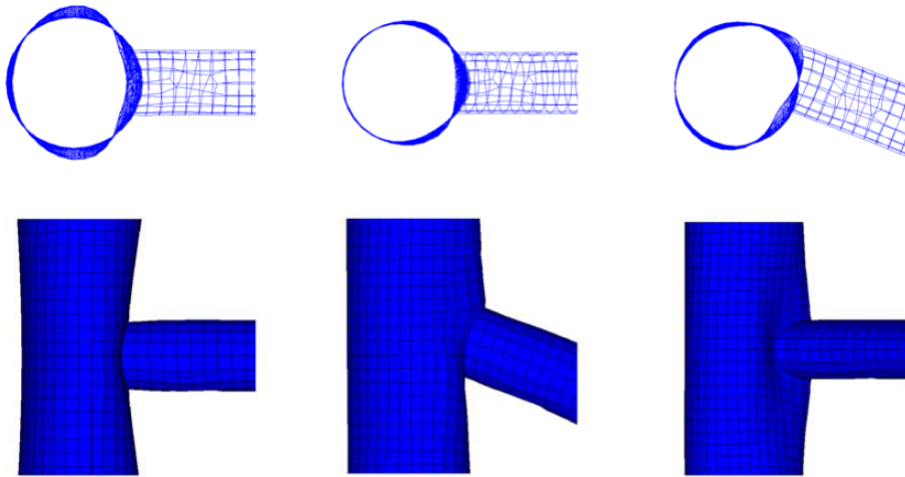


Figure 2.2: Deformations of a T-joint. From left to right: axial, in-plane bending and out-of-plane bending [6].

The deformations are the effect of a load. Axial force, out-of-plane bending moment and in-plane bending moment. Three flexibilities are defined: Axial flexibility, out-of-plane bending flexibility and in-plane bending flexibility. The flexibilities are the combination of the unit-load and the deformation and are defined following:

$$LJF_{AX} = \frac{\delta_1}{P_1} \quad (2.10)$$

$$LJF_{OPB} = \frac{\delta_2}{P_2} \quad (2.11)$$

$$LJF_{IPB} = \frac{\delta_3}{P_3} \quad (2.12)$$

Here, deformations and unit-loads are indexed under  $i$  and  $j$ . This notation becomes convenient later, for the application in multi-brace joints. Deformations are defined with  $\delta_i$  following:

- $\delta_1$  = axial deformation [m]
- $\delta_2$  = out-of-plane bending deformation [rad]
- $\delta_3$  = in-plane bending deformation [rad]

Unit-loads are defined with  $P_j$  following:

$P_1$  = axial force [N]  
 $P_2$  = out-of-plane bending moment [Nm]  
 $P_3$  = in-plane bending moment [Nm]

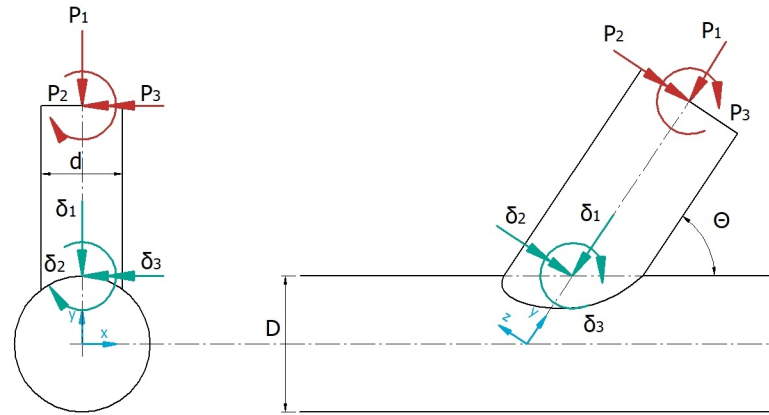


Figure 2.3: The flexibilities of a single-brace joint, defined in the local brace coordinate system

In literature, the flexibilities of the joint are defined in the local coordinate system of the brace. The three flexibilities are visualised in figure 2.3. For modelling of LJF, another coordinate system may be used. This coordinate system is discussed further in section 2.5.

The deformation-load relation of a T-joint subjected to an axial force is shown in figure 2.4a. The deformation-load relation of a T-joint subjected to an in-plane bending moment is shown in figure 2.4b. Both figures demonstrate that the flexibility until initial yielding is a linear relation which may be estimated with a constant value.

The previously defined flexibilities define the relation between a deformation and an unit-load in equal DOF. Additionally, there may be coupling between the unit-load in one DOF and the deformation in another DOF. E.g. axial deformations can appear as effect of an in-plane bending moment. The relation between deformations in the three DOF as effect of the three possible DOF unit-loads, are defined in the LJF matrix  $[LJF]$ . Because there are three DOF the dimension of this matrix is 3 x 3.

$$\underline{\Delta} = [LJF] \underline{P} \quad (2.13)$$

Written out:

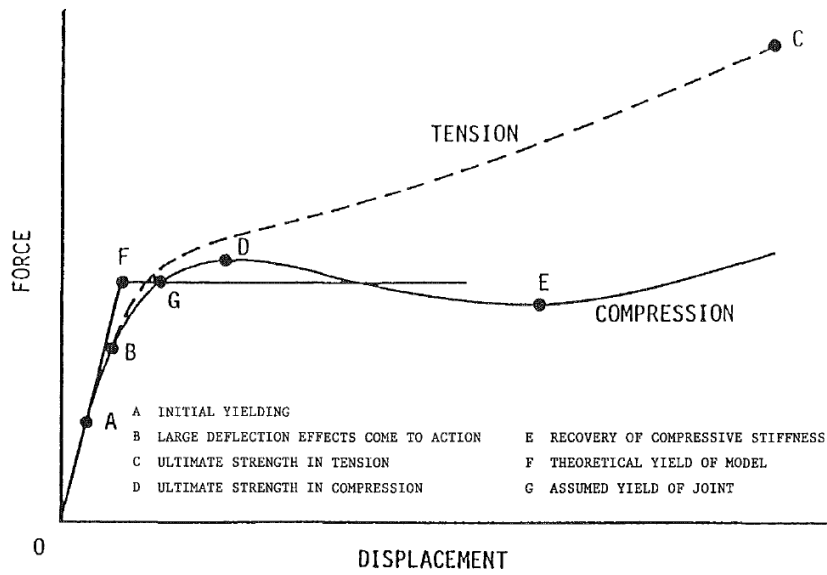
$$\begin{bmatrix} \delta_1 \\ \delta_2 \\ \delta_3 \end{bmatrix} = \begin{bmatrix} f_{11} & f_{12} & f_{13} \\ f_{21} & f_{22} & f_{23} \\ f_{31} & f_{32} & f_{33} \end{bmatrix} \begin{bmatrix} P_1 \\ P_2 \\ P_3 \end{bmatrix} \quad (2.14)$$

Here,  $f_{ij}$  represents the flexibility defined by a deformation in DOF  $i$  as effect of the unit-load in DOF  $j$ . The diagonal terms of the flexibility matrix represent the flexibility in the DOF equal to the load, discussed previously. This means:

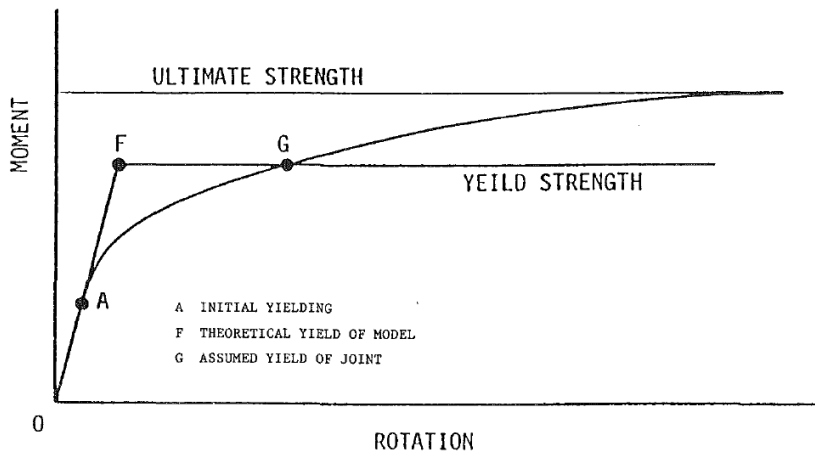
$$f_{11} = LJF_{AX} \quad (2.15)$$

$$f_{22} = LJF_{OPB} \quad (2.16)$$

$$f_{33} = LJF_{IPB} \quad (2.17)$$



(a) Subjected to an axial force



(b) Subjected to an in-plane bending moment

Figure 2.4: The typical load-displacement relationship of a T-joint [55]

Off-diagonal terms represent the flexibility between different DOF. E.g.  $f_{12}$  represents the axial deformation caused by an out-of-plane bending moment. Off-diagonal flexibilities can have unit  $\frac{rad}{Nm}$  or  $\frac{1}{N}$  or  $\frac{rad}{N}$ .

The Maxwell-Betti reciprocal work theorem states:

$$\sum_{n=1}^N P_n^i \delta_n^j = \sum_{n=1}^N P_n^j \delta_n^i \tag{2.18}$$

Therefore, the flexibility matrix shall theoretically be symmetrical. Fessler et al. [31]: “The  $f_{12}, f_{21}, f_{23}$  and  $f_{32}$  flexibilities are zero on account of (geometric) symmetry. The  $f_{13}$  and  $f_{31}$  flexibilities were found to be small and were assumed to be negligible as well. Thus only the three leading diagonal flexibilities are significant”. Literature comprises a difference in conception, considering accounting for out-of-plane bending ( $f_{22}$ ). Most authors include out-of-plane bending flexibility but Ueda et al. [54], Chen et al. [18] and Asgarian et al. [11] assume the influence is too small and neglect out-of-plane bending.

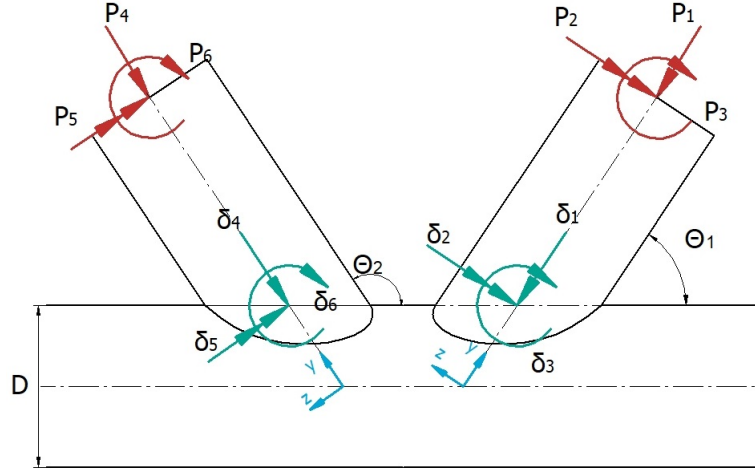


Figure 2.5: The flexibilities of a multi-brace joint, defined in the local brace coordinate system

### 2.2.3. Multi-brace joint flexibilities

When braces of a multi-brace joints are located close to each other, one brace can deform as effect of a load on an adjacent brace. The single-brace theorem for flexibilities is expanded for multi-brace joints. With every additional brace, three DOF deformations and three possible unit-loads are added to the joint. The deformations and loads are schematically shown in figure 2.5. The index for deformation  $\delta_i$  and unit-load  $P_j$  is expanded:

- $\delta_1$  = axial deformation of brace 1
- $\delta_2$  = out-of-plane bending deformation of brace 1
- $\delta_3$  = in-plane bending deformation of brace 1
- $\delta_4$  = axial deformation of brace 2
- $\delta_5$  = out-of-plane bending deformation of brace 2
- $\delta_6$  = in-plane bending deformation of brace 2

- $P_1$  = axial force on brace 1
- $P_2$  = out-of-plane bending moment on brace 1
- $P_3$  = in-plane bending moment on brace 1
- $P_4$  = axial force on brace 2
- $P_5$  = out-of-plane bending moment on brace 2
- $P_6$  = in-plane bending moment on brace 2

The flexibility matrix contains the relation between every DOF unit-load and every DOF deformation. The LJF matrix of a multi-brace joint is defined as:

$$\begin{bmatrix} \delta_1 \\ \delta_2 \\ \delta_3 \\ \delta_4 \\ \delta_5 \\ \delta_6 \\ \vdots \\ \delta_i \end{bmatrix} = \begin{bmatrix} f_{11} & f_{12} & f_{13} & f_{14} & f_{15} & f_{16} & \dots & f_{1j} \\ f_{21} & f_{22} & f_{23} & f_{24} & f_{25} & f_{26} & \dots & f_{2j} \\ f_{31} & f_{32} & f_{33} & f_{34} & f_{35} & f_{36} & \dots & f_{3j} \\ \hline f_{41} & f_{42} & f_{43} & f_{44} & f_{45} & f_{46} & \dots & f_{4j} \\ f_{51} & f_{52} & f_{53} & f_{54} & f_{55} & f_{56} & \dots & f_{5j} \\ f_{61} & f_{62} & f_{63} & f_{64} & f_{65} & f_{66} & \dots & f_{6j} \\ \vdots & \vdots & \vdots & \vdots & \vdots & \vdots & \ddots & \vdots \\ f_{i1} & f_{i2} & f_{i3} & f_{i4} & f_{i5} & f_{i6} & \dots & f_{ij} \end{bmatrix} \begin{bmatrix} P_1 \\ P_2 \\ P_3 \\ P_4 \\ P_5 \\ P_6 \\ \vdots \\ P_j \end{bmatrix} \quad (2.19)$$

The LJF matrix may be divided in sub-matrices, noted by  $[LJF_{bc}]$  with dimensions  $3 \times 3$ . The sub-matrix

contains the relation between the deformations of brace  $b$  notated with  $\underline{\Delta}_b$  as effect of the loads on brace  $c$  notated with  $\underline{P}_c$ .

$$\begin{bmatrix} \underline{\Delta}_1 \\ \underline{\Delta}_2 \\ \vdots \\ \underline{\Delta}_b \end{bmatrix} = \begin{bmatrix} [\mathbf{LJF}_{11}] & [\mathbf{LJF}_{12}] & \dots & [\mathbf{LJF}_{1c}] \\ [\mathbf{LJF}_{21}] & [\mathbf{LJF}_{22}] & \dots & [\mathbf{LJF}_{2c}] \\ \vdots & \vdots & \ddots & \vdots \\ [\mathbf{LJF}_{b1}] & [\mathbf{LJF}_{b2}] & \dots & [\mathbf{LJF}_{bc}] \end{bmatrix} \begin{bmatrix} \underline{P}_1 \\ \underline{P}_2 \\ \vdots \\ \underline{P}_c \end{bmatrix} \quad (2.20)$$

E.g.  $[\mathbf{LJF}_{21}]$  represents the deformation of brace 2 as effect of the possible loads on brace 1. The sub-matrix is defined as:

$$\begin{bmatrix} \delta_4 \\ \delta_5 \\ \delta_6 \end{bmatrix} = \begin{bmatrix} f_{41} & f_{42} & f_{43} \\ f_{51} & f_{52} & f_{53} \\ f_{61} & f_{62} & f_{63} \end{bmatrix} \begin{bmatrix} P_1 \\ P_2 \\ P_3 \end{bmatrix} \quad (2.21)$$

Deformations and unit-loads are both defined in the coordinate system of the brace of application. Therefore, when  $b \neq c$  the flexibilities are defined in a combination of two coordinate systems.

About the influence of adjacent braces on the flexibilities no clear conclusion is drawn in literature. MSL [45] applies a method ignoring the influence of surrounding braces in their investigation. This method is supported by ISO [42] and DNV-GL [22]. However, several publications write the importance of modelling the interaction between braces [4] [11] [30]. Ueda et al. [54] states that multi-brace joints with a gap ratio  $\zeta \geq 0.15$  may be treated as two separate joints. When the gap is less than  $0.15D$ , there is interaction between the joints [54].

## 2.3. Determination of LJF

In this section is elaborated on methods to determine the LJF of a tubular joint. Three methods are presented to determine the flexibilities: Physical measurements, Finite Element Analysis and parametric equations. The three methods are discussed further in the following sub-sections.

### 2.3.1. Physical measurements

In physical measurements a (scale) model of the tubular joint is fixed in a frame and physically loaded with a force or moment. With sensors the deformations of the chord wall are measured. For every measurement a model of the joint is required. By the knowledge of the author four publications containing measurements towards LJF are issued:

1. Fessler et al. [29] tested 25 joints, including seven multi-brace joints made of centrifugally cast araldite tubes. Araldite is a virtually linear elastic material.
2. Tebbett [53] measured the joint flexibility of five T-joints. Information considering the execution of the experiment could not be retrieved.
3. McDermott [26] according to [31], performed an unknown number of experiments measuring LJF. However, the research could not be accessed.
4. Fessler et al. [31] used 27 models made of centrifugally cast araldite tubes. All models are single-brace joints with varying  $\beta$ ,  $\gamma$  and  $\theta$ . Fessler et al. [31] did not take into account the brace wall thickness because they assumed that the influence on the LJF is negligible. A picture of the experiment is shown in figure 2.6. The full experiment is described in [28].

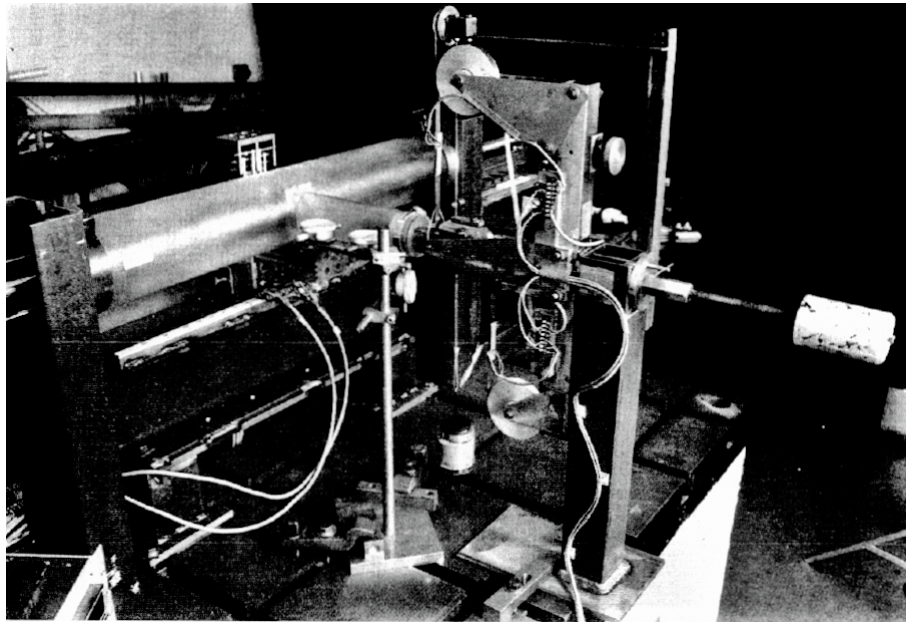


Figure 2.6: The test set-up used by Fessler et al. to measure the flexibilities of a tubular joint [31]

### 2.3.2. Finite Element Analysis

Finite Element Analysis (FEA) is used to numerically determine the flexibilities of a tubular joint. FEA is more cost effective than physical test and adjustable towards different joint geometries. Romeijn [48] investigated modelling tubular joints for joint flexibility and stress and strain concentration factors in FEA. When determining the flexibilities with FEA, the accuracy of the model is of high importance. Great attention needs to be paid to building a correct numerical model. The flexibility of a joint largely depends on the type of element, mesh refinement and the number of integration points [49]. An overview of the publications using FEA to determine the LJF is shown in table 2.2.

Two type of elements are common to model displacements in tubular joints, shell and solid elements. Shell models behave like plate elements and have four or eight nodes with six DOF. Solids have eight or twenty nodes with three DOF. Romeijn et al. [49] states about modelling tubular joints: “No general conclusion can be made on accuracy of 20-noded solid element against 8-noded shell elements, because this depends entirely on the geometry and type of loading”. The choices of authors investigating the joint flexibilities are shown in table 2.2.

Table 2.2: Element and software choices of authors investigating joint flexibility

Author	Year	Element type	Software
Hoshyari [38]	1993	quadrilateral plate assembled of four triangular elements [19]	ALGOR
Buitrago et al. [13]	1993	thick shell	PMBSHELL
Chen and Zhang [18]	1996	not mentioned	not mentioned
Qian et al. [47]	2013	20-node solid	PATRAN
Asgarian et al. [11]	2014	8-node shell	ANSYS
Jia and Chen [43]	2014	8-node thick shell	ABAQUS
Ahmadi et al. [1] [2] [3] [4] [5]	2017, 2018, 2019	8-node solid	ANSYS
Khan et al. [44]	2018	4-node shell	ABAQUS

### 2.3.3. Parametric equations

Determination of flexibilities of a joint with physical measurements or FEA is a time consuming matter. In the late 70's, investigation to equations to determine load-displacement relationships of different type of joints subjected to different load-cases started. The equations are generated by interpolation of results of physical measurements or FEA. The equations are dependent on the dimensionless geometric joint parameters and provide dimensionless flexibilities, for clarity topped with an asterisk.

$$f_{11} = \frac{f_{11}^*}{ED} \quad (2.22)$$

$$f_{22} = \frac{f_{22}^*}{ED^3} \quad (2.23)$$

$$f_{33} = \frac{f_{33}^*}{ED^3} \quad (2.24)$$

The dimensionless flexibility is geometry dependent only. Neither the size of the joint nor the elasticity of the material do have influence. This makes the dimensionless flexibility a very convenient definition for the comparison of flexibilities of different joint geometries.

The published parametric equations are developed for specific joint geometries for specific flexibilities. An overview of all published equations is shown in table 2.3. The equations presented in table 2.3 are shown in appendix H, including their validated domain. The equations are written out in an equal format and thus, if required, converted from their original notation to the authors notation. Out of the scope of this study, but worth to mention: Gho [35] showed the need for separate parametric equations for overlapped joints. These equations are determined by [32], [33], [34] and [13]. Nassiraei [46] [39] investigated the parametric equations for joints, strengthened with collar plates.

The presented equations have numerous variables which are dependent on each other and therefore hard to interpret. To gain insight in the parametric equations, the flexibility  $f_{33}^*$  of a tubular joint, according the equations of Efthymiou [24], Fessler et al. [31], Ueda et al. [54], Chen and Zhang [17], Buitrago et al. [13] and Asgarian et al. [11] are plotted in figure 2.7, 2.8, 2.9 and 2.10. The equations are dependent on geometric parameters  $\beta, \gamma, \theta, \tau, \beta_2, \theta_2$  and  $\zeta$ . In the plots, all parameters are kept fixed while one parameter is varied. The parameters are fixed on the following values:

$$\begin{aligned} \beta_1 &= 0.6 \\ \beta_2 &= 0.6 \\ \gamma &= 12 \\ \theta_1 &= 60 \\ \theta_2 &= 120 \\ \tau &= 0.6 \\ \zeta &= 0.05 \end{aligned}$$

Equations outside their validated domain are plotted with a dashed line. Moreover, equations which are independent of the plotted variable, are plotted with a dashed line as well and is shown as a reference to the other equations. The equations are written in Appendix H. Similar behaviour is seen for the equations of  $f_{11}^*$  and  $f_{22}^*$ . The plots of these flexibilities are presented in appendix I.

Large differences in predicted flexibility between different publications are observed. Nevertheless the difference between the flexibility of a Y- and a K-joint is small. The figures show that the flexibility decreases when  $\beta$  increases. The flexibility increases when  $\gamma$  increases, flexibility increases when  $\theta$  increases and  $\tau$  does not have a large influence according to most parametric equations.

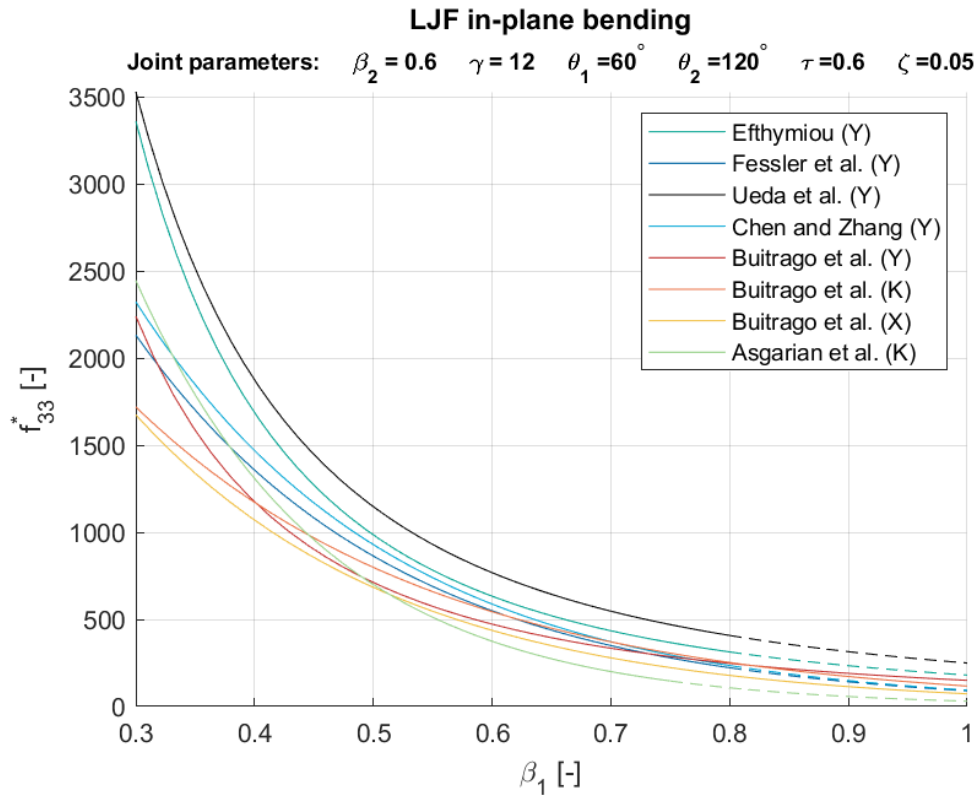


Figure 2.7: The influence of  $\beta_1$  on the dimensionless in-plane bending flexibility.

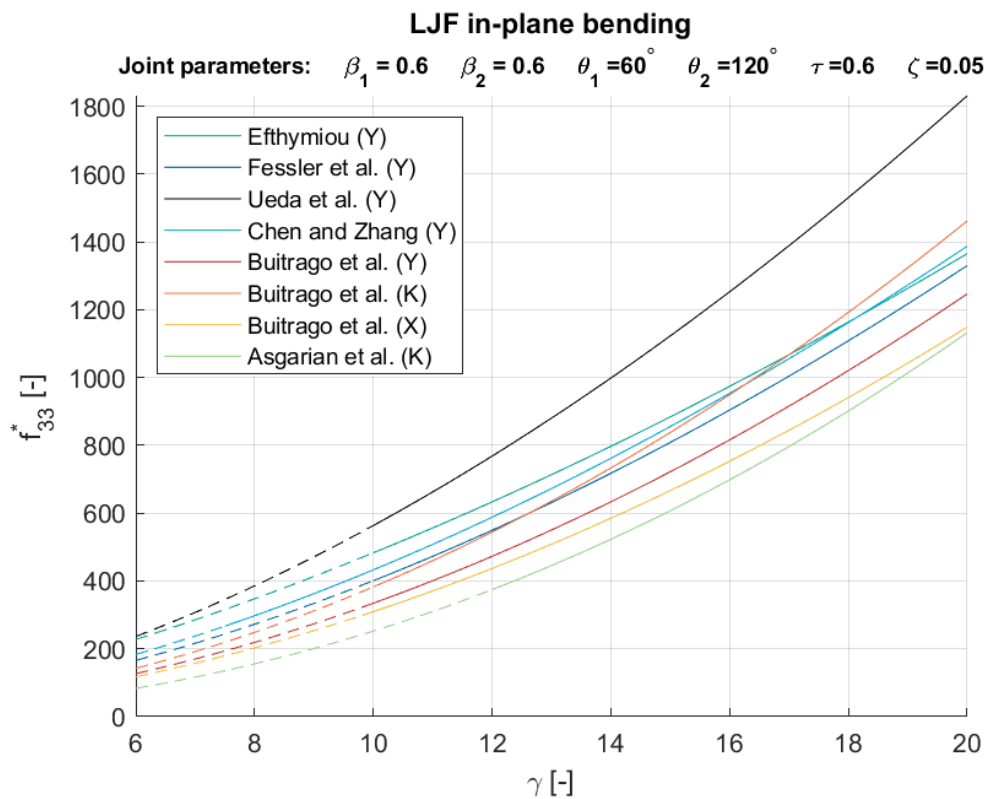


Figure 2.8: The influence of  $\gamma$  on the dimensionless in-plane bending flexibility.

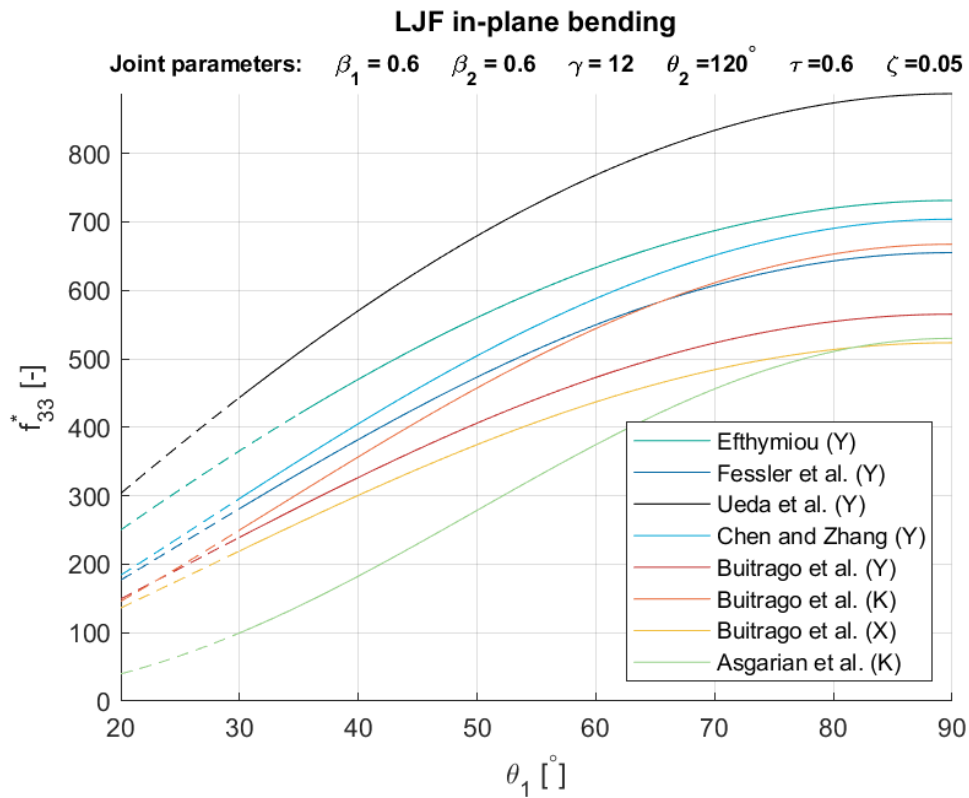


Figure 2.9: The influence of  $\theta_1$  on the dimensionless in-plane bending flexibility.

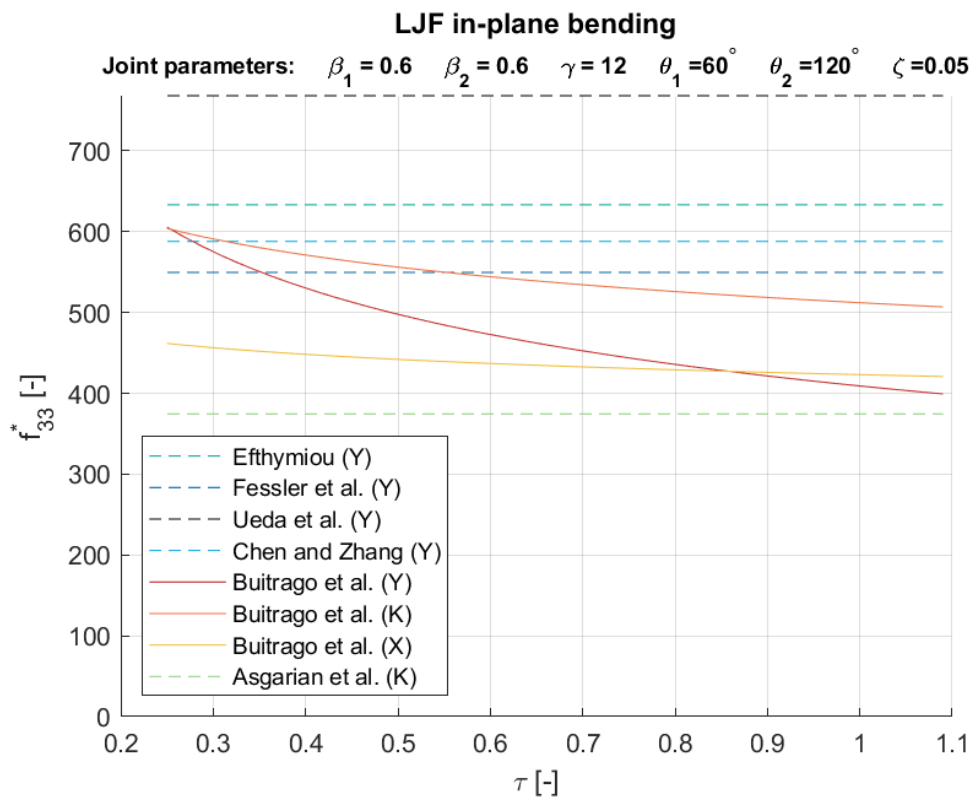


Figure 2.10: The influence of  $\tau$  on the dimensionless in-plane bending flexibility.

Table 2.3: List of publications of parametric equations

Publication	Joint classification	Flexibilities	Variables	Method of retrieval
Ahmadi and Nejad [3] [4] [5]	DK-joint	$f_{11}^*, f_{22}^*, f_{33}^*$	$\beta, \gamma, \theta, \tau$	FEA
Asgarian et al. [11]	YT/K-joint	$f_{11}^*, f_{22}^*, f_{33}^*$ $f_{14}^*, f_{25}^*, f_{36}^*$	$\beta_1, \beta_2, \gamma,$ $\theta_1, \theta_2, z$	FEA
Buitrago et al. [13]	Y/K/X-joint	$f_{11}^*, f_{22}^*, f_{33}^*$ $f_{14}^*, f_{25}^*, f_{36}^*$	$\beta, \gamma, \theta_1,$ $\theta_2, \tau, z$	FEA
Chen and Zhang [17]	Y/K-joint	$f_{11}^*, f_{33}^*$	$\beta, \gamma, \theta$	FEA
DNV [21] as cited in [17]	T-joint	$f_{22}^*, f_{33}^*$	$\beta, \gamma$	-
Efthymiou [24] as cited in [31]	Y-joint	$f_{22}^*, f_{33}^*$	$\beta, \gamma, \theta$	-
Fessler et al. [29] as cited in [17]	Y-joint	$f_{11}^*, f_{33}^*$	$\beta, \gamma, \theta$	Physical measurements
Fessler et al. [31]	Y-joint	$f_{11}^*, f_{22}^*, f_{33}^*$	$\beta, \gamma, \theta$	Physical measurements
Fessler et al. [30]	Y/TY/K/X-joints with brace under out-of-plane angle 0°, 90°, 180° and 270°	$f_{41}^*, f_{42}^*, f_{43}^*$ $f_{51}^*, f_{52}^*, f_{53}^*$ $f_{61}^*, f_{62}^*, f_{63}^*$	$\beta, \gamma, \theta$	Physical measurements
Hoshyari [38]	T-joint	$f_{11}^*, f_{22}^*, f_{33}^*$	$\beta, \gamma, \theta, \tau$	FEA
Khan et al. [44]	K-joint	$f_{11}^*, f_{22}^*, f_{33}^*$ $f_{52}^*, f_{63}^*$	$\beta, \gamma, \theta$	FEA
Ueda et al. [54]	Y/TY/K-joint	$f_{11}^*, f_{33}^*$	$\beta, \gamma, \theta$	FEA

## 2.4. Modelling of LJF

After the flexibility of a joint is determined, it is modelled in the beam model. This section discusses the methodologies published in literature. The concept behind modelling LJF is for all methods equal. The part of the brace element located within the chord surface, also referred to as brace extension element, is replaced by for another 2-node element (figure 2.11). One node is located on the outer chord wall, the second node in the extended of the brace tube at the intersection with the chord center. The length of the element is calculated with:

$$l_e = \frac{D}{2 \sin \theta} \quad (2.25)$$

The element receives the properties of the local joint flexibility's. Three methods are discussed in literature to represent the element: a spring element, a customized beam element and a global stiffness matrix (figure 2.12).

### 2.4.1. Spring element

With a spring element the stiffness between two nodes is added for translational or rotational DOF (figure 2.12 left). Implementation via a spring element is the most straightforward method to model LJF. Three springs can represent the axial, in-plane and out-of-plane flexibilities, where the stiffness constant  $k$  of each spring, is represented by the inverse of  $f_{11}, f_{22}, f_{33}$ . This methodology does not allow to model flexibilities between different DOF unit-load and deformation. Thus, it is not possible to model off-diagonal flexibilities and flexibilities between adjacent braces. Furthermore, unintentionally small deformations in the direction parallel to the chord are still included for joints with  $\theta \neq 90^\circ$ . This deviation is discussed further in sub-section 2.5.

### 2.4.2. Customized beam element

Because a spring element cannot always be implemented in FEA software, Buitrago et al. [13] propose application of a customized beam element with a geometry which possesses the computed LJF flexibil-

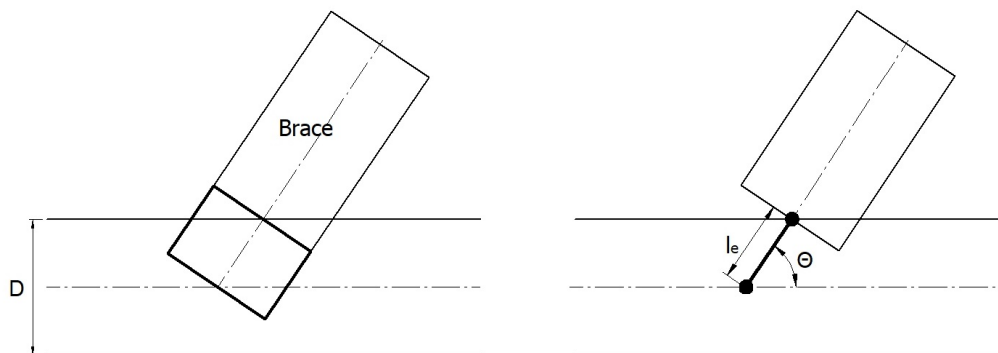


Figure 2.11: Schematic representation of the brace extension element (left) and the replaced LJF element (right)

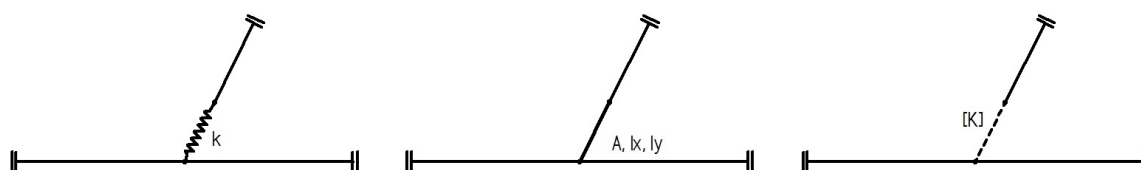


Figure 2.12: Different methods of modelling LJF of a single-brace joint. From left to right: spring element, customized beam element, global stiffness matrix

ities (figure 2.12 middle). In literature, this element is also referred to as 'flex element'. The flexibilities are represented by the cross-surface area (axial DOF) and the second moment of inertia (out-of-plane and in-plane DOF). The flexibilities of the element are calculated with:

$$A = \frac{l_e}{E * f_{11}} \quad (2.26)$$

$$I_{opb} = \frac{l_e}{E * f_{22}} \quad (2.27)$$

$$I_{ipb} = \frac{l_e}{E * f_{33}} \quad (2.28)$$

The customized beam element has the same properties as the spring element. It is unable to model off-diagonal flexibilities and unintended flexibility in the direction of the chord wall is modelled for joints with  $\theta \neq 90^\circ$ . According to Buitrago et al. [13], as the length of the element becomes shorter, the contribution of shear to the end rotations becomes negligible.

The method with the customized beam element is applied in the research of MSL [45]. The approach is recommended by ISO [42] and DNV-GL [20].

### 2.4.3. Global stiffness matrix

A beam model is a method to pre- and post- process a FEA. By generation of a beam element in the pre-processor, stiffness properties are calculated by the pre-processor and inserted into the global stiffness matrix. The global stiffness matrix, with applied loads and displacements is solved by the FEA solver, following:

$$[K] \underline{u} = \underline{P} \quad (2.29)$$

Alanjari et al. [6] [7], Golafshani et al. [36], Asgarian et al. [10] and Chen and Zhang [17] apply a method where a three-dimensional element is created, of which the stiffness matrix in the global coordinate system shall be defined (figure 2.12 right). With this method, stiffnesses in the global stiffness matrix are not calculated by the pre-processor, but inserted manually into the FEA solver.

Flexibilities are applied between two nodes. A single node possesses six DOF [tx, ty, tz, rx, ry, rz] thus the stiffness matrix of an element with two nodes is a 12 x 12 matrix. The matrix contains six DOF describing the flexibilities (between both nodes) and six DOF describing the rigid body moves (of both nodes). The stiffness matrix of the LJF element, is built out of four sub-matrices:

$$\begin{bmatrix} [F]^{-1} & [S] [F]^{-1} \\ [S] [F]^{-1} & [S] [F]^{-1} [S]^T \end{bmatrix} \begin{bmatrix} \underline{\Delta}_F \\ \underline{\Delta}_C \end{bmatrix} = \begin{bmatrix} \underline{P}_F \\ \underline{P}_C \end{bmatrix} \quad (2.30)$$

In here, subscript  $F$  represents the free DOF and subscript  $C$  the constrained DOF. Matrix  $[F]$  is the flexibility matrix which contains the flexibilities. The matrix describes the relation between the free deformations in 6 DOF [tx, ty, tz, rx, ry, rz] as effect of 6 unit-loads [Fx, Fy, Fz, Mx, My, Mz]. The other three sub-matrices are used to define the rigid body moves of the element. Those are calculated with transformation matrix  $[S]$  which connects basic and initial DOF. Matrix  $[S]$  is obtained by the method of unit-load application. In this method, unit-loads in all DOF are applied on one element end, while the corresponding reactions for static equilibrium are evaluated. The six different unit-loads and their reaction forces are shown in figure 2.13.

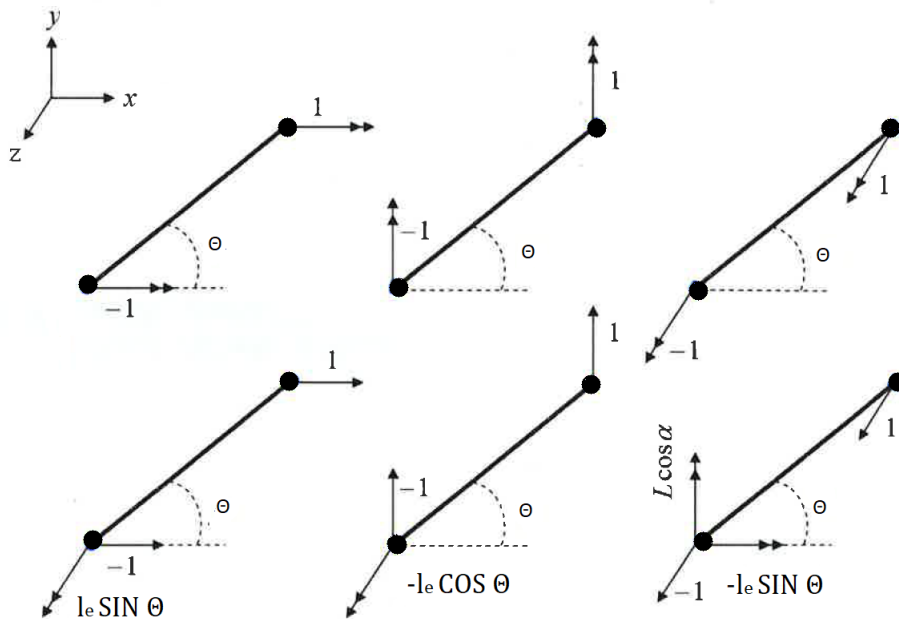


Figure 2.13: Six unit-loads with corresponding reaction forces for the determination of the transformation matrix [6]

$$[\mathbf{S}] = \begin{bmatrix} 1 & & & & & \\ & 1 & & & & \\ & & 1 & & & \\ & & -L \sin \theta & 1 & & \\ & & L \cos \theta & & 1 & \\ L \sin \theta & -L \cos \theta & & & & 1 \end{bmatrix} \quad (2.31)$$

Local flexibility matrix  $F$  contains the flexibilities of the element. The published articles focus on modelling the flexibilities on the diagonal flexibilities of matrix  $[\mathbf{LJF}]$  ( $f_{11}, f_{22}, f_{33}$ ).

The local flexibility matrix is defined in the local chord coordinate system (figure 2.16b). However, local joint flexibilities are defined in the local brace coordinate system (figure 2.16a). Therefore, the axial and out-of-plane flexibilities are transformed from local brace to local chord coordinate system. The transformation from local brace, to local chord coordinate system is an in-plane transformation, thus in-plane flexibility is not affected. Both coordinate systems are defined in appendix C. The differences between both coordinate systems are discussed in sub-section 2.5. The transformation is discussed in detail in sub-section 5.2.2. The local flexibility matrix  $F$  is given by [6]<sup>1</sup>:

$$[\mathbf{F}] = \begin{bmatrix} 0 & & & & & \\ & \frac{f_{11}}{\sin^2 \theta} & & & & \\ & & 0 & & & \\ & & & f_{33} & & \\ & & & & 0 & \\ & & & & & \frac{f_{22}}{\sin^2 \theta} \end{bmatrix} \quad (2.32)$$

The constructed stiffness matrix is defined in the local joint coordinate system (for a single brace joint, the local joint coordinate system is equal to local chord coordinate system). Because the stiffness matrix is inserted in the global stiffness matrix which is defined in the global coordinate system, the stiffness matrix with LJF flexibilities shall be rotated towards the global coordinate system. The rotation is performed with rotation matrix  $[\mathbf{R}^{local \rightarrow global}]$ . Application of rotation matrices is discussed in detail by Greenwood [37]. The rotation follows:

$$[\mathbf{K}_{global}] = [\mathbf{R}^{local \rightarrow global}]^T [\mathbf{K}] [\mathbf{R}^{local \rightarrow global}] \quad (2.33)$$

Alanjari et al. [6] [7], Golafshani et al. [36] and Asgarian et al. [10] [11] implemented this method in FEA program OpenSees. Comparable methods applying this methodology are discussed by Ueda et al. [54], Hu et al. [40] and Chen and Zhang [18]. Although not applied in their publications, this method would be suitable for modelling off-diagonal flexibilities.

#### 2.4.4. Expansion of methodologies to multi-brace elements

Foregoing mentioned methods are used to model the interaction between brace and chord. The methodologies can be applied for multi-brace joints, but do not take the reciprocal interaction among adjacent braces into account ( $f_{14}, f_{15}, f_{16}, f_{24}, f_{25}, f_{26}, f_{34}, f_{35}$  and  $f_{36}$ ). Preceding mentioned methods can be expanded to methods suitable for multi-brace joints. However, the number of publications considering the interaction among braces is low. Ueda et al. [54] proposes to create an extra customized beam element between two braces to simulate the interaction (figure 2.14 middle). However, Ueda et

<sup>1</sup>Orientation of axis [xyz] is rewritten to authors notation

al. [54] find the bending stiffness of the interaction element is so small compared to the bending stiffness of the joint elements and therefore concludes the interaction is not represented well in the model. Hu et al. [40], Chen and Zhang [18] and Alanjari et al. [7] create a stiffness matrix for an element with three nodes (figure 2.14 right). One node is connected to the chord the other two nodes each to a brace. The global stiffness matrix of the new element is determined in similar method as previously presented. No literature investigating a multi-brace model with multiple springs is found (figure 2.14left).

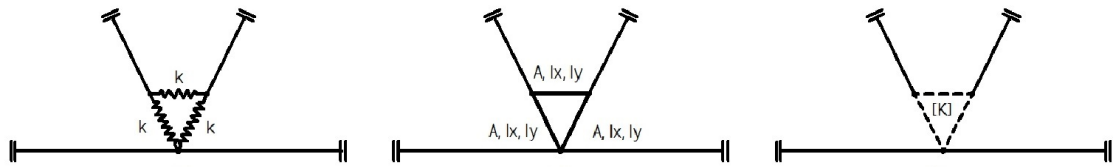


Figure 2.14: Different methods of modelling LJF of a multi-brace joint. From left to right: spring element, customized beam element, global stiffness matrix

## 2.5. Definition of orientation of flexibilities

A contradictory definition of the coordinate systems in which the flexibilities are defined is observed in literature. In the definition of LJF, deformations are assumed to appear due to bending of the chord wall. In the direction parallel to the chord wall, the joint is subjected to shear loads and it is assumed the deformation is negligible. This theorem is substantiated with figure 2.15, which shows the deformations of an Y-joint as effect of an axial force. The deformations appear perpendicular to the chord wall and not in axial direction.

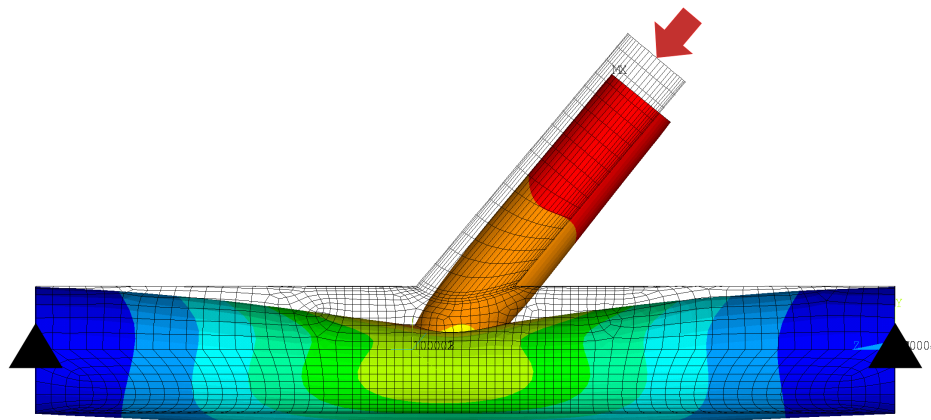
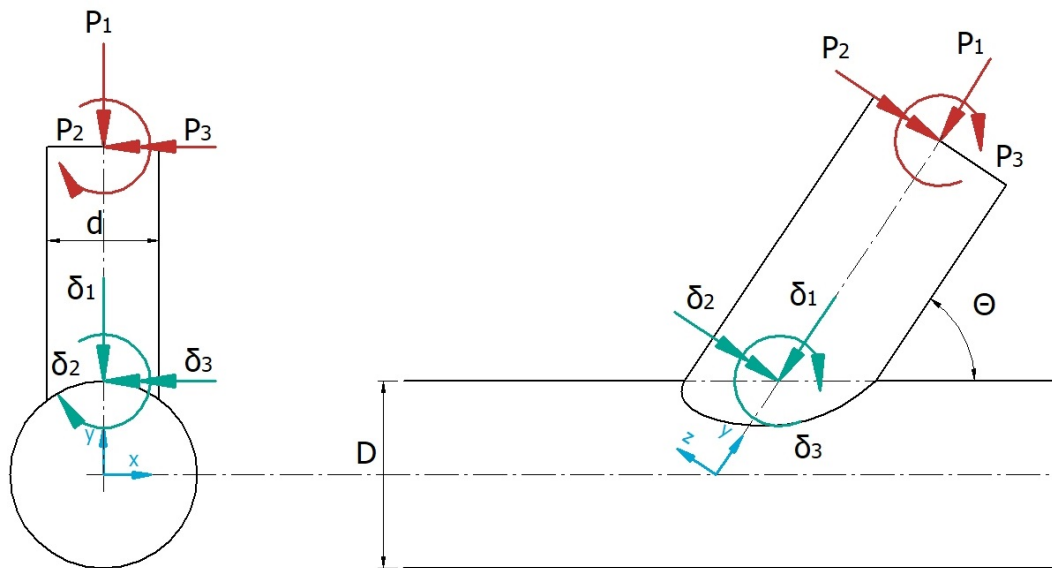


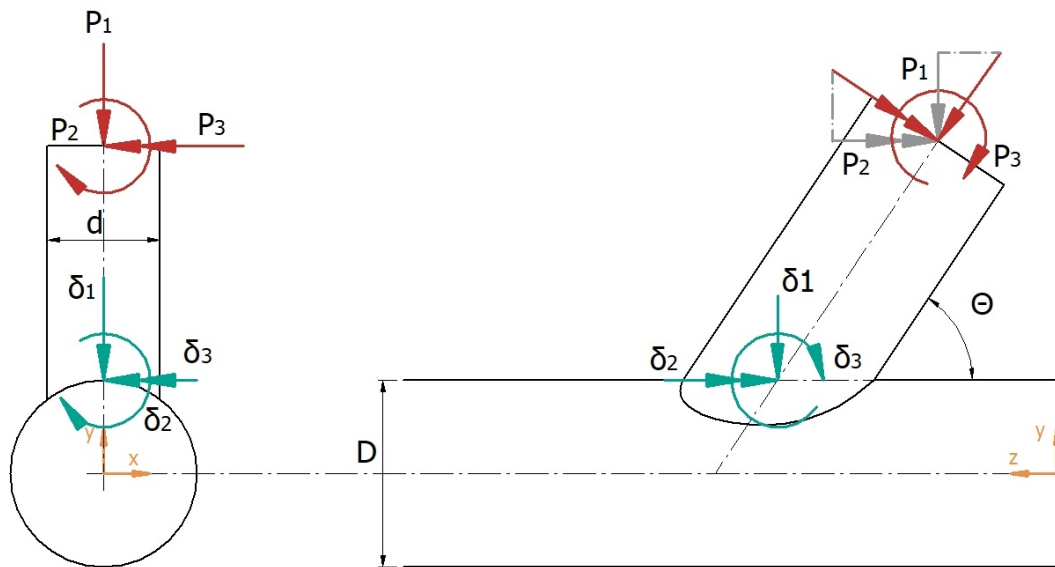
Figure 2.15: Shell model, representing the chord wall deformations as effect of an axial force.

In sub-section 2.2.2, the flexibilities are defined in the local brace coordinate system. This definition is applied by all authors who investigated the determination of LJF in tubular joints (table 2.3) and a part of the authors who developed a method to model LJF. The definition of the flexibilities in a brace oriented coordinate system allows deformation in the axial direction (figure 2.16a). Thereby, deformation in the direction parallel to the chord wall is allowed for joints with  $\theta \neq 90^\circ$ .

The correct definition of the deformations is, in whats referred to as the 'local chord coordinate system', which is aligned with the chord wall. The orientation of the local chord oriented coordinate system is shown in figure 2.16b. The approach is applied by [6] [7] [10] [11] [36]. The deformations are the effect of member-loads in the brace oriented coordinate system, but only the vector aligned with the chord oriented coordinate system contributes to the deformations.



(a) The flexibilities of a single-brace joint defined in the local brace coordinate system



(b) The flexibilities of a single-brace joint defined in the local chord coordinate system

Figure 2.16: Comparison of the flexibilities of a single-brace joint, defined in different coordinate systems

The local chord coordinate system is described in appendix C.3. The transformation from local brace to local chord coordinate system is described in appendix 5.2.2.

The difference in definition is expected to be related to the methodology applied to model LJF in the beam model. When modelling LJF in a beam model with a spring or customized beam element, only three flexibilities can be modelled (sub-section 2.4.1 and 2.4.2). Flexibilities are aligned with the element and therefore, application via the brace oriented coordinate system is the only possibility. Modelling LJF with a stiffness matrix, allows to model the flexibility in any DOF, independent of the orientation. Thereby, flexibilities defined in a chord oriented coordinate can be modelled. As a result, modelling LJF via a stiffness matrix is more accurate. The magnitude of the deviations and the influence on the final predicted fatigue assessment are unknown. This could be a topic for further research.

## 2.6. Conclusion

LJF is defined as the flexibility through local chord wall deformation as effect of a load on the brace. A single-brace tubular joint possesses three considerable DOF flexibilities: axial, out-of-plane bending and in-plane bending flexibility. In other degrees the chord is subjected to shear loads for which the flexibility is assumed to be zero. Until initial yielding joints show linear elastic behaviour. Plasticity is not considered, hence the flexibility can be defined with a constant value.

The flexibilities of a single-brace joint are defined in flexibility matrix  $[LJF]$  which gives the relation between deformations in three DOF as effect of unit-loads in the same three DOF, resulting in a 3x3 matrix. The matrix is symmetrical and off-diagonal terms are small. For multi-brace joints, the matrix is expanded, defining the flexibility of both braces, and additionally the relation between deformations of one brace as effect of a load on a adjacent brace.

Three methods to determine the LJF of a tubular joint are discussed in literature: physical experiments, Finite Element Analysis and parametric equations. Three methods to model the LJF in a beam model are discussed in literature: a spring element, a customized beam element, and via a global stiffness matrix. The global stiffness matrix represents the flexibilities more accurate because these can be defined in the local chord coordinate system. In the next chapter, the most suitable methodology for this project is discussed.

# 3

## Determination of methodology

### 3.1. Introduction

In the previous chapter three methods to determine the flexibilities of a joint and three methods to model the flexibilities in a beam member model are presented. In this chapter, the most suitable method for application within this project is determined. In section 3.2, the joints present in the stinger are discussed. In section 3.3, the decision making for the most suitable methodology for application within this project is discussed. The conclusion is discussed in section 3.4. Thereby, the sub-question: “What are the most suitable methodologies, to determine and model Local Joint Flexibility in a beam model, in order to determine its influence?” is answered.

### 3.2. Specification of joints in a stinger

The research is applied and limited to Solitaire stinger section 1. The full stinger of Solitaire consist out of three parts. Section 1 is the frame on the ship side, highlighted in red in figure 3.1. Section 1 is the newest stinger section and representative for the stingers utilized within Allseas. Other than most stingers, section 1 contains mostly tubular joints without reinforcements making it suitable for this study.

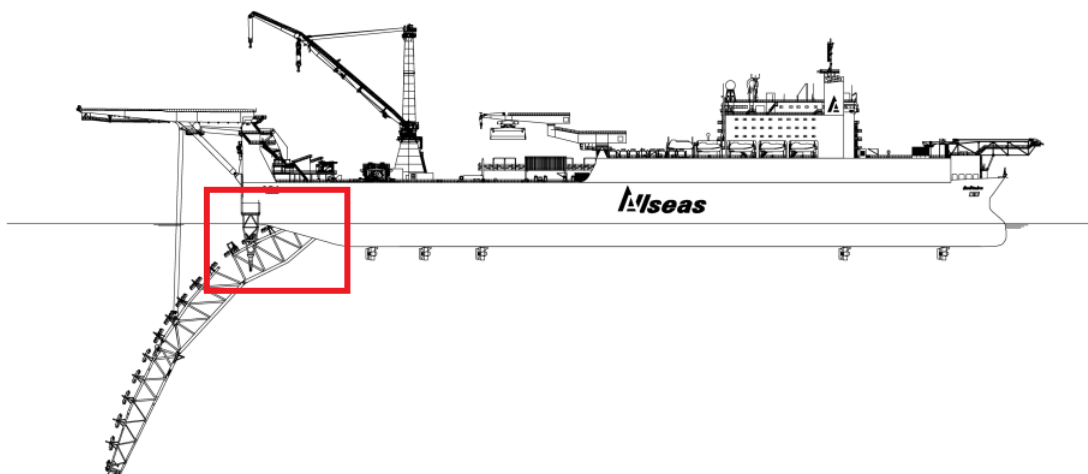


Figure 3.1: The Solitaire with highlighted stinger section 1

A detailed image of the stinger section is shown in confidential appendix O.1. The stinger section contains a total of 67 tubular joints, with 152 braces. A large part of the joints are multi-brace joints, with

up to six braces, in up to three different planes. Almost every joint has different geometric parameters. The joints are grouped into four categories with comparable geometric parameters. The categories are discussed below. The geometric parameters of the categories can be found in confidential appendix O.2.

**Category 1: Main-joints** The main joints are located on the four main chords of the stinger. The joints connect the four main chords directly to each other, creating the main structure. Stinger section 1 has a total of 22 main joints. Most of the joints are multi-brace joints with up to six braces in multiple planes. Furthermore, low values for  $\gamma$  are observed. No parametric equations are available for direct determination of the LJF of the joints. The gaps between the braces are a minimum of  $0.05m$  for welding. In non-dimensional parameters, equal to  $\zeta \approx 0.05$

**Category 2: Cross-joints** The cross joints are classified as X-joints and have two braces under equal angle in the same plane. The joints have geometric parameter  $\beta = 1$ . In the literature review, it is observed that these joints have a extremely low flexibility. No parametric equations for the determination of the joints are present.

**Category 3: Support joints** The support joints are located on the braces of the previously mentioned main joints. The support joints are single-planar Y-, T-, YT- or K-joints. Parametric equations for these classification joints are widely published. However, because of the low  $\gamma$  values of the joints in the stinger, a part of the joints is out of the validated domain of the parametric equations.

**Category 4: Stiffened joints** This category contains all joints which are stiffened with reinforcements. The joints are not discussed further, because they are out of the scope of the project (section 1.6).

### 3.3. Determination of methodologies

In this section, the most suitable method to determine and model LJF for the application within this research is discussed. In sub-section 3.3.1, the approach behind the decision making is discussed. In sub-section 3.3.2, the most suitable methodology to determine the LJF is selected. In sub-section 3.3.3, the most suitable methodology to model the LJF is selected.

#### 3.3.1. Approach

The main objective of the project is the development of a valid method to account for LJF and to determine the magnitude of the influence on the predicted fatigue life. Within the field of determining and modelling LJF there are uncertainties about which factors do have to be taken into account and which ones do not. E.g.: Geometric parameters, flexibilities, interaction with adjacent braces, the coordinate system of definition of LJF. No clear conclusion can be made based on the published literature. To answer the main research question, it is important to decrease the number of uncertainties as much as possible. Simplifications of which the influence is unclear should be avoided. Therefore, the most suitable methodology for application is the most accurate methodology, which can be applied within the timeline of this project.

The most accurate approach it not necessarily be the approach which is the most accessible for implementation. It is possible that with certain allowable simplifications a methodology which is easier to implement can be applied as well to determine and model LJF. The research towards simplifications to improve the ease of application, is considered as a possible follow-up of the project. First it is required to determine the influence of modelling LJF so it can be decided whether modelling LJF is beneficial or not.

#### 3.3.2. Methodology to determine LJF

It is decided to determine the LJF of tubular joints with FEA. In section 3.2 it is shown that the stinger contains many different joint geometries. FEA is able to determine the flexibility of any joint geometry. The accuracy of the parametric equations is unknown, the equations are limited to standard joint

geometries and the equations are not validated for the domain of the geometries of the joints in the stinger. Especially for the main joints in category 1, it is questionable if application of parametric equations is valid. The determination of the flexibility with physical experiments is not considered, because the development of the test setup, and the fact that for every joint geometry a unique test joint is required, does not fit in the timeline of this project. The FEA can be validated with results of experiments by other authors, to secure accurate results.

### 3.3.3. Methodology to model LJF

It is decided to model LJF of tubular joints with a stiffness matrix in the beam model. The stiffness matrix is a general approach wherein it is possible, but not required, to model flexibilities in every DOF. The spring- and customized beam- element are limited to the diagonal terms of the flexibility matrix. Modelling LJF with a stiffness matrix is more accurate because it allows modelling LJF in a chord oriented coordinate system instead of a brace oriented system (section 2.5). Furthermore, it allows to model interaction between adjacent braces, which is though/not possible with the spring- and customized beam- element. The disadvantage of the stiffness matrix is its complexity of implementation. The stiffness matrix is defined in the global coordinate system and several calculations are required before insertion.

## 3.4. Conclusion

The joints in the stinger are categorized into four groups with comparable geometries. It is observed that the majority of the joints in the stinger consists of up to six braces in multiple planes, resulting in a complicated geometry to determine and model LJF. The joints in category 1 are considered as the main joints and are all located on the four chords of the stinger. The cross joints of category 2, have geometric parameter  $\beta = 1$  leading to a very low flexibility. The third category consists of single-plane joints, supporting the main structure. The joints in category 4 are stiffened and therefore out of the scope of the project.

The most suitable methodologies for application are the most accurate methodologies, which can be applied within the timeline of this project. The most accurate approach is not necessarily be the approach which is the most accessible for implementation. A study towards simplifications to improve the ease of application, is considered as a possible sequel of the project. It is decided to determine the LJF of tubular joints with FEA. It is decided to model LJF of tubular joints with a stiffness matrix in the beam model. Both methods are the most flexible and accurate methodology, but lack in ease of implementation, if not automated.



# 4

## Development of method to determine the LJF of tubular joints

### 4.1. Introduction

In the previous chapter, it is decided to determine the LJF of tubular joints with FEA. In this chapter is elaborated on how this methodology is applied. The determination of the LJF of a tubular joint is a complex procedure, thus it is decided to start with the development, verification and validation of a numerical model for single-brace joints. Thereafter, the numerical model is expanded to a model for multi-brace, multi-planar joints. Because the multi-brace model is an expansion of the single-brace model, a large part performs equally, hence only adaptations towards a multi-brace model are discussed.

The methodology of the model which determines the LJF of single-brace tubular joints is explained in section 4.2. In section 4.3, the results of the single-brace numerical model are verified and in section 4.4, the results of the single-brace numerical model are validated by comparing the results to results of published physical experiments. In section 4.5, the expansion to a multi-brace model is discussed. In section 4.6, the multi-brace numerical model is verified and in section 4.7, the validation of the multi-brace numerical model is discussed. The conclusion is provided in section 4.8. Thereby the sub-question: “How can the local joint flexibility of joints in a stinger be determined, and with what accuracy? How can this method be verified and validated?” is answered.

### 4.2. Methodology single-brace numerical model

In this section the methodology applied to determine the LJF of single-brace joints is discussed. The construction of a FEA model, performance of the analysis and calculation of the LJF of a tubular joint is a time consuming task. For single-brace joints this approach is doable, but keeping in mind the expansion towards multi-brace joints, it is decided to develop a code to automate the procedure. The FEA is performed in ANSYS APDL (ANSYS Parametric Design Language) because of its suitability for parametric design and automation of design tasks. Around the FEA a code is written in MATLAB to direct ANSYS APDL and calculate the LJF. The input of the code are the geometric and material properties of the joint. The output is the LJF matrix. In sub-section 4.2.1, a general overview of the numerical model is provided. In the following sub-sections, specific parts of the numerical model are discussed in detail.

#### 4.2.1. General model overview

A schematic overview of the numerical model is given in figure 4.1. The inputs of the model are the geometric properties of the joint  $\beta$ ,  $\gamma$ ,  $\theta$ ,  $\tau$ , chord diameter  $D$  and the material properties, described with Young's modulus  $E$  and Poisson's ratio  $\nu$ . Geometric parameters  $\alpha$  and  $\alpha_b$  do not influence the LJF and thus are not required as input. The output of the model is flexibility matrix  $[LJF]$ . In the literature

review in chapter 2, it is found that a single-brace joint can deform in three DOF as effect of three DOF loads. Therefore flexibility matrix [**LJF**] has dimensions 3x3. Three deformations notated with  $\delta_i$  and three unit-loads notated with  $P_j$  are defined:

- $\delta_1$  = axial deformation [m]
- $\delta_2$  = out-of-plane bending deformation [rad]
- $\delta_3$  = in-plane bending deformation [rad]
- $P_1$  = axial force [N]
- $P_2$  = out-of-plane bending moment [Nm]
- $P_3$  = in-plane bending moment [Nm]

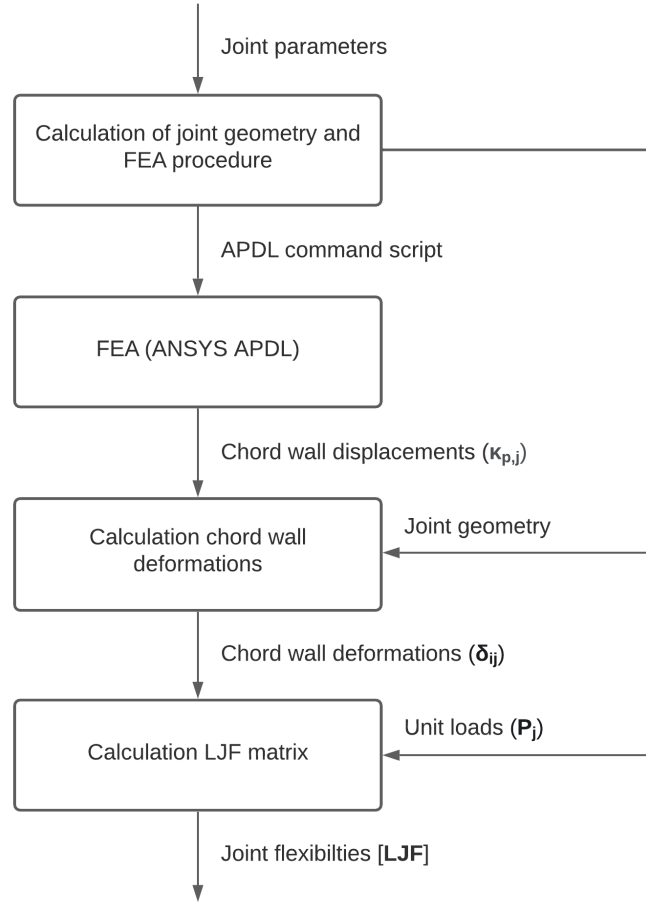


Figure 4.1: Schematic presentation of the numerical model.

The LJF matrix is defined in the local coordinate system of the brace. The flexibility matrix of a single-brace joint is defined as:

$$\begin{bmatrix} \delta_{11} & \delta_{12} & \delta_{13} \\ \delta_{21} & \delta_{22} & \delta_{23} \\ \delta_{31} & \delta_{32} & \delta_{33} \end{bmatrix} \begin{bmatrix} \frac{1}{P_1} \\ \frac{1}{P_2} \\ \frac{1}{P_3} \end{bmatrix} = \begin{bmatrix} f_{11} & f_{12} & f_{13} \\ f_{21} & f_{22} & f_{23} \\ f_{31} & f_{32} & f_{33} \end{bmatrix} \quad (4.1)$$

Deformations and unit-loads are determined/applied in the local brace coordinate system, as schematically presented in figure 4.2. In section 2.5, it is discussed that the definition of flexibilities in the local

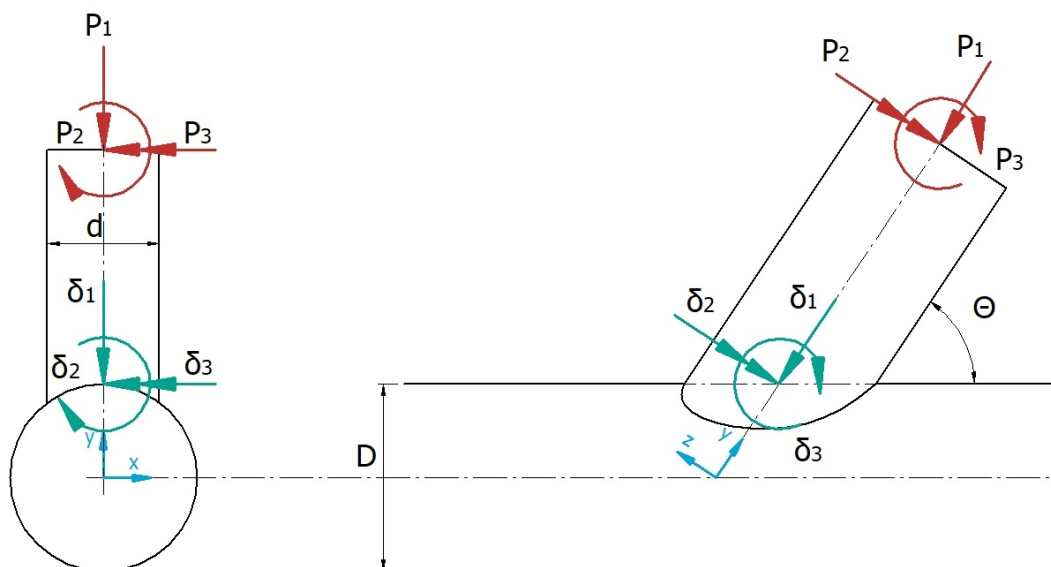


Figure 4.2: The flexibilities of a single-brace joint defined in the local brace coordinate system

brace coordinates system is not correct. However, this definition is followed in accordance to the definition applied by other publications[13] [24] [31] [53] [54], so the results of the numerical model can be compared in the verification and validation of the numerical model. In chapter 5, where the flexibilities are modelled in a beam model, the flexibilities are transformed to the local chord coordinate system whereby deviations are excluded.

The numerical model consists out of four steps (figure 4.1). The first step is the preparation of the FEA. Based on the input, the code creates a command script for APDL. Within this step the complete procedure of the FEA is generated. The output of this step is a command script for ANSYS APDL. The code is presented in appendix Q. The code itself is not discussed further, because of its complexity and explanation does not contribute to the research question. However, an overview of the APDL command language is provided by ANSYS [8]. The second step is the FEA. This step is performed in APDL. In APDL the joint is constructed and meshed, unit-loads and constraints are applied, the model is solved for every load-case  $P_j$  and chord wall displacements  $\kappa_{p,j}$  as effect of every load case are measured and saved. The FEA is discussed in detail in section 4.2.2. In the third step, chord wall deformations  $\delta_{ij}$  are computed. Deformations are computed based on the chord wall displacements  $\kappa_{p,j}$ . Out of every set of chord wall displacements as effect of unit-load  $P_j$ , the deformations in every DOF  $\delta_{ij}$  as effect of the load-case  $j$  are computed. The output of step three is the deformation matrix  $[\Delta]$ , containing the deformations as results of the unit-loads. The calculation of the chord wall deformations is discussed in detail in section 4.2.3. In the fourth step, the dimensional and non-dimensional LJF is computed. The LJF matrix defined in the local brace coordinate system is the output of the numerical model. The calculation of the LJF matrix is discussed in detail in section 4.2.4.

The compatible domain of the geometries of which the numerical model is able to calculate the flexibility, is taken as large as possible, taking into consideration the typical joint geometries of the stinger, determined in section 3.2. The numerical model is compatible for single-brace joints within the following geometric domain:

$$\begin{aligned}
 0 < D &\rightarrow \infty \\
 0.3 &\leq \beta \leq 0.9 \\
 7.5 &\leq \gamma \leq 40 \\
 26^\circ &\leq \theta \leq 154^\circ \\
 0.20 &\leq \tau \leq 1.0
 \end{aligned}$$

The joints in the stinger are multi-brace joints thus the model is unable to determine the flexibilities for the joints. However, several authors [13], [45] and [54] simplify their models and treat multi-brace joints as single-brace joints. With this simplification the numerical model is able to calculate the flexibilities for the main joints in *category 1*. The model is not able to calculate the flexibilities for joints with  $\beta = 1$ , due to limitations of the geometry in the FEA. Thus, the cross joints in *category 2* cannot be modelled. However, in section 4.4.2 it can be seen that the flexibility in a joint without LJF is comparable to the flexibility of a joint with LJF for joints with high  $\beta$  values. It is expected, that not modelling LJF in the X-joint, does not lead to large deviations. The flexibility of every joint in *category 3* with  $\beta \neq 1$  can be determined.

#### 4.2.2. FEA

In this section, the specification of the FEA is discussed. In the following sub-sub-section, there is elaborated on: the element type, the element location and offset, modelling of welds, the mesh, application of unit-loads, application of constraints, the material properties, the applied analysis and solver and the output data.

##### Element type

The model uses 8-noded shell elements (figure 4.3), also referred to as ANSYS SHELL281 elements [9]. Shell elements are suitable for thin to moderately-thick shell structures [9]. Four nodes are located on the corners and four nodes on the mid-sides. An 8-noded shell element is selected because it provides a higher accuracy than 4-noded shell elements. The nodes have six DOF: three translations over the x-, y- and z-axis, and three rotations around the x-, y- and z-axis.

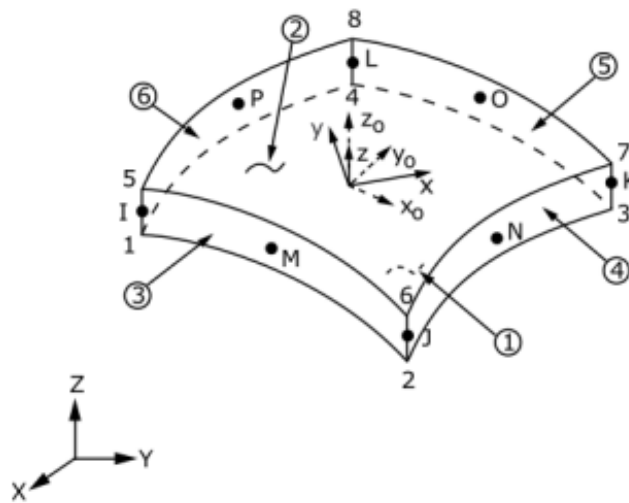


Figure 4.3: SHELL281 element (ANSYS) [9].

Shell elements are preferred over solid elements. Although solid elements are more accurate in a fully refined mesh, large calculation times are induced. In less refined meshes, solid elements have the risk of locking. Locking refers to excessive stiffness in a certain deformation mode, caused by the inability of solid elements to exhibit pure bending. With a lower number of elements, a model built of shell elements is more accurate. Elements are preferred to have a squared or tetragonal shape, above triangular or hexagonal because a higher accuracy is obtained. Due to the complex geometry of a tubular joint it is difficult to create a satisfactory mesh. Because shell elements are 2-dimensional, instead of 3-dimensional solid elements, shell elements are less demanding to generate a squared elements.

A 2x2x3 integration scheme is applied. This is the most suitable integration scheme according to

Romeijn [48]. Furthermore, no considerable difference in results with a 2x2x5 scheme is noticed (Appendix D).

#### Element location and offset

In the conventional method of modelling, the nodes of a shell elements are located at the mid-surface of a geometry, in case of a tubular joint on  $D - T$  and  $d - t$  (figure 4.4 blue). The area of the footprint of the brace is then  $\approx 0.5 * \pi(d - t)^2$ . However, the actual area of the footprint is  $\approx 0.5 * \pi(d)^2$ . Thereby the footprint of the brace on the chord wall is underestimated in the conventional method of modelling. As a results of the smaller area, deformations as effect of the unit-load are larger and the flexibility of the local chord wall is overestimated. For normal thin-walled shell structures this deviation is negligible but in section 3.2 it is found that especially joints in the stinger obtain thick walls (low  $\gamma$ ).

To avoid underestimation of the footprint area of the brace on the chord, the elements in the numerical model are located on the outer diameter of the geometry  $D$  and  $d$  also referred to as top-surface (figure 4.4 red). The element offset is adapted to the plane where the element is modelled to maintain (virtually) an equal joint geometry. In the validation in section 4.4, the results of the numerical model are compared with the results of a model with elements on the mid-surface. It is shown that the model with elements on the top-surface, determines the flexibilities of single-brace joints more accurately than the model with elements on the mid-surface.

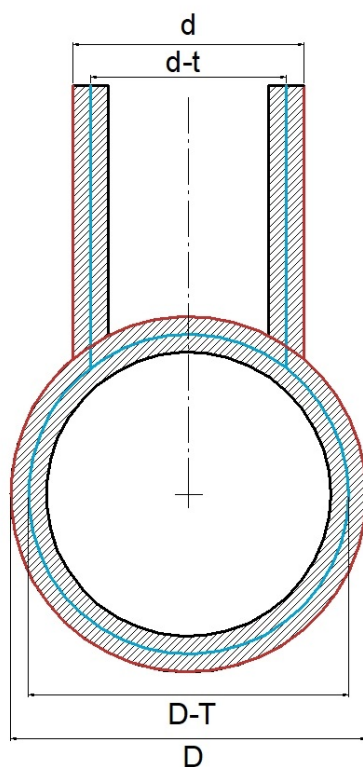


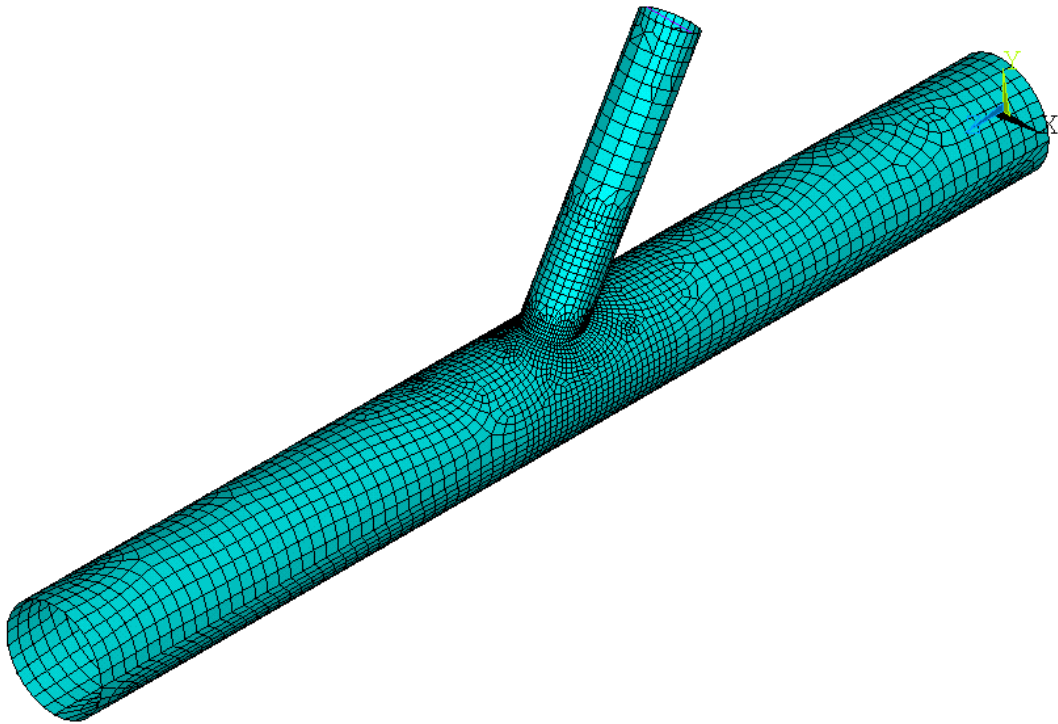
Figure 4.4: Schematic presentation of the location of the elements for mid-surface model (blue) and top-surface model (red).

#### Weld

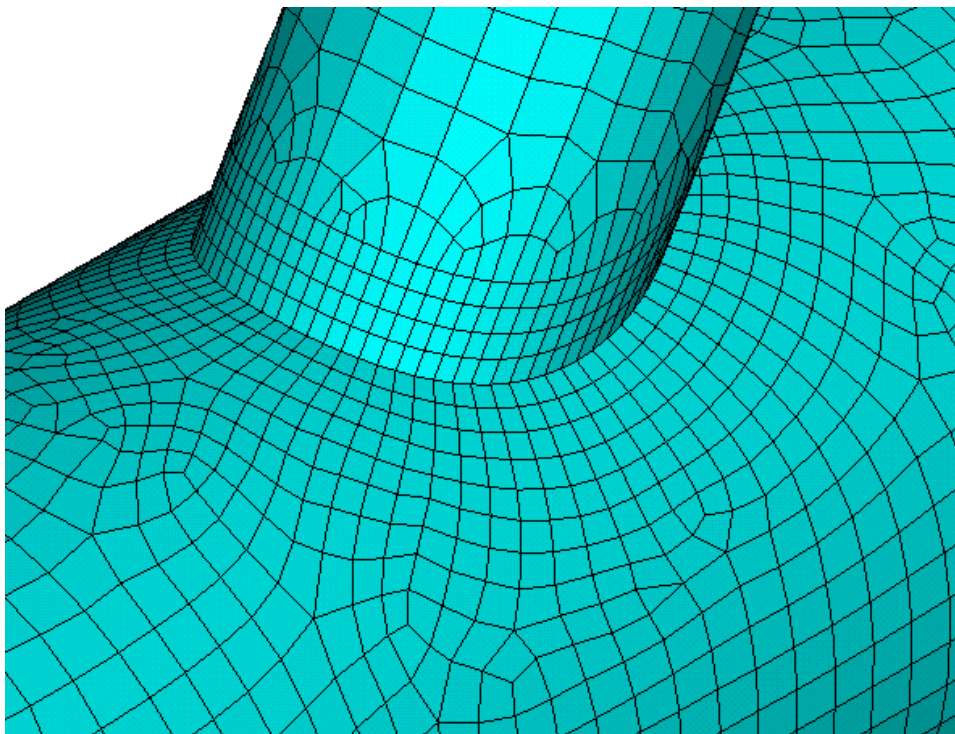
Weld are not taken into account in the FEA. This is a standard approach for models with shell elements. Although uncommon, an approach to model welds in a shell model is published by van der Vegte et al. [56]. For the scope of this project their approach is too complex. However, the addition of welds to the model could be investigated for future improvement of the model.

#### Mesh

The geometry of the joint is discretized into a mathematical model, through meshing. The mesh quality determines the accuracy of the results thus special attention is paid to the generation of a suitable



(a) General mesh



(b) The mesh around the chord/brace intersection

Figure 4.5: Example of the applied mesh in the FEA

mesh. An example of a meshed joint is shown in figure 4.5a. To reduce the amount of elements, three levels of mesh refinement are applied. A coarse mesh is applied at the brace and chord ends. At these points accuracy is not important. Closer to the intersection a finer mesh is applied. On and around the chord and brace intersection the displacements are measured and therefore a fine mesh is applied in this area.

Beside refinement, the shape of the element strongly influences the accuracy. Squared shell elements with a height width ratio of  $\approx 1:1$  supply the most accurate results and are therefore preferred to lay on the surface where chord and brace intersect and displacements are measured. Because two curved surfaces merge at the intersection, it is tough to obtain perfectly square elements in this area. APDL is not able to automatically create a satisfactory mesh and support is required. The chord brace intersection and surrounding contours of elements are constructed following an approach applied by Cao et al. [15] and Ermolaeva et al. [27]. The approach is explained further in appendix B.1. The result is squared elements at the chord/brace intersection. An example of the elements is shown in figure 4.5b.

The element length and width on the surfaces around the intersection is equal to, or smaller than the chord wall thickness  $T$ . Romeijn [48] recommends having a maximum element length of  $1/12$  of the total length around the perimeter of the brace to chord intersection. DNV-GL [23] recommends for FEA elements with dimensions of  $T \times T$  up to  $2T \times 2T$ . Both recommendations are clearly obeyed. The mesh refinement is verified in sub-section 4.3.2.

### Boundary conditions

Unit-loads are applied in the center of the brace end. The nodes at the ends of the brace wall are connected fully rigid to each other. Via a rigid beam element, connected to the nodes on the brace wall, the load is applied. An example is shown in figure 4.6a. The loads are applied in the local coordinate system of the brace, as schematically shown in figure 4.2.

Displacements in six DOF are restricted for the nodes located at both ends of the chord wall. This constraint is also referred to as F/F (fixed/fixed). An example is shown in figure 4.6b. This approach is supported by Romeijn et al. [50]. Numerical tests with other constraints, such as pinned support (P) or roller support (R), did not result into considerable differences. The results of the numerical tests are shown in appendix D.

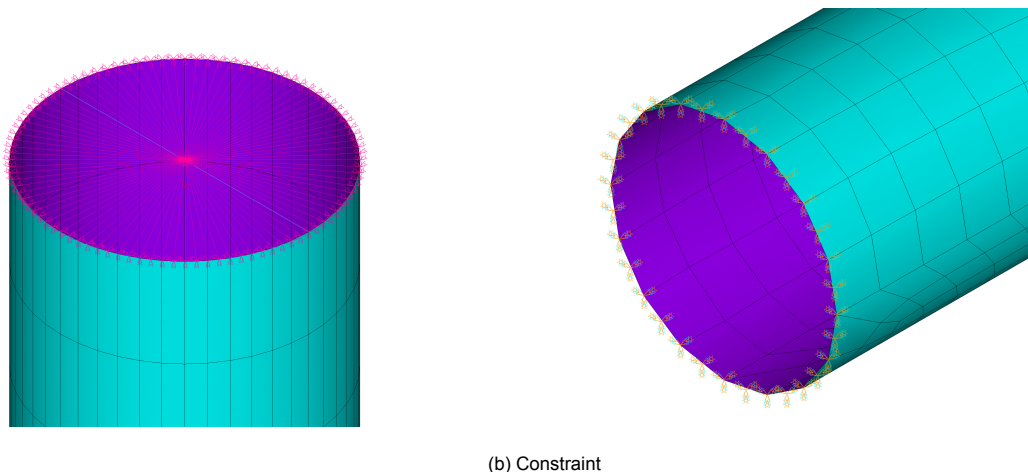


Figure 4.6: Example of the applied boundary conditions

### Material properties

The flexibility of a joint is dependent on the material properties of the joint. Both Young's modulus  $E$  and Poisson's ratio  $\nu$  do affect the flexibility. The relation between Young's modulus and flexibility is linear. This is also observed in the verification in section 4.3. The Young's modulus does not affect the non-dimensional flexibility. Poisson's ratio does affect both dimensional and non-dimensional flexibility. In

the verification of section 4.3 it can be seen it leads to considerable differences. Both material properties are dependent on the joint of consideration and need to be chosen carefully.

### Analysis

The LJF is a linear value hence a static linear analysis is performed. The analysis is solved with the sparse direct equation solver. This solver is recommended by ANSYS for models consisting of shell and/or beam elements [9].

### Output data

The output of the FEA are the chord wall displacements, noted with  $\kappa_{p,j}$ . The chord wall displacements are dependent on the location  $p$  and the unit-load  $P_j$ . The displacements are a nodal solution which means they are retrieved directly from the location of the node. The locations whereat the displacements are measured and in which direction, is discussed in sub-section 4.2.3.

### 4.2.3. Calculation chord wall deformation

In this sub-section, it is discussed how the chord wall deformations  $\delta_{ij}$  are computed out of the chord wall displacements  $\kappa_{p,j}$ . The chord wall deformations  $\delta_{ij}$  are determined in three DOF  $i$  as effect of the unit-load  $P_j$ . The deformations are notated in deformation matrix  $[\Delta]$ . The deformation matrix has an equal layout as the flexibility matrix.

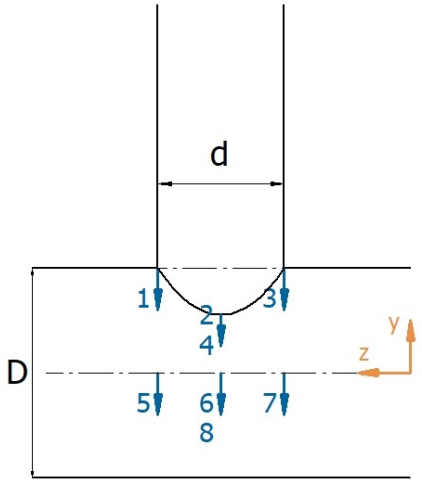
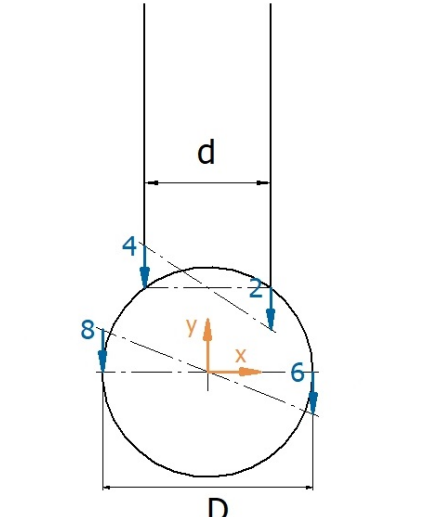
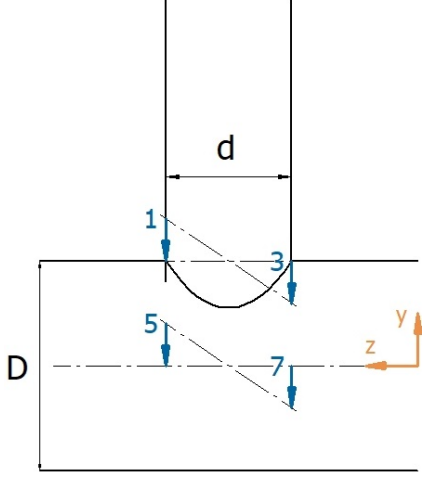
$$[\Delta] = \begin{bmatrix} \delta_{11} & \delta_{12} & \delta_{13} \\ \delta_{21} & \delta_{22} & \delta_{23} \\ \delta_{31} & \delta_{32} & \delta_{33} \end{bmatrix} \quad (4.2)$$

For every load-case  $P_j$  the displacements  $\kappa_{p,j}$  of eight points  $p$  are measured in the FEA. Out of every set of displacements, the deformations in the three DOF  $i$  are computed. The displacements are a nodal solution and therefore, taken from the surface upon which the elements are located. For the numerical model, which has elements on the top-surface, this is on  $D$  and  $d$ . For a model with elements on the mid-surface this would be on  $D - T$  and  $d - t$ . The displacements are measured in the local chord coordinate system, in the direction normal to the chord axis. In figure 4.7 this is the direction of the negative y-axis. In the calculation of the chord wall deformations, a transformation to the local brace coordinate system is made through multiplication with  $\sin \theta$ . In the experiments which are used in the validation [31] an equal approach is applied. In those experiments this method is applied because displacements need to be measured with sensors. Although the FEA can measure displacements in any direction, an equal approach is used, to reduce deviations between experiment and numerical model.

Point 1, 2, 3, and 4 are located on the chord/brace intersection. Point 1 and 3 lay on the crown-toe and crown-heel, point 2 and 4 lay on both saddle points. The chord wall deformations are computed based on the displacement of these four points. However, the displacements in point 1, 2, 3 and 4 include displacements due to 'beam behavior' of the chord. As effect of axial force or in-plane bending moment, the chord bends like a beam and as effect of out-of-plane bending moment, the chord twists. Examples of these displacements are shown in figure 4.8. Point 5, 6, 7 and 8 serve to subtract the displacements due to beam behavior. Point 5, 6, 7 and 8 are located on the chord wall, at center height and do only account for displacements due to bending and torsion of the chord.

The equations to determine the chord wall deformations are dependent on the DOF deformation  $i$  in combination with the unit-load  $P_j$  of application, resulting in nine equations. The equations are shown in table 4.1. The equations are notated for the top-surface model where the elements are located on  $D$  and  $d$ . For the mid-surface model the elements are located on the outer diameter  $D - T$  and  $d - t$ . The equations for  $\delta_{11}$ ,  $\delta_{22}$  and  $\delta_{33}$  are also applied by Fessler et al. [31] and by Ahmadi and Nejad [3] [4] [5].

Table 4.1: Overview of equations to calculate the chord wall deformations

<p><b>Axial deformation as effect of unit axial force</b></p> $\delta_{11} = \frac{\kappa_{1,1} - \kappa_{5,1} + \kappa_{2,1} - \kappa_{6,1} + \kappa_{3,1} - \kappa_{7,1} + \kappa_{4,1} - \kappa_{8,1}}{4} \sin \theta \quad (4.3)$	
<p><b>Axial deformation as effect of unit out-of-plane bending moment</b></p> $\delta_{12} = \frac{\kappa_{1,2} + \kappa_{2,2} + \kappa_{3,2} + \kappa_{4,2}}{4} \sin \theta \quad (4.4)$	
<p><b>Axial deformation as effect of unit in-plane bending moment</b></p> $\delta_{13} = \frac{\kappa_{1,3} - \kappa_{5,3} + \kappa_{2,3} - \kappa_{6,3} + \kappa_{3,3} - \kappa_{7,3} + \kappa_{4,3} - \kappa_{8,3}}{4} \sin \theta \quad (4.5)$	
<p><b>Out-of-plane bending as effect of unit axial force</b></p> $\delta_{21} = \left( \frac{\kappa_{2,1} - \kappa_{4,1}}{d} - \frac{\kappa_{6,1} - \kappa_{8,1}}{D} \right) \sin \theta \quad (4.6)$	
<p><b>Out-of-plane bending as effect of unit out-of-plane bending moment</b></p> $\delta_{22} = \left( \frac{\kappa_{2,2} - \kappa_{4,2}}{d} - \frac{\kappa_{6,2} - \kappa_{8,2}}{D} \right) \sin \theta \quad (4.7)$	
<p><b>Out-of-plane bending as effect of unit in-plane bending moment</b></p> $\delta_{23} = \left( \frac{\kappa_{2,3} - \kappa_{4,3}}{d} - \frac{\kappa_{6,3} - \kappa_{8,3}}{D} \right) \sin \theta \quad (4.8)$	
<p><b>In-plane bending as effect of unit axial force</b></p> $\delta_{31} = \frac{\kappa_{3,1} - \kappa_{7,1} - \kappa_{1,1} + \kappa_{5,1}}{d} \sin \theta \quad (4.9)$	
<p><b>In-plane bending as effect of unit out-of-plane bending moment</b></p> $\delta_{32} = \frac{\kappa_{3,2} - \kappa_{1,2}}{d} \sin \theta \quad (4.10)$	
<p><b>In-plane bending as effect of unit in-plane bending moment</b></p> $\delta_{33} = \frac{\kappa_{3,3} - \kappa_{7,3} - \kappa_{1,1} + \kappa_{5,3}}{d} \sin \theta \quad (4.11)$	

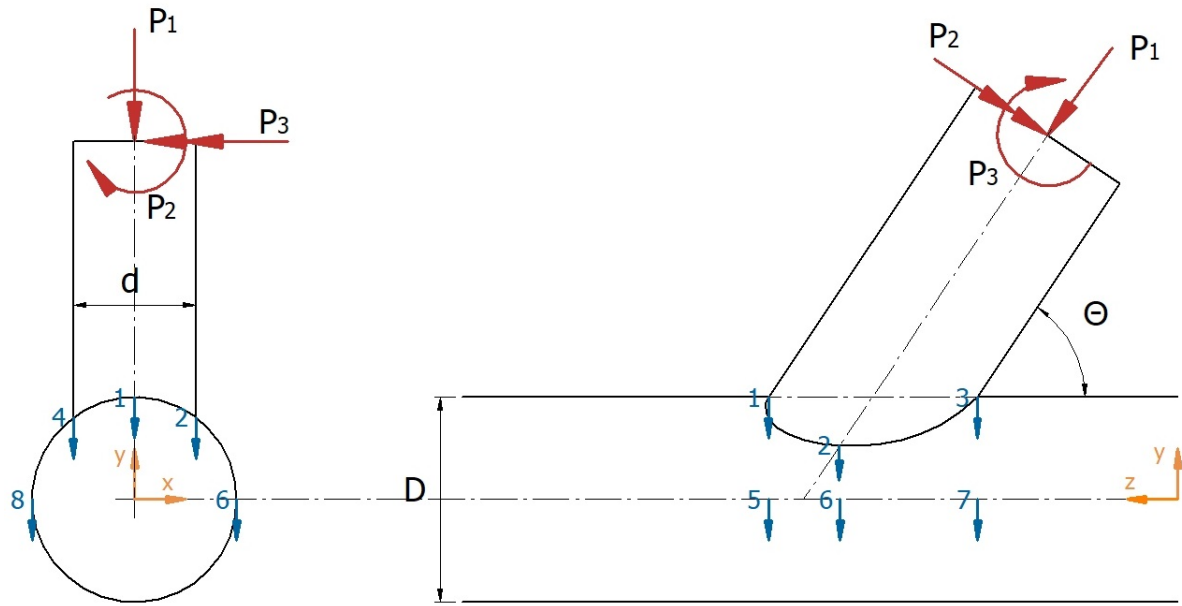


Figure 4.7: Location, and direction of measured displacements  $\kappa_{p,j}$  in points  $p$

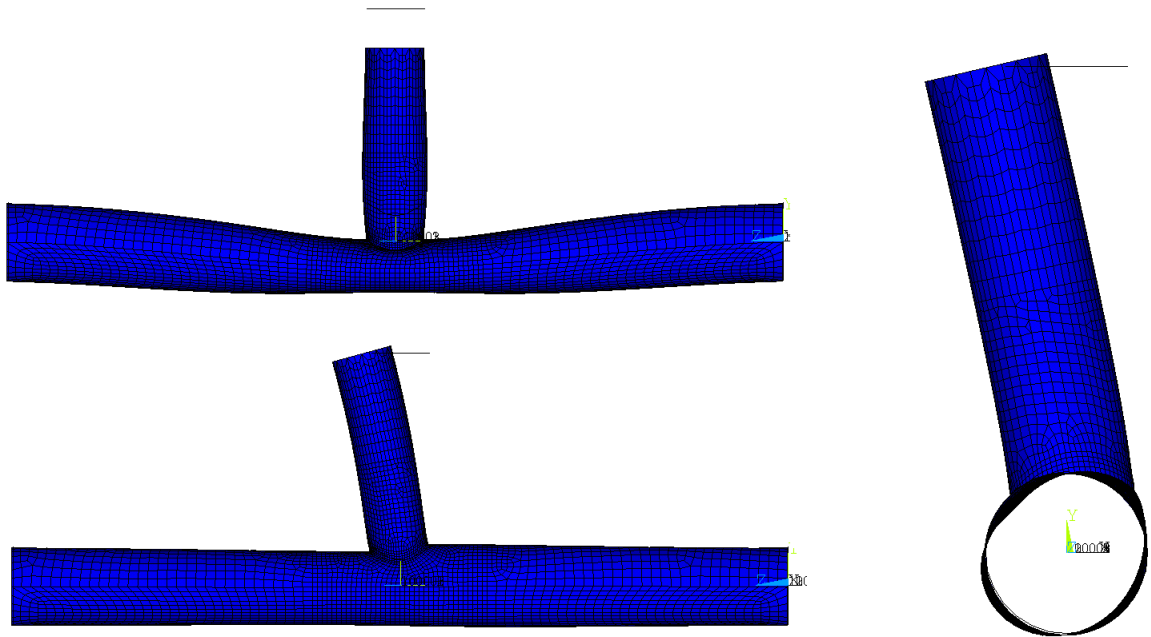


Figure 4.8: Chord wall displacements as effect of axial, out-of-plane and in-plane load-case.

#### 4.2.4. Calculation flexibility matrix

In the previous sub-section the chord wall displacements as effect of every unit-load are computed. In this sub-section, the flexibility matrix is computed. The flexibility matrix is computed by dividing the deformations over the unit-load of application.

$$[LJF] = [\Delta] [P]$$

$$(4.12)$$

$$[P] = \begin{bmatrix} \frac{1}{P_1} & & \\ & \frac{1}{P_2} & \\ & & \frac{1}{P_3} \end{bmatrix} \quad (4.13)$$

To relate to the flexibilities and compare them, the non-dimensional flexibility matrix is computed. Flexibilities are a combination of a deformation and a unit-load. Both the unit-load and deformation shall be made non-dimensional. Flexibilities of which the deformation is defined by a translation (unit m) are made non-dimensional by division over the chord diameter. Flexibilities of which the deformation is defined by a rotation [rad] are already non-dimensional. Flexibilities of which the unit-load is defined by a force [1/N] and are multiplied with  $ED^2$  [N]. Flexibilities of which the unit-load is defined by a bending moment [1/Nm] and multiplied with  $ED^3$  [Nm]. In matrix notation it follows that:

$$[LJF^*] = [Q_\Delta] [\Delta] [P] [Q_P] \quad (4.14)$$

Where:

$$[Q_\Delta] = \begin{bmatrix} \frac{1}{D} & & \\ & 1 & \\ & & 1 \end{bmatrix} \quad (4.15)$$

$$[Q_P] = \begin{bmatrix} ED^2 & & \\ & ED^3 & \\ & & ED^3 \end{bmatrix} \quad (4.16)$$

Written out:

$$[LJF^*] = \begin{bmatrix} f_{11}^* & f_{12}^* & f_{13}^* \\ f_{21}^* & f_{22}^* & f_{23}^* \\ f_{31}^* & f_{32}^* & f_{33}^* \end{bmatrix} = \begin{bmatrix} \frac{1}{D} & & \\ & 1 & \\ & & 1 \end{bmatrix} \begin{bmatrix} \delta_{11} & \delta_{12} & \delta_{13} \\ \delta_{21} & \delta_{22} & \delta_{23} \\ \delta_{31} & \delta_{32} & \delta_{33} \end{bmatrix} \begin{bmatrix} ED^2 & & \\ & ED^3 & \\ & & ED^3 \end{bmatrix} \begin{bmatrix} \frac{1}{P_1} & & \\ & \frac{1}{P_2} & \\ & & \frac{1}{P_3} \end{bmatrix} \quad (4.17)$$

The equations for the nine non-dimensional flexibilities are written out in Appendix G.1.

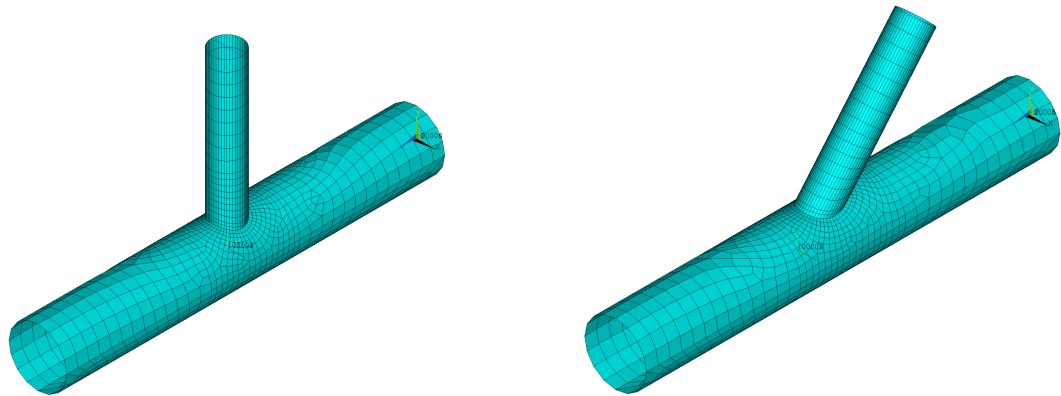
### 4.3. Verification single-brace numerical model

The numerical model is subjected to three tests for verification. In paragraph 4.3.1, the results of the model are analyzed and compared with results described in literature. In paragraph 4.3.2, the mesh refinement is verified. In paragraph 4.3.3, numerical tests are performed whose results is known because of simplicity. The results of the numerical tests can be found in appendix D.

#### 4.3.1. Analysis of results and comparison to literature

The flexibilities of two different joints are determined with the numerical model. The difference between joint 1 and joint 2 is the in-plane angle  $\theta$ . The joints are shown in figure 4.9. The properties of both joints are shown in table 4.2. The chord wall displacements measured in the FEA are presented shown in appendix M

The resulting LJF according the numerical model and the parametric equations of joint 1 are shown in table 4.3. The resulting LJF according to the numerical model and the parametric equations of joint 2 are shown in table 4.4. It can be seen that the equations of Buitrago et al. [13] provide a slightly higher flexibility for  $f_{11}$  and  $f_{22}$ , and a lower flexibility for  $f_{33}$ . However, a strong correlation between the numerical model and the equations is clearly visible. The exact reason for the differences cannot be



(a) Joint 1

(b) Joint 2

Figure 4.9: The two joints for the verification of the single-brace model

Table 4.2: Geometrical properties of test joints

Joint property (section 4.2.2)	Joint 1	Joint 2
$\beta$ [-]	0.53	0.53
$\gamma$ [-]	10	10
$\tau$ [-]	0.5	0.5
$\theta$ [°]	90	50
Element-plane	Top	Top
Integration scheme	2x2x3	2x2x3
Constraint	F/F	F/F
Load [-]	1	1
Element-size [mm]	T	T
E [MPa]	2.1e5	2.1e5
$\nu$ [-]	0.3	0.3
D [mm]	132	132
Chord length [mm]	10*D	10*D
Brace length [mm]	3*d	3*d

retrieved because insufficient details about the experiment performed by Buitrago et al.[13] is provided. However, it is assumed the differences are the effect of different methods of modelling the joint in FEA. In the validation in section 4.4, the accuracy of the determination of the diagonal flexibilities is assessed further.

The results of the numerical models show that there is no coupling between axial and out-of-plane bending flexibility ( $f_{12}^*$  and  $f_{21}^* = 0$ ) and between in-plane bending- and out-of-plane bending flexibility ( $f_{32}^*$  and  $f_{23}^* = 0$ ). This observation is confirmed in literature [13] [17] [31] [54]. In the flexibilities of joint 2, small coupling between axial flexibility and in-plane bending ( $f_{13}^*$  and  $f_{31}^*$ ) is noticed. This is caused by the asymmetric shape of the chord/brace intersection. The reciprocal theorem states that the flexibility

Table 4.3: Comparison between LJF of joint 1 according to the numerical model and parametric equation of Buitrago et al. [13]

	LJF* of joint 1 according to: [-]					
	Numerical model			Buitrago et al.		
	$f_{i1}^*$	$f_{i2}^*$	$f_{i3}^*$	$f_{i1}^*$	$f_{i2}^*$	$f_{i3}^*$
$f_{1j}^*$	73.6	0	0	147.4		
$f_{2j}^*$	0	1117.5	0		1929.3	
$f_{3j}^*$	0	0	537.3			556.2

Table 4.4: Comparison between LJF of joint 2 according to the numerical model and parametric equation of Buitrago et al. [13]

	LJF* of joint 2 according to: [-]					
	Numerical model			Buitrago et al.		
	$f_{i1}^*$	$f_{i2}^*$	$f_{i3}^*$	$f_{i1}^*$	$f_{i2}^*$	$f_{i3}^*$
$f_{1j}^*$	43.2	0	10.1	92.0		
$f_{2j}^*$	0	623.5	0		1168.0	
$f_{3j}^*$	-7.53	0	378.4			399.6

matrix is symmetrical. However, a small deviation is noticed. The literature considering off-diagonal flexibilities is limited. Fessler et al. [31] is the only publications discussing these off-diagonal flexibilities and face similar deviations. The deviations expose the simplification which is made while converting the flexibility behaviour of tubular joints to a flexibility matrix.

### 4.3.2. Mesh refinement

The mesh size determines the accuracy of the discretization and thereby the accuracy of the results of the numerical model. Sufficient refinement is required for accurate results. Three simulations of the numerical model with different mesh refinement are performed. A course mesh with 3043 elements, a fine mesh with 11440 elements and an extra fine mesh with 44607 elements. Examples of the meshes are shown in figure 4.10. The results of the different simulations are shown in table 4.5. The difference between a coarse and extra fine mesh is less than 0.1 %. It is concluded that the coarse mesh has sufficient accuracy. The computational time of the course mesh is within several seconds.

Table 4.5: Results of a course, fine and extra fine mesh

Mesh	Apr. elem. size at intersection [T]	$f_{11}^*[-]$	$f_{22}^*[-]$	$f_{33}^*[-]$
Coarse (3043 elements)	1	98.83	1631.83	799.16
Fine (11440 elements)	0.5	98.87	1631.97	799.16
Extra fine (44607 elements)	0.25	98.87	1631.90	799.11

### 4.3.3. Consistency of results

Tests are performed to control the consistency of the results of the numerical model. Several numerical model parameters which theoretically do not influence the LJF matrix are varied and the influence on the results is checked. Performed numerical tests are shown in table 4.6. The results of all numerical tests are presented in appendix D. It can be seen that the model provides consistent results.

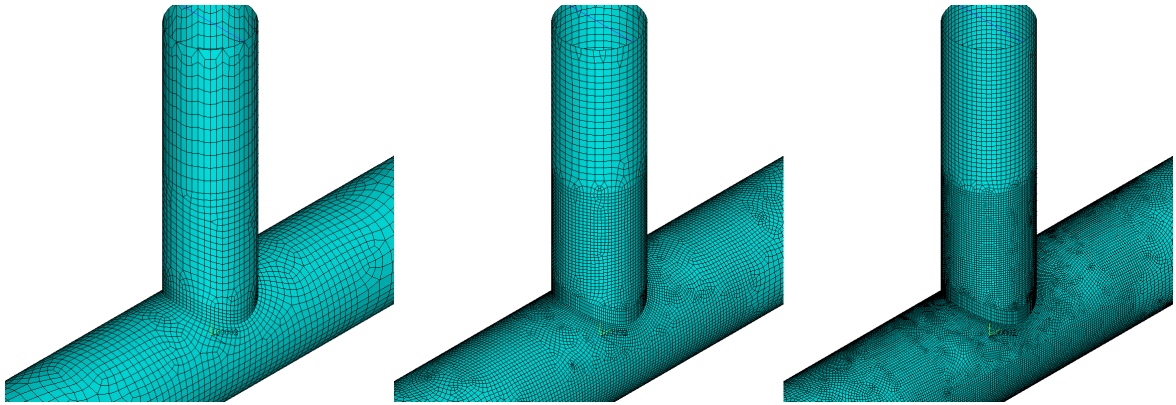


Figure 4.10: Example of the different mesh sizes, from left to right: coarse, fine and extra fine mesh

Table 4.6: Test for verification of the model

Variable	Required outcome	Pass test
Out-of-plane angle $\phi$	The out-of-plane angle of a single-brace joint does not affect the LJF. The result under a different out-of-plane angle needs to be equal.	√
Load sign +−	The numerical model is linear. Therefore, the sign does not affect the flexibility. The results under varying sign need to be equal.	√
Load magnitude $P$	The magnitude of the unit-load affects deformations of the chord wall. However, as the model is linear and flexibility is defined as the deformation per unit-load. Results obtained with a different unit-load need to be equal.	√
Joint size $D$	The dimensionless flexibility is dependent of the joint parameters. The size of the joint does not affect the LJF if the geometry is respected. The required result needs to be equal.	√
Brace length $l$	The length of the brace does not affect the flexibility (taking into account a minimum length of $3D$ for stress redistribution. Results under a variable brace length are required to be equal.	√
Chord length $L$	The length of the chord does not affect the flexibility (taking into account a minimum length of $6D$ for stress redistribution. Results under a variable chord length are required to be equal.	√
Young's modulus $E$	The non-dimensional LJF is independent of the Young's modulus. Calculations with another Young's modulus are required to provide equal results.	√

#### 4.4. Validation single-brace numerical model

In this section, the single-brace numerical model is validated. The results of the numerical model are compared to experimental data of publications. Application of the numerical model is justified by proving that the flexibilities according to the model are a more accurate representation of the joint flexibilities, than the flexibilities present in a beam model without LJF. It is shown that the numerical model with elements on the top-surface (sub-section 4.2.2) is more accurate than the model with elements on the mid surface. The accuracy of the numerical model is compared to the accuracy of parametric equations presented by other authors. In sub-section 4.4.1, the experimental data which is compared to is discussed. In sub-section 4.4.2, the flexibilities according to the different methods are discussed. In sub-section 4.4.3, the accuracy of the methods is computed and compared. In sub-section 4.4.4, the reliability of the experiments, used for the validation, is discussed.

##### 4.4.1. Data for comparison

In this sub-section, the data which is compared with each other is discussed. First the experimental data to which all results are compared to is discussed. Secondly the flexibility of the joint in a model without LJF is discussed. Latest the retrieval of flexibilities according to the parametric equations is discussed.

### Experimental data

The validation is performed based on the experimentally measured flexibilities in 27 experiments by Fessler et al. [31] and four experiments by Tebbett [53]. These are the only two available single-brace experiments, published in literature. The performance of own experiments to measure the flexibility of tubular joints is considered as too complex and time consuming for application within this project. The experiment setup by Fessler et al. [31] is described accurately by Fessler et al. [28]. Details about the experiment setup of Tebbett [53] could not be retrieved. The flexibilities for the 31 joint geometries according to the experiments are shown in appendix E.

In the 31 experiments, the three diagonal terms of the flexibility matrix are measured ( $f_{11}$ ,  $f_{22}$  and  $f_{33}$ ), for 31 different joint geometries, leading to a total of 93 measurements. For unknown reason Tebbett has not been able to measure for every experiment every flexibility, leading to 89 'valid' measurements.

In the publication of Fessler et al. [28] it can be seen that the araldite test models applied in the experiments by Fessler et al. [31] contain deviations in dimensions. E.g., a joint which is in the article noted as  $\gamma = 20$ , actually had  $\gamma \approx 19.6$ . By investigating the deviations a part of the geometric parameters could be tracked and adapted. Furthermore neither Fessler et al. [31] nor Tebbett [53] did take the brace wall thickness into account. For Fessler et al. [31], the brace wall thickness of the joints applied in the experiment could still be computed with the information provided by Fessler et al. [28]. For Tebbett [53] the brace wall thickness is unknown and  $\tau = 0.50$  is taken. The geometric parameters of the 27 joints of the experiments by Fessler et al. [31] are within the following domain:

$$\begin{aligned} 0.333 &\leq \beta \leq 0.756 \\ 10.0 &\leq \gamma \leq 19.6 \\ 35^\circ &\leq \theta \leq 90^\circ \\ 0.379 &\leq \tau \leq 0.970 \end{aligned}$$

The geometric parameters of the four joints of the experiments by Tebbett [53] are within the following domain:

$$\begin{aligned} 0.331 &\leq \beta \leq 0.924 \\ 20.0 &\leq \gamma \leq 32.0 \\ \theta &= 90^\circ \\ \tau &= 0.500 \end{aligned}$$

Because the measured flexibilities are defined as non-dimensional values, Young's modulus does not affect the flexibility. However, Poisson's ratio  $\nu$  does affect the flexibility. Both authors do not provide information considering the Poisson's ratio of their test models. For the araldite models of Fessler et al. [31] a global estimation of  $\nu = 0.375$  is made in consultation with the manufacturer of araldite, Huntsman [41]. For the experiment by Tebbett [53], steel models are applied for which Poisson's ratio  $\nu = 0.30$  is taken.

Tebbett [53] determined the axial flexibility  $f_{11}$  as effect of tension as well as effect of compression. In his experiment, considerable differences are noticed. Theoretically the flexibility is a linear value and no difference between tension and compression should exist. During the validation, the average value of the flexibility as effect of compression and tension is taken.

### Flexibilities of brace extension element

In figure 4.11 a schematic presentation of the brace extension element in a beam model without LJF, and the new element in a model with LJF is presented. In a model without LJF, the beam element of the brace is extended from the chord wall to the center of the chord, also referred to as brace extension element. The flexibilities of the brace extension element are computed and compared to the actual experimentally determined flexibility in order to determine the accuracy of the flexibility in a model without LJF.

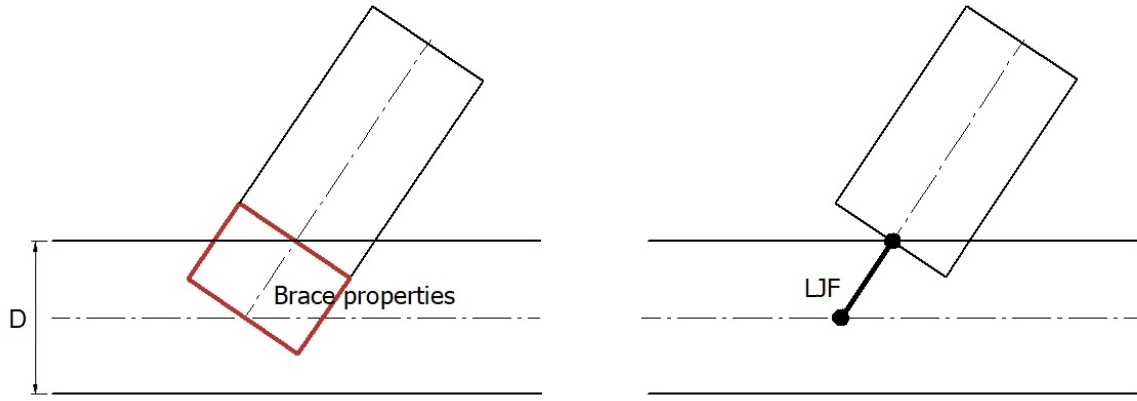


Figure 4.11: Schematic presentation of the brace extension element (left) and a beam model with LJF element (right).

The axial-, out-of-plane bending- and in-plane bending- flexibilities of the brace extension element possess the flexibility properties of the brace element. The flexibilities are dependent on: the length of the element  $l_e$ , Young's modulus  $E$ , the cross surface area of the brace  $A$  and the second moment of the cross surface area of the brace  $I$ . The flexibilities are calculated with:

$$f_{11} = \frac{l_e}{E * A} \quad (4.18)$$

$$f_{22} = f_{33} = \frac{l_e}{E * I} \quad (4.19)$$

Here:

$$A = \pi(r^2 - (r - t)^2) \quad (4.20)$$

$$I = \frac{\pi}{4} (r^4 - (r - t)^4) \quad (4.21)$$

$$l_e = \frac{D}{2 \sin(\theta)} \quad (4.22)$$

The flexibilities are converted to non-dimensional flexibilities to compare them:

$$f_{11}^* = f_{11} * ED = \frac{D^2}{\pi(r^2 - (r - t)^2) * 2 \sin(\theta)} \quad (4.23)$$

$$f_{22}^* = f_{33}^* = f_{22} * ED^3 = f_{33} * ED^3 = \frac{2D^4}{\pi (r^4 - (r - t)^4) * \sin(\theta)} \quad (4.24)$$

Substitution of the non-dimensional parameters gives:

$$f_{11}^* = \frac{\gamma}{\pi \tau \left( \beta - \frac{\tau}{2\gamma} \right) \sin(\theta)} \quad (4.25)$$

$$f_{22}^* = f_{33}^* = \frac{32}{\pi \left( \beta^4 - \frac{(\beta\gamma - \tau)^4}{\gamma^4} \right) * \sin(\theta)} \quad (4.26)$$

The flexibilities of the brace extension element in the model without LJF, are computed for the 31 experiments. The flexibilities are presented in appendix E.

### Parametric equations

The flexibilities according to the parametric equations by Fessler et al. [31], Buitrago et al. [13], Chen and Zhang [17], Ueda et al. [54] and Efthymiou [24] are computed. All these published equations are for single-brace joints. The equations by DNV [21] as stated by Fessler et al. [31] and Hoshyari [38] are not discussed because these are only valid for T-joints. The equations are presented in appendix H.

### 4.4.2. Analysis of results

In this sub-section, the flexibilities according to the experiments, the numerical model and the brace extension element are analysed and compared.

The in-plane bending flexibilities ( $f_{33}^*$ ) of the joint geometries discussed by Fessler et al. [31] are plotted for different joint geometries as function of  $\beta$ ,  $\gamma$  and  $\theta$ . The plots are shown in figure 4.12 up to figure 4.14. Similar plots for axial and out-of-plane bending flexibility are presented in appendix F.

Comparing the flexibilities of the numerical model with the experimentally measured flexibilities, a strong relation is observed. The deviations mostly seem random deviations which cannot be appointed to a single cause. No clear pattern in the deviations is noticed. Only for out-of-plane bending, the numerical model tends to slightly overestimate the flexibilities for  $\beta = 0.333$  and underestimate the flexibilities for  $\beta = 0.756$  (figure F.4). This might be caused through the method applied to compensate for the 'beam behaviour', either by the author or by Fessler et al. [31].

Comparing the brace extension flexibilities of the joint to the experimentally measured flexibilities, no strong relationship is observed. In figure F.2, F.5 and 4.13 it can be seen that the flexibility of the brace extension element is not influenced by the chord wall thickness. However, the experimental flexibilities show that the LJF is strongly influenced by the chord wall thickness. In figure F.3, F.6 and 4.14 it can be seen that as effect of an increasing in-plane angle the LJF increases while the flexibility of the brace extension element decreases. The decrease of flexibility of the brace extension element can be explained by the shortening of the element which lays between chord wall and chord centerline, notated with  $l_e$ .

Analysing the graphs, it is observed that the LJF of a joint is not necessary higher than the brace extension flexibility of a joint without LJF. It can be seen that especially joints with a combination of low  $\gamma$ , and low  $\theta$  possess a lower out-of-plane- and in-plane- bending flexibility in a model with LJF than in a model without LJF. Thereby it is concluded that modelling LJF does not only lead to an increase of flexibility but possibly can lead to a decrease in flexibility, in comparison to a model without LJF included.

### 4.4.3. Accuracy of methodologies

In this section the accuracy of: the LJF according to the numerical model, the flexibility in a model without LJF and the flexibility according to the parametric equations of other authors, are computed and compared. The accuracy of the methodologies is compared by calculation of the deviations towards the LJF according to the experiments. Therefore, it is required to assume that the flexibilities according to the experiments are completely accurate. Whether this is a valid assumption is discussed further in sub-section 4.4.4. The deviation  $\omega$  from the experiment is defined as:

$$\omega = \left( \frac{f_{methodology}}{f_{experiment}} - 1 \right) * 100\% \quad (4.27)$$

The mean  $\mu$  deviation, and the SD (standard deviation)  $\sigma$  of the deviation, is calculated following:

$$\mu = \frac{1}{N} \sum_{n=1}^N \omega_n \quad (4.28)$$

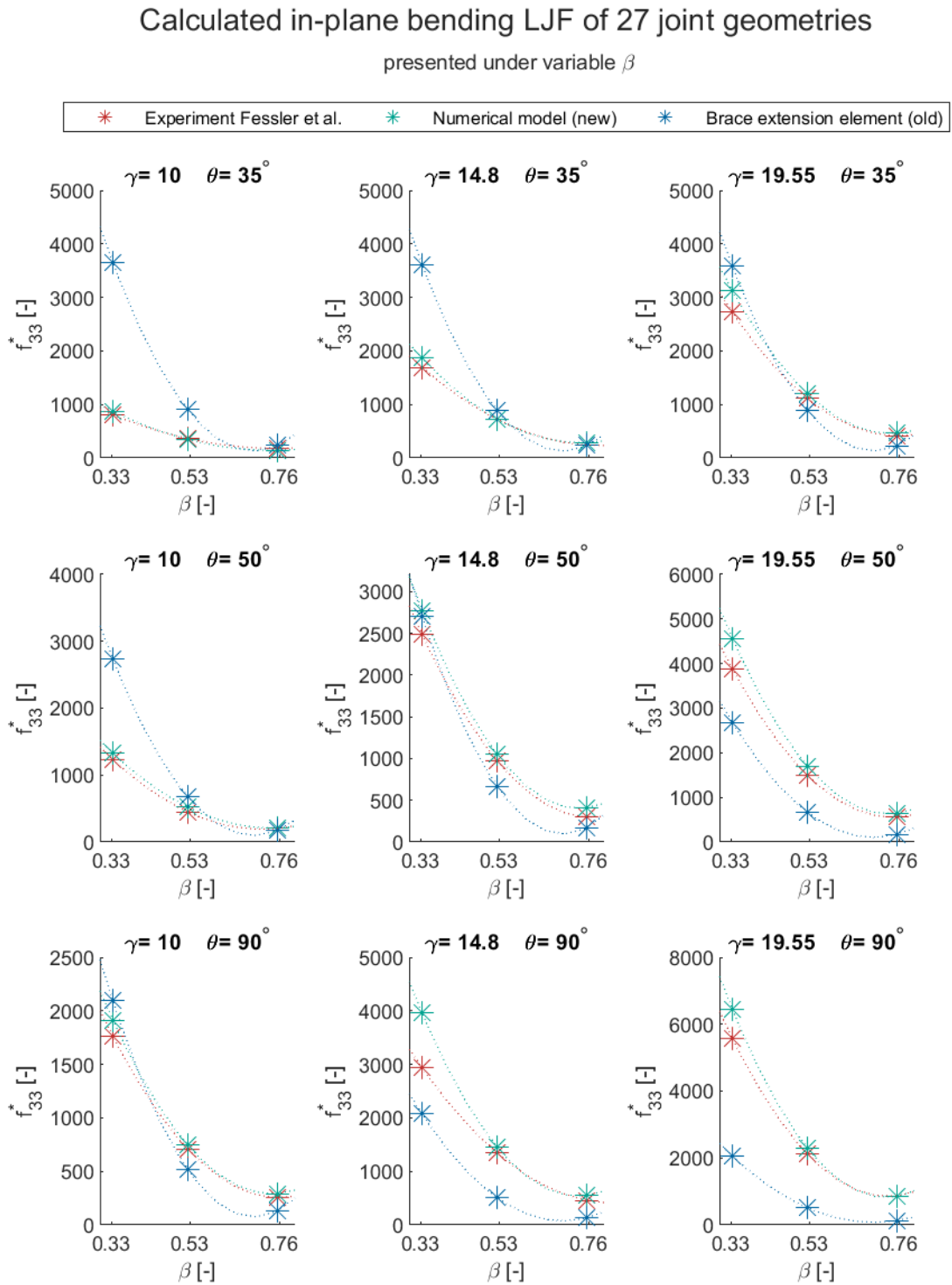


Figure 4.12: The in-plane bending LJF of the 27 joint geometries investigated by Fessler et al., according to: the experiment of Fessler et al., the numerical model and the flexibility of the brace extension element, presented under a variable  $\beta$

### Calculated in-plane bending LJF of 27 joint geometries

presented under variable  $\gamma$

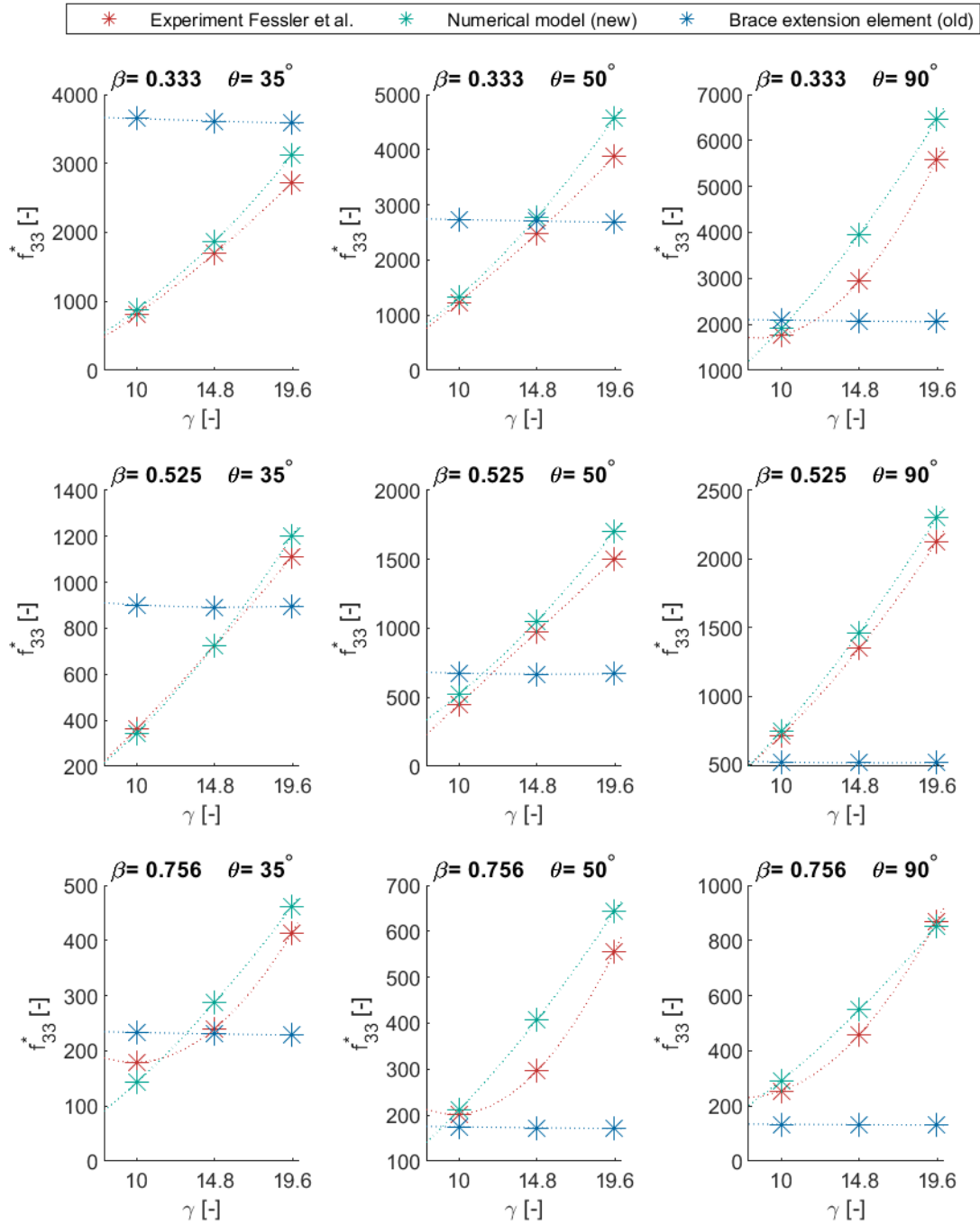


Figure 4.13: The in-plane bending LJF of the 27 joint geometries investigated by Fessler et al., according to: the experiment of Fessler et al., the numerical model and the flexibility of the brace extension element, presented under a variable  $\gamma$

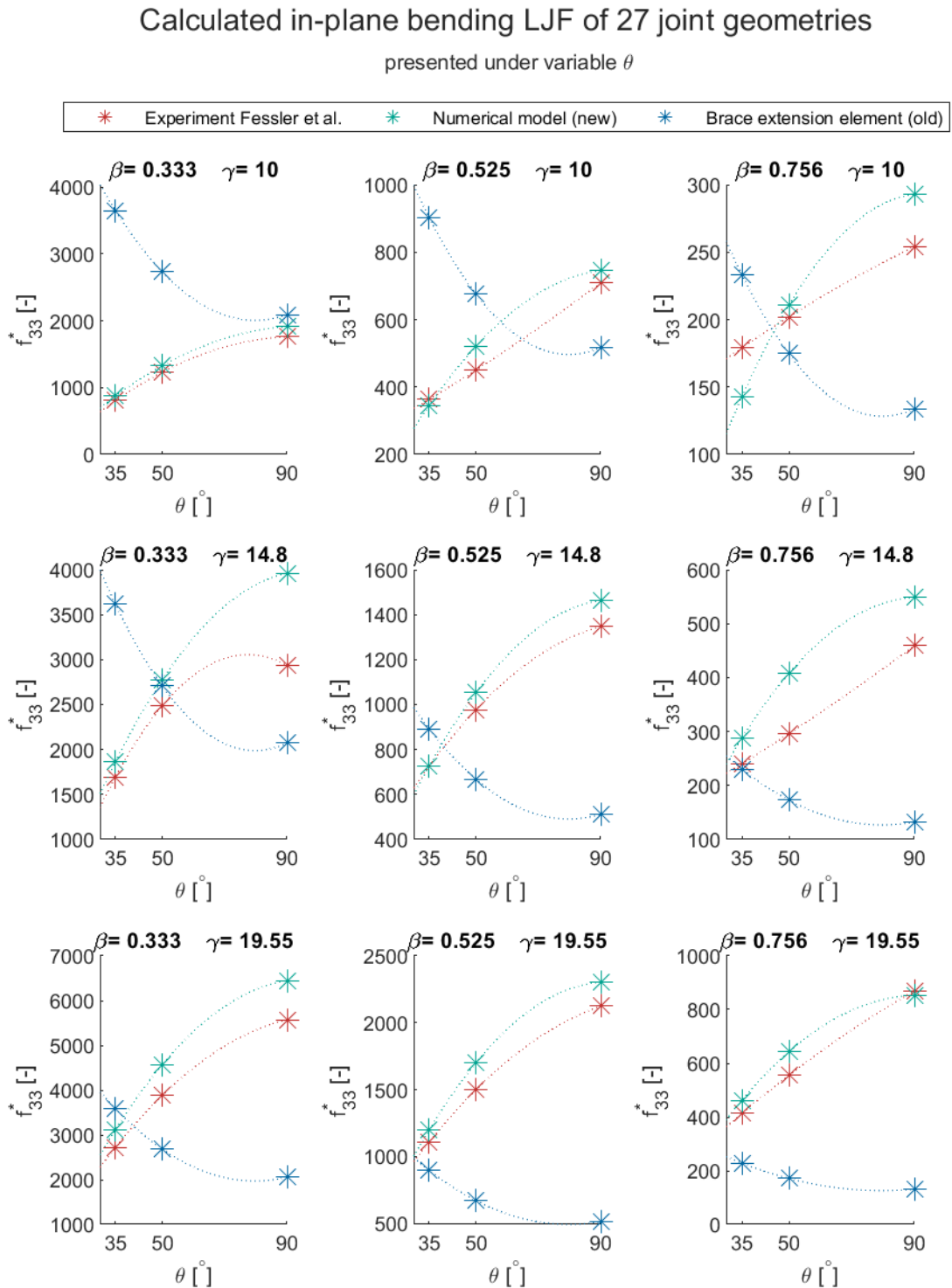


Figure 4.14: The in-plane bending LJF of the 27 joint geometries investigated by Fessler et al., according to: the experiment of Fessler et al., the numerical model and the flexibility of the brace extension element, presented under a variable  $\theta$

$$\sigma = \sqrt{\frac{1}{N} \sum_{n=1}^N (\omega_n - \mu)^2} \quad (4.29)$$

In these equations  $N$  is the total number of samples and  $\omega_n$  the deviation of sample  $n$ . The mean and SD of the deviations are determined for the experiments of both Fessler et al. [31] and Tebbett [53]. The deviations to the experiments of Fessler et al. [31] are considered as stronger because of the higher number of samples  $N$  compared with Tebbett. [53]. The results are shown in table 4.7 and discussed in the following sub-sub-sections.

#### Accuracy of flexibilities brace extension element

In table 4.7 it can be seen that the flexibilities of the brace extension element in a model without LJJ do not approach the experimentally measured flexibilities. A mean deviation of -36% with a SD of 74% is measured to the experiments of Fessler et al. [31] A mean deviation of 85% with a SD of 18% to the experiments of Tebbett [53] is computed. It can be seen that the numerical model has a mean deviation of +3% with a SD of 20% to the experiments by Fessler et al. [31], and a mean deviation of -1% with a SD of 23% to the experiments by Tebbett. It is concluded that the flexibilities computed by the numerical model are more accurately than the flexibilities of the brace extension element in a model without LJJ.

#### Accuracy of numerical model with elements on mid- and top-surface

In sub-section 4.2.2 it is discussed that the numerical model is built with elements on the top-surface of the brace and chord. The accuracy of the model is compared to the accuracy of a model with elements on the mid-surface. In table 4.7 it can be seen that modelling with elements on the top-surface is more accurate than a method with elements on the mid-surface. The flexibilities of the model with elements on the top-surface provides slightly smaller flexibilities than the model with elements on the mid-surface. This can be explained by the larger brace footprint, which provides a larger area to deform and thereby a higher stiffness.

#### Accuracy of parametric equations

To relate to the accuracy of the numerical model, the accuracy of the flexibilities according to the parametric equations of other authors is computed. Fessler et al. [31] published parametric equations for the three flexibilities of a single-brace joint. The equations of Fessler et al. [31] are derived by fitting a curve through the presented 27 experiments of Fessler et al. [31] hence the equations do not provide a reliable representation of the accuracy of the equations. However, the equations show the accuracy lost when transforming experiments to parametric equation. Buitrago et al. [13] published equations for all three main flexibilities of a single-brace joint. The equations of Buitrago et al. are derived of a FEA. It can be seen that the equations of Buitrago et al. [13] tend to overestimate the axial and out-of-plane flexibility. Chen and Zhang [17], Ueda et al. [54] and Efthymiou [24] equations are limited to flexibilities in certain DOF. The results in table 4.7 show that the numerical model calculates, on average, the flexibilities more accurate than the parametric equations. Noteworthy is the accuracy for in-plane bending according the methodologies of Buitrago et al. [13] and of Chen and Zhang [17]. Their approach can be investigated for future improvement of the numerical model.

### 4.4.4. Discussion of reliability of experiments

The reliability of the published experiments is questioned. Without discussion the experiments together provide a good representation of the flexibilities in a joint and provide a convincing validation. As shown in the previous sub-section the numerical model has a mean deviation of only +2.8% to the experiments by Fessler. Deviations of the numerical model to the experiments are not consistent. Though, it is assumed that the FEA provides very consistent results compared to physical experiments. Furthermore several remarkable observations indicate the presence of random errors.

Deviations in the dimensions of the test joints are observed in Fessler et al. [28]. Tubes have a mean deviation in diameter of up to 0.7%, out of roundness of up to 0.25%, mean deviation in wall thickness

Table 4.7: The mean deviation and standard deviation of the deviation, of the L.J.F according to the methodology towards the experimentally determined L.J.F

Experiment	Flexibility	N	Mean and standard deviation of the deviation of the L.J.F according to the methodology to experimental flexibility $\mu \pm \sigma$ [%]							
			No L.J.F (old model)			Parametric equation				
			Brace extended element	Numerical model (top-plane)	(mid-plane)	Fessler et al.	Buitrago and Healy	Chen and Zhang	Ueda et al.	Efthymiou
Fessler et al.	$f_{11}^*$	27	-74.3±21.3	+2.1±19.9	+7.7±20.8	-4.3±17.4	+54.6±36.1	+35.0±25.3	+66.7±46.0	-
	$f_{22}^*$	27	-37.9±67.9	-4.5±22.6	-1.1±25.3	+8.1±20.4	+32.7±26.2	-	-	+51.1±30.2
	$f_{33}^*$	27	+4.8±90.9	+10.9±11.0	+21.9±12.3	-4.5±8.4	-7.8±9.3	+1.3±9.0	+48.5±17.9	+24.4±19.8
	Average	81	-35.8±74.0	+2.8±19.6	+9.5±22.3	-0.2±17.2	+26.5±36.9	-	-	-
Tebbett	$f_{11}^*$	3	-98.4±0.5	-4.9±26.3	-2.7±29.2	-13.0±2.4	+23.8±21.9	+16.6±8.0	+68.5±42.5	-
	$f_{22}^*$	2	-92.0±4.2	-5.4±6.6	-3.3±3.8	-17.1±14.6	+2.0±12.4	-	-	-6.1±1.6
	$f_{33}^*$	3	-66.3 ± 18.0	+6.2±25.0	+11.4±28.7	-14.5±12.5	-32.9±20.4	-11.1±15.1	+15.6±25.2	-10.3±25.2
	Average	8	-84.8±18.4	-0.8±23.1	+2.4±26.1	-14.6±10.8	-2.9±41.3	-	-	-

of up to 9.5% and thickness variations along the wall of up to 6.9%. In table 4.8 the influence of the most extreme combination of deviations in the dimensions on the calculated flexibility is presented. It can be seen that as effect of inaccuracies in the dimensions of the araldite test joints, deviations in flexibility of up to  $\approx 25\%$  are introduced.

The deviations lead to considerable differences in the measured LJF according to the numerical model.

Table 4.8: Comparison of influence of deviations in joint dimension on calculated LJF.

		Local joint flexibilities of tubular joint with:		
		nominal dimension	deviations in dimension leading to an increased calculated flexibility	deviations in dimension leading to a decreased calculated flexibility
Geometry	$D$	1	1	1
	$\beta$ [-]	0.525	+0.7%	-0.7%
	$\gamma$ [-]	19.6	-9.5%	+9.5%
	$\tau$ [-]	0.746	+9.5%	-9.5%
	$\theta$ [°]	90	90	90
LJF	$f_{11}^*[-]$	476.6	358.9	594.2
	$f_{22}^*[-]$	7928.7	6007.1	10223.1
	$f_{33}^*[-]$	2282.8	1865.6	2750.8

Joint geometries of experiment 21 and 23 by Fessler et al. [31] are similar to the geometries of experiment 29 and 30 by Tebbett. Large differences, in flexibility, of up to 75% are noticed. In appendix E it can be seen that the results of parametric equations by Buitrago et al., Efthymiou, Chen and Zhang and Ueda et al., converge towards the experiments of Tebbett [53], making it probable that deviations have appeared in the experiments of Fessler et al.

Comparing the axial flexibilities of experiment 9, 18 and 27 (table E.1), it can be seen all parameters are equal except  $\gamma$  (the influence of  $\tau$  is assumed to be negligible). By increasing  $\gamma$  from 10 to 14.8, the flexibility increases from 57 to 65 (+14%). By increasing  $\gamma$  from 14.8 to 19.6, the flexibility increases from 65 to 219 (+237%). The increase of flexibility for  $\gamma$  from 14.8 to 19.6 seems disproportionate, especially when analyzing increases of other experiments with similar geometries under increasing  $\gamma$ .

It is hard to elaborate on the accuracy of the experiments by Tebbett [53]. No information about the methodology applied to perform the experiments is found. Furthermore, the number of published experiments is low.

The performance of own, more accurate experiments could be considered. It could possibly lead to a reduction of the SD. However, this is out of the scope for this project.

## 4.5. Methodology multi-brace numerical model

The single-brace numerical model is expanded to a multi-brace numerical model. In this section the adaptations are discussed. In sub-section 4.5.1 the general model setup is discussed. In sub-section 4.5.2, adaptations to the FEA are discussed. In sub-section 4.5.3, the expansion of the calculation of the chord wall deformations is discussed and in sub-section 4.5.4, is explained how to calculate the LJF matrix for multi-brace joints.

### 4.5.1. General model overview

The numerical model follows the same procedure as the single-brace model, discussed in section 4.2. In the multi-brace model, two extra dimensions are added. Index  $b$  representing the number of the brace on which the deformations are considered and variable  $c$  representing the number of the brace on

which the unit-load is applied. The total number of braces is notated under  $B$  and  $C$ . Several geometric properties are dependent on the brace number and therefore, in the multi-brace model, defined as  $\beta_b, \theta_b, \tau_b$ . Joint properties  $\gamma$ , chord diameter  $D$  and material properties  $E$  and  $\nu$  are independent of the brace number. Additionally geometric properties: out-of-plane angle  $\psi_b$  and brace gap  $\epsilon_b$  are added to the model.

The output of the model is the flexibility matrix  $[LJF]$ . In a multi-brace model, the local chord wall deformation of a brace can be, not only the result of a load on the brace itself, but also the result of loads on adjacent braces. With every additional brace, three DOF are added. The deformations  $\delta_i$  and unit-loads  $P_j$  are defined as:

- $\delta_1$  = axial deformation of brace 1
- $\delta_2$  = out-of-plane bending deformation of brace 1
- $\delta_3$  = in-plane bending deformation of brace 1
- $\delta_4$  = axial deformation of brace 2
- $\delta_5$  = out-of-plane bending deformation of brace 2
- $\delta_6$  = in-plane bending deformation of brace 2
- $\delta_7$  = etc.

- $P_1$  = axial force on brace 1
- $P_2$  = out-of-plane bending moment on brace 1
- $P_3$  = in-plane bending moment on brace 1
- $P_4$  = axial force on brace 2
- $P_5$  = out-of-plane bending moment on brace 2
- $P_6$  = in-plane bending moment on brace 2
- $P_7$  = etc.

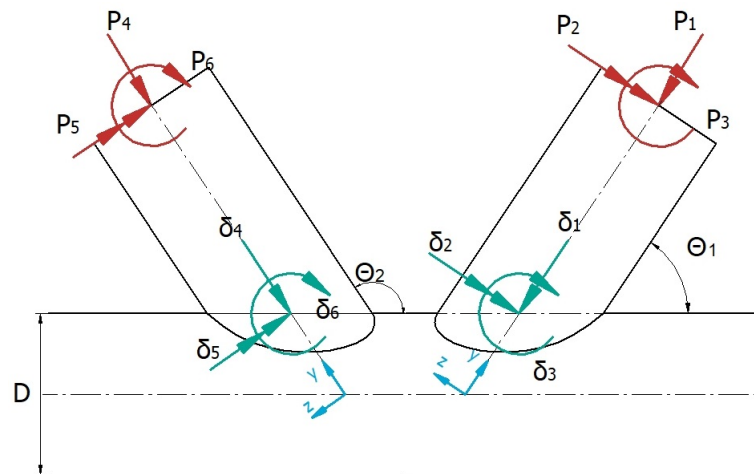


Figure 4.15: The flexibilities of a multi-brace joint defined in the local brace coordinate system

An example of the deformations and unit-loads is shown in 4.15. The flexibility matrix is defined as:

$$\begin{bmatrix} \delta_{11} & \delta_{12} & \delta_{13} & \delta_{14} & \delta_{15} & \delta_{16} & \dots & \delta_{1j} \\ \delta_{21} & \delta_{22} & \delta_{23} & \delta_{24} & \delta_{25} & \delta_{26} & \dots & \delta_{2j} \\ \delta_{31} & \delta_{32} & \delta_{33} & \delta_{34} & \delta_{35} & \delta_{36} & \dots & \delta_{3j} \\ \delta_{41} & \delta_{42} & \delta_{43} & \delta_{44} & \delta_{45} & \delta_{46} & \dots & \delta_{4j} \\ \delta_{51} & \delta_{52} & \delta_{53} & \delta_{54} & \delta_{55} & \delta_{56} & \dots & \delta_{5j} \\ \delta_{61} & \delta_{62} & \delta_{63} & \delta_{64} & \delta_{65} & \delta_{66} & \dots & \delta_{6j} \\ \vdots & \vdots & \vdots & \vdots & \vdots & \vdots & \ddots & \vdots \\ \delta_{i1} & \delta_{i2} & \delta_{i3} & \delta_{i4} & \delta_{i5} & \delta_{i6} & \dots & \delta_{ij} \end{bmatrix} \begin{bmatrix} \frac{1}{P_1} \\ \frac{1}{P_2} \\ \frac{1}{P_3} \\ \frac{1}{P_4} \\ \frac{1}{P_5} \\ \frac{1}{P_6} \\ \dots \\ \frac{1}{P_j} \end{bmatrix} = \begin{bmatrix} f_{11} & f_{12} & f_{13} & f_{14} & f_{15} & f_{16} & \dots & f_{1j} \\ f_{21} & f_{22} & f_{23} & f_{24} & f_{25} & f_{26} & \dots & f_{2j} \\ f_{31} & f_{32} & f_{33} & f_{34} & f_{35} & f_{36} & \dots & f_{3j} \\ f_{41} & f_{42} & f_{43} & f_{44} & f_{45} & f_{46} & \dots & f_{4j} \\ f_{51} & f_{52} & f_{53} & f_{54} & f_{55} & f_{56} & \dots & f_{5j} \\ f_{61} & f_{62} & f_{63} & f_{64} & f_{65} & f_{66} & \dots & f_{6j} \\ \vdots & \vdots & \vdots & \vdots & \vdots & \vdots & \ddots & \vdots \\ f_{i1} & f_{i2} & f_{i3} & f_{i4} & f_{i5} & f_{i6} & \dots & f_{ij} \end{bmatrix} \quad (4.30)$$

The flexibility matrix is built out of  $B \times C$  sub-matrices defined as:

$$[\mathbf{LJF}] = \begin{bmatrix} [\mathbf{LJF}_{11}] & [\mathbf{LJF}_{12}] & \dots & [\mathbf{LJF}_{1c}] \\ [\mathbf{LJF}_{21}] & [\mathbf{LJF}_{22}] & \dots & [\mathbf{LJF}_{2c}] \\ \vdots & \vdots & \ddots & \vdots \\ [\mathbf{LJF}_{b1}] & [\mathbf{LJF}_{b2}] & \dots & [\mathbf{LJF}_{bc}] \end{bmatrix} \quad (4.31)$$

Here,  $[\mathbf{LJF}_{bc}]$  is the flexibility sub-matrix describing the deformations of brace  $b$  caused by a load on brace  $c$ . E.g.  $f_{53}$  is located in sub-matrix  $[\mathbf{LJF}_{21}]$ , represents the out-of-plane deformation at brace 2 as effect of an in-plane bending moment of brace 1. Similar as the single-brace model, loads and deformations are defined in the local brace coordinate system. This is schematically presented in figure 4.15. This means that when  $b \neq c$  the flexibilities are defined in a combination of two coordinate systems.

The multi-brace numerical model is compatible to determine the flexibilities for any non-overlapping joint, within the following geometric domain:

$$\begin{aligned} 0 &< D \rightarrow \infty \\ 0.3 &\leq \beta_b \leq 0.9 \\ 7.5 &\leq \gamma \leq 40 \\ 26^\circ &\leq \theta_b \leq 154^\circ \\ 0^\circ &\leq \psi_b \leq 360^\circ \\ 0.20 &\leq \tau_b \leq 1.0 \\ 0.01 &\leq \epsilon_b \rightarrow \infty \end{aligned}$$

In section 3.2, the joints are categorized. The multi-brace numerical model is able to calculate the flexibilities of every main joint in *category 1*. The model is not able to calculate the flexibilities for joints with  $\beta = 1$  in *category 2*, due to limitations of the geometry in the FEA. However, in section 4.4.2 it can be seen that the flexibility of the brace extension element and the LJF, for high  $\beta$  values, is comparable. It is expected that not modelling LJF in the X-joint with  $\beta = 1$ , does not lead to large deviations. The flexibilities of the joints in *category 3* with  $\beta \neq 1$  can be determined.

### 4.5.2. FEA

In this section adaptations to the FEA as part of the expansion to a multi-brace model are discussed. An example of a multi-brace joint in APDL is shown in figure 4.16. Two adaptations are made towards the FEA. An algorithm which calculates the chord length and an algorithm which detects elements of surrounding braces within the mesh generation.

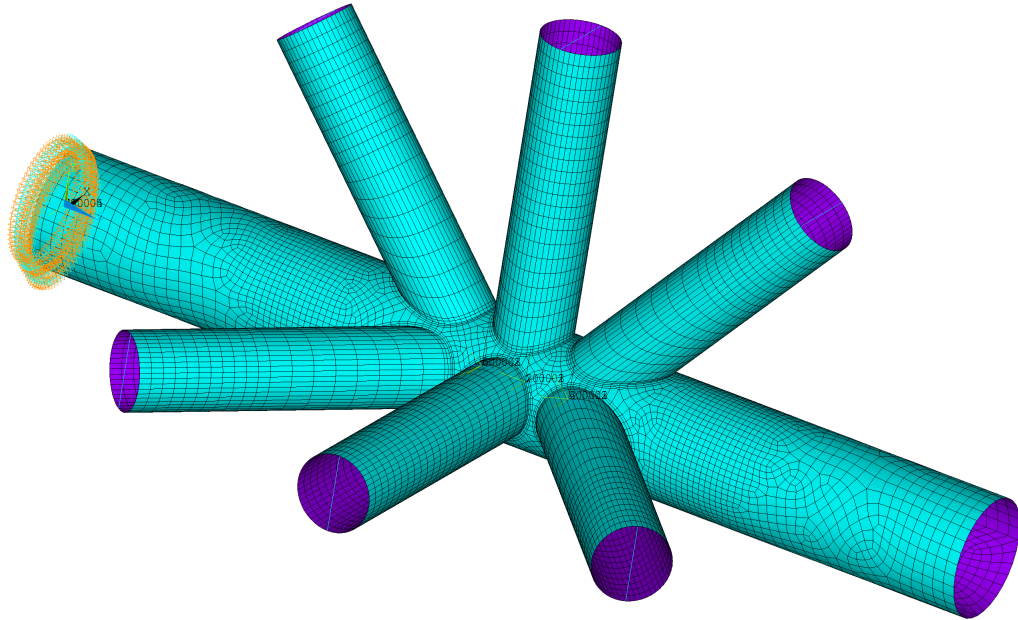


Figure 4.16: Example of a multi-brace joint in the FEA

#### Chord and brace length

The chord length used in the numerical model, is dependent on the number of braces. The center of the chord is also dependent on the location of the braces. An algorithm is developed which automatically detects the points of intersection between chord and brace wall. From the points at the begin and end of the chord, an extra chord length of  $3D$  is added. Braces have a standard length of  $3D$  measured from the intersection of the chord surface.

#### Mesh

When multiple braces are located close to each other, the mesh contours discussed in subsection 4.2.2 intersect each other. Intersection of mesh contours leads to unwanted element shapes. An algorithm is developed which detects intersecting mesh contours. In case of intersection, the mesh contour width  $w$  is decreased with mesh contour reduction  $w_r$ . The mathematics behind this algorithm are explained in appendix B.2. A top view of an example of the mesh contours after reduction, is shown in figure 4.17. It can be seen that the mesh contours close to the intersection are cropped towards each other. An example of a mesh in the numerical model is shown in figure 4.18.

### 4.5.3. Calculation chord wall deformation

Deformations of the chord wall are described in the deformation matrix. Deformation matrix  $[\Delta]$  has dimensions  $i \times j$  equal to  $3B \times 3B$  and is defined with:

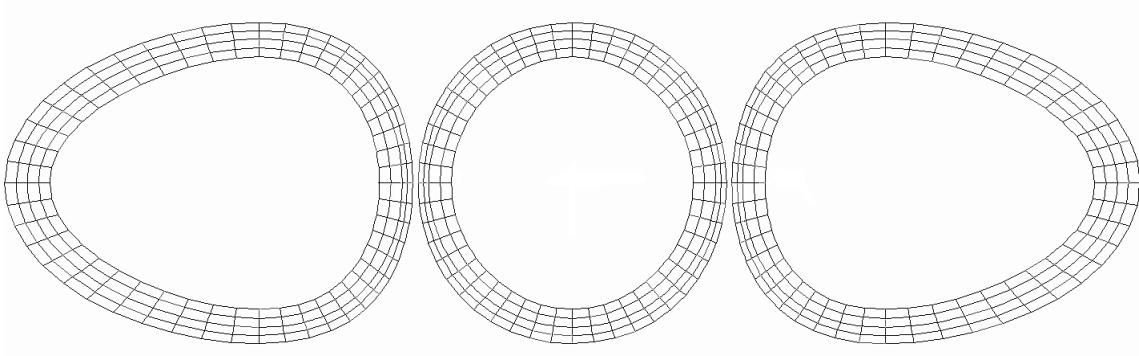


Figure 4.17: Example of mesh contours after reduction of the contour width

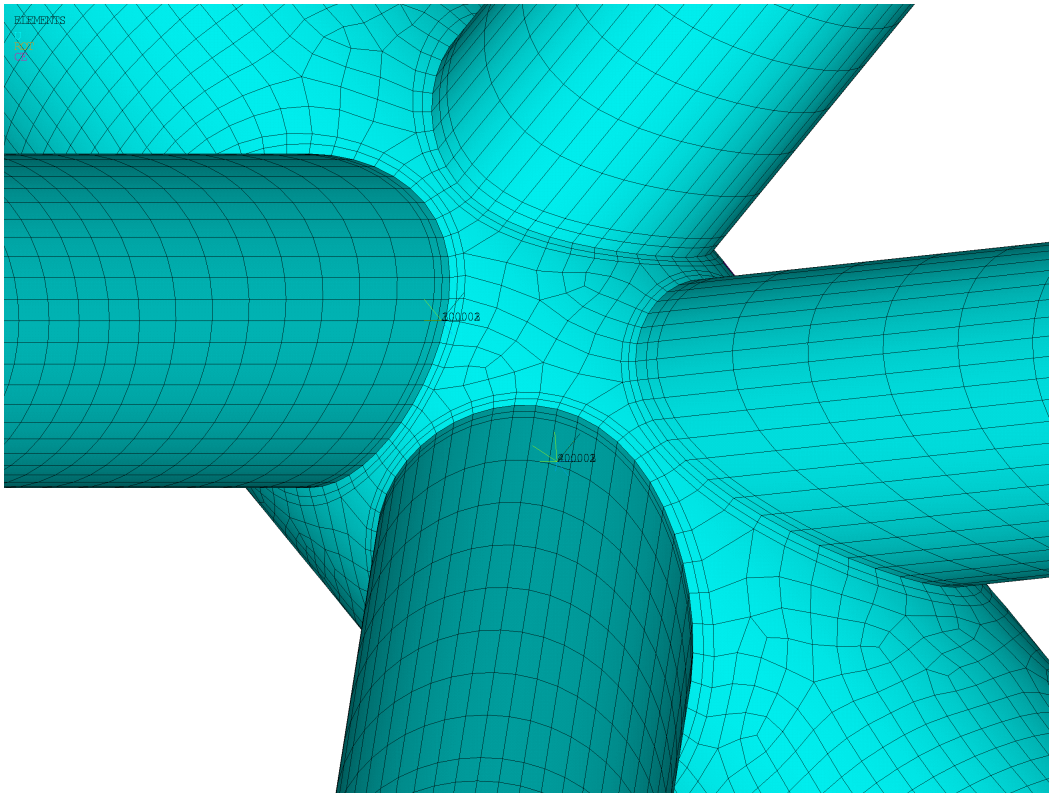


Figure 4.18: Example of a meshed joint after reduction of the contour width

$$[\Delta] = \begin{bmatrix} \delta_{11} & \delta_{12} & \delta_{13} & \delta_{14} & \delta_{15} & \delta_{16} & \dots & \delta_{1j} \\ \delta_{21} & \delta_{22} & \delta_{23} & \delta_{24} & \delta_{25} & \delta_{26} & \dots & \delta_{2j} \\ \delta_{31} & \delta_{32} & \delta_{33} & \delta_{34} & \delta_{35} & \delta_{36} & \dots & \delta_{3j} \\ \delta_{41} & \delta_{42} & \delta_{43} & \delta_{44} & \delta_{45} & \delta_{46} & \dots & \delta_{4j} \\ \delta_{51} & \delta_{52} & \delta_{53} & \delta_{54} & \delta_{55} & \delta_{56} & \dots & \delta_{5j} \\ \delta_{61} & \delta_{62} & \delta_{63} & \delta_{64} & \delta_{65} & \delta_{66} & \dots & \delta_{6j} \\ \vdots & \vdots & \vdots & \vdots & \vdots & \vdots & \ddots & \vdots \\ \delta_{i1} & \delta_{i2} & \delta_{i3} & \delta_{i4} & \delta_{i5} & \delta_{i6} & \dots & \delta_{ij} \end{bmatrix} \tag{4.32}$$

The chord wall deformations are computed from the chord wall displacements  $\kappa_{p,j,b}$  of the eight points

around the brace intersection. For the multi-brace model every brace has eight points describing the displacements and therefore,  $\kappa_{p,j,b}$  is indexed under brace number  $b$ . The loaded brace causing the displacements is indirectly indexed within variable  $j$ . Two examples of a multi-brace joint are shown in figure 4.19 and 4.20. The chord wall displacements of brace 1 are shown in green and of brace 2 in blue.

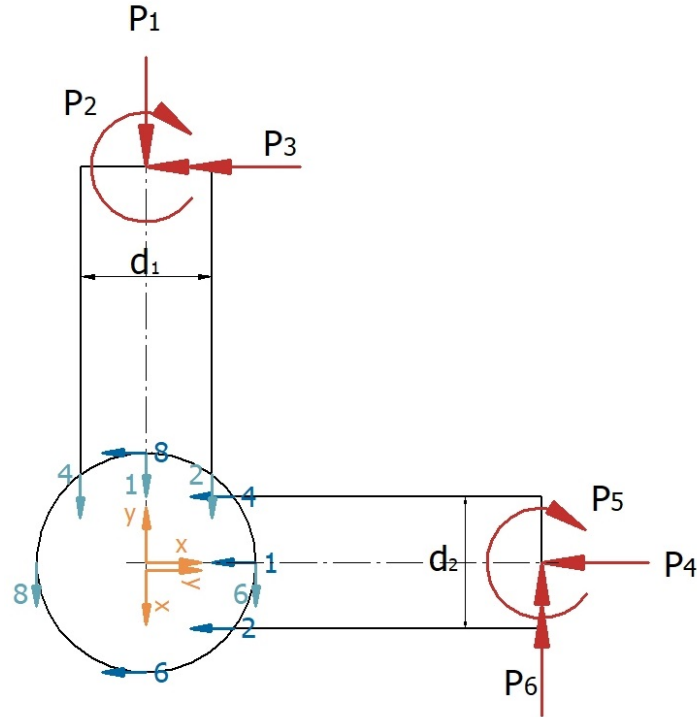


Figure 4.19: Example of displacements of a multi-brace DT-joint

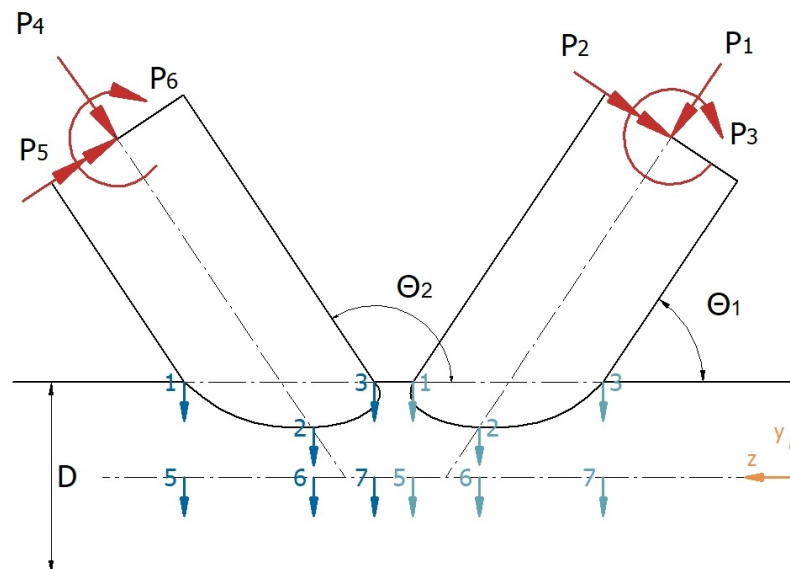
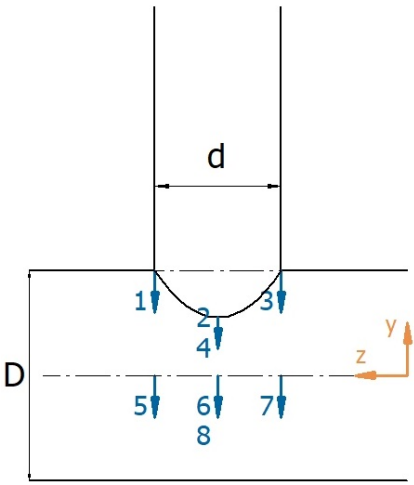
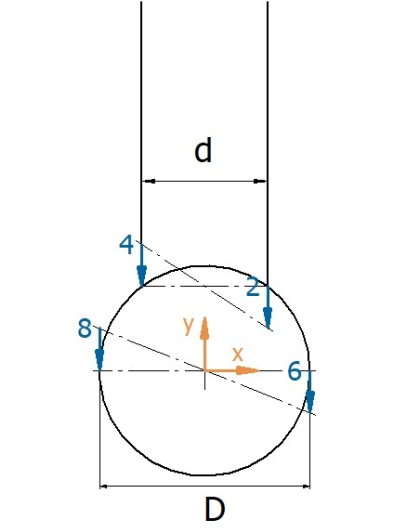
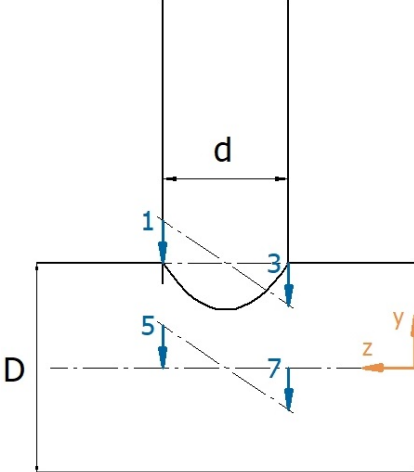


Figure 4.20: Example of displacements of a multi-brace K/TY-joint

The chord wall displacements are measured in the local chord coordinate system, in the direction nor-

Table 4.9: Overview of equations to calculate the chord wall deformations of a multi-brace joint

<p><b>Axial deformation as effect of unit axial force</b></p> $\delta_{ij} = \frac{\kappa_{1,1,b} - \kappa_{5,j,b} + \kappa_{2,j,b} - \kappa_{6,j,b} + \kappa_{3,j,b} - \kappa_{7,j,b} + \kappa_{4,j,b} - \kappa_{8,j,b}}{4} \sin \theta_b \quad (4.33)$	
<p><b>Axial deformation as effect of unit out-of-plane bending moment</b></p> $\delta_{ij} = \frac{\kappa_{1,j,b} + \kappa_{2,j,b} + \kappa_{3,j,b} + \kappa_{4,j,b}}{4} \sin \theta_b \quad (4.34)$	
<p><b>Axial deformation as effect of unit in-plane bending moment</b></p> $\delta_{ij} = \frac{\kappa_{1,j,b} - \kappa_{5,j,b} + \kappa_{2,j,b} - \kappa_{6,j,b} + \kappa_{3,j,b} - \kappa_{7,j,b} + \kappa_{4,j,b} - \kappa_{8,j,b}}{4} \sin \theta_b \quad (4.35)$	
<p><b>Out-of-plane bending as effect of unit axial force</b></p> $\delta_{ij} = \left( \frac{\kappa_{2,j,b} - \kappa_{4,j,b}}{d_b} - \frac{\kappa_{6,j,b} - \kappa_{8,j,b}}{D} \right) \sin \theta_b \quad (4.36)$	
<p><b>Out-of-plane bending as effect of unit out-of-plane bending moment</b></p> $\delta_{ij} = \left( \frac{\kappa_{2,j,b} - \kappa_{4,j,b}}{d_b} - \frac{\kappa_{6,j,b} - \kappa_{8,j,b}}{D} \right) \sin \theta_b \quad (4.37)$	
<p><b>Out-of-plane bending as effect of unit in-plane bending moment</b></p> $\delta_{ij} = \left( \frac{\kappa_{2,j,b} - \kappa_{4,j,b}}{d_b} - \frac{\kappa_{6,j,b} - \kappa_{8,j,b}}{D} \right) \sin \theta_b \quad (4.38)$	
<p><b>In-plane bending as effect of unit axial force</b></p> $\delta_{ij} = \frac{\kappa_{3,j,b} - \kappa_{7,j,b} - \kappa_{1,j,b} + \kappa_{5,j,b}}{d_b} \sin \theta_b \quad (4.39)$	
<p><b>In-plane bending as effect of unit out-of-plane bending moment</b></p> $\delta_{ij} = \frac{\kappa_{3,j,b} - \kappa_{1,j,b}}{d_b} \sin \theta_b \quad (4.40)$	
<p><b>In-plane bending as effect of unit in-plane bending moment</b></p> $\delta_{ij} = \frac{\kappa_{3,j,b} - \kappa_{7,j,b} - \kappa_{1,j,b} + \kappa_{5,j,b}}{d_b} \sin \theta_b \quad (4.41)$	

mal to the chord axis. Therefore, the nine equations, applied to determine the chord wall deformations in a single-brace model, are applied for the multi-brace model too. As discussed for the single-brace model, the type of equation is dependent on the load- and deformation direction. However, the equation is not dependent on the brace upon which it is applied. E.g. the axial deformation at any brace, caused by the in-plane bending moment on another brace, can be computed with the same equation. The equations of the single-brace model are rewritten for multi-brace joints and shown in table 4.9.

#### 4.5.4. Calculation flexibility matrix

The flexibility matrix is computed similar to a single-brace numerical model. The difference is the size of the matrices. The first step is dividing the deformation over the unit-load of applications. This is the same equation as applied in the single-brace model (equation 4.12).

$$[LJF] = [\Delta] [P] \quad (4.42)$$

Matrix  $[P]$  is built up of sub-matrices  $[P_c]$  and contains the applied unit-loads  $P_j$  for every DOF  $j$ , defined as:

$$[P] = \begin{bmatrix} [P_1] & & & \\ & [P_c] & & \\ & & \ddots & \\ & & & [P_c] \end{bmatrix} = \begin{bmatrix} \frac{1}{P_1} & & & \\ & \frac{1}{P_2} & & \\ & & \frac{1}{P_3} & \\ & & & \ddots \\ & & & & \frac{1}{P_j} \end{bmatrix} \quad (4.43)$$

The transformation to the non-dimensional flexibility is dependent on the load and deformation combination and is for every sub-matrix equal. The transformation vectors are extended, dependent on the number of braces. It follows that:

$$[LJF^*] = \begin{bmatrix} [Q_{\Delta 1}] & & & \\ & [Q_{\Delta b}] & & \\ & & \ddots & \\ & & & [Q_{\Delta B}] \end{bmatrix} [\Delta] [P] \begin{bmatrix} [Q_{P 1}] & & & \\ & [Q_{P c}] & & \\ & & \ddots & \\ & & & [Q_{P c}] \end{bmatrix} \quad (4.44)$$

Here:

$$[Q_{\Delta b}] = \begin{bmatrix} \frac{1}{D} & & \\ & 1 & \\ & & 1 \end{bmatrix} \quad (4.45)$$

$$[Q_{P c}] = \begin{bmatrix} ED^2 & & \\ & ED^3 & \\ & & ED^3 \end{bmatrix} \quad (4.46)$$

The equations for the nine non-dimensional flexibilities are written out in Appendix G.2.

## 4.6. Verification multi-brace numerical model

### 4.6.1. Analysis of results

The flexibility matrices of four different joints are determined with the expanded numerical model. First, a single-plane KT-joint is assessed (Joint 1). Secondly a multi-plane DX-joint is assessed (Joint 2). Both joints consists of braces with two different geometries. The flexibility of these braces in a single-brace model is determined (Joint 3 and 4) and serves as a comparison to the first two joints. The

single-brace model is validated in section 4.4 and hence assumed to provide reliable results which are used as reference flexibility. The joints are shown in figure 4.21. The geometries of the joints are shown in table 4.10. The LJF matrices according to the numerical model are shown in table 4.11. The results are verified by testing the results to three criteria, which are discussed in the following sub-sub-sections.

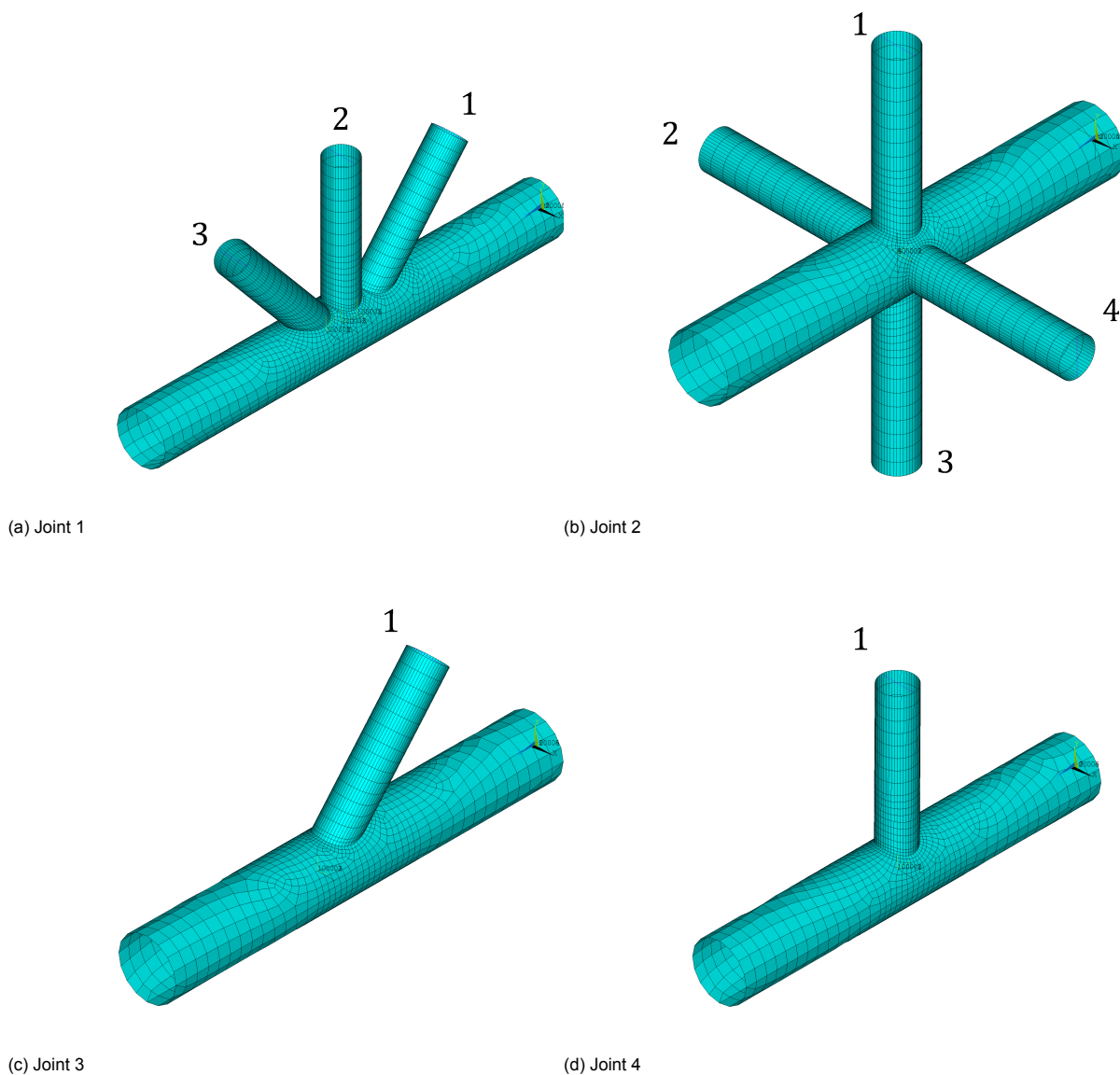


Figure 4.21: The four joints for the verification of the multi-brace model

### Symmetry of matrix

In section 2.2.2, it is shown that the flexibility matrix theoretically is symmetrical because of Maxwell Betti reciprocal theorem. It can be seen that the resulting flexibility matrices of the numerical model is symmetrical except small deviations which are also observed in the single brace numerical model.

### Comparison to flexibilities of single-brace joints

The flexibilities of the multi-brace model are compared with the flexibilities of the single-brace joints. The flexibilities of the single-brace joints are verified and validated in section 4.3 and 4.4 and hence a valid reference. It is expected that braces with similar geometry possess comparable flexibility compared to the single-brace joint. Because of the presence of adjacent braces the stiffness of the multi-brace joints is slightly higher (more material) thus the flexibilities are slightly lower than for a single-brace joint.

Table 4.10: Geometries of the four joints used for verification

Geometry property	Joint 1	Joint 2	Joint 3	Joint 4
$D[m]$	1	1	1	1
$E[N/m^2]$	2.1e11	2.1e11	2.1e11	2.1e11
$\gamma [-]$	10	10	10	10
$\zeta [-]$	$\approx 0.05$	$\approx 0.14$	-	-
$\beta_1 [-]$	0.60	0.60	0.60	0.60
$\tau_1 [-]$	0.50	0.50	0.50	0.50
$\theta_1 [-]$	50	90	50	90
$\psi_1 [-]$	0	0	0	0
$\epsilon_1 [-]$	-0.32	0	0	0
$\beta_2 [-]$	0.60	0.60	-	-
$\tau_2 [-]$	0.50	0.50	-	-
$\theta_2 [-]$	90	90	-	-
$\psi_2 [-]$	0	90	-	-
$\epsilon_2 [-]$	0	0	-	-
$\beta_3 [-]$	0.60	0.60	-	-
$\tau_3 [-]$	0.5	0.50	-	-
$\theta_3 [-]$	130	90	-	-
$\psi_3 [-]$	0	180	-	-
$\epsilon_3 [-]$	0.32	0	-	-
$\beta_4 [-]$	-	0.6	-	-
$\tau_4 [-]$	-	0.50	-	-
$\theta_4 [-]$	-	90	-	-
$\psi_4 [-]$	-	270	-	-
$\epsilon_4 [-]$	-	0	-	-

The reductions of flexibility is also observed in the parametric equations of Buitrago et al. for Y-, K and X-joints [13] and can be seen in figure 2.7, 2.8, 2.10 and 2.9. Furthermore, the presence of adjacent braces can cause an asymmetrical chord brace intersection. Therefore, off-diagonal flexibilities in the multi-brace model can increase compared to the single-brace joint. The following braces have an equal geometry:

Joint 1:

$$[LJF^*_{11}] (1) = [LJF^*_{33}] (1) \approx [LJF^*_{11}] (3) \quad (4.47)$$

$$[LJF^*_{22}] (1) \approx [LJF^*_{11}] (3) \quad (4.48)$$

Joint 2:

$$[LJF^*_{11}] (2) = [LJF^*_{22}] (2) = [LJF^*_{33}] (2) = [LJF^*_{44}] (2) \approx [LJF^*_{11}] (4) \quad (4.49)$$

The results of the numerical model obey this theorem. A reduction of up to 30 % as effect of surrounding braces is observed.

Table 4.11: The non-dimensional LJF matrices of the four joints presented in table 4.10, according to the numerical model

Joint	[LJF]*
1	$\begin{bmatrix} 36.9 & 0 & 19.6 & 28.8 & 0 & 46.5 & 8.6 & 0 & 17.3 \\ 0 & 550.5 & 0 & 0 & 348.1 & 0 & 0 & 138.4 & 0 \\ 8.1 & 0 & 335.7 & -52.7 & 0 & -98.6 & -19.5 & 0 & -18.9 \\ 30.3 & 0 & -41.6 & 61.8 & 0 & 0 & 30.3 & 0 & 41.6 \\ 0 & 370.2 & 0 & 0 & 952.4 & 0 & 0 & 370.2 & 0 \\ 48.3 & 0 & -64.1 & 0 & 0 & 449.5 & -48.3 & 0 & -64.1 \\ 8.6 & 0 & -17.3 & 28.7 & 0 & -46.5 & 36.9 & 0 & -19.6 \\ 0 & 138.4 & 0 & 0 & 348.1 & 0 & 0 & 550.5 & 0 \\ 19.5 & 0 & -18.9 & 52.7 & 0 & -98.6 & -8.1 & 0 & 335.7 \end{bmatrix}$
2	$\begin{bmatrix} 50.3 & 0 & 0 & -38.5 & -32.8 & 0 & 37.2 & 0 & 0 & -38.5 & 32.8 & 0 \\ 0 & 965.2 & 0 & 31.4 & -464.6 & 0 & 0 & 330.2 & 0 & -31.5 & -464.6 & 0 \\ 0 & 0 & 499.9 & 0 & 0 & -163.8 & 0 & 0 & 112.7 & 0 & 0 & -163.7 \\ -38.5 & 32.7 & 0 & 50.3 & 0 & 0 & -38.5 & -32.8 & 0 & 37.2 & 0 & 0 \\ -31.5 & -464.6 & 0 & 0 & 965.1 & 0 & 31.5 & -464.6 & 0 & 0 & 330.1 & 0 \\ 0 & 0 & -163.7 & 0 & 0 & 499.9 & 0 & 0 & -163.8 & 0 & 0 & 112.7 \\ 37.2 & 0 & 0 & -38.5 & 32.7 & 0 & 50.3 & 0 & 0 & -38.5 & -32.8 & 0 \\ 0 & 330.2 & 0 & -31.5 & -464.6 & 0 & 0 & 965.2 & 0 & 31.5 & -464.6 & 0 \\ 0 & 0 & 112.6 & 0 & 0 & -163.7 & 0 & 0 & 500.1 & 0 & 0 & -163.8 \\ -38.5 & -32.8 & 0 & 37.2 & 0 & 0 & -38.5 & 32.8 & 0 & 50.3 & 0 & 0 \\ 31.5 & -464.6 & 0 & 0 & 330.2 & 0 & -31.5 & -464.6 & 0 & 0 & 965.2 & 0 \\ 0 & 0 & -163.6 & 0 & 0 & 112.6 & 0 & 0 & -163.8 & 0 & 0 & 500.0 \end{bmatrix}$
3	$\begin{bmatrix} 41.3 & 0 & 9.8 \\ 0 & 594.7 & 0 \\ -6.8 & 0 & 370.5 \end{bmatrix}$
4	$\begin{bmatrix} 70.4 & 0 & 0 \\ 0 & 1069.5 & 0 \\ 0 & 0 & 527.3 \end{bmatrix}$

### Geometrical symmetry

The multi-brace joints are a combination of only two geometrically different braces. Therefore, a large part of the flexibilities shall be equal because of geometrical symmetry. E.g. in join 2; the deformations of brace 1 as effect of an unit load on brace 3, are equal to the deformations of brace 2 as effect of an unit load on brace 4. In several cases, the flexibilities can be negative because the flexibilities are defined in the coordinate system of the brace. Nevertheless the magnitudes of the flexibilities shall be equal. Because of geometrical symmetry the following sub-matrices shall be equal:

Joint 1:

$$[LJF^*_{11}] (1) = [LJF^*_{33}] (1) \quad (4.50)$$

$$[LJF^*_{21}] (1) = [LJF^*_{23}] (1) \quad (4.51)$$

$$[LJF^*_{31}] (1) = [LJF^*_{13}] (1) \quad (4.52)$$

Joint 2:

$$[LJF^*_{11}] (2) = [LJF^*_{22}] (2) = [LJF^*_{33}] (2) = [LJF^*_{44}] (2) \quad (4.53)$$

$$[LJF^*_{13}] (2) = [LJF^*_{24}] (2) = [LJF^*_{31}] (2) = [LJF^*_{42}] (2) \quad (4.54)$$

$$[LJF^*_{12}] (2) = [LJF^*_{23}] (2) = [LJF^*_{34}] (2) = [LJF^*_{41}] (2) \quad (4.55)$$

$$[LJF^*_{14}] (2) = [LJF^*_{21}] (2) = [LJF^*_{32}] (2) = [LJF^*_{43}] (2) \quad (4.56)$$

The directions of displacements and the deformations as effect of an unit-load are investigated in sub-section 5.3. It is concluded there, that the flexibilities are determined in the correct direction.

## 4.7. Validation multi-brace numerical model

The number of physical experiments, suitable for the validation of a multi-brace model is very limited. Fessler et al. [30] is the only author who performed experiments to the flexibility of multi-brace joints. However, the number of experiments is very limited and in section 4.4.4, it is shown that the experiments do not have a high reliability. For multi-brace joints the deviations are only expected to increase. It is decided to not perform any additional validation for the multi-brace expansion because due to a shortage of reliable experiments. The validation of the single-brace numerical model in combination with the verification of the multi-brace numerical model are considered as sufficient.

Ahmadi et al. [3][4][5] published parametric equations for DK-joints. Comparison could be investigated in future.

## 4.8. Conclusion

A numerical model to determine the flexibilities of tubular joints is developed in MATLAB. The inputs of the model are the geometric and material properties of the joint, the output is the flexibility matrix. The FEA is performed in Ansys. The joint is modelled with 8-noded shell elements, and solved with a 2x2x3 integration scheme.

Initially a model which is able to determine the flexibilities of single-brace joints is developed. The mesh is divided in 3 areas with different refinement. A special approach is followed to lay squared elements on the intersection between brace and chord where the displacements are measured. A mesh with size with element dimensions equal to T, in this report referred to as 'coarse mesh', appeared to reach sufficient accuracy. Welds are not taken into account in the model. The unit-loads are applied at the

brace end, and the chord ends are constrained in all 6 DOF. The displacements are measured at four points located at the crown toe, heel and both saddle points and four points to compensate for beam behavior of the chord. From the chord wall displacements the chord wall deformations are computed. From the chord wall deformations the flexibility matrix is computed.

The single-brace model is verified through several numerical tests which show that the numerical model functions as expected. The numerical model is validated by comparing the results with 27 experiments of Fessler et al. [31] and four experiments by Tebbett [53]. The experiments of Fessler et al. [31] are considered as leading because they are described more detailed and a higher number of experiments is performed. Statistics show that the numerical model is able to determine the flexibilities of tubular joints, with a mean deviation of +3% with a SD of  $\pm 20\%$  to the experiments of Fessler et al. [31]. The flexibilities of the single-brace numerical model are compared to the flexibilities of the brace extension element which is present in a model without LJF. The flexibilities of the brace extension element do not have any correlation with the measured flexibilities in the experiments. Statistics show that the flexibilities of the brace extension element have a mean deviation of  $-36\%$  with a SD of  $\pm 74\%$  towards the experimentally determined flexibilities. Thereby it is proven, that the flexibilities according to the numerical model provide a more accurate representation of the LJF than the model without LJF. A comparison of the results for single brace joints, according to the numerical model and the published parametric equations, shows that the numerical model determines the LJF of a tubular joint more accurately than the parametric equations published in literature.

The numerical model is expanded to a multi-brace model, which is able to determine the flexibilities of every non-overlapping joint in the stinger, except joints with  $\beta = 1$ . With special algorithms the mesh and chord and brace length is regulated. Because LJF is defined in the local coordinate system of the brace, the same method as applied in the single-brace model is applied to calculate the LJF matrix. In the verification, it is shown that the model behaves exactly as expected. Because a shortage of suitable data for the validation of the numerical model, it is decided to not perform any additional validation. The single-brace model validation in combination with the verification of the multi-brace model is considered as sufficient.

To improve the accuracy of the model, it is recommended to investigate the influence of modelling welds. Furthermore, it is recommended to perform own physical experiments to measure the flexibility of joints, especially the flexibility of multi-brace joints. Beside strengthening the validation of the model, it could result in the observation of a higher accuracy.



# 5

## Development of a method to model LJF in a beam model

### 5.1. Introduction

In the previous chapter, a method to determine the LJF of a tubular joint is discussed. In this chapter, a method to model LJF in the beam model is discussed. In chapter 3, it is decided that the most suitable method to model LJF in a beam model is with a global stiffness matrix. Application of the methodology is discussed in detail in section 5.2. In section 5.3, the methodology is verified and in section 5.4, the validation of the methodology is discussed. In section 5.5, the conclusion is given. Thereby the sub-question: "How can local joint flexibility of joints in a stinger be modelled in a beam member model and with what accuracy? How can this method be verified and validated?" is answered.

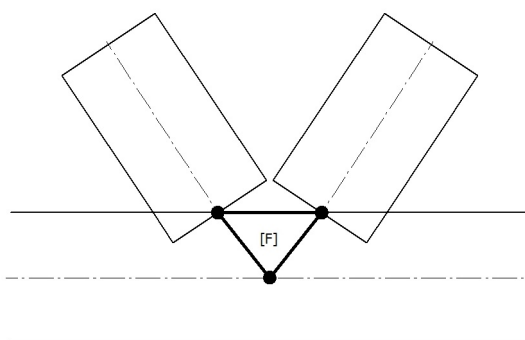


Figure 5.1: Schematic presentation of a global flexibility element.

### 5.2. Methodology

In this section, the methodology applied to model LJF in a beam model is discussed (figure 5.1). A schematic overview of the calculation is shown in figure 5.2. The input of the methodology is the LJF matrix, determined for tubular joints according to chapter 4. The LJF matrix is defined in the local coordinate system of the braces. Via several transformations and rotations the LJF properties are rewritten to a global flexibility matrix. The calculation of the global flexibility matrix is discussed in sub-section 5.2.1 up to sub-section 5.2.6. The global flexibility matrix is inserted in Simcenter FEMAP (2020.2). Within FEMAP, the global flexibility matrix is transformed to a global stiffness matrix. The insertion of the global flexibility matrix in FEMAP is discussed in sub-section 5.2.7.

An abstract but important concept, applied in the methodology, is the rotation of flexibility matrices. Flexibilities are a combination of an unit-load and a deformation. Therefore, the rotation of a flexibility involves the rotation of both the unit-load and the deformation. It is defined that:

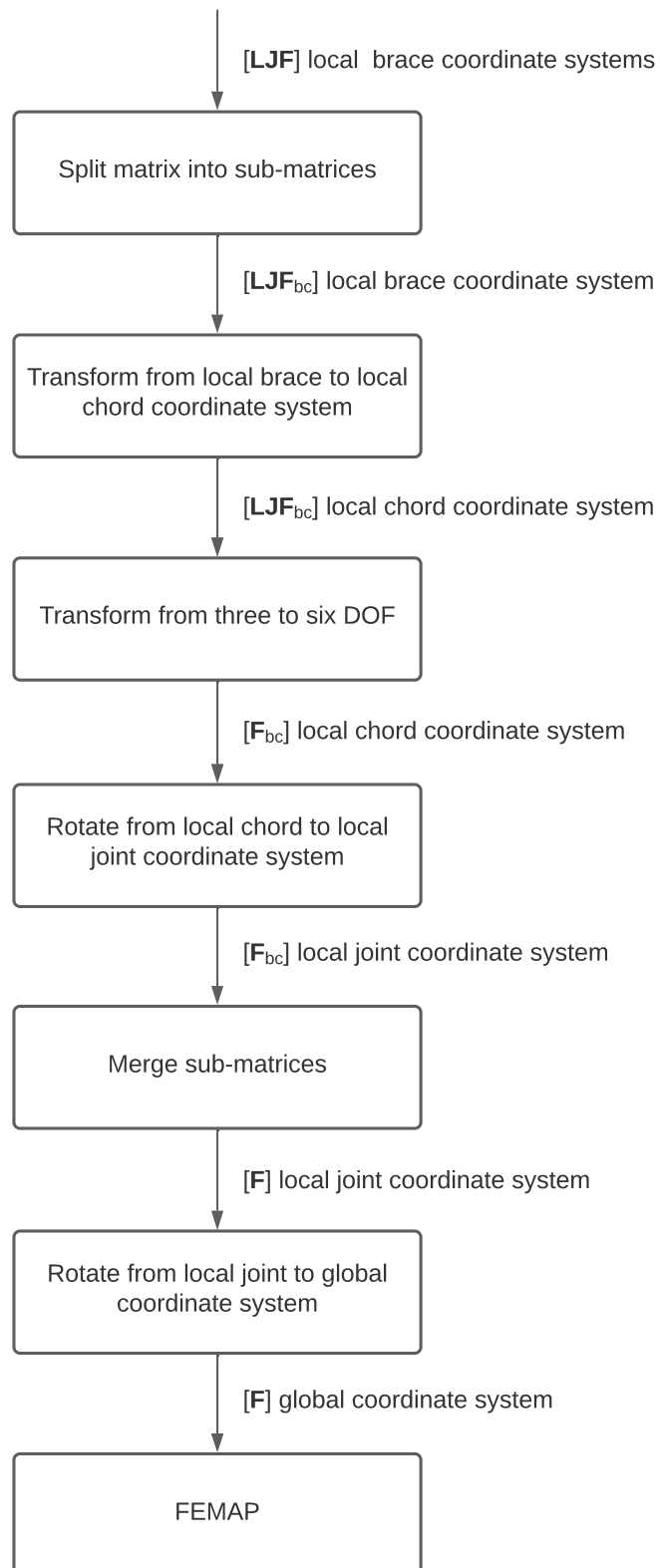


Figure 5.2: Schematic overview of the calculation to model LJF in FEMAP

$$[\mathbf{LJF}_{bc}^{CS1}] = [\mathbf{R}_{\Delta b}^{2 \rightarrow 1}]^T [\mathbf{LJF}_{bc}^{CS2}] [\mathbf{R}_{Pc}^{2 \rightarrow 1}] \quad (5.1)$$

Here  $[\mathbf{R}_{Pc}^{2 \rightarrow 1}]$  represents the rotation matrix to rotate the unit-loads from coordinate system 2 to coordinate system 1.  $[\mathbf{R}_{\Delta b}^{2 \rightarrow 1}]$  represents the rotation matrix to rotate the deformations from coordinate system 2 to coordinate system 1. In a standard situation, the unit-loads and deformations are both defined in the same coordinate system. For instance the flexibility matrix of a single brace joint, or the sub-matrices of a multi-brace joint located on the diagonal of the flexibility matrix. Moreover, when  $b = c$ :

$$[\mathbf{R}_{Pc}^{2 \rightarrow 1}] = [\mathbf{R}_{\Delta b}^{2 \rightarrow 1}] \quad (5.2)$$

However, the LJF matrix of a multi-brace joint contains flexibilities defining the relations between deformations of brace  $b$  as effect of an unit-load on brace  $c$ . Both are defined in the coordinate system of the brace of application. Therefore, when  $b \neq c$ , and a rotation to one single coordinate system is performed, the rotation matrix for the deformations and unit-loads might be different.

### 5.2.1. Split matrix into sub-matrices

Accounting for the rotation of the flexibility matrices as explained before, first the flexibility matrix of the joint is split into sub-matrices with dimensions 3x3 (equation 5.3). The matrix of a single-brace joint is already 3x3. Every sub-matrix relates the three DOF deformations of brace  $b$  as effect of the three DOF unit-load applied on brace  $c$ , hence every sub-matrix is defined in the same combination of coordinate systems.

$$[\mathbf{LJF}] = \begin{bmatrix} [\mathbf{LJF}_{11}] & [\mathbf{LJF}_{12}] & \dots & [\mathbf{LJF}_{1c}] \\ [\mathbf{LJF}_{21}] & [\mathbf{LJF}_{22}] & \dots & [\mathbf{LJF}_{2c}] \\ \vdots & \vdots & \ddots & \vdots \\ [\mathbf{LJF}_{b1}] & [\mathbf{LJF}_{b2}] & \dots & [\mathbf{LJF}_{bc}] \end{bmatrix} \quad (5.3)$$

(5.4)

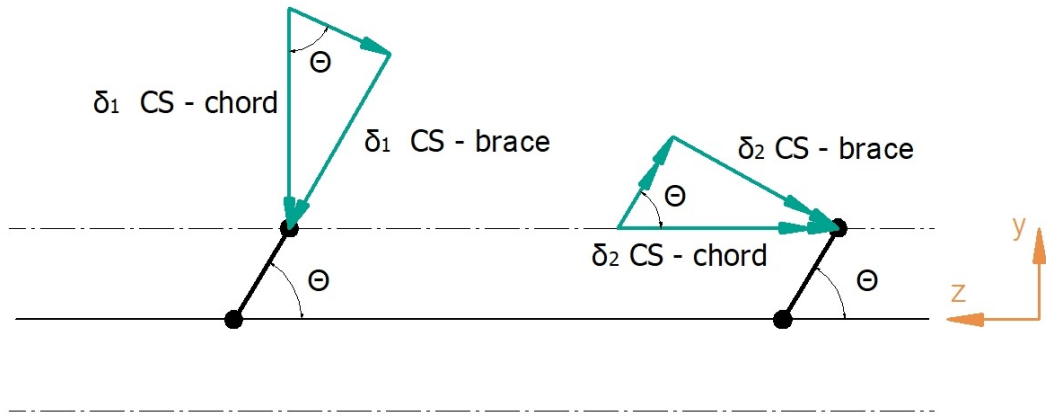
### 5.2.2. Transformation from local-brace to local-chord coordinate system

In section 2.5 it is discussed that definition in the local brace coordinate system is not a correct definition thus, the flexibilities are rotated to the local chord coordinate system. This transformation from local brace to local chord is an in-plane transformation, defined with:

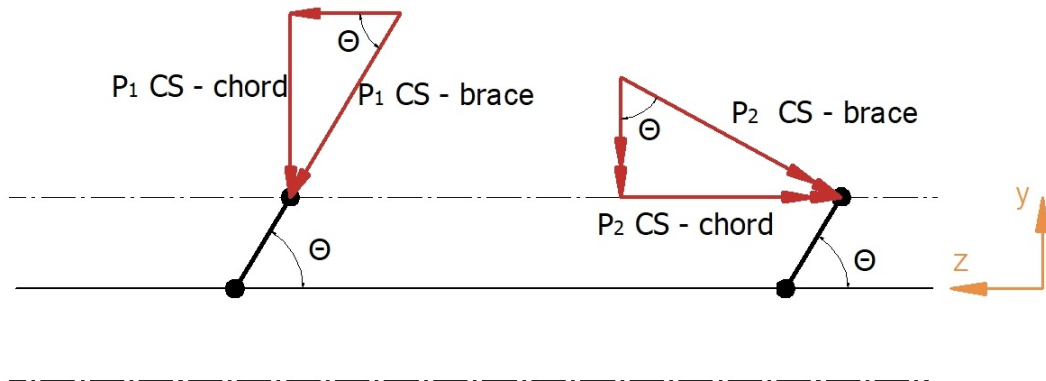
$$[\mathbf{LJF}_{bc}^{chord}] = [\mathbf{T}_{\Delta b}^{brace \rightarrow chord}] [\mathbf{LJF}_{bc}^{brace}] [\mathbf{T}_{Pc}^{brace \rightarrow chord}] \quad (5.5)$$

The transformation of the axial and out-of-plane bending deformation is shown in figure 5.3a. Axial and out-of-plane deformations are divided by  $\sin \theta_b$ . The in-plane deformation is not affected by the rotation. It follows that:

$$[\mathbf{R}_{\Delta b}^{brace \rightarrow chord}] = \begin{bmatrix} \frac{1}{\sin \theta_b} & & \\ & \frac{1}{\sin \theta_b} & \\ & & 1 \end{bmatrix} \quad (5.6)$$



(a) Transformation of deformations



(b) Transformation of loads

Figure 5.3: The transformation of axial and out-of plane loads/deformations from local brace to local chord coordinate system.

The transformation of the axial force and out-of plane bending moment is shown in figure 5.3b. The loads are multiplied with  $\sin \theta_c$ . Because the load is the denominator of the flexibility, the multiplication turns into a division. The in-plane deformation is not affected by the rotation. It follows that:

$$[\mathbf{R}_{p\ c}^{brace \rightarrow chord}] = \begin{bmatrix} \frac{1}{\sin \theta_c} & & & \\ & \frac{1}{\sin \theta_c} & & \\ & & & 1 \end{bmatrix} \quad (5.7)$$

### 5.2.3. Transformation from three to six DOF

Matrix  $[\mathbf{LJF}]$  only considers flexible DOF. Other DOF were assumed rigid and were not further considered. To describe the flexibilities in a three dimensional environment, a notation in a matrix containing every DOF is required. The LJF sub-matrix is transformed to a general flexibility matrix notated with  $[\mathbf{F}]$ . The flexibility matrix has dimension 6x6 and contains the relation between deformation and load for all possible six DOF  $[tx, ty, tz, rx, ry, rz]$ . In the previous step, the flexibilities are aligned with the coordinate system of the chord. The same orientation is maintained when transforming from LJF to general flexibility matrix. The axial DOF is aligned with the y-axis, the out-of-plane bending flexibility aligned with the z-axis of rotation and the in-plane bending flexibility aligned with the x-axis of rotation (figure 5.4). The pivots of the matrix cannot be zero and are therefore the rigid DOF are assumed to possess 10% of the flexibility of the other pivots, noted with  $u$ . The transformation is defined as:

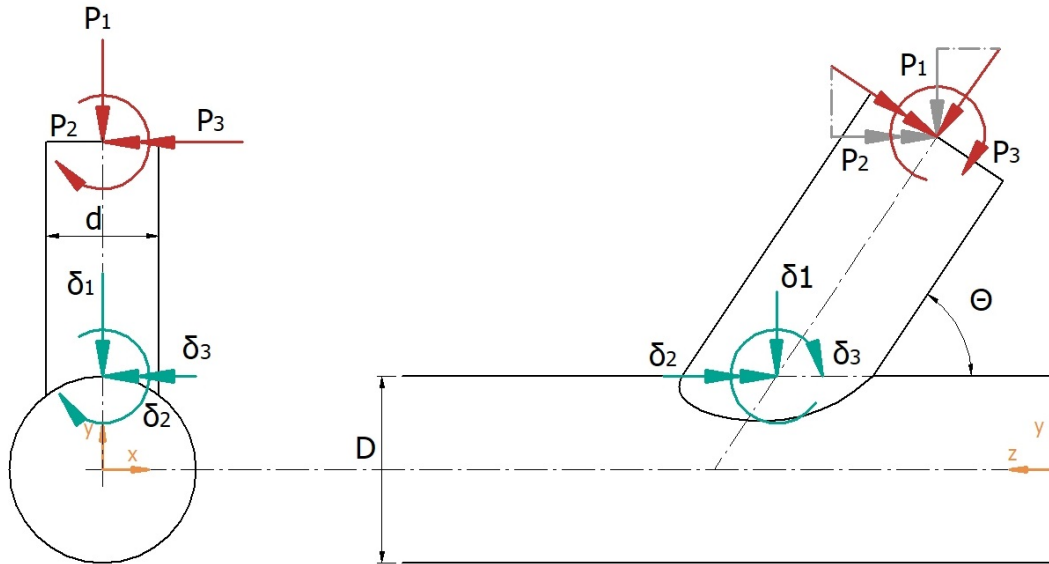


Figure 5.4: The flexibilities defined in the local chord coordinate system

$$[L]F_{bc}^{chord} \rightarrow [F_{bc}^{chord}] \quad (5.8)$$

Written out:

$$\begin{bmatrix} f_{b1c1} & f_{b1c2} & f_{b1c3} \\ f_{b2c1} & f_{b2c2} & f_{b2c3} \\ f_{b3c1} & f_{b3c2} & f_{b3c3} \end{bmatrix} \rightarrow \begin{bmatrix} u & 0 & 0 & 0 & 0 & 0 \\ 0 & f_{b1c1} & 0 & f_{b1c3} & 0 & f_{b1c2} \\ 0 & 0 & u & 0 & 0 & 0 \\ 0 & f_{b3c1} & 0 & f_{b3c3} & 0 & f_{b3c2} \\ 0 & 0 & 0 & 0 & u & 0 \\ 0 & f_{b2c1} & 0 & f_{b2c3} & 0 & f_{b2c2} \end{bmatrix} \quad (5.9)$$

#### 5.2.4. Rotation from local chord to local joint coordinate system

Sub-matrix  $[F_{bc}^{chord}]$  is oriented in a coordinate system aligned with the chord wall and the brace. This is a unique orientation for every sub-matrix. The sub-matrices of the joint are rotated towards the local joint coordinate system (figure C.1). This is an out-of-plane rotation, around the z-axis with a magnitude equal to the out-of-plane angle of the brace shown in figure 5.5. The rotation is performed with standard rotation matrices  $[R_{Pc}^{chord \rightarrow joint}]$  and  $[R_{\Delta b}^{chord \rightarrow joint}]$ . The rotation is defined as:

$$[F_{bc}^{joint}] = [R_{Pc}^{chord \rightarrow joint}] [F_{bc}^{chord}] [R_{\Delta b}^{chord \rightarrow joint}]^T \quad (5.10)$$

with:

$$[R_{Pc}^{chord \rightarrow joint}] = \begin{bmatrix} \cos \psi_c & -\sin \psi_c & 0 & 0 & 0 & 0 \\ \sin \psi_c & \cos \psi_c & 0 & 0 & 0 & 0 \\ 0 & 0 & 1 & 0 & 0 & 0 \\ 0 & 0 & 0 & \cos \psi_c & -\sin \psi_c & 0 \\ 0 & 0 & 0 & \sin \psi_c & \cos \psi_c & 0 \\ 0 & 0 & 0 & 0 & 0 & 1 \end{bmatrix} \quad (5.11)$$

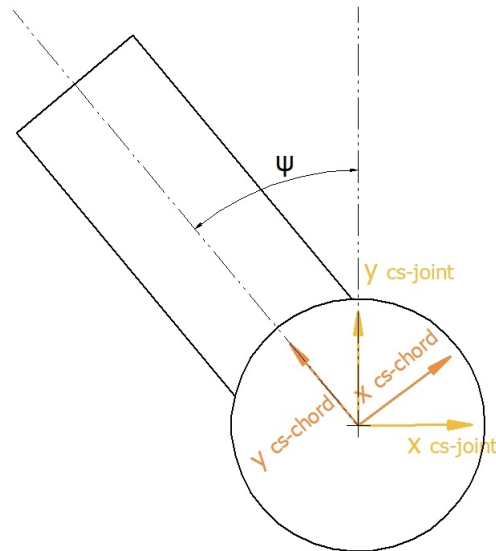


Figure 5.5: Rotation from local chord coordinate system to local joint coordinate system.

$$[\mathbf{R}_{\Delta b}^{chord \rightarrow joint}] = \begin{bmatrix} \cos \psi_b & -\sin \psi_b & 0 & 0 & 0 & 0 \\ \sin \psi_b & \cos \psi_b & 0 & 0 & 0 & 0 \\ 0 & 0 & 1 & 0 & 0 & 0 \\ 0 & 0 & 0 & \cos \psi_b & -\sin \psi_b & 0 \\ 0 & 0 & 0 & \sin \psi_b & \cos \psi_b & 0 \\ 0 & 0 & 0 & 0 & 0 & 1 \end{bmatrix} \quad (5.12)$$

More information considering rotation matrices is discussed by Greenwood [37].

### 5.2.5. Merge sub-matrices

In the previous step the LJF sub-matrices are rotated to the coordinate system of the joint thus all sub-matrices have the same orientation. The sub-matrices are merged together into the flexibility matrix  $[\mathbf{F}^{joint}]$  of the joint. The flexibility matrix has an equal layout to the LJF matrix and has dimensions  $6B \times 6B$ .

$$[\mathbf{F}^{joint}] = \begin{bmatrix} [\mathbf{F}_{11}^{joint}] & [\mathbf{F}_{12}^{joint}] & \dots & [\mathbf{F}_{1c}^{joint}] \\ [\mathbf{F}_{21}^{joint}] & [\mathbf{F}_{22}^{joint}] & \dots & [\mathbf{F}_{2c}^{joint}] \\ \vdots & \vdots & \ddots & \vdots \\ [\mathbf{F}_{b1}^{joint}] & [\mathbf{F}_{b2}^{joint}] & \dots & [\mathbf{F}_{bc}^{joint}] \end{bmatrix} \quad (5.13)$$

### 5.2.6. Rotation from local joint to global coordinate system

The last step before the flexibilities are inserted in FEMAP is the rotation of the flexibility matrix to the global coordinate system. This rotation is dependent on the orientation of the joint in the global coordi-

nate system. The rotation is performed with two rotation matrices  $[R_2^{joint \rightarrow global}]$  and  $[R_1^{joint \rightarrow global}]$ . In the first rotation the chord is rotated and in the second rotation the braces are rotated.

The orientation of the chord, in its local joint coordinate system (z-axis) is notated with vector  $\underline{v}_{chord}^{CS\ joint}$ . The orientation of the chord in the global coordinate system is notated with  $\underline{v}_{chord}^{CS\ global}$ . The orientation is defined in the x,y,z direction following:

$$\underline{v} = \begin{bmatrix} v_x \\ v_y \\ v_z \end{bmatrix} \quad (5.14)$$

Having two vectors, the axis of rotation  $\underline{a}_1$  is defined as the cross product between both vectors:

$$\underline{a}_1 = \underline{v}_{chord}^{CS\ joint} \times \underline{v}_{chord}^{CS\ global} \quad (5.15)$$

The angle of rotation is defined with the dot product divided over the product of the magnitudes of both vectors:

$$\phi_1 = \frac{\underline{v}_{chord}^{CS\ joint} \cdot \underline{v}_{chord}^{CS\ global}}{\|\underline{v}_{chord}^{CS\ joint}\| \cdot \|\underline{v}_{chord}^{CS\ global}\|} \quad (5.16)$$

The rotation matrix is then given by [37]:

$$[R^{joint \rightarrow global}] = \begin{bmatrix} R_{xx} & R_{xy} & R_{xz} & 0 & 0 & 0 \\ R_{yx} & R_{yy} & R_{yz} & 0 & 0 & 0 \\ R_{zx} & R_{zy} & R_{zz} & 0 & 0 & 0 \\ 0 & 0 & 0 & R_{xx} & R_{xy} & R_{xz} \\ 0 & 0 & 0 & R_{yx} & R_{yy} & R_{yz} \\ 0 & 0 & 0 & R_{zx} & R_{zy} & R_{zz} \end{bmatrix} \quad (5.17)$$

$$R_{xx} = (1 - \cos \phi) a_x^2 + \cos \phi \quad (5.18)$$

$$R_{yy} = (1 - \cos \phi) a_y^2 + \cos \phi \quad (5.19)$$

$$R_{zz} = (1 - \cos \phi) a_z^2 + \cos \phi \quad (5.20)$$

$$R_{xy} = (1 - \cos \phi) a_x a_y + a_z \sin \phi \quad (5.21)$$

$$R_{yx} = (1 - \cos \phi) a_x a_y - a_z \sin \phi \quad (5.22)$$

$$R_{xz} = (1 - \cos \phi) a_x a_z + a_y \sin \phi \quad (5.23)$$

$$R_{zx} = (1 - \cos \phi) a_x a_z - a_y \sin \phi \quad (5.24)$$

$$R_{yz} = (1 - \cos \phi) a_y a_z + a_x \sin \phi \quad (5.25)$$

$$R_{zy} = (1 - \cos \phi) a_y a_z - a_x \sin \phi \quad (5.26)$$

A second rotation is performed for the correct orientation of the braces. The same procedure is repeated, but now the rotation is determined based on the orientation of the braces. The orientation of the brace in the local joint coordinate system ( $y$ -axis) is notated with vector  $\underline{v}_{brace}^{CS\ joint}$  and the orientation of the brace in the global coordinate system is notated as  $\underline{v}_{brace}^{CS\ global}$ . Because already one rotation is performed, the orientation of the brace in the local coordinate system has changed with first rotation matrix  $[\mathbf{R}_1^{joint \rightarrow global}]$ . The axis of the second rotation is given by:

$$\underline{a}_2 = \left( [\mathbf{R}_1^{joint \rightarrow global}] \underline{v}_{brace}^{CS\ joint} \right) \times \underline{v}_{brace}^{CS\ global} \quad (5.27)$$

The angle of the second rotation is given by:

$$\phi_2 = \frac{\left( [\mathbf{R}_1^{joint \rightarrow global}] \underline{v}_{brace}^{CS\ joint} \right) \cdot \underline{v}_{brace}^{CS\ global}}{\| \left( [\mathbf{R}_1^{joint \rightarrow global}] \underline{v}_{brace}^{CS\ joint} \right) \| \cdot \| \underline{v}_{brace}^{CS\ global} \|} \quad (5.28)$$

The second rotation matrix  $[\mathbf{R}_2^{joint \rightarrow global}]$  is constructed with equation 5.17. The global flexibility matrix is calculated with:

$$[\mathbf{F}^{CS\ global}] = [\mathbf{R}_2^{joint \rightarrow global}]^T [\mathbf{R}_1^{joint \rightarrow global}]^T [\mathbf{F}^{CS\ joint}] [\mathbf{R}_1^{joint \rightarrow global}] [\mathbf{R}_2^{joint \rightarrow global}] \quad (5.29)$$

### 5.2.7. Insert global flexibility matrix in FEMAP

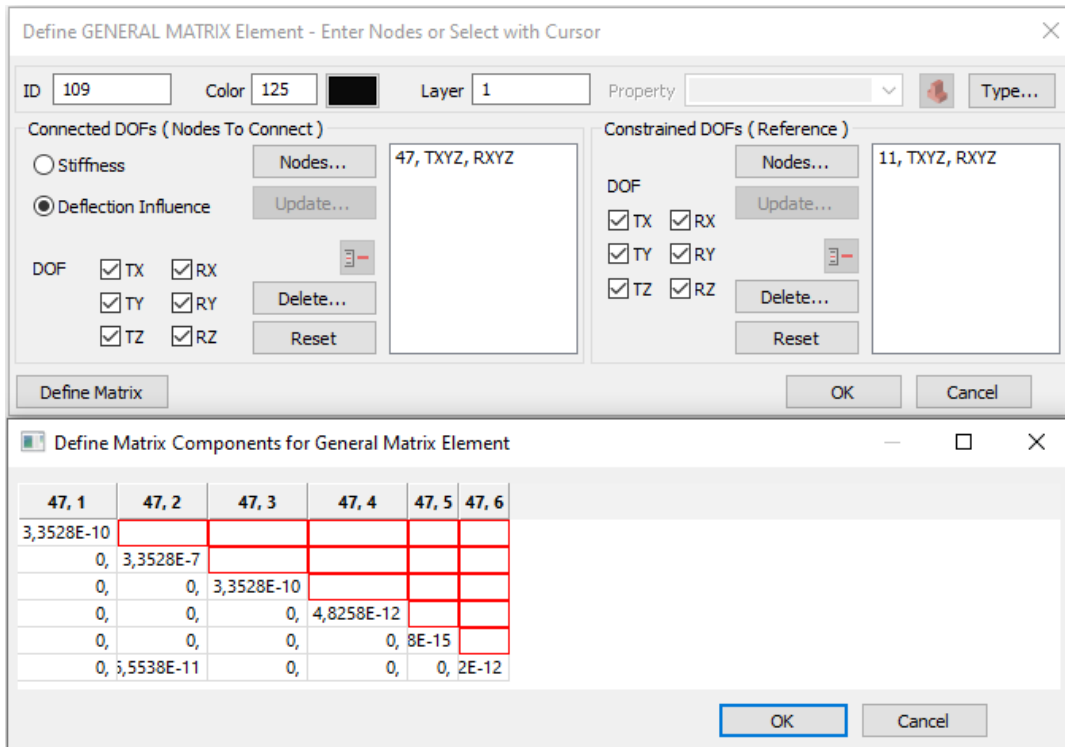
To insert the global flexibility matrix in FEMAP a new element is created. The beam members of the braces are split in two parts at the location where the brace element intersects the outer chord wall. The brace extension element, located within the chord surface, is replaced for a general element, also referred to as GENEL [52]. With the GENEL, flexibilities between nodes can be inserted directly in the Simcenter NASTRAN solver. The GENEL is available from FEMAP version 2020.2 on-wards. Flexibilities in the GENEL are oriented in the global coordinate system. Via the button 'define matrix' the flexibilities between the nodes can be inserted. Two examples are shown in figure 5.6 and 5.7.

The flexibilities are inserted excluding rigid body motions. The rigid body motions are computed by FEMAP itself. Therefore, the node located at the center of the chord. The flexibility matrix including rigid body modes is defined as:

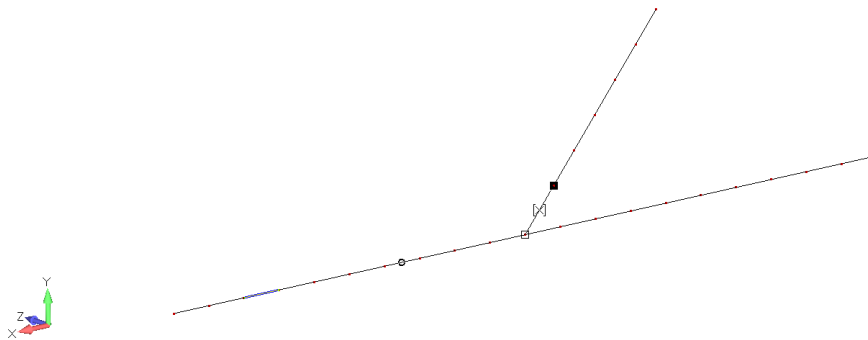
$$\begin{bmatrix} \underline{\Delta}_F \\ \underline{P}_C \end{bmatrix} = \begin{bmatrix} [\mathbf{F}^{global}] & [\mathbf{S}] \\ [-\mathbf{S}]^T & [\mathbf{0}] \end{bmatrix} \begin{bmatrix} \underline{P}_F \\ \underline{\Delta}_C \end{bmatrix} \quad (5.30)$$

Because the flexibility matrix is theoretically symmetrical, only the lower half of the matrix can be inserted in FEMAP. In chapter 4, it is found that the LJF matrix is not always symmetrical. Therefore the average flexibility of two transposed flexibilities is taken:

$$\overline{f}_{ij} = \frac{f_{ij} + f_{ji}}{2} \quad (5.31)$$



(a) Input window



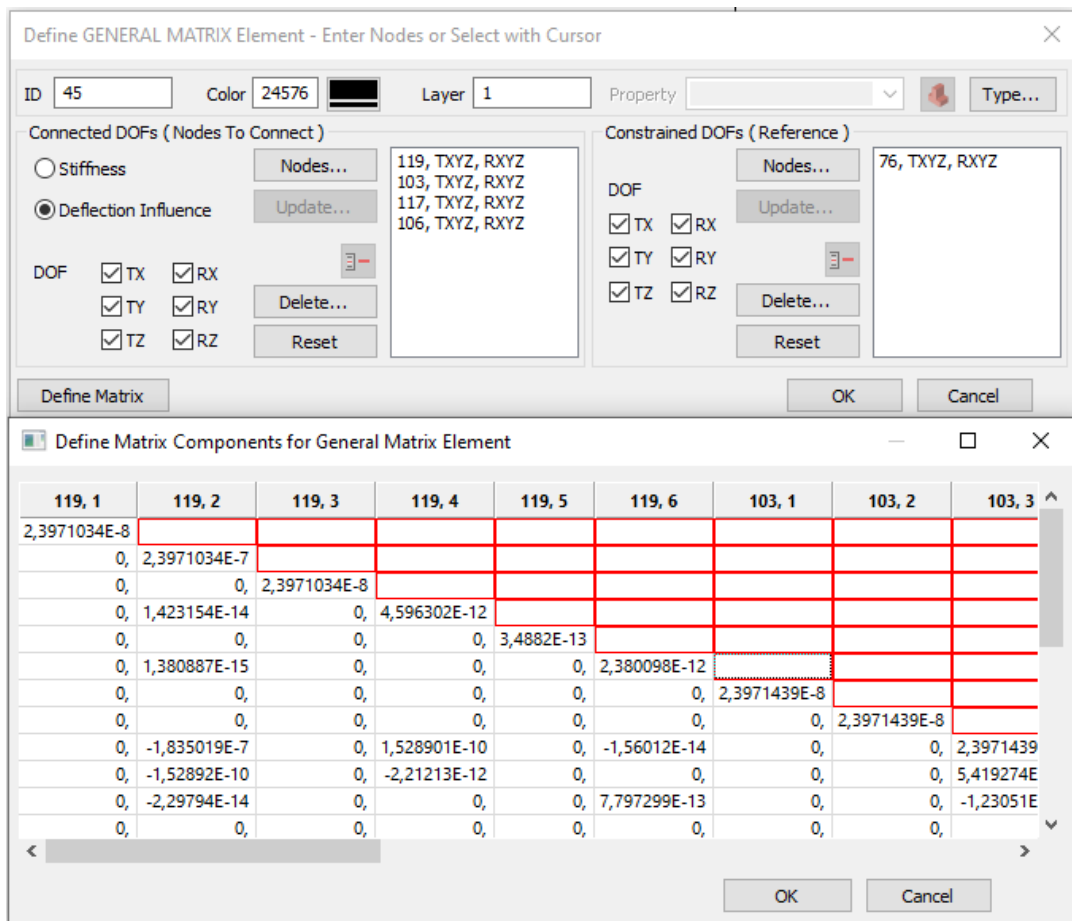
(b) GENEL in FEMAP environment

Figure 5.6: Example of insertion of the GENEL in FEMAP for a single-brace joint

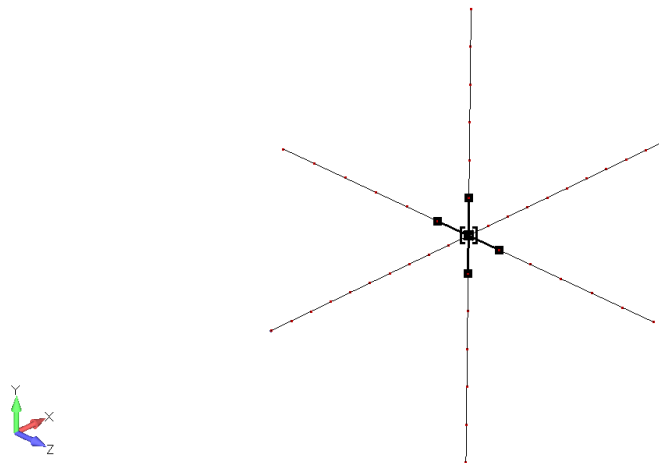
### 5.3. Verification

The methodology is verified by comparison of the deformations caused by an unit-load, according to the beam model without LJF element, the beam model with LJF and the shell model. Deformations according to the shell model are computed with the method applied in sub-section 4.2.3 and 4.5.3. The deformations are represented in matrix  $[\Delta]$ . The deformations according to the beam model are retrieved from FEMAP and transformed to the local coordinate system of the brace. Joint geometries discussed in section 4.6, table 4.10 are reused in this section. The joints are referred to as joint 1, 2, 3, and 4.

First the deformations in the single-brace joints 3 and 4 is investigated. The deformations of joint 3 and 4 according to the shell model, the beam model with LJF element and the beam model without LJF element, as effect of different unit-loads are shown in table 5.2 and 5.1. It can be seen that the



(a) Input window



(b) GENEL in FEMAP environment

Figure 5.7: Example of insertion of the GENEL in FEMAP for a multi-brace joint

deformations according to the shell model and beam model with LJF element are equal. This result is also expected because the implementation of LJF in a beam model is a purely mathematical procedure. Small deviations are observed in the off-diagonal flexibilities of joint 3. The deviations are caused through averaging of transposed flexibilities, discussed in sub-section 5.2.7. The deviations do origin in uncertainties in the methodology which is used to determine the LJF.

Table 5.1: Comparison of local chord wall deformations joint 4 according to a model with shell elements, beam model with LJF and a beam model without LJF

	Local chord wall deformations joint 4 as effect of load case $j$ [mm] or [rad]								
	j=1 (100 [kN])			j=2 (1000 [Nm])			j=3 (1000 [Nm])		
	Shell	Beam with LJF	Beam without LJF	Shell	Beam with LJF	Beam without LJF	Shell	Beam with LJF	Beam without LJF
$\delta_{1j}$	-3.34e-2	-3.34e-2	-5.27e-3	0	0	0	0	0	0
$\delta_{2j}$	0	0	0	5.09e-6	5.10e-6	1.27e-6	0	0	0
$\delta_{3j}$	0	0	0	0	0	0	2.51e-6	2.51e-6	1.27e-6

Table 5.2: Comparison of local chord wall deformations joint 3 according to a model with shell elements, beam model with LJF and a beam model without LJF

	Local chord wall deformations joint 3 as effect of load case $j$ [mm] or [rad]								
	j=1 (100 [kN])			j=2 (1000 [Nm])			j=3 (1000 [Nm])		
	Shell	Beam with LJF	Beam without LJF	Shell	Beam with LJF	Beam without LJF	Shell	Beam with LJF	Beam without LJF
$\delta_{1j}$	1.97e-2	1.97e-2	6.88e-3	0	0	0	4.65e-5	3.60e-5	0
$\delta_{2j}$	0	0	0	2.83e-6	2.83e-6	1.66e-6	0	0	0
$\delta_{3j}$	3.26e-6	3.99e-6	0	0	0	0	1.76e-6	1.76e-6	1.66e-6

The same investigation is performed on multi-brace joints 1 and 2. Plots of the displacements according to the FEA are added, to verify that translations and rotations are performed in the correct direction and DOF. The chord wall deformations and global displacements according to the shell model, the beam model with LJF element and the beam model without LJF element loaded by an unit-load are shown in figure 5.3 up to figure 5.8. It can be seen clearly that the displacements of the beam model with LJF correspond with the displacements of the shell model. In the beam model without LJF no interaction between braces is present. Displacements are solely caused as effect of bending of the chord. As observed for single-brace joints, deviations in off-diagonal deformations according to the beam model with LJF are present due to deviations between transposed flexibilities. This deviations origins in uncertainties of the methodology used to determine the LJF.

## 5.4. Validation

Modelling of LJF in a beam model is a purely mathematical procedure which does not lead to any deviations. This in contrast to implementation via a spring- or customized- beam-element which is discussed in section 2.5. The accuracy in the beam model is purely dependent on the accuracy of the method to determine the LJF. Inaccuracies are introduced because the inserted flexibility matrix is required to be symmetrical. No validation is performed.

## 5.5. Conclusion

A method is developed to model LJF of tubular joints into a beam model. The methodology is developed for FEMAP 2020.2 software. The brace extension element, located within the chord surface is replaced by a GENEL. With the GENEL, flexibilities between nodes, defined in the global coordinate system, can be inserted. Via several transformations and rotations the LJF matrix, obtained in chapter 4 is transformed to the global flexibility matrix in the global coordinate system.

In the verification, it is shown that the methodology works correctly and no deviations are introduced. Because the flexibility matrix is only theoretically symmetrical, before insertion, off-diagonal flexibilities

Table 5.3: Comparison of deformations and displacements, as effect of an axial load on brace 2, according to a shell model, a beam model without LJF and a beam model with LJF.

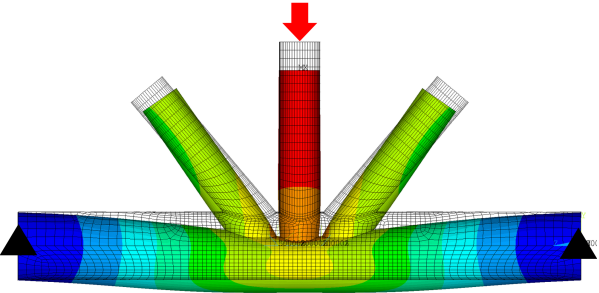
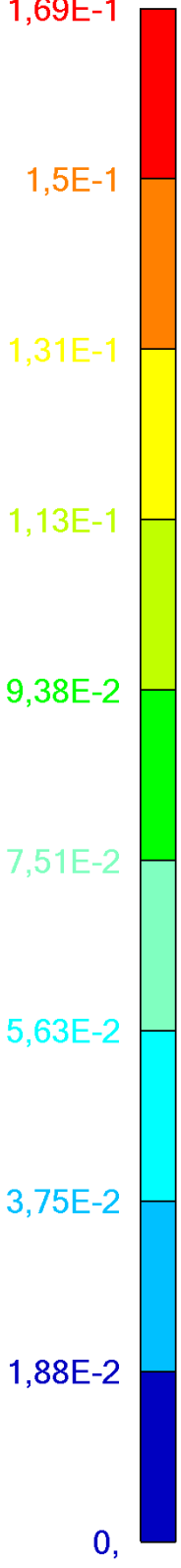
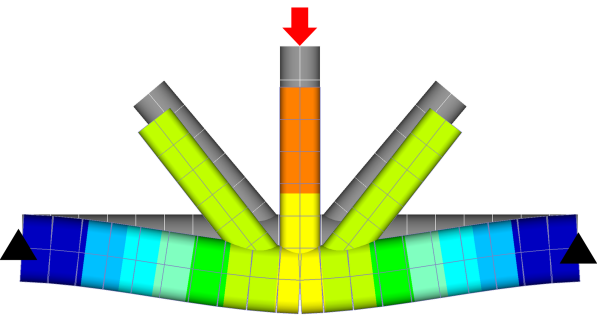
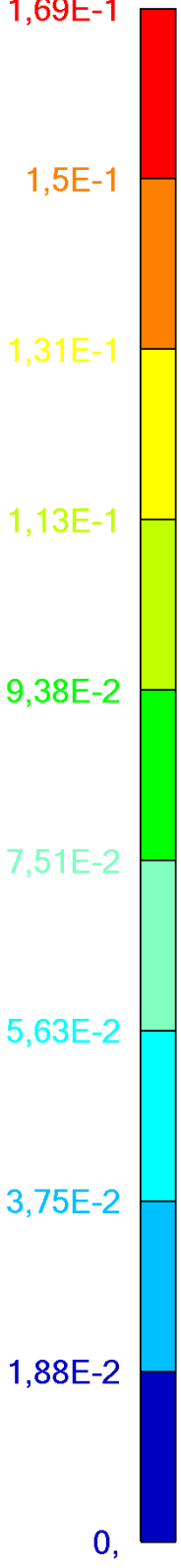
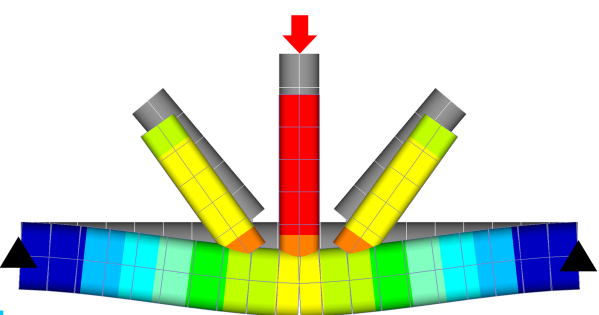
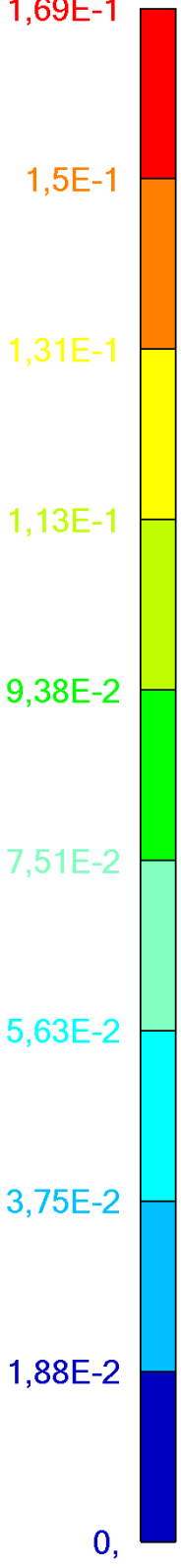
		Effect of axial force (100 kN) on brace 2 ( $i = 4$ )	
	Chord wall de-formation in local brace CS [mm] / [rad]	Global translation [mm]	
Shell model (ANSYS)	$\delta_{41}=1.37e-2$		
	$\delta_{42}=6.60e-10$		
	$\delta_{43}=-2.51e-5$		
	$\delta_{44}=2.94e-2$		
	$\delta_{45}=2.23e-9$		
	$\delta_{46}=1.67e-9$		
	$\delta_{47}=1.37e-2$		
	$\delta_{48}=4.73e-9$		
	$\delta_{49}=2.51e-5$		
Beam model without LJF (FEMAP)	$\delta_{41}=0$		
	$\delta_{42}=0$		
	$\delta_{43}=0$		
	$\delta_{44}=-5.27e-3$		
	$\delta_{45}=0$		
	$\delta_{46}=0$		
	$\delta_{47}=0$		
	$\delta_{48}=0$		
	$\delta_{49}=0$		
Beam model with LJF (FEMAP)	$\delta_{41}=1.83e-2$		
	$\delta_{42}=5.05e-10$		
	$\delta_{43}=-2.25e-5$		
	$\delta_{44}=2.94e-2$		
	$\delta_{45}=1.74e-9$		
	$\delta_{46}=1.03e-90$		
	$\delta_{47}=1.83e-2$		
	$\delta_{48}=5.81e-9$		
	$\delta_{49}=2.25e-5$		

Table 5.4: Comparison of deformations and displacements, as effect of an out-of-plane bending moment on brace 2, according to a shell model, a beam model without LJF and a beam model with LJF.

Effect of out-of-plane bending moment (1000 Nm) on brace 2 ( $i = 5$ )		
	Chord wall de-formation in local brace CS [mm] / [rad]	Global translation [mm]
Shell model (ANSYS)	$\delta_{51}=2.11e-8$	
	$\delta_{52}=1.66e-6$	
	$\delta_{53}=0$	
	$\delta_{54}=1.24e-8$	
	$\delta_{55}=4.53e-6$	
	$\delta_{56}=-0$	
	$\delta_{57}=9.50e-9$	
	$\delta_{58}=1.66e-6$	
	$\delta_{59}=0$	
Beam model without LJF (FEMAP)	$\delta_{51}=0$	
	$\delta_{52}=0$	
	$\delta_{53}=0$	
	$\delta_{54}=0$	
	$\delta_{55}=1.27e-6$	
	$\delta_{56}=0$	
	$\delta_{57}=0$	
	$\delta_{58}=0$	
	$\delta_{59}=0$	
Beam model with LJF (FEMAP)	$\delta_{51}=3.53e-8$	
	$\delta_{52}=2.22e-6$	
	$\delta_{53}=0$	
	$\delta_{54}=1.74e-8$	
	$\delta_{55}=4.53e-6$	
	$\delta_{56}=0$	
	$\delta_{57}=1.83e-8$	
	$\delta_{58}=2.23e-6$	
	$\delta_{59}=0$	

Table 5.5: Comparison of deformations and displacements, as effect of an in-plane bending moment on brace 2, according to a shell model, a beam model without LJF and a beam model with LJF.

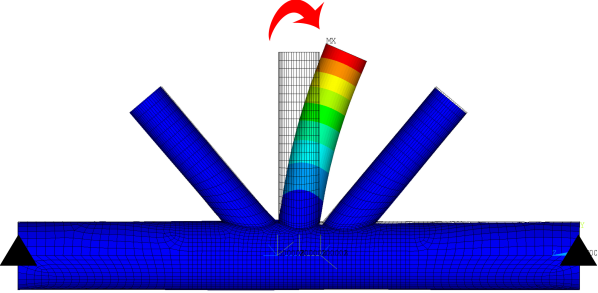
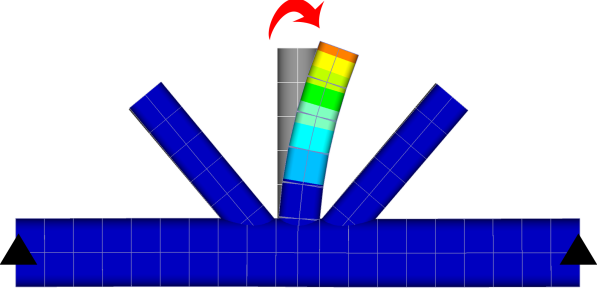
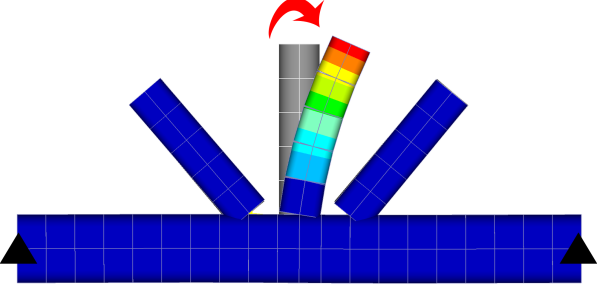
Effect of in-plane bending moment (1000 Nm) on brace 2 ( $i = 6$ )			
	Chord wall de-formation in local brace CS [mm] / [rad]	Global translation [mm]	
Shell model (ANSYS)	$\delta_{61}=2.22e-4$		
	$\delta_{62}=0$		
	$\delta_{63}=4.69e-7$		
	$\delta_{64}=3.88e-9$		
	$\delta_{65}=0$		
	$\delta_{66}=2.14e-6$		
	$\delta_{67}=-2.21e-4$		
	$\delta_{68}=0$		
	$\delta_{69}=-4.69e-7$		
Beam model without LJF (FEMAP)	$\delta_{61}=0$		
	$\delta_{62}=0$		
	$\delta_{63}=0$		
	$\delta_{64}=0$		
	$\delta_{65}=0$		
	$\delta_{66}=1.27e-6$		
	$\delta_{67}=0$		
	$\delta_{68}=0$		
	$\delta_{69}=0$		
Beam model with LJF (FEMAP)	$\delta_{61}=2.95e-4$		
	$\delta_{62}=0$		
	$\delta_{63}=3.87e-7$		
	$\delta_{64}=1.03e-8$		
	$\delta_{65}=0$		
	$\delta_{66}=2.14e-6$		
	$\delta_{67}=-2.95e-4$		
	$\delta_{68}=0$		
	$\delta_{69}=-3.87e-7$		

Table 5.6: Comparison of deformations and displacements, as effect of an axial load on brace 1, according to a shell model, a beam model without LJF and a beam model with LJF.

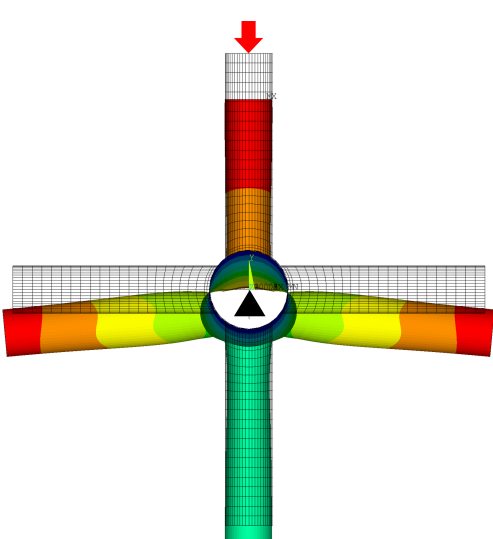
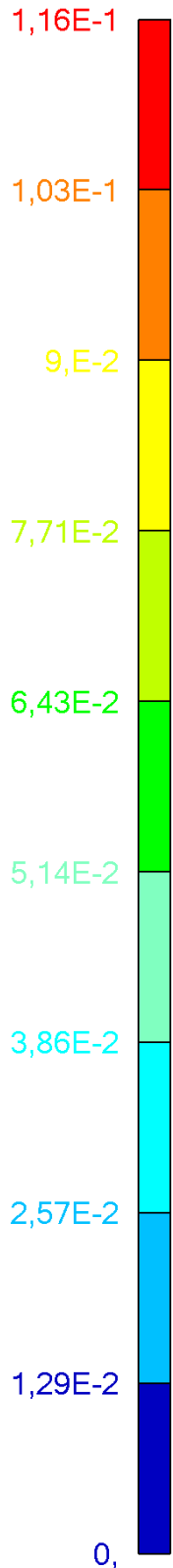
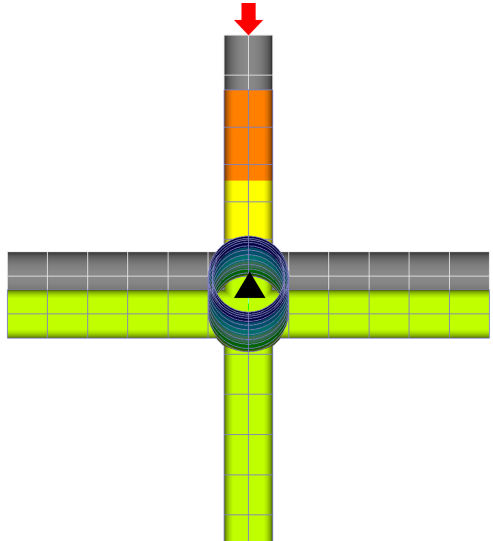
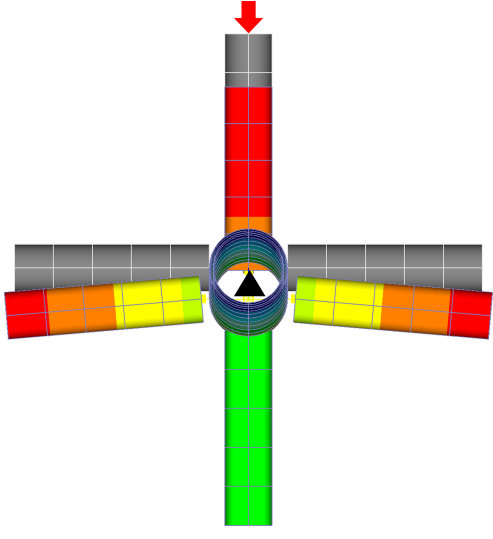
		Effect of axial force (100 kN) on brace 1 ( $i = 1$ )	
	Chord wall de-formation in local brace CS [mm] / [rad]	Global translation [mm]	
Shell model (ANSYS)	$\delta_{11}=2.40e-2$		
	$\delta_{12}=1.45e-9$		
	$\delta_{13}=8.97e-11$		
	$\delta_{14}=-1.84e-2$		
	$\delta_{15}=-1.50e-5$		
	$\delta_{16}=-2.79e-9$		
	$\delta_{17}=1.77e-2$		
	$\delta_{18}=3.13e-9$		
	$\delta_{19}=3.64e-9$		
	$\delta_{1-10}=-1.83e-2$		
	$\delta_{1-11}=1.50e-5$		
	$\delta_{1-12}=1.13e-9$		
Beam model without LJF (FEMAP)	$\delta_{11}=-5.27e-3$		
	$\delta_{12}=0$		
	$\delta_{13}=0$		
	$\delta_{14}=0$		
	$\delta_{15}=0$		
	$\delta_{16}=0$		
	$\delta_{17}=0$		
	$\delta_{18}=0$		
	$\delta_{19}=0$		
	$\delta_{1-10}=0$		
	$\delta_{1-11}=0$		
	$\delta_{1-12}=0$		
Beam model with LJF (FEMAP)	$\delta_{11}=2.40e-2$		
	$\delta_{12}=1.42e-9$		
	$\delta_{13}=1.38e-10$		
	$\delta_{14}=-1.84e-2$		
	$\delta_{15}=-1.53e-5$		
	$\delta_{16}=-1.20e-9$		
	$\delta_{17}=1.77e-2$		
	$\delta_{18}=3.06e-9$		
	$\delta_{19}=2.62e-9$		
	$\delta_{1-10}=-1.84e-2$		
	$\delta_{1-11}=1.53e-5$		
	$\delta_{1-12}=2.30e-9$		

Table 5.7: Comparison of deformations and displacements, as effect of an out-of-plane bending moment on brace 1, according to a shell model, a beam model without LJF and a beam model with LJF.

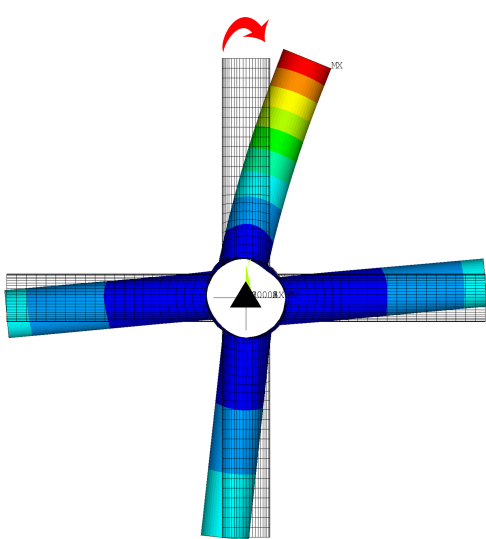
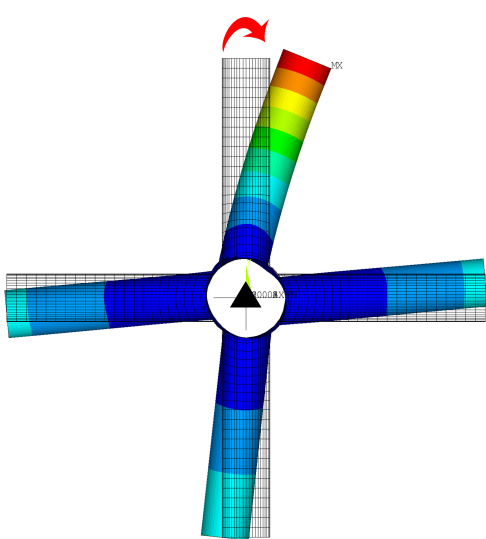
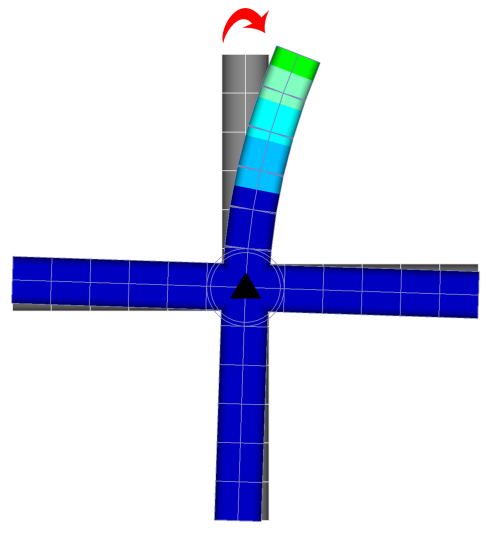
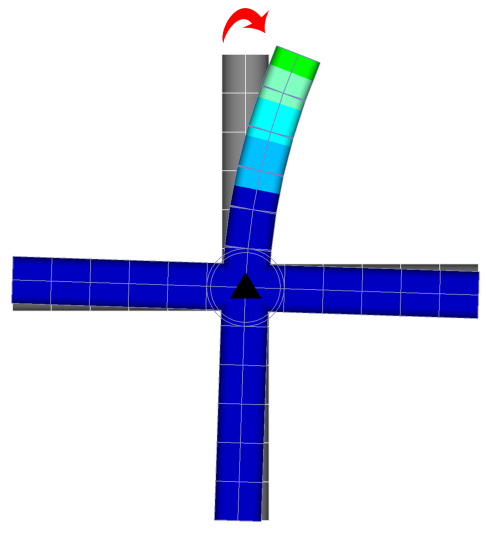
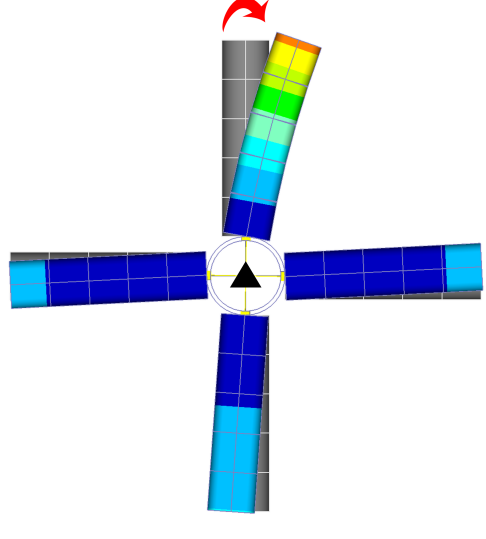
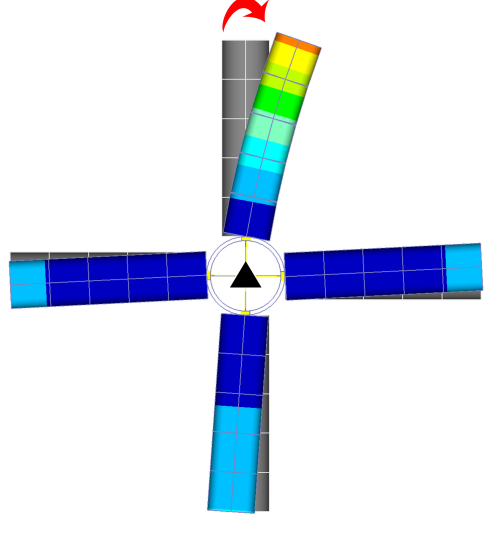
		Effect of out-of-plane bending moment (1000 Nm) on brace 1 ( $i = 2$ )	
		Chord wall de-formation in local brace CS [mm] / [rad]	Global translation [mm]
Shell model (ANSYS)	$\delta_{21}=1.39e-8$		
	$\delta_{22}=4.60e-6$		
	$\delta_{23}=0$		
	$\delta_{24}=1.56e-4$		
	$\delta_{25}=-2.21e-6$		
	$\delta_{26}=0$		
	$\delta_{27}=-1.70e-8$		
	$\delta_{28}=-1.57e-6$		
	$\delta_{29}=0$		
	$\delta_{2-10}=-1.56e-4$		
	$\delta_{2-11}=-2.21e-6$		
	$\delta_{2-12}=0$		
Beam model without LJF (FEMAP)	$\delta_{21}=0$		
	$\delta_{22}=1.27e-6$		
	$\delta_{23}=0$		
	$\delta_{24}=0$		
	$\delta_{25}=0$		
	$\delta_{26}=0$		
	$\delta_{27}=0$		
	$\delta_{28}=0$		
	$\delta_{29}=0$		
	$\delta_{2-10}=0$		
	$\delta_{2-11}=0$		
	$\delta_{2-12}=0$		
Beam model with LJF (FEMAP)	$\delta_{21}=1.42e-8$		
	$\delta_{22}=4.60e-6$		
	$\delta_{23}=0$		
	$\delta_{24}=1.53e-4$		
	$\delta_{25}=-2.21e-6$		
	$\delta_{26}=0$		
	$\delta_{27}=-1.50e-8$		
	$\delta_{28}=-1.57e-6$		
	$\delta_{29}=0$		
	$\delta_{2-10}=-1.53e-4$		
	$\delta_{2-11}=-2.21e-5$		
	$\delta_{2-12}=0$		

Table 5.8: Comparison of deformations and displacements, as effect of an in-plane bending moment on brace 1, according to a shell model, a beam model without LJF and a beam model with LJF.

Effect of in-plane bending moment (1000 Nm) on brace 1 ( $i = 3$ )		
	Chord wall deformation in local brace CS [mm] / [rad]	Global translation [mm]
Shell model (ANSYS)	$\delta_{31} = -3.66e-9$	
	$\delta_{32} = 0$	
	$\delta_{33} = 2.38e-6$	
	$\delta_{34} = 1.19e-8$	
	$\delta_{35} = 0$	
	$\delta_{36} = -7.80e-7$	
	$\delta_{37} = -1.43e-8$	
	$\delta_{38} = 0$	
	$\delta_{39} = 5.36e-7$	
	$\delta_{3-10} = 2.89e-8$	
	$\delta_{3-11} = 0$	
	$\delta_{3-12} = -7.80e-7$	
Beam model without LJF (FEMAP)	$\delta_{31} = 0$	
	$\delta_{32} = 0$	
	$\delta_{33} = -1.27e-6$	
	$\delta_{34} = 0$	
	$\delta_{35} = 0$	
	$\delta_{36} = 0$	
	$\delta_{37} = 0$	
	$\delta_{38} = 0$	
	$\delta_{39} = 0$	
	$\delta_{3-10} = 0$	
	$\delta_{3-11} = 0$	
	$\delta_{3-12} = 0$	
Beam model with LJF (FEMAP)	$\delta_{31} = -3.66e-9$	
	$\delta_{32} = 0$	
	$\delta_{33} = 2.38e-6$	
	$\delta_{34} = 1.37e-8$	
	$\delta_{35} = 0$	
	$\delta_{36} = -7.80e-7$	
	$\delta_{37} = -1.56e-8$	
	$\delta_{38} = 0$	
	$\delta_{39} = 5.36e-7$	
	$\delta_{3-10} = 1.56e-8$	
	$\delta_{3-11} = 0$	
	$\delta_{3-12} = -7.80e-7$	

are averaged with their transposed flexibility. Thereby, small deviations in the off-diagonal flexibilities are introduced. The deviations origin in the inaccuracy of the numerical model which determines the flexibilities of the joint. Because the insertion of the flexibilities is a purely mathematical operation, no validation is performed.

# 6

## Numerical test-case of model with LJF

### 6.1. Introduction

In the previous two chapters, a methodology to determine and model LJF within a beam model is developed. In this chapter, the influence of modelling LJF, on the predicted fatigue life of the joints in the stinger is investigated, through a numerical test-case. The predicted fatigue life according to two models is computed. One model with LJF, and another without LJF. Apart from the difference in LJF, both models are identical. The results according to both models are compared. The setup of the numerical test-case is discussed in section 6.2. The performed fatigue assessment is discussed in section 6.3.

It is observed that through the modification of the flexibility elements, large variations in results appear. To enhance understanding of the influence of modelling LJF, precursory several simplified numerical test-cases are investigated. The preliminary results are discussed in section 6.4. The results of the entire numerical test-case are discussed in section 6.5. In section 6.6, the results are compared to those obtained in literature. In section 6.7, the conclusion is given. Thereby the sub-question: "What is the influence, of accounting for local joint flexibility in a beam model, on the fatigue assessment of a stinger? " is answered.

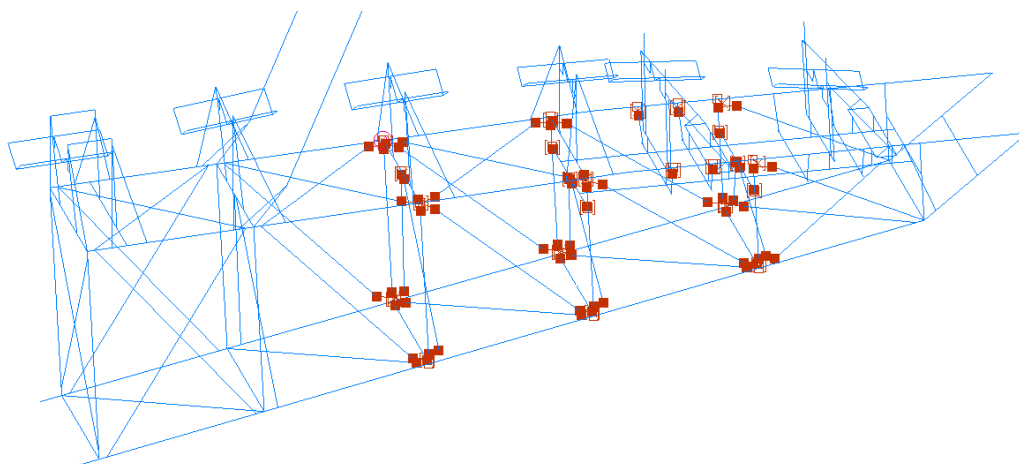


Figure 6.1: Beam model of stinger section 1 with LJF elements.

## 6.2. Numerical test-case setup

In this section, the setup of the numerical test-case is discussed. The numerical test is performed on Solitaire's stinger. Because the fatigue damage is influenced by numerous factors (joint geometry, frame geometry, load-case), it is decided to stick close to the real scenario and avoid simplifications. A beam model in FEMAP of the stinger is made available by Allseas Engineering. For the numerical test-case, two identical models are used. In one model LJF is modelled and in another, no LJF is modelled. The results of both models are compared, in order to determine the influence of modelling LJF in the beam model. In sub-section 6.2.1, the geometry of the joints and stinger is discussed. In sub-section 6.2.2, the load-cases to which the stinger is subjected, are discussed.

### 6.2.1. Geometry and joints of interest

Fatigue assessment is a complex and extensive calculation, hence only a limited number of joints is assessed. Seven joints with a total of 22 braces are investigated. The braces are numbered following *joint-number.brace-number*. E.g. brace 2.3 refers to brace number three of joint number 2. The braces are all located in a single section, shown in figure 6.2. The location of the joints in the stinger is shown in confidential appendix P.1. In figure 6.1 the beam model of Solitaire stinger section 1 with LJF elements is presented. The flexibilities of the brace extension element in a model without LJF, and the LJF of the brace, are presented in appendix N. The geometric parameters of the joints are presented in confidential appendix P.3.

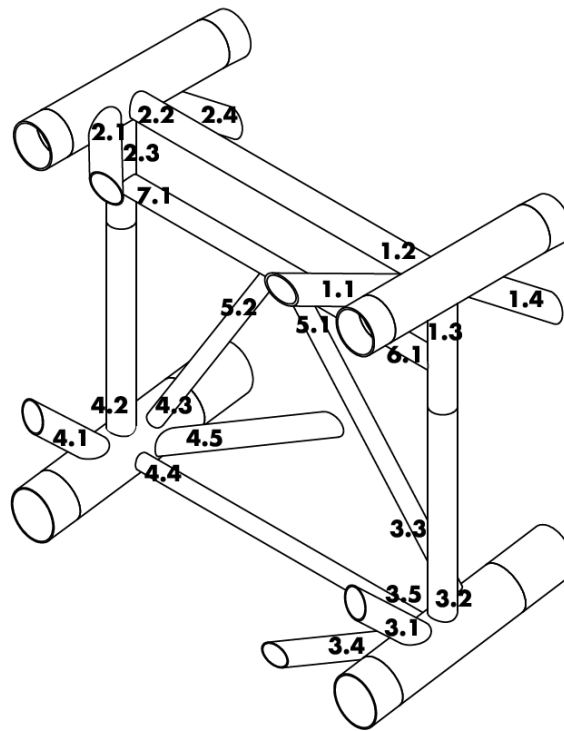


Figure 6.2: Overview of braces/joints of interest.

The joints are located in one plane, distant from stiffeners and additional boundary conditions in the stinger. In section 3.2, the joints are categorized. The selection of joints covers joints of *category 1, 3, and 4*. The model is not able to calculate the flexibilities for joints with  $\beta = 1$  in *category 2*, due to limitations of the geometry in the FEA. However, in section 4.4.2, it can be seen that the flexibility of the brace extension element and the LJF, for high  $\beta$  values is comparable. It is expected that not modelling LJF in the X-joint does not lead to large deviations.

The geometry of the stinger is asymmetrical. Moreover, on the port-side of the stinger, a damper is

attached to prevent the stinger to swing in the horizontal plane. Therefore, comparable fatigue damage and fatigue life of symmetrical braces on starboard and port-side of the stinger is not guaranteed.

### 6.2.2. Load-case

The numerical test-case is limited to the hydrodynamic loads due to waves. Functional loads are not considered. The hydrodynamic loads are provided by Allseas. The hydrodynamic loads as effect of the waves on the stinger are computed in AQWA simulations. A statistical analysis is applied to find the maximum and minimum forces on the stinger in surge, sway and heave direction, with a probability of exceedance of  $10^{-3}$  during 3-hours of exposure. The maximum and minimum force in three dimensions are applied on the beam model in six sub-load-cases ( $F_{x-max}$ ,  $F_{y-max}$ ,  $F_{z-max}$ ,  $F_{x-min}$ ,  $F_{y-min}$  and  $F_{z-min}$ ). The different sub-load-cases later determine the stress range in the joints as effect of the load-case. The forces are applied on the nodes in the beam model.

During the study, it is found that the fatigue damage is strongly load-case dependent (sub-section 6.4.3). However, due to the limitation of the project, application of all possible load-cases is too complex. To retrieve reliable and representative results, the stinger is exposed to a total of sixteen different hydrodynamic load-cases of three hours each. The load-cases concern loads as effect of waves with varying headings, but identical wave height and period. An overview of the load-cases is presented in table 6.1. The definition of the wave heading is shown in figure 6.3.

Table 6.1: Overview of load-cases

load-case	wave height [m]	wave heading [°]	wave period [s]	exposure time [hrs]
1	2.5	0	8.5	3
2	2.5	22.5	8.5	3
3	2.5	45	8.5	3
4	2.5	67.5	8.5	3
5	2.5	90	8.5	3
6	2.5	112.5	8.5	3
7	2.5	135	8.5	3
8	2.5	157.5	8.5	3
9	2.5	180	8.5	3
10	2.5	202.5	8.5	3
11	2.5	225	8.5	3
12	2.5	247.5	8.5	3
13	2.5	270	8.5	3
14	2.5	292.5	8.5	3
15	2.5	315	8.5	3
16	2.5	337.5	8.5	3

## 6.3. Fatigue assessment

The fatigue assessment is performed following the procedure applied by Allseas [25]. The procedure follows DNV-RP-C203 [23]. A simplified schematic overview of the fatigue assessment approach for tubular joints in a stinger, used by Allseas is presented in figure 1.3. The fatigue assessment is performed for each of the 22 braces.

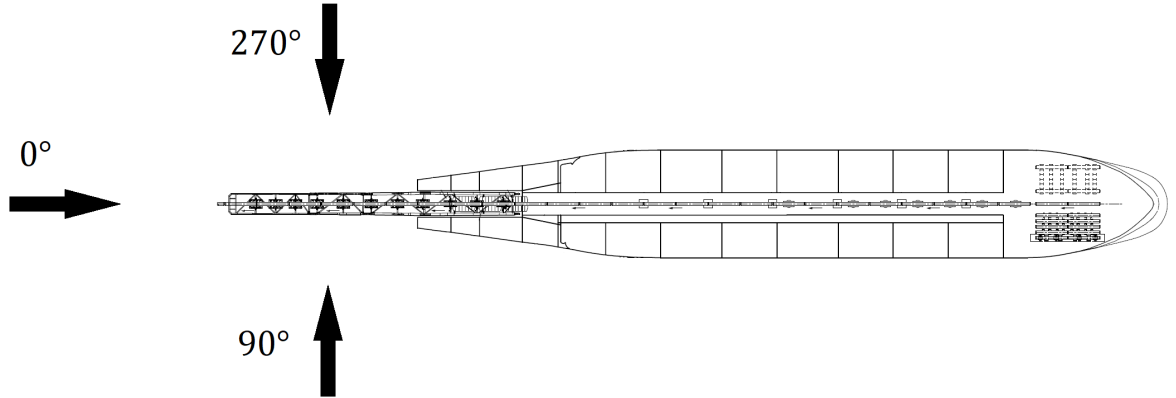


Figure 6.3: Definition of wave heading.

### 6.3.1. Member-loads and nominal stresses

The input of the fatigue assessment are the member-forces on the braces, according to the beam model, as effect of each sub-load-case. This concerns the axial force and the out-of-plane- and in-plane- bending moment. The FEA is solved for every sub-load-case. The beam member loads are defined in the coordinate system of the brace as shown in figure 6.5. The nominal stresses due to axial force ( $\sigma_x$ ), out-of-plane bending moment ( $\sigma_{mz}$ ) and in-plane bending moment ( $\sigma_{my}$ ), are calculated following:

$$\sigma_x = \frac{F_{AX}}{A} \quad (6.1)$$

$$\sigma_{my} = \frac{M_{IPB}}{W} \quad (6.2)$$

$$\sigma_{mz} = \frac{M_{OPB}}{W} \quad (6.3)$$

$$W = \frac{I}{r} \quad (6.4)$$

### 6.3.2. Hot spot stress range

With the nominal stresses, the hot spot stresses at sixteen locations in the chord/brace intersection, as effect of each sub-load-case, are computed. The locations are also referred to as 'hot spots'. Eight hot spots are located on the chord wall and eight hot spots are located on the brace wall, as shown in figure 6.6. Superposition of the hot-spot stresses is applied. The hot spot stresses are computed in every hot spot as effect of each sub-load-case. The difference in stress among the sub-load-cases determines later the stress range in each hot spot. The hot spot stresses are computed with the following equations[23]:

$$\sigma_1 = SCF_{AC}\sigma_x + SCF_{MIP}\sigma_{my} \quad (6.5)$$

$$\sigma_2 = \frac{1}{2}(SCF_{AC} + SCF_{AS})\sigma_x + \frac{1}{2}\sqrt{2} SCF_{MIP}\sigma_{my} - \frac{1}{2}\sqrt{2} SCF_{MOP}\sigma_{mz} \quad (6.6)$$

$$\sigma_3 = SCF_{AS}\sigma_x - SCF_{MOP}\sigma_{mz} \quad (6.7)$$

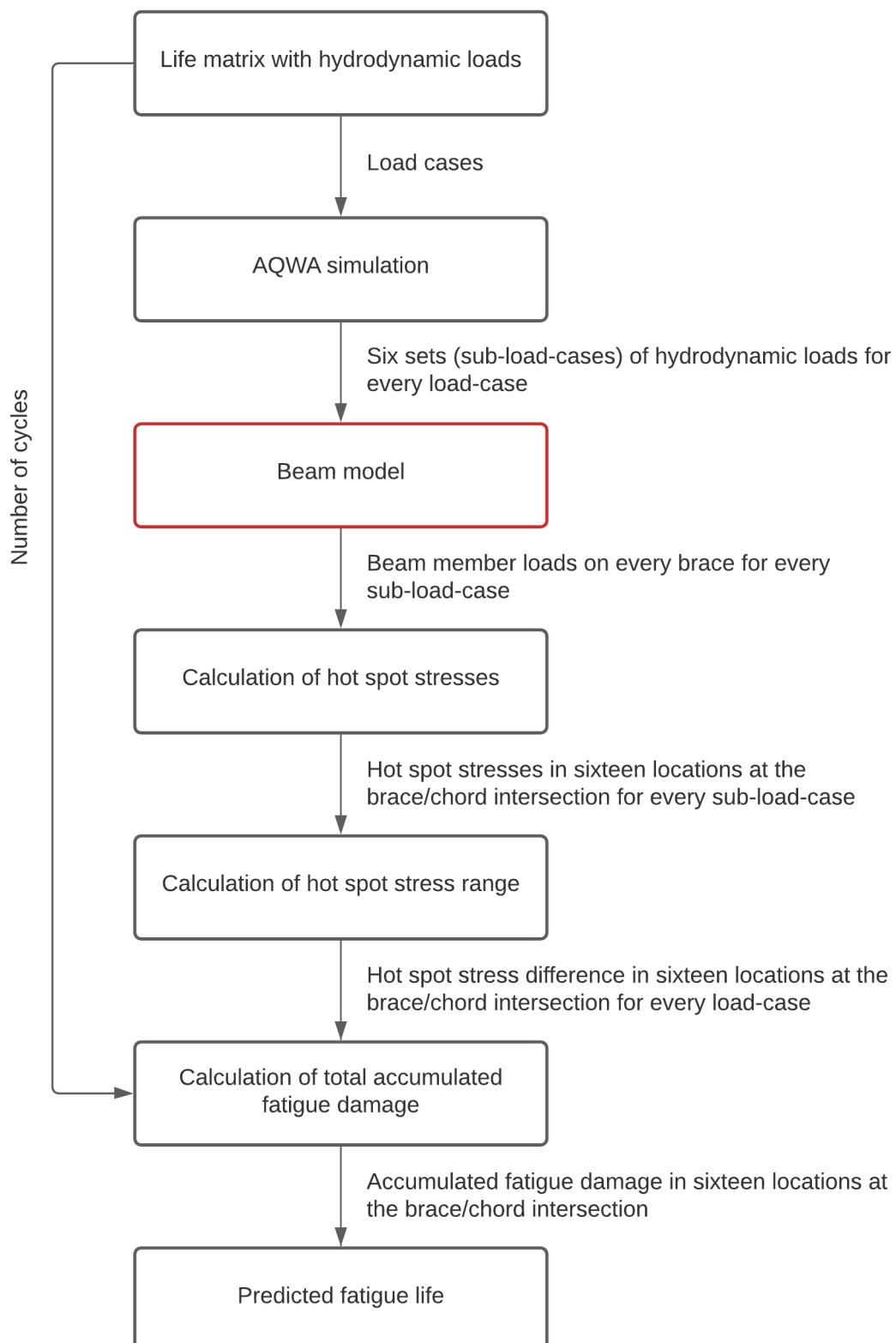


Figure 6.4: Schematic overview of the fatigue assessment for tubular joints in a beam model

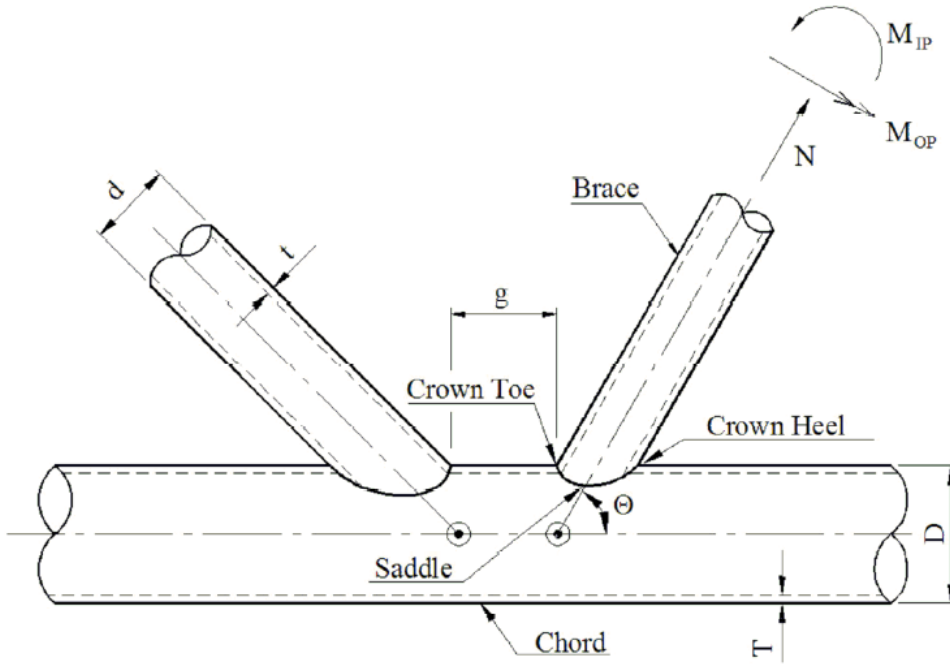


Figure 6.5: Orientation of the member loads according to DNV [23].

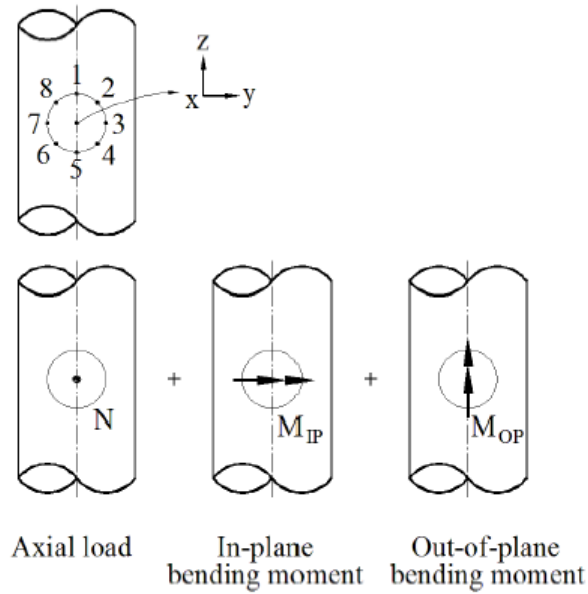


Figure 6.6: Hot spot locations and superposition of stresses [23]

$$\sigma_4 = \frac{1}{2}(SCF_{AC} + SCF_{AS})\sigma_x - \frac{1}{2}\sqrt{2} SCF_{MIP}\sigma_{my} - \frac{1}{2}\sqrt{2} SCF_{MOP}\sigma_{mz} \tag{6.8}$$

$$\sigma_5 = SCF_{AC}\sigma_x - SCF_{MIP}\sigma_{my} \tag{6.9}$$

$$\sigma_6 = \frac{1}{2}(SCF_{AC} + SCF_{AS})\sigma_x - \frac{1}{2}\sqrt{2} SCF_{MIP}\sigma_{my} + \frac{1}{2}\sqrt{2} SCF_{MOP}\sigma_{mz} \quad (6.10)$$

$$\sigma_7 = SCF_{AS}\sigma_x + SCF_{MOP}\sigma_{mz} \quad (6.11)$$

$$\sigma_8 = \frac{1}{2}(SCF_{AC} + SCF_{AS})\sigma_x + \frac{1}{2}\sqrt{2} SCF_{MIP}\sigma_{my} + \frac{1}{2}\sqrt{2} SCF_{MOP}\sigma_{mz} \quad (6.12)$$

SCF's (Stress Concentration Factors) are computed following parametric equations of DNV [23]. The equations are presented in appendix J. SCF's are joint geometry but also joint classification dependent. The joint classification is dependent on the member-loads, in particular the forces perpendicular to the chord wall. These decide whether SCF's for Y- or K-joints are applied. For every sub-load-case the joint can have a different classification. Furthermore, joint classification is not limited to one classification but can be a combination of two classifications. In that regard, the SCF is a combination of the SCF's of both classifications, following:

$$SCF = \lambda_Y SCF_Y + \lambda_K SCF_K \quad (6.13)$$

Here  $\lambda$  represents the fraction of the joint classification. The fraction of classification is calculated following:

$$\lambda_K = \frac{F_{AXa} \sin \theta_a}{-F_{AXb} \sin \theta_b} \quad (6.14)$$

$$\lambda_Y = 1 - \lambda_K \quad (6.15)$$

In appendix K.2, several examples of joint classification according to DNV [23] are presented. In confidential appendix P, the SCF's of the seven joints of consideration are presented. The hot spot stress in the sixteen hot spots is computed for each sub-load-case. The hot spot stress range, notated with  $\Delta\sigma$ , is computed for the maximum stress difference in every hot spot among the six sub-load-cases. This can be a different combination of sub-load-cases for every hot spot.

### 6.3.3. Accumulated fatigue damage

With the hot spot stress range, the accumulated fatigue damage in each hot spot, as result of exposure to the load-case is calculated. The basic design S-N curve is given as:

$$\log N = \log a - m \log \left( \Delta\sigma \left( \frac{t}{t_{ref}} \right)^k \right) \quad (6.16)$$

Here:

- $N$  = predicted number of cycles to failure
- $\Delta\sigma$  = stress range [MPa]
- $m$  = negative inverse of slope of S-N curve
- $\log a$  = intercept of log N-axis by design S-N curve
- $t_{ref}$  = reference thickness [mm], 16 for tubular joints [23]
- $t$  = thickness through which the crack will grow [mm].  $t = t_{ref}$  for thicknesses less than  $t_{ref}$
- $k$  = thickness exponent

The DNV [23] S-N curve for tubular joints in air is applicable (figure 6.7). This is a two slope curve. The following parameters are taken:

$$\begin{aligned}
m_1 &= 3.0 \\
\log a_1 &= 12.480 \\
m_2 &= 5.0 \\
\log a_2 &= 16.130 \\
\sigma_0 &= 67.09 \text{ [MPa]} \\
k &= 0.25 \\
t_{ref} &= 16 \text{ [mm]}
\end{aligned}$$

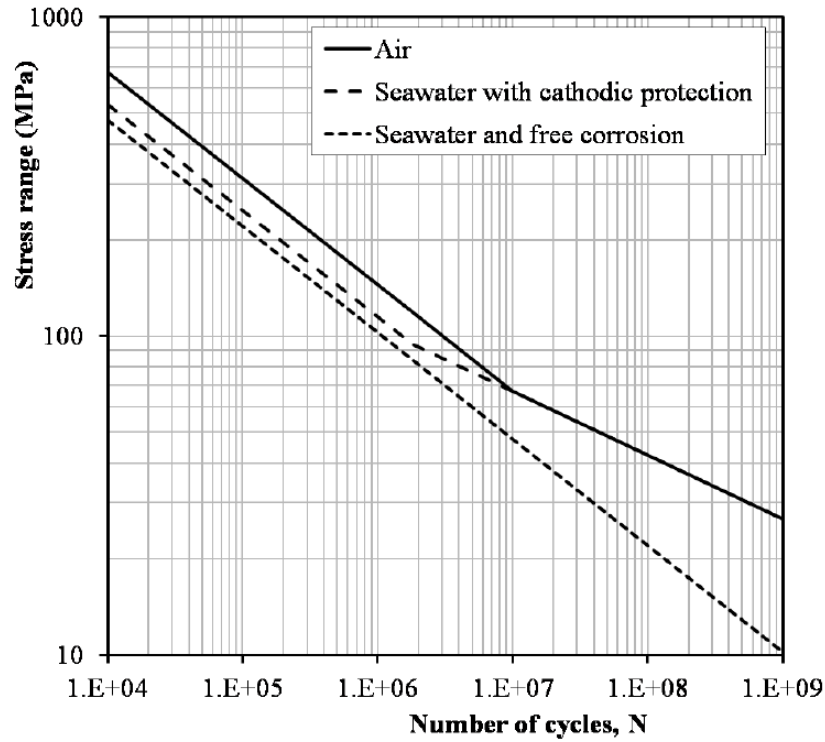


Figure 6.7: S-N curve for tubular joints in air and in seawater with cathodic protection [23].

The minimum and maximum stresses, and thereby the stress range  $\Delta\sigma(Q)$  is determined in a 3-hour AQWA run. A probability of exceedance of  $10^{-3}$  is taken, assuming the Rayleigh distribution [14]. The Rayleigh probability density function is given by:

$$f(\sigma) = \frac{2\sigma}{\sigma_{rms}^2} \exp\left(-\frac{\sigma^2}{\sigma_{rms}^2}\right) \quad (6.17)$$

Here  $\sigma_{rms}$  is the mode  $\cdot\sqrt{2}$ . The probability of exceedance  $Q$  is defined as:

$$Q = \int_{\sigma(Q)}^{\infty} f(\sigma) d\sigma \quad (6.18)$$

Combining equations 6.17 and 6.18 gives:

$$\sigma_{rms} = \frac{\Delta\sigma(Q)}{\sqrt{-\ln Q}} \quad (6.19)$$

The accumulated fatigue damage is calculated following the Palmgren-Miner rule and the two slope S-N curve, including a correction due to wall thickness [25]:

$$D = n_0 \left[ \frac{(\sigma_{rms} * corr)^{m_1}}{a_1} \Gamma \left( \frac{m_1}{2} + 1; \left( \frac{\sigma_0}{\sigma_{rms}} \right)^2 \right) + \frac{(\sigma_{rms} * corr)^{m_2}}{a_2} \gamma \left( \frac{m_2}{2} + 1; \left( \frac{\sigma_0}{\sigma_{rms}} \right)^2 \right) \right] \quad (6.20)$$

Here:

- $D$  = accumulated fatigue damage
- $n_0$  = the number of cycles per load case
- $corr$  = correction for wall thickness  $\left( \frac{t}{t_{ref}} \right)^k$
- $\Gamma(a, x)$  = gamma function  $\int_x^\infty t^{a-1} \exp(-t) dt$
- $\gamma(a, x)$  = incomplete gamma function  $\int_0^\infty t^{a-1} \exp(-t) dt$

The stinger is exposed to every load-case for three hours each. With a wave period of 8.5 seconds, a total of  $n_0 = 1270$  cycles have occurred<sup>1</sup>. The accumulated fatigue damage in the hot spots as effect of the sixteen load-cases is the summation of the accumulated damage as effect of each load case, for every hot spot.

#### 6.3.4. Predicted fatigue life

The predicted fatigue life of the brace is dependent on the accumulated damage in the most affected hot spot. When a brace is subjected to multiple load-cases, the accumulated fatigue damage in each hot spot is the summation of the accumulated fatigue damage in each load-case in the hot spot. The predicted fatigue life is dependent on the damage in the most affected hot spot. The predicted fatigue life  $L$  after a life-long exposure to the same load-profile, affecting the total damage in years, is calculated following:

$$L = \frac{T}{D_{mostaffected} * 24 * 365} \quad (6.21)$$

Here  $T$  is the time in hours, in which the damage is accumulated.

<sup>1</sup>The accumulated fatigue damage has a linear relation with the number of cycles. Therefore, the number of cycles does not affect the difference in results according to a model with and without LJJ.

## 6.4. Preliminary results

As result of the modification to a beam model with LJF elements, large alternations in results are observed. The alternations are complex to relate to. In order to verify the results of the model, and understand the influence of modelling LJF, two simplified cases, where LJF is modelled in one single brace solely, are investigated. In sub-section 6.4.1, the results of modelling LJF solely in a brace of which flexibility is underestimated is investigated. In sub-section 6.4.2, the results of modelling LJF solely in a brace of which flexibility is overestimated is investigated. Results are found to be load-case dependent. This is discussed in sub-section 6.4.3.

### 6.4.1. Modelling LJF solely in a brace with underestimated flexibility

In this sub-section, the effect of modelling LJF solely in one brace is discussed. LJF is modelled in brace 1.3. This brace is picked because the flexibility is underestimated in a model without LJF. The most influential (non-dimensional) flexibilities of brace 1.3, in a model with and without LJF, are presented in table 6.2. By modelling LJF, the flexibilities in brace 1.3 increase. The influence of modelling LJF in brace 1.3, is investigated within load-case 6. This load-case has appeared as the most damaging load-case (sub-section 6.4.3) and is thereby considered as a representative load-case.

Table 6.2: Comparison of the diagonal flexibilities (non-dimensional) of brace 1.3 in a model with and without LJF

Non-dimensional flexibility	Model without LJF	Model with LJF
$f_{11}^*[-]$	10.7	53.5
$f_{22}^*[-]$	302.1	953.5
$f_{33}^*[-]$	302.1	495.9

To begin, the member-loads and nominal stresses according to the beam model with and without LJF are compared. The member-loads and nominal stresses on brace 1.3 as effect of the six sub-load-cases of load-case 6, according to both models, are presented in figure 6.8a. As effect of modelling LJF, the axial force in the six sub-load-cases has slightly decreased. The out-of-plane bending moment has reduced with up to 20% for every sub-load-case. The alteration of the in-plane bending moment is sub-load-case dependent. The maximum in-plane-bending moments have decreased and the minimum in-plane moments have increased hence a convergence of bending moment is observed. Analysing the contribution of the member forces to the nominal stress, it can be seen that out-of-plane bending moment causes the largest stresses.

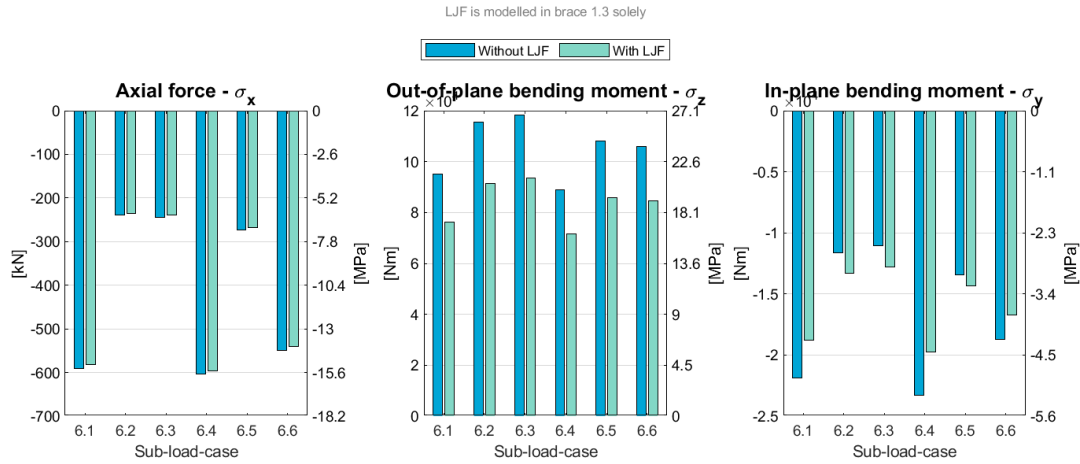
In figure 6.8b the stress range and accumulated fatigue damage, in the sixteen hot spots of brace 1.3 as effect of load-case 6 according to a model with and without LJF is presented. The effect of modelling LJF is different for every hot spot. Through the reduction of member-loads in the model with LJF, the stress ranges have reduced in most hot spots. Especially the hot-spots with the highest stress range, benefit from the decrease. The large decrease of stress range in hot spot 6, 7, 8 (figure 6.6) can be appointed to the decrease in out-of-plane- and in-plane- bending moment.

With the stress range, the accumulated fatigue damage in the hot spots is computed. Through the decrease of stress range in a model with LJF, the accumulated fatigue damage has decreased also. Due to the nature of fatigue, the small reduction in stress range has led to a large reduction in fatigue damage in the hot spots. Especially large decreases in the most damaged hot spots are observed. This is positive because the predicted fatigue life of the brace is determined by the hot spot with the most accumulated damage.

The predicted fatigue life is dependent on the accumulated damage in the most affected hot spot. In this scenario this is hot spot 8 at the chord wall, according to both models. As effect of modelling LJF, the accumulated fatigue damage in the most affected hot spot of brace 1.3 changes with factor:

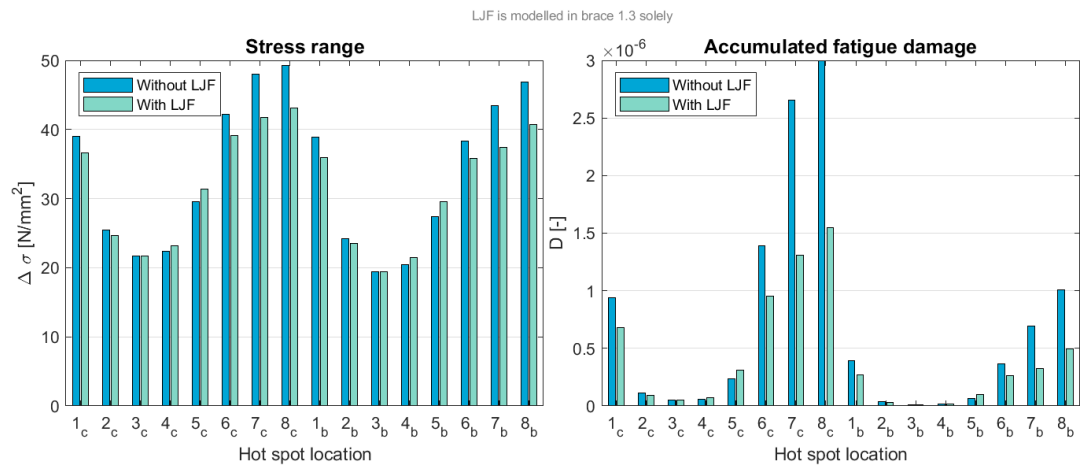
$$\text{Ratio accumulated fatigue damage} = \frac{D_{\text{with LJF}}}{D_{\text{without LJF}}} = \frac{1.55 * 10^{-6}}{2.99 * 10^{-6}} = 0.52 \quad (6.22)$$

Beam-member-loads and nominal stresses on brace 1.3 as effect of load-case 6



(a) Member-loads

Stress range and accumulated fatigue damage in 16 hot spots of brace 1.3 as effect of load-case 6



(b) Stress range and accumulated fatigue damage in 16 hot spots

Figure 6.8: The effects of load-case 6 on brace 1.3

If brace 1.3 would only be exposed to load-case 6, the predicted fatigue life would change, as effect of modelling LJF in brace 1.3, with factor:

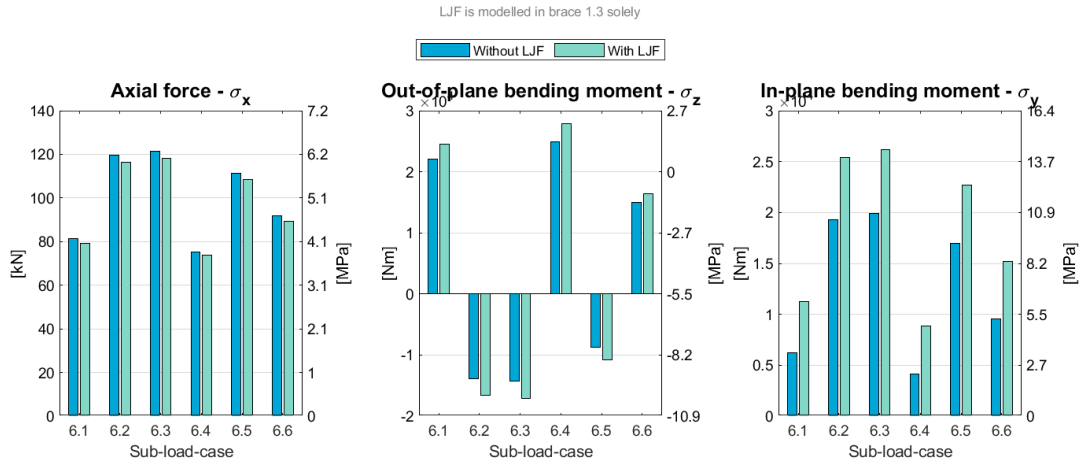
$$Ratio\ predicted\ fatigue\ life = \frac{D_{without\ LJF}}{D_{with\ LJF}} = \frac{2.99 \cdot 10^{-6}}{1.55 \cdot 10^{-6}} = 1.93 \tag{6.23}$$

The predicted fatigue life of brace 1.3 would increase as effect of modelling LJF solely in brace 1.3.

It is shown that as effect of modelling LJF in brace 1.3, the predicted fatigue life of brace 1.3 increases. However, it is observed that member-loads on surrounding braces have altered too. In figure 6.9a, the member-loads and nominal stresses on brace 6.1 as effect of the sub-load-cases of load-case 6 are presented, according to a model with and without LJF. By modelling LJF in brace 1.3, the axial force on brace 6.1 has decreased but the out-of-plane- and in-plane- bending moment on brace 6.1 have increased. Especially the out-of-plane moment increases for both sub-load-cases with positive and negative out-of-plane bending moment. The increase of in-plane bending moment and the divergence of the out-of-plane bending moment will contribute to an increase of stress range.

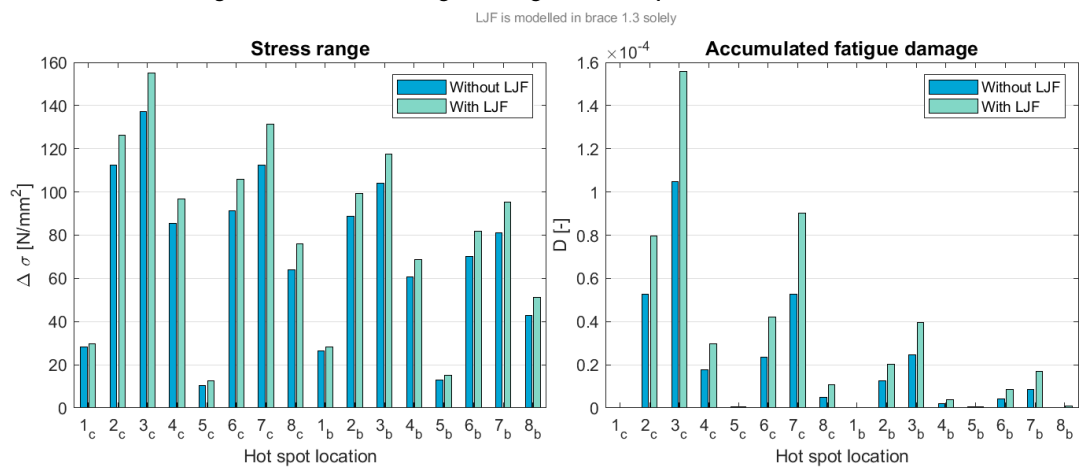
As a consequence of the increased member-loads, the stress range and thereby the accumulated damage, in the hot spots of brace 6.1 have increased. This is shown in figure 6.9b. The effect of

### Beam-member-loads and nominal stresses on brace 6.1 as effect of load-case 6



(a) Member-loads

### Stress range and accumulated fatigue damage in 16 hot spots of brace 6.1 as effect of load-case 6



(b) Stress range and accumulated fatigue damage in 16 hot spots

Figure 6.9: The effects of load-case 6 on brace 6.1

modelling LJF is different for every hot spot. Especially the hot-spots with the highest stress range, encounter the largest accumulated damage increase. As effect of modelling LJF, the accumulated fatigue damage in the most affected hot spot of brace 6.1 changes with factor:

$$\text{Ratio accumulated fatigue damage} = \frac{D_{\text{with LJF}}}{D_{\text{without LJF}}} = \frac{1.56 * 10^{-4}}{1.05 * 10^{-4}} = 1.49 \quad (6.24)$$

If brace 6.1 would only be exposed to load-case 6, the predicted fatigue life would change, as effect of modelling LJF in brace 1.3, with factor:

$$\text{Ratio predicted fatigue life} = \frac{D_{\text{without LJF}}}{D_{\text{with LJF}}} = \frac{1.05 * 10^{-4}}{1.56 * 10^{-4}} = 0.67 \quad (6.25)$$

The predicted fatigue life of brace 6.1 would decrease as effect of modelling LJF solely in brace 1.3.

With this example, it is shown that through modelling LJF the member-loads in the stinger have redistributed. Because the flexibility of brace 1.3 is increased, the member-loads, and thereby the accumulated fatigue damage in the brace have decreased, with a longer predicted fatigue life as result. As side effect, member-loads on surrounding braces and thereby, the accumulated fatigue damage, have increased with a shorter predicted fatigue life as result.

The effect of different load-cases, and the resulting accumulated fatigue damage in the 22 braces after exposure to the sixteen load-cases according to the model with LJF in brace 1.3 and without LJF is discussed in sub-section 6.4.3.

### 6.4.2. Modelling LJF solely in a brace with overestimated flexibility

In section 4.4, it is found that a brace does not always gain flexibility through modelling LJF. For braces with a combination of high  $\beta$ , low  $\gamma$  and low  $\theta$  it is possible that in the beam model the flexibility is overestimated. In this sub-section the effect of modelling LJF in a brace with overestimated flexibility is discussed.

Table 6.3: Comparison of the diagonal flexibilities of brace 1.4 in model with and without LJF

Flexibility	Model without LJF	Model with LJF
$f_{11}^*[-]$	22.0	20.1
$f_{22}^*[-]$	605.5	332.6
$f_{33}^*[-]$	605.5	251.7

LJF is modelled solely in brace 1.4. The most influential non-dimensional flexibilities of brace 1.4 are shown in table 6.3. Through modelling LJF the flexibility of the brace decreases. The influence of modelling LJF in brace 1.4 is investigated for exposure to load-case 4. This load-case has appeared as the most damaging load-case for this brace. (sub-section 6.4.3) and is thereby seen a representative load-case.

Firstly the influence of modelling LJF in brace 1.4 is investigated for the brace itself. The member-loads on brace 1.4 as effect of the six sub-load-cases of load-case 4 according to a model with and without LJF, are presented in figure 6.10a. As effect of modelling LJF the axial force in the six sub-load-cases has slightly reduced. For the out-of-plane bending moment a divergence of bending moments is observed. Large bending moments have increased and small bending moments have decreased. Furthermore, the in-plane bending moment has increased for every sub-load-case.

In figure 6.10b the stress range and accumulated fatigue damage, in the sixteen hot spots of brace 1.4 as effect of load-case 4, according to a model with and without LJF, are presented. It can be seen that the effect of modelling LJF is different for every hot spot. As effect of the increased member-loads in the model with LJF, the stress ranges increased. Especially at the most affected locations, with the largest stress range, the stress range increased. Because of the increase of stress range in a model with LJF, the accumulated fatigue damage has increased also. As effect of modelling LJF, the accumulated fatigue damage in the most affected hot spot of brace 1.4 changes with factor:

$$\text{Ratio accumulated fatigue damage} = \frac{D_{\text{with LJF}}}{D_{\text{without LJF}}} = \frac{1.38 * 10^{-5}}{1.14 * 10^{-5}} = 1.21 \quad (6.26)$$

If brace 1.4 would only be exposed to load-case 4, the predicted fatigue life would change, as effect of modelling LJF in brace 1.4, with factor:

$$\text{Ratio predicted fatigue life} = \frac{D_{\text{without LJF}}}{D_{\text{with LJF}}} = \frac{1.14 * 10^{-5}}{1.38 * 10^{-5}} = 0.83 \quad (6.27)$$

The predicted fatigue life of brace 1.4 would decrease as effect of modelling LJF solely in brace 1.4.

It is shown that as effect of modelling LJF in brace 1.4, its member loads have increased and thereby, the predicted fatigue life decreased. It is observed that member-loads on surrounding braces have decreased. In figure 6.11a the member-loads on brace 1.3 as effect of load-case 4 are presented

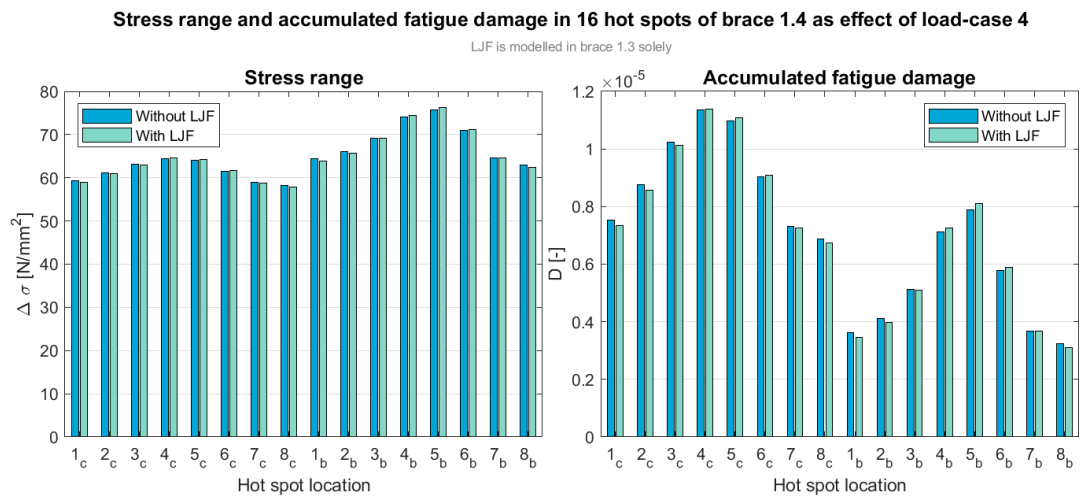
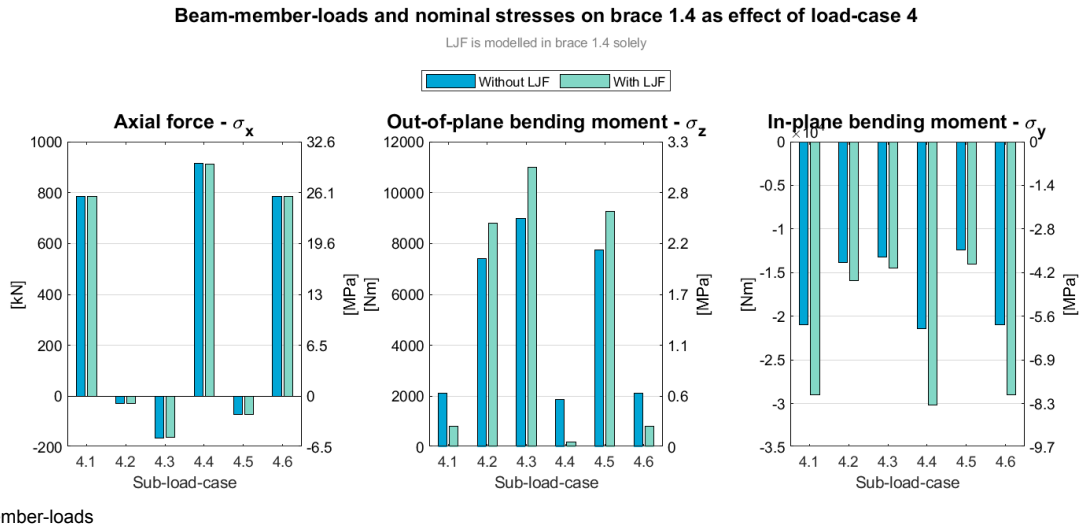


Figure 6.10: The effects of load-case 4 on brace 1.4

according to a model with LJJ and without LJJ. It can be seen that by modelling LJJ in brace 1.4, the axial force on brace 1.3 has decreased and the out-of-plane- and in-plane- bending moment on brace 1.3 have decreased slightly. As a consequence, the stress range in the hot spots and thereby the accumulated fatigue damage in the brace have decreased. This is shown in figure 6.11b. As effect of modelling LJJ, the accumulated fatigue damage in the most affected hot spot of brace 1.3 changes with factor:

$$\text{Ratio accumulated fatigue damage} = \frac{D_{\text{with LJJ}}}{D_{\text{without LJJ}}} = \frac{6.25 * 10^{-6}}{6.51 * 10^{-6}} = 0.96 \quad (6.28)$$

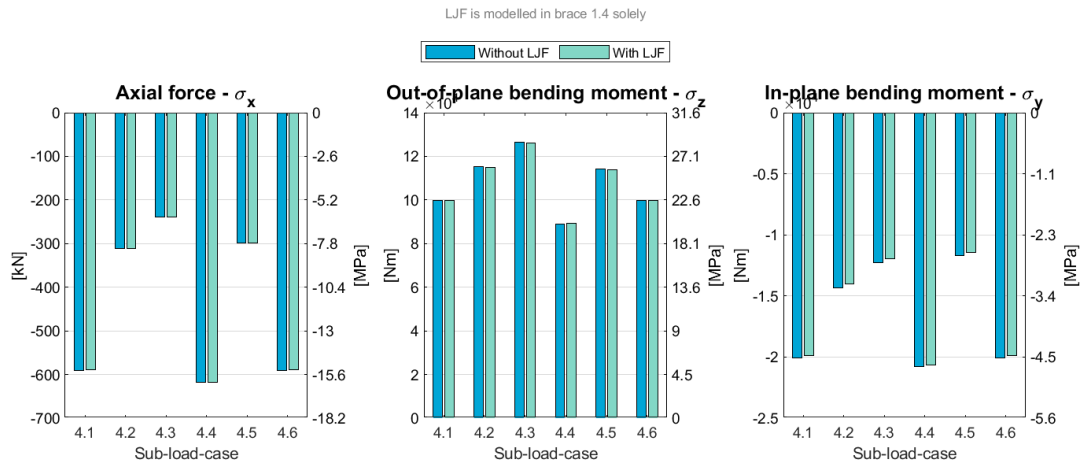
If brace 1.3 would only be exposed to load-case 4, the predicted fatigue life would change, as effect of modelling LJJ in brace 1.4, with factor:

$$\text{Ratio predicted fatigue life} = \frac{D_{\text{without LJJ}}}{D_{\text{with LJJ}}} = \frac{6.51 * 10^{-6}}{6.25 * 10^{-6}} = 1.04 \quad (6.29)$$

The predicted fatigue life of brace 1.3 would increase as effect of modelling LJJ solely in brace 1.4.

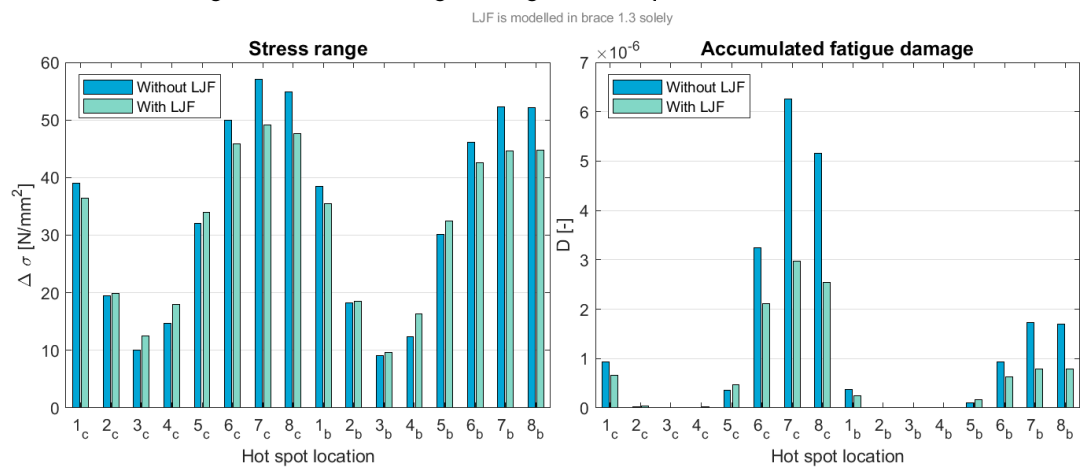
Because the flexibility of brace 1.4 is decreased, the member-loads, and thereby the accumulated fatigue damage in the brace have increased, with a lower predicted fatigue life as result. As side effect,

Beam-member-loads and nominal stresses on brace 1.3 as effect of load-case 4



(a) Member-loads

Stress range and accumulated fatigue damage in 16 hot spots of brace 1.3 as effect of load-case 4



(b) Stress range and accumulated fatigue damage in 16 hot spots

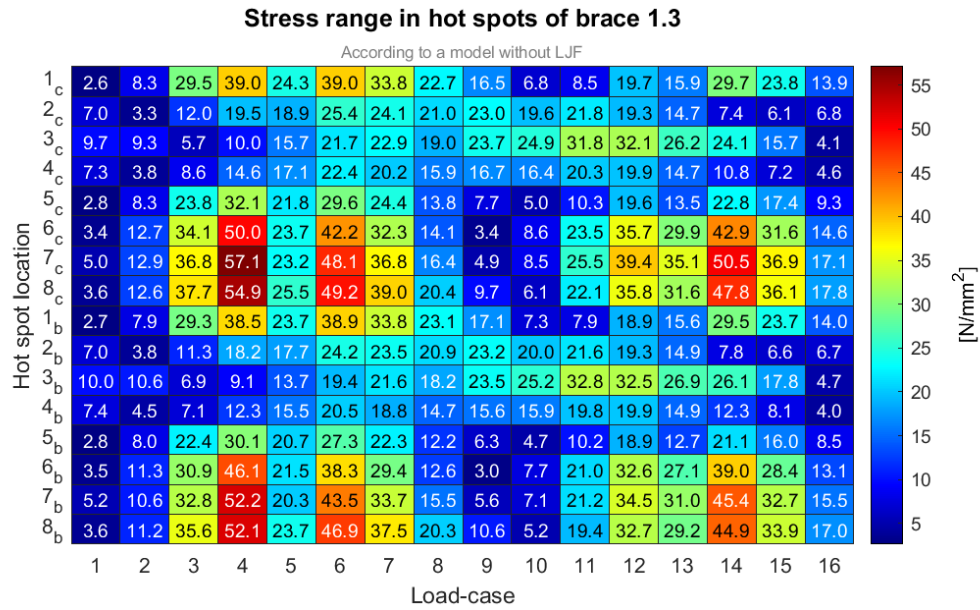
Figure 6.11: The effects of load-case 4 on brace 1.3

member-loads on surrounding braces and thereby, the accumulated fatigue damage have decreased. These braces will have a longer predicted fatigue life as effect of modelling LJF. With this example, it is shown again that through modelling LJF the member-loads in the stinger have redistributed. The effect of different load-cases, and the resulting fatigue damage to the 22 braces after exposure to these sixteen load-cases according to the model with LJF in brace 1.3 and without LJF is discussed in sub-section 6.4.3.

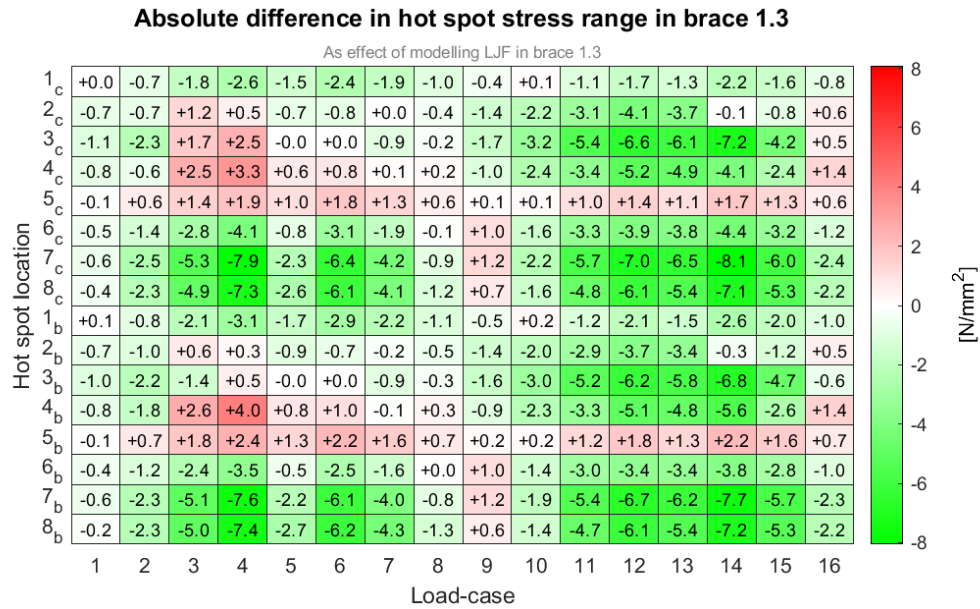
### 6.4.3. Influence of different load-cases

In the previously discussed sub-section, an insight into the effect of modification of the flexibilities of a single brace is given. However, the previously discussed results are obtained for load-cases that are specifically chosen. It is observed that for different load-cases different results are obtained. In this sub-section the differences for different load-cases is discussed.

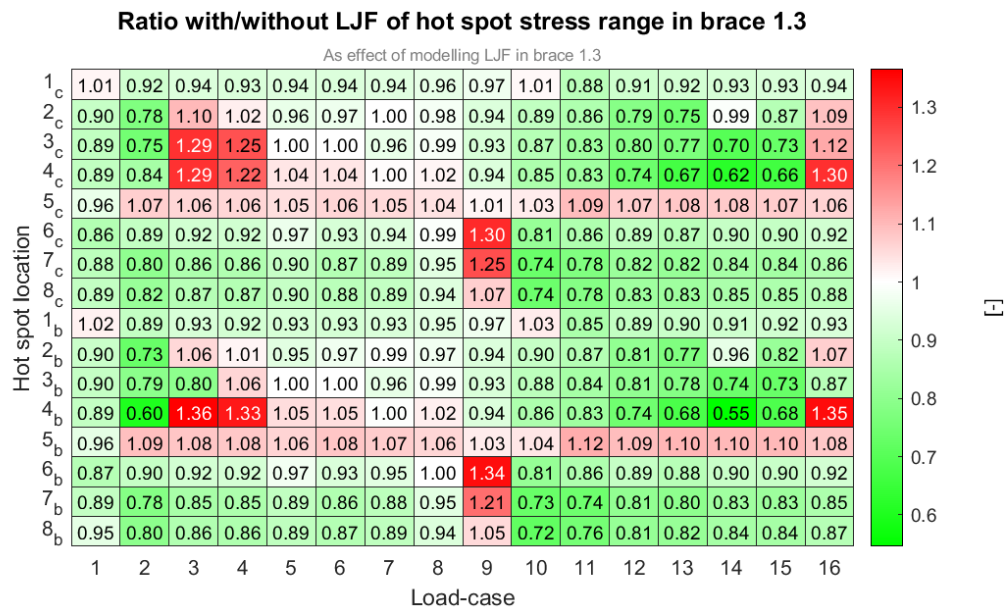
The scenario of modelling LJF solely in brace 1.3, described in sub-section 6.4.1, is investigated again. In figure 6.12a, the stress range in the sixteen hot spots of brace 1.3, as effect of exposure to each of the sixteen load-cases, according to the model without LJF, is presented. The columns represent the different load-cases. The stress ranges in column 6 are equal to the presented stress ranges in figure 6.8b. Load-case 4, 6 and 14 provide the highest stress ranges. The stress range in the hot spots is



(a) According to a model without LJF.

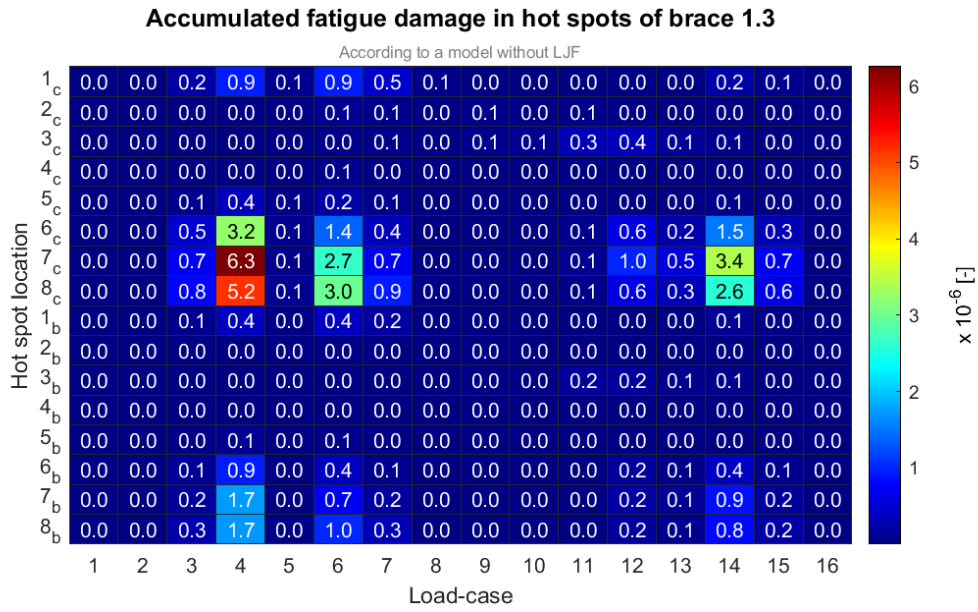


(b) The absolute difference as effect of modelling LJF in brace 1.3

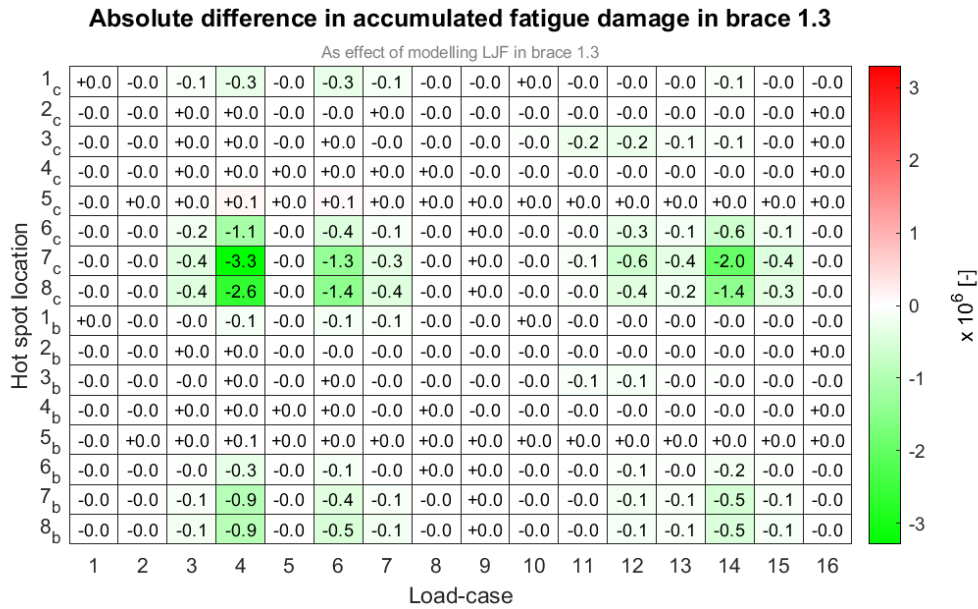


(c) The ratio with/without LJF as effect of modelling LJF in brace 1.3.

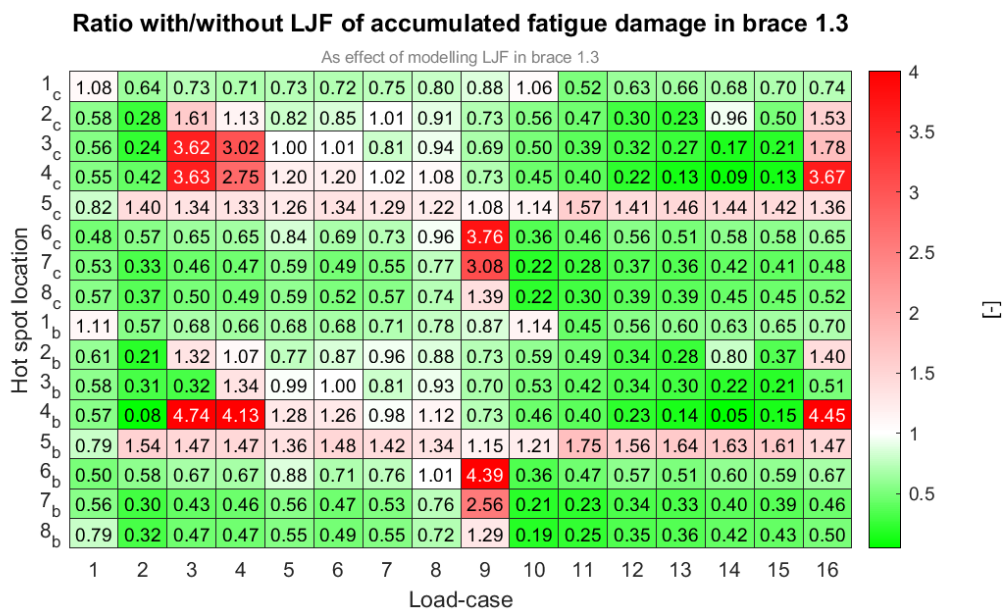
Figure 6.12: The stress range in the hot spots of brace 1.3 as effect of the sixteen load-cases



(a) According to a model without LJF.



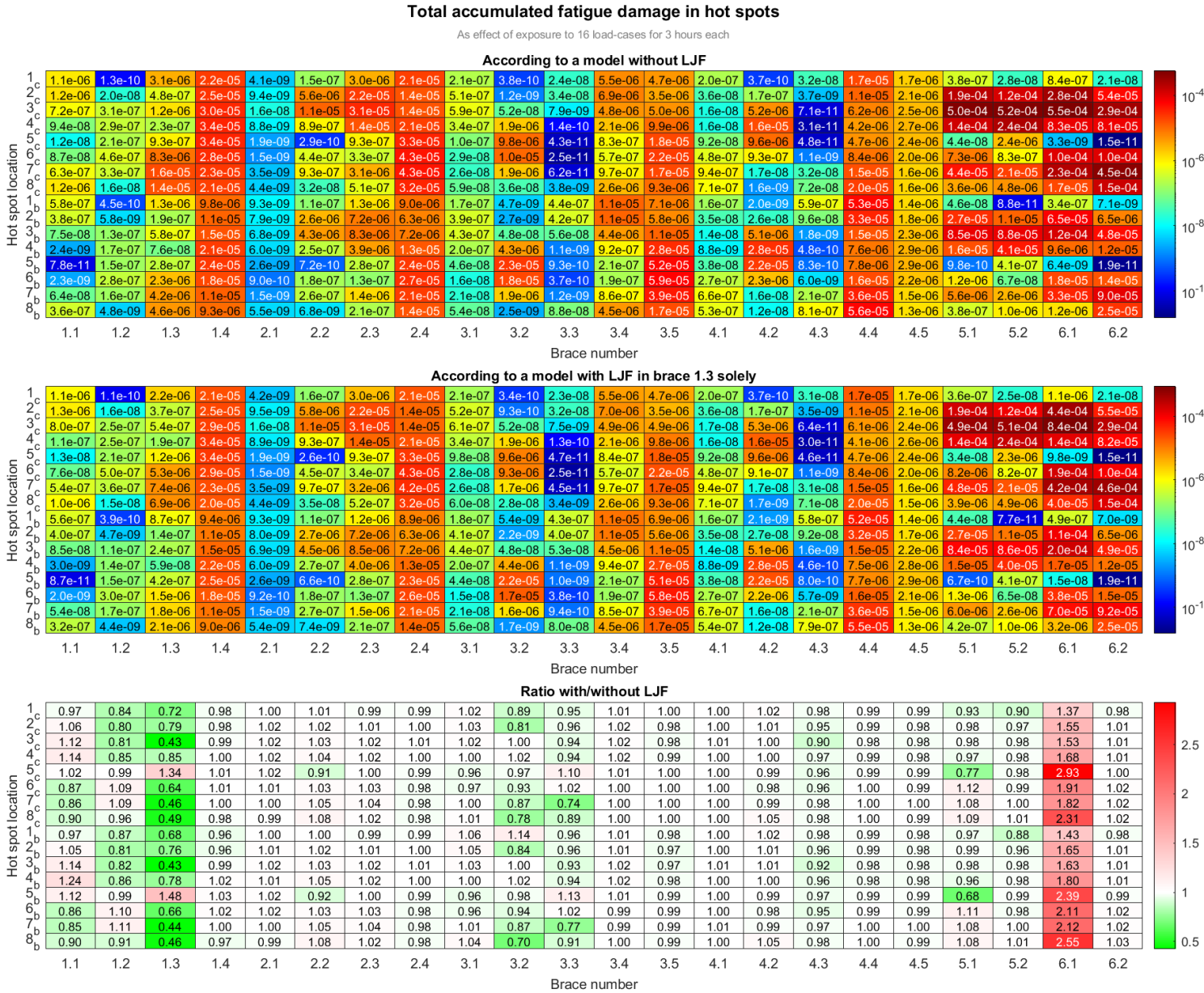
(b) The absolute difference as effect of modelling LjF in brace 1.3



(c) The ratio with/without LjF as effect of modelling LjF in brace 1.3.

Figure 6.13: The accumulated fatigue damage in the hot spots of brace 1.3 as effect of the sixteen load-cases

different for each hot spot and different for each load-case. In figure 6.12b the absolute difference in stress range obtained when modelling LJJ in brace 1.3 is shown. The effect of modelling LJJ is different in each hot spot location and for each load-case. In several hot spots, it is load-case dependent whether the stress range increases or decreases. E.g: As effect of modelling the stress range in hot spot 4 on the brace wall, the stress range is increased with 3.3 MPa in load-case 4, but is decreased with 5.2 MPa in load-case 12. In figure 6.12c the ratio with/without LJJ of the stress range in the hot spots of brace 1.3 as effect of modelling LJJ in brace 1.3 is presented. Ratios of 0.55 up to 1.35 are obtained.



determined after all load-cases are investigated. In figure 6.13b the absolute difference in accumulated fatigue damage to the sixteen hot spots of brace 1.3, after exposure to each load-case, as effect of modelling LJF in brace 1.3 is shown. By modelling LJF, the damage in the most affected locations decreased. In figure 6.13c the ratio with/without LJF of the accumulated fatigue damage in the hot spots of brace 1.3 as effect of modelling LJF in brace 1.3 is presented. Ratios of 0.05 up to 4.74 are obtained.

The results show, that the effect of modelling LJF is strongly load-case dependent. To retrieve reliable results of the influence of modelling LJF on the predicted fatigue life, the total accumulated fatigue damage in the braces of the stinger after exposure to the 16 load-cases for three hours each is taken. The total accumulated fatigue damage of each hot spot in each brace as effect of exposure to the 16 load-cases for three hours each, according to a model without LJF and according to a model with LJF in brace 1.3 is presented in figure 6.14. In the lower table, the ratio between the accumulated fatigue damage according to a model with and without LJF is presented. As effect of modelling LJF the fatigue damage in brace 1.3 has decreased in most hot spots. As effect of modelling LJF in brace 1.3, the fatigue damage in brace 6.1 has increased. The modification of the flexibility in brace 1.3 does not affect the other braces considerably.

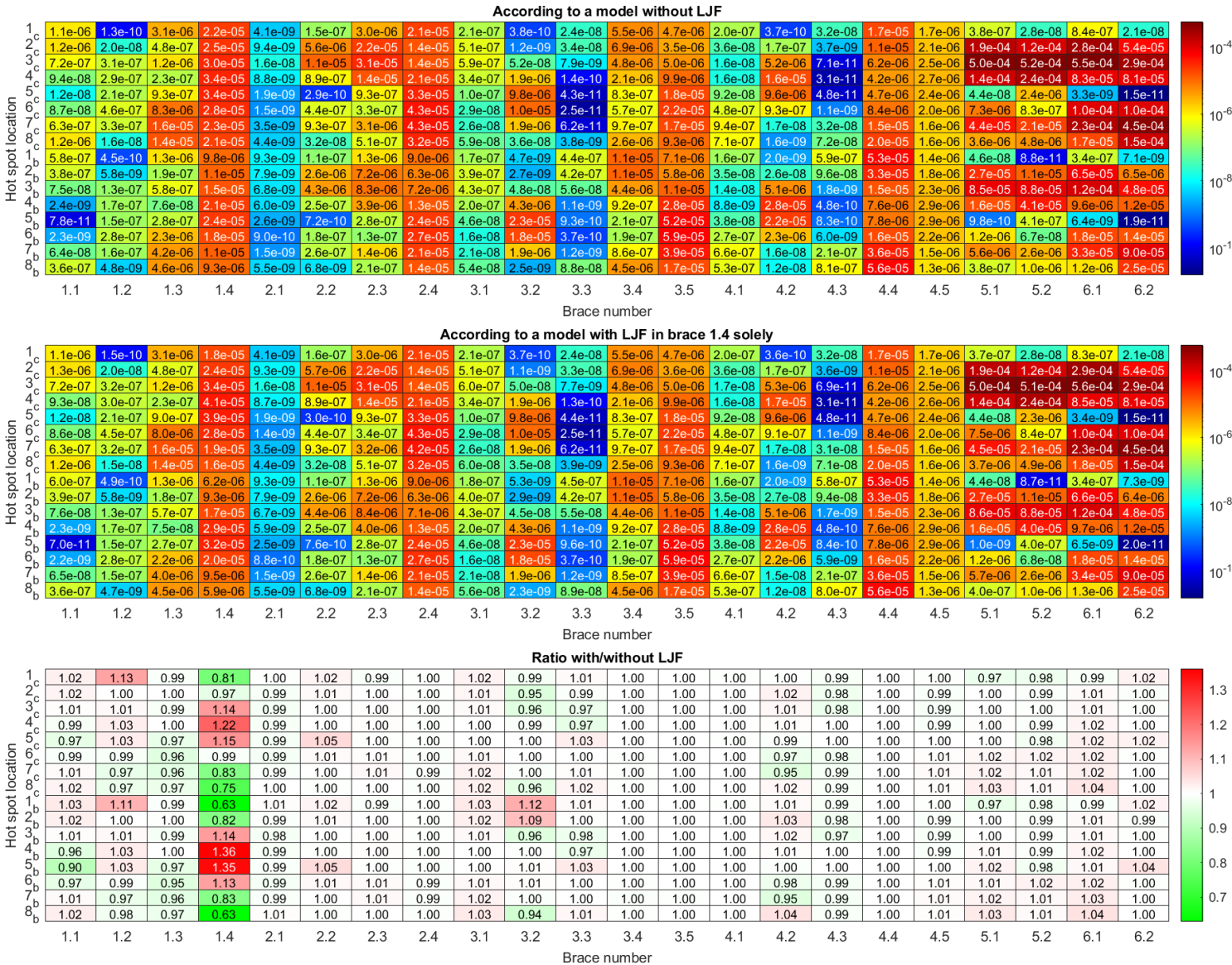
Table 6.4: Comparison of critical fatigue damage according to a model with and without LJF

Joint no.	Brace no.	Model without LJF		Model with LJF in brace 1.3		Ratio [-] with/without
		Most affected hot spot	Calculated fatigue damage	Most affected hot spot	Calculated fatigue damage	
1	1	2 <sub>c</sub>	1.24 e-06	2 <sub>c</sub>	1.32 e-06	1.06
	2	6 <sub>c</sub>	4.59 e-07	6 <sub>c</sub>	5.01 e-07	1.09
	3	7 <sub>c</sub>	1.62 e-05	7 <sub>c</sub>	7.36 e-06	0.46
	4	4 <sub>c</sub>	3.38 e-05	5 <sub>c</sub>	3.39 e-05	1.00
2	1	3 <sub>c</sub>	1.59 e-08	3 <sub>c</sub>	1.62 e-08	1.02
	2	3 <sub>c</sub>	1.11 e-05	3 <sub>c</sub>	1.15 e-05	1.03
	3	3 <sub>c</sub>	3.07 e-05	3 <sub>c</sub>	3.14 e-05	1.02
	4	6 <sub>c</sub>	4.34 e-05	6 <sub>c</sub>	4.27 e-05	0.98
3	1	3 <sub>c</sub>	5.93 e-07	3 <sub>c</sub>	6.07 e-07	1.02
	2	5 <sub>b</sub>	2.27 e-05	5 <sub>b</sub>	2.22 e-05	0.98
	3	1 <sub>b</sub>	4.45 e-07	1 <sub>b</sub>	4.25 e-07	0.96
	4	1 <sub>b</sub>	1.12 e-05	1 <sub>b</sub>	1.12 e-05	1.01
	5	6 <sub>b</sub>	5.88 e-05	6 <sub>b</sub>	5.85 e-05	0.99
4	1	7 <sub>c</sub>	9.36 e-07	7 <sub>c</sub>	9.41 e-07	1.00
	2	4 <sub>b</sub>	2.76 e-05	4 <sub>b</sub>	2.76 e-05	1.00
	3	8 <sub>b</sub>	8.10 e-07	8 <sub>b</sub>	7.94 e-07	0.98
	4	8 <sub>b</sub>	5.56 e-05	8 <sub>b</sub>	5.53 e-05	1.00
	5	5 <sub>b</sub>	2.90 e-06	5 <sub>b</sub>	2.85 e-06	0.99
5	1	3 <sub>c</sub>	5.00 e-04	3 <sub>c</sub>	4.92 e-04	0.98
	2	3 <sub>c</sub>	5.17 e-04	3 <sub>c</sub>	5.08 e-04	0.98
6	1	3 <sub>c</sub>	5.54 e-04	3 <sub>c</sub>	8.45 e-04	1.53
7	1	7 <sub>c</sub>	4.49 e-04	7 <sub>c</sub>	4.56 e-04	1.02

The predicted fatigue life of a brace, is dependent on the damage in the most affected location. Damage in other locations does not contribute to the predicted fatigue life. To compare the influence of modelling LJJ the most affected damage in the braces according to a model with and without LJJ is compared. The damage according to both models is presented in table 6.4. In the table, it can be seen that the accumulated fatigue damage in the most affected hot spot of brace 1.3 has changed with 0.46 (decrease). Thereby the predicted fatigue life of the brace will change with factor  $\frac{1}{0.46} = 2.17$  (increase). The accumulated fatigue damage in the most affected hot spot of brace 6.1 has changed with 1.53 (increase). Thereby the predicted fatigue life of the brace will change with factor  $\frac{1}{1.53} = 0.65$  (decrease).

**Total accumulated fatigue damage in hot spots**

As effect of exposure to 16 load-cases for 3 hours each



damage in brace 1.4 has increased in most hot spots. As effect of modelling LJF the fatigue damage in brace 1.4 has decreased.

The predicted fatigue life is dependent on the accumulated damage in the most affected location. To compare the influence of modelling LJF the damage in the most affected braces according to a model with and without LJF is compared and presented in table 6.5. The accumulated fatigue damage in the most affected hot spot of brace 1.4 has changed with 1.22 (increase). Thereby the predicted fatigue life of the brace will change with factor  $\frac{1}{1.22} = 0.82$  (decrease). The accumulated fatigue damage in the most affected hot spot of brace 1.3 has changed with 0.96 (decrease). Thereby the predicted fatigue life of the brace will change with factor  $\frac{1}{0.96} = 1.04$  (increase).

Table 6.5: Comparison of critical fatigue damage according to a model with and without LJF

Joint no.	Brace no.	Model without LJF		Model with LJF in brace 1.4		Ratio [-] with/without
		Most affected hot spot	Calculated fatigue damage	Most affected hot spot	Calculated fatigue damage	
1	1	2 <sub>c</sub>	1.24 e-06	2 <sub>c</sub>	1.26 e-06	1.02
	2	6 <sub>c</sub>	4.59 e-07	6 <sub>c</sub>	4.54 e-07	0.99
	3	7 <sub>c</sub>	1.62 e-05	7 <sub>c</sub>	1.55 e-05	0.96
	4	4 <sub>c</sub>	3.38 e-05	4 <sub>c</sub>	4.13 e-05	1.22
2	1	3 <sub>c</sub>	1.59 e-08	3 <sub>c</sub>	1.57 e-08	0.99
	2	3 <sub>c</sub>	1.11 e-05	3 <sub>c</sub>	1.12 e-05	1.00
	3	3 <sub>c</sub>	3.07 e-05	3 <sub>c</sub>	3.09 e-05	1.00
	4	6 <sub>c</sub>	4.34 e-05	6 <sub>c</sub>	4.32 e-05	1.00
3	1	3 <sub>c</sub>	5.93 e-07	3 <sub>c</sub>	5.99 e-07	1.01
	2	5 <sub>b</sub>	2.27 e-05	5 <sub>b</sub>	2.28 e-05	1.01
	3	1 <sub>b</sub>	4.45 e-07	1 <sub>b</sub>	4.49 e-07	1.01
	4	1 <sub>b</sub>	1.12 e-05	1 <sub>b</sub>	1.12 e-05	1.00
	5	6 <sub>b</sub>	5.88 e-05	6 <sub>b</sub>	5.87 e-05	1.00
4	1	7 <sub>c</sub>	9.36 e-07	7 <sub>c</sub>	9.36 e-07	1.00
	2	4 <sub>b</sub>	2.76 e-05	4 <sub>b</sub>	2.77 e-05	1.01
	3	8 <sub>b</sub>	8.10 e-07	8 <sub>b</sub>	8.01 e-07	0.99
	4	8 <sub>b</sub>	5.56 e-05	8 <sub>b</sub>	5.56 e-05	1.00
	5	5 <sub>b</sub>	2.90 e-06	5 <sub>b</sub>	2.89 e-06	1.00
5	1	3 <sub>c</sub>	5.00 e-04	3 <sub>c</sub>	5.01 e-04	1.00
	2	3 <sub>c</sub>	5.17 e-04	3 <sub>c</sub>	5.15 e-04	1.00
6	1	3 <sub>c</sub>	5.54 e-04	3 <sub>c</sub>	5.60 e-04	1.01
7	1	7 <sub>c</sub>	4.49 e-04	7 <sub>c</sub>	4.49 e-04	1.00

## 6.5. Results

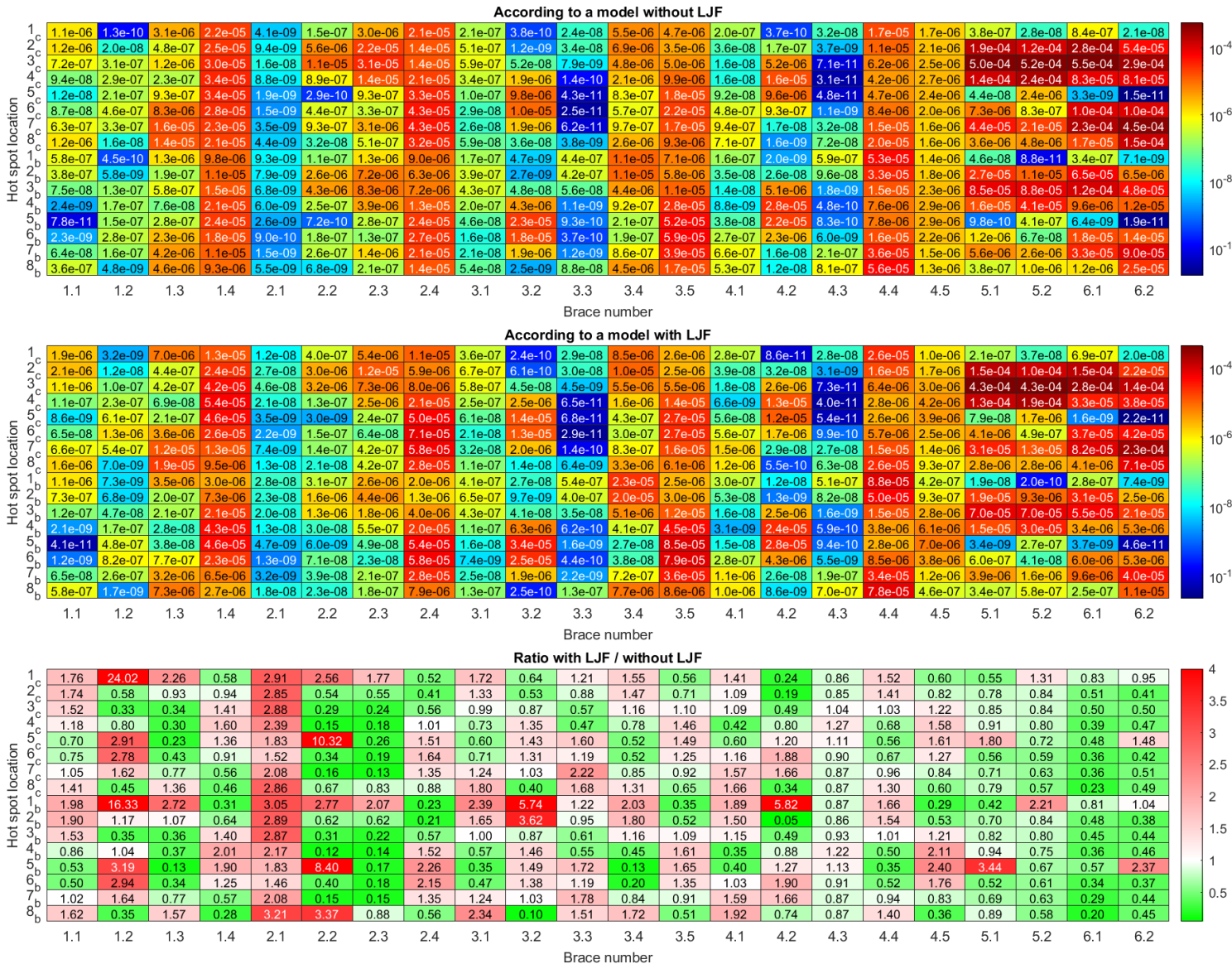
In this section, the result of modelling LJF in the stinger is discussed. In the previous section, it is shown that modelling LJF does not only affect the predicted fatigue life of the brace itself but also of adjacent and surrounding braces. In fact the modification of the flexibility in a joint leads to the redistribution of the member loads through the full stinger frame. To determine the influence of modelling LJF in a stinger, LJF is modelled for the seven joints of which the fatigue assessment is performed, but also all

surrounding joints, highlighted in orange in confidential appendix P.1.

As effect of the modification of the flexibilities of a large number of braces, a total redistribution of the member loads through the stinger appears. The redistribution cannot be abbreviated to certain properties of a single joint but is the effect of the reciprocal flexibility modification of all joints in the stinger. Furthermore, the influence of LJJ has appeared to be strongly load-case dependent. A detailed analysis of the influence on each brace for each load-case is too complicated for the scope of this project. Figures with the member-loads, stress range, and accumulated fatigue damage for each brace as effect of each load-case are presented in appendix L but not discussed further.

**Total accumulated fatigue damage in hot spots**

As effect of exposure to 16 load-cases for 3 hours each



is investigated.

The total accumulated fatigue damage of each hot spot in each brace as effect of exposure to the 16 load-cases for three hours each, is presented in figure 6.16. Differences in fatigue damage in the hot spot of factor 0.10 up to 24.02 are observed. However, not all of these ratios provide a reliable impression as the extreme ratios are only obtained in non-critical locations. modelling LJF does not lead to a complete redistribution of the most affected hot spots and of the critical braces. In both models these are almost equal.

The accumulated fatigue damage in the most affected hot spot of each brace in the stinger as effect of exposure to the sixteen load-cases for three hours each, according to a model with and without LJF, is shown in table 6.6. Several braces have benefited and others have taken disadvantage of modelling LJF. The accumulated fatigue damage in the most affected hot spots of the braces has changed with factor 0.29 up to factor 2.88. An increase of fatigue damage with factor 3 may seem large but due to the nature of fatigue is only the results of an increase in stress range of  $\sqrt[5]{3} = 1.25$ . Here 5 is the slope of the SN curve for stresses below 67 MPa.

Table 6.6: Comparison of critical fatigue damage according to a model with and without LJF

Joint no.	Brace no.	Model without LJF		Model with LJF		Ratio [-] with/without
		Most affected hot spot	Calculated fatigue damage	Most affected hot spot	Calculated fatigue damage	
1	1	2 <sub>c</sub>	1.24 e-06	2 <sub>c</sub>	2.15 e-06	1.74
	2	6 <sub>c</sub>	4.59 e-07	6 <sub>c</sub>	1.27 e-06	2.78
	3	7 <sub>c</sub>	1.62 e-05	8 <sub>c</sub>	1.94 e-05	1.20
	4	4 <sub>c</sub>	3.38 e-05	4 <sub>c</sub>	5.40 e-05	1.60
2	1	3 <sub>c</sub>	1.59 e-08	3 <sub>c</sub>	4.59 e-08	2.88
	2	3 <sub>c</sub>	1.11 e-05	3 <sub>c</sub>	3.25 e-06	0.29
	3	3 <sub>c</sub>	3.07 e-05	2 <sub>c</sub>	1.22 e-05	0.40
	4	6 <sub>c</sub>	4.34 e-05	6 <sub>c</sub>	7.12 e-05	1.64
3	1	3 <sub>c</sub>	5.93 e-07	2 <sub>c</sub>	6.74 e-07	1.14
	2	5 <sub>b</sub>	2.27 e-05	5 <sub>b</sub>	3.39 e-05	1.49
	3	1 <sub>b</sub>	4.45 e-07	1 <sub>b</sub>	5.43 e-07	1.22
	4	1 <sub>b</sub>	1.12 e-05	1 <sub>b</sub>	2.27 e-05	2.03
	5	6 <sub>b</sub>	5.88 e-05	5 <sub>b</sub>	8.54 e-05	1.45
4	1	7 <sub>c</sub>	9.36 e-07	7 <sub>c</sub>	1.47 e-06	1.57
	2	4 <sub>b</sub>	2.76 e-05	5 <sub>b</sub>	2.77 e-05	1.00
	3	8 <sub>b</sub>	8.10 e-07	8 <sub>b</sub>	7.02 e-07	0.87
	4	8 <sub>b</sub>	5.56 e-05	1 <sub>b</sub>	8.77 e-05	1.58
	5	5 <sub>b</sub>	2.90 e-06	5 <sub>b</sub>	6.96 e-06	2.40
5	1	3 <sub>c</sub>	5.00 e-04	3 <sub>c</sub>	4.26 e-04	0.85
	2	3 <sub>c</sub>	5.17 e-04	3 <sub>c</sub>	4.32 e-04	0.84
6	1	3 <sub>c</sub>	5.54 e-04	3 <sub>c</sub>	2.78 e-04	0.50
7	1	7 <sub>c</sub>	4.49 e-04	7 <sub>c</sub>	2.29 e-04	0.51

The change in predicted fatigue life as effect of modelling LJF, is equal to the inverse of the change in

computed fatigue damage. By modelling LJF in the joint of the stinger, differences in predicted fatigue life of  $\frac{1}{0.29} = 3.45$  up to  $\frac{1}{2.88} = 0.35$  are observed. These values are not expected to be the maximum and minimum values, in exceptional cases these values can be exceeded. However, the values are considered as a reliable impression of the influence of modelling LJF in the joints of the stinger.

The influence of modelling LJF is most important on the critical braces in the stinger. For the test-case this appears to be brace 5.1, 5.2, 6.1, 6.2. In table 6.6 it can be seen that the four braces all benefit from modelling LJF, as the predicted fatigue life changes with factor 1.17 - 2.00. Thus modelling LJF does not only provide a more accurate predicted fatigue life but additionally can help to improve the predicted fatigue life.

## 6.6. Discussion

In the numerical test-case, differences in predicted fatigue life of factor 0.35 up to 3.45 are observed. This observation does not correspond with the findings of MSL Engineering Ltd. [45]. In their publication, MSL Engineering Ltd. [45] found an average increased predicted fatigue life of factor 8.0 up to factor 19.3 for different joint types. The alternation in predicted fatigue life in the research of MSL Engineering Ltd. is larger than observed in this research. Furthermore, no decreases in predicted fatigue life are found by MSL Engineering Ltd. [45]. The difference in results might be obtained for the following reasons:

To begin with, MSL Engineering Ltd. [45] only modelled LJF to a selection of braces. An example is presented in figure 6.17. In sub-section 6.4.1, it is observed that by modelling LJF in one brace, its predicted fatigue life increases, but as effect the predicted fatigue life of adjacent and surrounding braces decreases. The fatigue life of the adjacent braces is not mentioned in the research of MSL Engineering Ltd. Furthermore, modelling LJF in adjacent and surrounding braces, might have led to a decrease in predicted fatigue life of the braces of consideration.

In addition, MSL Engineering Ltd. Models LJF with a 'customized beam element' (sub-section 2.4.2). In this methodology, the LJF flexibilities are defined in the coordinate system of the brace. The definition of the flexibilities in this coordinate system allows deformations in the direction perpendicular to the chord. A direction that is according to LJF theorem assumed to be stiff. The definition in this coordinate system is discussed in section 2.5.

Furthermore, in the publication of MSL Engineering Ltd. it is suggested that joints have a relatively high  $\gamma$  value ( $\gamma > 15$ ). In chapter 4, it is shown that joints with higher  $\gamma$  values possess higher flexibilities, resulting in larger alternations in predicted fatigue life. Furthermore, MSL Engineering Ltd. determines the LJF with the parametric equations of Buitrago et al. [13]. In sub-section 4.4.3, it is shown that the parametric equations of Buitrago et al. tend to overestimate the LJF.

The observations of this research correspond partially with the observations in the research of Golafshani et al. [36]. Golafshani et al. model LJF in another jacket and models LJF in relatively more joint in the structure. Golafshani et al. [36] do not calculate the predicted fatigue life, but provide the member forces as result of modelling LJF. Golafshani et al. [36] do observe the increase as well as decrease of member loads as effect of modelling LJF, this increase and decrease of predicted fatigue life.

For both researches, it is hard to take a conclusion about the reason for the different results, due to the limited available data.

## 6.7. Conclusion

A numerical test-case is performed to investigate the influence of modelling LJF on the predicted fatigue life of the braces in the stinger. The fatigue assessment is performed for two beam models. One model with LJF and another, without LJF. Apart from the difference in LJF both models are identical. The results are compared.

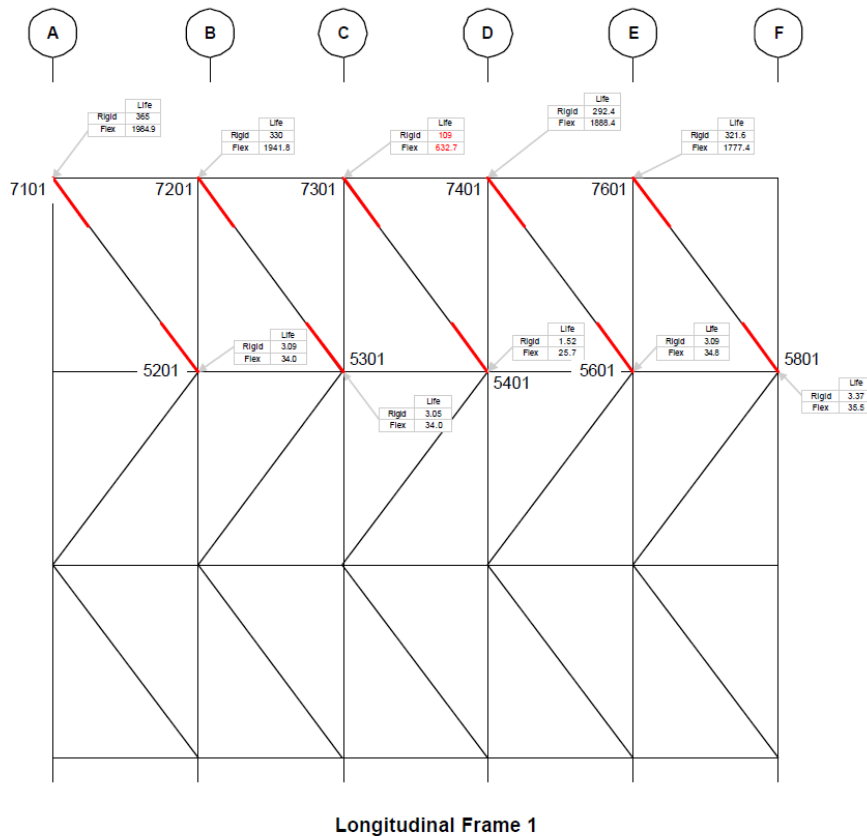


Figure 6.17: An overview of the braces in which LJF is modelled in the research of MSL Engineering Ltd. [45].

In two test scenarios, the influence of modelling LJF in one single brace solely is investigated. It is observed that when a brace increases flexibility through modelling LJF, its member loads decrease and the predicted fatigue life increases. As effect, the member loads on surrounding braces increase and fatigue life of decreases. When modelling LJF in a brace which decreases in flexibility through modelling LJF, its member loads increase and thereby its predicted fatigue life decreases. As effect, the member loads on surrounding joints decrease and the predicted fatigue life increases. Because of the interaction among braces, it is required to model LJF in all surrounding braces of the brace of interest, to retrieve reliable results.

The above observations are generally valid but large influences of different load-cases are observed. In several cases modelling LJF can lead to a decrease of fatigue damage in one load-case and to an increase in another load-case.

To determine the influence of modelling LJF in a stinger, LJF is modelled for seven joints of which the fatigue assessment is performed, but also in all surrounding joints. As effect of the modification of the flexibilities of a large number of braces, a total redistribution of the member loads through the stinger appears. Because the influence of LJF has appeared to be strongly load-case dependent, the total accumulated damage in the hot spots of the braces, as effect of exposure to 16 load-cases for three hours each, is computed. The accumulated fatigue damage, according to a model with and without LJF, is compared. The accumulated fatigue damage in the most affected hot spots of the braces has changed with factor 0.29 up to factor 2.88 as effect of LJF. The change in predicted fatigue life as effect of modelling LJF, is equal to factor 3.45 up to 0.35. These values are not expected to be the maximum and minimum values, in exceptional cases these values can be exceeded. However, because the fatigue assessment is performed over sixteen load-cases in total, the values are considered as a reliable prediction of the possible influence of modelling LJF in the joints of the stinger. No large alterations in

most critical braces or most affected hot spots within the brace, as effect of modelling LJF are observed. Thus, modelling LJF would not lead to a different fatigue monitoring.

The results do not correspond with the result obtained by MSL Engineering Ltd. [45]. The results of MSL Engineering Ltd. [45] are expected to be different because: they only model LJF to a segment of the tubular joints, model LJF with an element that allows deformations in a different direction, use parametric equations which tend to overestimate LJF and are expected to use joint geometries which possess more flexibility. The results do partially correspond with the results obtained by Golafshani et al. [36]. In both research an increase, as well as an decrease in member-loads as effect of modelling LJF is observed. Though, the magnitude of the influence of modelling LJF appears to be larger in the research performed by Golafshani et al. [36].

# 7

## Conclusion

In this chapter, the conclusion and recommendations are discussed.

### 7.1. Conclusion

The main research question of this study is stated as:

***“How can Local Joint Flexibility be modelled in a beam model of a stinger and what is the influence on the predicted fatigue life?”***

To answer the main research question, the six sub-questions are answered:

#### ***1. What is local joint flexibility and what flexibilities do tubular joints have?***

LJF is defined as the flexibility through local chord wall deformation caused by an external load on the brace. The brace can deform in three DOF (axial, out-of-plane bending, in-plane bending) as effect of three possible DOF unit-loads (axial force, out-of-plane bending moment, in-plane bending moment), applied on the brace itself or adjacent braces. Until initial yielding, joints show linear elastic behaviour, hence the flexibilities can be described by a constant value.

#### ***2. What methodologies to determine and model local joint flexibility are presented in literature?***

Three methodologies to determine the LJF of a tubular joint are discussed in literature: physical experiments, Finite Element Analysis and parametric equations. Three methods to model the LJF in a beam model are discussed in literature: a spring element, a customized beam element, and a global stiffness matrix.

#### ***3. What methodology is the most suitable to determine and model the local joint flexibility in a stinger?***

The majority of the joints in the stinger, concerns multi-brace joints with up to six braces in multiple planes, resulting in a complicated geometry to determine and model LJF. The most suitable methodologies for application, are the most accurate methodologies, executable within the timeline of the project. It is decided to determine the LJF of tubular joints with FEA, using shell elements and to model LJF via the global stiffness matrix of the beam model. Both methodologies are the most accurate solution, provide the possibility to modify parameters, but lack in ease of implementation.

#### ***4. How can the local joint flexibility of joints in a stinger be determined, and with what accuracy? How can this method be verified and validated?***

A numerical model to determine the flexibilities of tubular joints is developed in MATLAB. The model requires the geometric and material properties as input and automatically calculates the LJF matrix. The FEA, as part of the numerical model is performed in Ansys. Initially, a numerical model to determine the flexibilities of single-brace joints is developed. The single-brace model is verified with several numerical tests, which prove that the numerical model performs as expected. The single-brace model is validated

by comparing the results to 27 experiments of Fessler et al. [31] and four experiments by Tebbett [53]. The experiments of Fessler et al. [31] are considered as leading, because they are described in more detail and a higher number of experiments is performed. Statistics show that the flexibilities according to the numerical model have a mean deviation of +3% with a SD of  $\pm 20\%$  to the experiments of Fessler et al. [31]. The accuracy of the numerical model is compared to the accuracy of the brace extension element, present in the beam model without LJF. The flexibilities of the brace extension element, have a mean deviation of  $-36\%$  with a SD of  $\pm 74\%$  to the experiments of Fessler et al. [31]. Thereby, it is proven that the flexibilities according to the numerical model, provide a more accurate representation of the LJF than the brace extension element in a beam model without LJF. The numerical model is expanded to a multi-brace model, which is able to determine the flexibilities of every non-overlapping multi-brace joint, except joints with  $\beta = 1$ . Due to a shortage of suitable data for the validation of the numerical model, no additional validation of the multi-brace numerical model is performed. The validation for single-brace joints, in combination with the verification for multi-brace joints, is considered as sufficient.

**5. How can local joint flexibility of joints in a stinger be modelled in a beam member model and with what accuracy? How can this method be verified and validated?**

A methodology is developed, to model LJF of tubular joints into a beam model. The brace extension element, located within the chord surface, is replaced by a GENEL in FEMAP. The GENEL is an element, which allows inserting stiffnesses or flexibilities between nodes, directly in the global stiffness matrix in the Simcenter NASTRAN solver. Because the flexibilities are inserted in the global coordinate system, several transformations and rotations are performed. In the verification, it is shown that the model performs correctly and the inserted flexibilities, are represented without deviation in the beam model. However, because the flexibility is only theoretically symmetrical, transposed, off-diagonal flexibilities are averaged, before insertion, hence small deviations in the off-diagonal flexibilities are introduced. The deviations originate in the inaccuracy of the numerical model which determines the flexibilities of the joint. Because the methodology is a purely mathematical operation, no validation is performed.

**6. What is the influence of accounting for local joint flexibility in a beam model on the fatigue assessment of a stinger?**

A numerical test-case is performed to investigate the influence of modelling LJF on the predicted fatigue life of the joints in the stinger. The results of two beam models are investigated. One model with LJF and another, without LJF. The fatigue assessment is performed according to DNV-RP-C203 [23]. Due to the complexity of fatigue assessment, a limited number of 7 joints with 22 braces is investigated. It is found that modelling LJF in one brace, affects adjacent and surrounding braces, therefore, LJF is modelled in the joints of interest, and additionally in the surrounding joints. The influence of LJF has appeared to be strongly load-case dependent, thus the total accumulated damage as effect of exposure to 16 load-cases for three hours each is calculated. The accumulated fatigue damage in the critical hot spot of the braces, as effect of exposure to the sixteen load-cases for three hours each, has changed with factor 0.29 up to factor 2.88 as effect of LJF. The change in predicted fatigue life as effect of modelling LJF, is equal to factor 0.35 up to 3.45. These values are not expected to be the absolute maximum and minimum values, in exceptional cases these values can be exceeded. Though, because the fatigue assessment is performed over sixteen load-cases in total, the values are considered as a reliable representation of the influence of modelling LJF. No large alterations in most critical braces nor most critical hot spot within the brace, as effect of modelling LJF is observed. Thus, based on the performed study, modelling LJF would not lead to a different fatigue monitoring approach. The results of this research, do not correspond with the result obtained by MSL Engineering Ltd. [45]. MSL Engineering Ltd. [45] does not observe any decrease in predicted fatigue life, and the observed influence of modelling LJF is larger (factor 8.0 - 19.3). The difference in results can possibly be caused because MSL Engineering Ltd. [45]: only models LJF to a segment of the tubular joints, only performs the fatigue assessment to a segment of the tubular joints, models LJF with an element that allows deformation perpendicular to the chord wall, use parametric equations which tend to overestimate LJF and suggests to apply LJF on joint geometries, which possess more flexibility. The results of this project, do partially correspond with the results obtained by Golafshani et al. [36]. In both the publication of Golafshani et al. [36] and this research, an increase as well as a decrease of member-loads as effect of modelling LJF is observed.

Concluding, 22 braces are investigated and increases as well as decreases in predicted fatigue life are observed (change in predicted fatigue life of factor 0.35 up to 3.45). Especially in the numerical test-case, the observed influence has appeared to be beneficial for the four most critical braces of consideration (brace 5.1, 5.2, 6.1, 6.2), which endure an increase of predicted fatigue life of factor 1.17 up to 2.00 as effect of modelling LJF. Thus modelling LJF does not only provide a more accurate predicted fatigue life but additionally can help to increase the predicted fatigue life. On the other hand, implementation of LJF is a time-demanding job, mistakes are easily made and tough to notice in the model. A recommendation about whether it is feasible to implement this method or not, cannot be provided by the author, because of insufficient knowledge about the fatigue assessment as a whole. Furthermore, a recommendation about the application of LJF is situation dependent. However, with this report information about the influence, advantages and disadvantages of modelling LJF is provided. Thereby, the stinger designer is presumed to be able to make a well-considered deliberation about whether to model LJF into the stinger.

## 7.2. Recommendations

A method is developed to accurately model the flexibility of the stinger, in order to obtain more accurate member-forces and thereby, a more accurate: stress range, accumulated fatigue damage and predicted fatigue life. Considerable differences in predicted fatigue life are obtained as result of modelling LJF. However, more research is required to determine the accuracy of the new methodology..

To begin, it is recommended to compare the results of both a model with and without LJF, to the results according to a stinger model with shell elements. Theoretically, the results according to the shell model are more accurate and are a good comparison. Because modelling of the stinger in shell elements is time demanding, modelling could be limited to a selection of joints in the stinger.

In addition, it is recommended to perform the fatigue assessment of an 'old' stinger and compare the predicted fatigue life according to the three methods (beam model with LJF, beam model without LJF and shell model), with the actual observed fatigue life of the stinger, thus a clear overview of the accuracy of the results according to the three methodologies can be obtained.

The current methodology is only valid for unstiffened and non-overlapping joints. Generally looking, the stinger contains numerous stiffened joints. These joints have a high stiffness thus low flexibility. In 6.4, it is shown that stiff joints attract larger member loads, which can lead to the reduction of member loads on surrounding joints. It is recommended to investigate modelling LJF for these joints.

The developed methodology can be improved on two aspects, accuracy and ease of implementation. To increase the accuracy of the methodology it is recommended to:

1. In the validation in section 4.4, large deviations in the results of the physical experiments are observed. Furthermore, no suitable experiments for the validation of the flexibilities in a multi-brace joint is obtained. Experiments could be performed in order to more accurately determine the accuracy of the numerical model and validate the results for multi-brace joints. Though, the performance of physical experiments is considered as a cost and time ineffective method and thus should be carefully considered.
2. During this study, it is found that the braces possess small flexibility in the other three DOF where the brace is loaded on shear. In this research, these DOF are neglected, but in future, the influence of modelling these flexibilities could be investigated. The current methodology to model LJF with a stiffness matrix, is a convenient method to model the extra DOF.
3. In the validation in section 4.4.3, it is found that Buitrago et al. [13] and Chen and Zhang [17] are able to determine the in-plane bending flexibility ( $f_{33}$ ) more accurate than the methodology of this research. The approach of Buitrago et al. [13] and Chen and Zhang [17] could be investigated in order to increase the accuracy of the numerical model.
4. In the current numerical model of chapter 4, the LJF of tubular joints is determined with a FEA in which weld are neglected. modelling welds in the FEA could lead to a more accurate determi-

nation of the LJF. A method to model welds with shell elements is already published by van der Vegte et al. [56].

5. The numerical model is able to determine the LJF of any non-overlapping joints. It is recommended to expand the numerical model towards a model which also can determine the LJF of overlapping and reinforced joints. These joints are expected to decrease considerably in flexibility as effect of modelling LJF. Especially adjacent and surrounding joints can benefit from this.

The current methodology, applied to determine LJF and model LJF in a beam model, is complicated due to the large number of calculations which is performed before LJF is modelled. Furthermore, the current method allows to easily include errors without noticing. To improve ease of implementation it is recommended to:

1. Determination of LJF with parametric equations is faster than FEA. Research towards the application of parametric equations and the development of own parameter equations is recommended to perform. Results of the developed numerical model can be used in order to develop parametric equations.
2. modelling LJF via the GENEL is complicated because a large number of flexibilities needs to be transformed to the global coordinate system, which is dependent on the orientation of the joint. Research towards modelling LJF with a different type of element, oriented in the local coordinate system of the joint or brace is recommended.

The two aspects of improvement are strongly related to each other. By increasing the accuracy of the model, the ease of implementation decreases, and by making more assumptions the ease of implementation improves, but the accuracy decreases. Research towards the influence of the improvements needs to be performed in order to determine whether the improvements are profitable.

Latest, it is recommended to perform research towards automation of the developed methodology. Software that automatically detect joints, in order to calculate the LJF and which automatically can adapt the beam model and replace the beam extension elements for GENEL's with LJF properties, can be developed. Thereby, the ease of implementation will be increased without loss of accuracy.

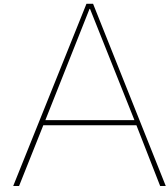
# Bibliography

- [1] H. Ahmadi and V. Mayeli. "Development of a probability distribution model for the LJF factors in offshore two-planar tubular DK-joints subjected to OPB moment loading". In: *Marine Structures* 63 (2019), pp. 196–214. DOI: 10.1016/j.marstruc.2018.09.009.
- [2] H. Ahmadi and V. Mayeli. "Probabilistic analysis of the local joint flexibility in two-planar tubular DK-joints of offshore jacket structures under in-plane bending loads". In: *Applied Ocean Research* 81 (2018), pp. 126–140. DOI: 10.1016/j.apor.2018.10.011.
- [3] H. Ahmadi and A. Ziaei Nejad. "A study on the local joint flexibility (LJF) of two-planar tubular DK-joints in jacket structures under in-plane bending loads". In: *Applied Ocean Research* 64 (2017), pp. 1–14. DOI: 10.1016/j.apor.2017.02.002.
- [4] H. Ahmadi and A. Ziaei Nejad. "Geometrical effects on the local joint flexibility of two-planar tubular DK-joints in jacket substructure of offshore wind turbines under OPB loading". In: *Thin-Walled Structures* 114 (2017), pp. 122–133. DOI: 10.1016/j.tws.2017.02.001.
- [5] H. Ahmadi and A. Ziaei Nejad. "Local joint flexibility of two-planar tubular DK-joints in OWTs subjected to axial loading: parametric study of geometrical effects and design formulation". In: *Ocean Engineering* 136 (2017), pp. 1–10. DOI: 10.1016/j.oceaneng.2017.03.011.
- [6] P. Alanjari, B. Asgarian, and M. Kia. "Nonlinear joint flexibility element for the modeling of jacket-type offshore platforms". In: *Applied Ocean Research* 33.2 (2011), pp. 147–157. DOI: 10.1016/j.apor.2010.12.005.
- [7] P. Alanjari, B. Asgarian, and N. Salari. "Elastic tubular joint element for modelling of multi-brace, uni-planar tubular connections". In: *Ships and Offshore Structures* 10.4 (2015), pp. 404–415. DOI: 10.1080/17445302.2014.942077.
- [8] ANSYS Inc. *ANSYS Mechanical APDL command reference*. Tech. rep. 2010.
- [9] ANSYS Inc. *ANSYS Mechanical APDL element reference*. Tech. rep. 2011.
- [10] B. Asgarian, P. Alanjari, and V. Aghaeidoost. "Three-dimensional joint flexibility element for modeling of tubular offshore connections". In: *Schmerz* 29.6 (2015), pp. 629–639. DOI: 10.1007/s00773-015-0317-2.
- [11] B. Asgarian, V. Mokarram, and P. Alanjari. "Local joint flexibility equations for Y-T and K-type tubular joints". In: *Ocean Systems Engineering* 4.2 (2014), pp. 151–167.
- [12] J.G. Bouwkamp et al. "Effects of joint flexibility on the response of offshore towers". In: *Proceedings of the Annual Offshore Technology Conference* 1980-May (1980), pp. 455–464. DOI: 10.4043/3901-ms.
- [13] J. Buitrago, B.E. Healy, and T.Y. Chang. "Local joint flexibility of tubular joints". In: *Proceedings of the International Conference on Offshore Mechanics and Arctic Engineering - OMAE* 1 (1993), pp. 405–411.
- [14] J.J. van der Cammen. "Fatigue prediction and response monitoring on a FPSO". In: (2008).
- [15] J. Cao, G. Yang, and J. A. Packer. "FE mesh generation for circular tubular joints with or without cracks". In: *Proceedings of the International Offshore and Polar Engineering Conference* 4 (1997), pp. 98–105.
- [16] J.J. Cao et al. "Crack modeling in FE analysis of circular tubular joints". In: *Engineering Fracture Mechanics* 61.5-6 (1998), pp. 537–553. DOI: 10.1016/S0013-7944(98)00091-5.
- [17] B. Chen, Y. Hu, and M. Tan. "Local joint flexibility of tubular joints of offshore structures". In: *Marine Structures* 3.3 (1990), pp. 177–197. DOI: 10.1016/0951-8339(90)90025-M.
- [18] T.-Y. Chen and H.-Y. Zhang. "Stress analysis of spatial frames with consideration of local flexibility of multiplanar tubular joint". In: *Engineering Structures* 18.6 (1996), pp. 465–471. DOI: 10.1016/0141-0296(95)00109-3.

- [19] R. Clough and C. Felippa. "A Refined Quadrilateral Element for Analysis of Plate Bending". In: *Proc. 2nd Conf. on Matrix Methods in Structural Mechanics* AFFDL-TR-68-150 (Oct. 1968), p. 43.
- [20] DNV. *DNV-OS-J101 Design of offshore wind turbine structures*. 2014.
- [21] DNV. *Rules for the design, construction and inspection of offshore structures*. 1977.
- [22] DNV GL. *DNVGL-OS-C101 Design of offshore steel structures, general LRFD method*. 2015.
- [23] DNV GL. *DNVGL-RP-C203 Fatigue design of offshore steel structures*. 2019.
- [24] M. Efthymiou. *Local rotational stiffness of unstiffened tubular joints*. Report No. RKER.85.199. Koninklijke/Shell exploratie en productie laboratorium, Rijswijk, 1985.
- [25] Allseas engineering. *SOL - Fatigue analysis of stinger tubular joints*. SO-929-X1-R-38. Nov. 2019.
- [26] McDermott Engineering. "Occidental of Britain Inc. Piper A jacket, static load tests on model of 12 3/4 / 24 inch tubular joint." In: (1979).
- [27] N. Ermolaeva, Y. Yu, and L. Zhao. "Design and fatigue assessment of a stinger". In: *Tubular Structures XIII - Proceedings of the 13th International Symposium on Tubular Structures* (2010), pp. 547–555. DOI: 10.1201/b10564-76.
- [28] H. Fessler, P.B. Mockford, and J.J. Webster. "An experimental technique for determining the flexibility of tubular joints in offshore structures". In: *The Journal of Strain Analysis for Engineering Design* 22.1 (1987), pp. 7–15. DOI: 10.1243/03093247V221007.
- [29] H. Fessler and H. Spooner. "Experimental determination of stiffness of tubular joints". In: *Proc. 2nd International Symposium on Integrity of Offshore Structures, Institute of Shipbuilders and Engineers* (1981), pp. 493–511.
- [30] H. Fessler, J.J. Webster, and P.B. Mockford. "Parametric equations for the flexibility matrices of multi-brace tubular joints in offshore structures." In: *INST. CIV. ENGRS. PROC. PART 2*. 81 , Dec. 1986 (1986), pp. 675–696.
- [31] H. Fessler, J.J. Webster, and P.B. Mockford. "Parametric equations for the flexibility matrices of single brace tubular joints in offshore structures." In: *INST. CIV. ENGRS. PROC. PART 2*. 81 , Dec. 1986 (1986), pp. 659–673.
- [32] F. Gao and B. Hu. "Local joint flexibility of completely overlapped tubular joints under out-of-plane bending". In: *Journal of Constructional Steel Research* 115 (2015), pp. 121–130. DOI: 10.1016/j.jcsr.2015.08.016.
- [33] F. Gao, B. Hu, and H.P. Zhu. "Local joint flexibility of completely overlapped tubular joints under in-plane bending". In: *Journal of Constructional Steel Research* 99 (2014), pp. 1–9. DOI: 10.1016/j.jcsr.2014.03.004.
- [34] F. Gao, B. Hu, and H.P. Zhu. "Parametric equations to predict LJJ of completely overlapped tubular joints under lap brace axial loading". In: *Journal of Constructional Steel Research* 89 (2013), pp. 284–292. DOI: 10.1016/j.jcsr.2013.07.010.
- [35] W. Gho. "Local joint flexibility of tubular circular hollow section joints with complete overlap of braces". In: (Sept. 2008), pp. 607–614. DOI: 10.1201/9780203882818.ch69.
- [36] A.A. Golafshani, M. Kia, and P. Alanjari. "Local joint flexibility element for offshore platforms structures". In: *Marine Structures* 33 (2013), pp. 56–70. DOI: 10.1016/j.marstruc.2013.04.003.
- [37] D. T. Greenwood. *Advanced Dynamics*. Cambridge University Press, Aug. 23, 2006. 436 pp. ISBN: 0521029937. URL: [https://www.ebook.de/de/product/5965987/donald\\_t\\_greenwood\\_advanced\\_dynamics.html](https://www.ebook.de/de/product/5965987/donald_t_greenwood_advanced_dynamics.html).
- [38] I. Hoshyari and R. Kohoutek. "Rotational and axial flexibility of tubular T-joints". In: *Proceedings of the Third (1993) International Offshore and Polar Engineering Conference* (1993), pp. 192–198.
- [39] H. Hossein. "Local joint flexibility of CHS T/Y-connections strengthened with collar plate under in-plane bending load: parametric study of geometrical effects and design formulation". In: *Ocean Engineering* 202 (Apr. 2020), p. 107054. DOI: 10.1016/j.oceaneng.2020.107054.

- [40] Y. Hu, B. Chen, and J. Ma. "An equivalent element representing local flexibility of tubular joints in structural analysis of offshore platforms". In: *Computers and Structures* 47.6 (1993), pp. 957–969. DOI: 10.1016/0045-7949(93)90300-3.
- [41] Huntsman. Private communication. Contact person: L. Chouvet. Jan. 2021.
- [42] International standard. *ISO 19902 Petroleum and natural gas industries - fixed steel offshore structures*. Tech. rep. International standard, 2007.
- [43] L. J. Jia and Y. Y. Chen. "Evaluation of elastic in-plane flexural rigidity of unstiffened multiplanar CHS X-joints". In: *International Journal of Steel Structures* 14.1 (Mar. 2014), pp. 23–30. DOI: 10.1007/s13296-014-1003-7.
- [44] R. Khan, K. Smith, and I. Kraincanic. "Improved LJF equations for the uni-planar gapped K-type tubular joints of ageing fixed steel offshore platforms". In: *Journal of Marine Engineering and Technology* 17.3 (2018), pp. 121–136. DOI: 10.1080/20464177.2017.1299613.
- [45] MSL Engineering Ltd. "The effect of local joint flexibility on the reliability of fatigue life estimates and inspection planning". In: 2001/056 (2001).
- [46] H. Nassiraei. "Local joint flexibility of CHS X-joints reinforced with collar plates in jacket structures subjected to axial load". In: *Applied Ocean Research* 93 (2019). DOI: 10.1016/j.apor.2019.101961.
- [47] X. Qian, Y. Zhang, and Y.S. Choo. "A load-deformation formulation for CHS X- and K-joints in push-over analyses". In: *Journal of Constructional Steel Research* 90 (Nov. 2013), pp. 108–119. DOI: 10.1016/j.jcsr.2013.07.024.
- [48] A. Romeijn. "Stress and strain concentration factors of welded multiplanar tubular joints". PhD thesis. Delft University of Technology, 1994.
- [49] A. Romeijn, K.S. Puthli, and J. Wardenier. "Finite element modelling of multiplanar joint flexibility in tubular structures". In: (1992), pp. 420–429.
- [50] A. Romeijn, K.S. Puthli, and J. Wardenier. "The flexibility of uniplanar and multiplanar joints made of circular hollow sections". In: (1991).
- [51] Dikshant Singh Saini, Debasis Karmakar, and Samit ray chaudhuri. "A Review of Stress Concentration Factors in Tubular and Non-Tubular Joints for Design of Offshore Installations". In: *Journal of Ocean Engineering and Science* 1 (Aug. 2016). DOI: 10.1016/j.joes.2016.06.006.
- [52] Siemens. *Simcenter nastran element library reference*. Siemens, 2020.
- [53] I.E. Tebbett. "The reappraisal of steel jacket structures allowing for the composite action of grouted piles". In: *Proceedings of the Annual Offshore Technology Conference* 1982-May (1982), pp. 329–333. DOI: 10.4043/4194-ms.
- [54] Y. Ueda, S.M.H. Bashed, and K. Nakacho. "An improved joint model and equations for flexibility of tubular joints". In: *Journal of Offshore Mechanics and Arctic Engineering* 112.2 (1990), pp. 157–168. DOI: 10.1115/1.2919850.
- [55] Y. Ueda et al. "Flexibility and yield strength of joints in analysis of tubular offshore structures". In: II (1986), pp. 293–302. DOI: 10.1115/1.2919850.
- [56] G.J. van der Vegte et al. "Numerical simulation of experiments on multiplanar tubular steel X-joints". In: *International Journal of Offshore and Polar Engineering* 1.1 (1991), pp. 42–52.





## Academic essay

# Local Joint Flexibility: A study to modelling LJF into a beam model for fatigue design of a stinger.

E. Wierenga \* X.L. Jiang \*\* N. Ermolaeva \*\*\* Y. Yu \*\*\* D.L. Schott \*\*

\* Student at the department of Maritime and Transport Technology, Delft University of Technology

\*\* Department of Maritime and Transport Technology, Delft University of Technology

\*\*\* Allseas Engineering B.V. Delft

**Abstract:** As part of the fatigue assessment of a stinger, member loads on the tubular joints are determined with a beam model. A beam model is a simplified method of modelling complex structures out of circular hollow sections. In a standard beam model, no attention is paid to modelling the tubular joint itself. In the model, beam elements of the braces are extended from the surface of the chord to the centerline of the chord. This connection is considered as rigid. In reality, tubular joints possess considerable elastic flexibility through local deformation of the chord wall. It is suggested that modelling local joint flexibly leads to a reduction of member-loads and thereby an increase of predicted fatigue life. A method to determine and model local joint flexibility in a beam model is developed. A numerical test-case is performed to investigate the influence of modelling LJF on the predicted fatigue life of the braces in the stinger. As effect of modelling LJF, the accumulated fatigue damage in the critical hot spots of the braces has changed with factor 0.29 up to factor 2.88. This would result in a change in predicted fatigue of factor 0.35 up to 3.45 as effect of modelling LJF.

**Keywords:** Local Joint Flexibility, LJF, tubular joint, fatigue assessment, stinger, pipe laying, beam model, chord wall deformation

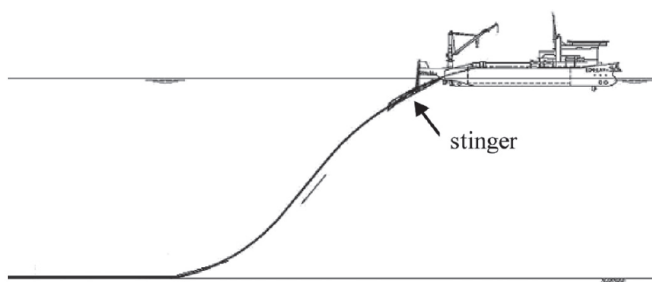


Fig. 1. S-lay pipeline configuration [17]

## 1. INTRODUCTION

Allseas Group S.A. is a Swiss based offshore contractor and global leader in offshore pipeline installation and subsea construction. Allseas uses several ships to lay pipelines following the S-lay method. In this configuration, pipelines are assembled horizontally on a vessel and guided into the water by a stinger frame, to reduce strain in the pipeline and prevent it of buckling (figure 1). In the production line, also called 'firing line' pipe joints are welded together to a pipeline. After completion of the connection of a new joint the vessel moves forward and a part of the pipeline is guided into the water. The stinger is made of a steel space frame structure and mounted on the bow or stern on a vessel. The stinger frame is made of steel tubular sections. In particular circular hollow sections are commonly used in offshore structures because of their good properties for resisting compression, tension, bending and torsion forces but also their low drag coefficients when being subjected to wind and wave loads. The stinger structure is made of upper and lower chords supported by horizontal, vertical and diagonal

braces. The braces and chord are welded together in uni- and multi-planar joints.

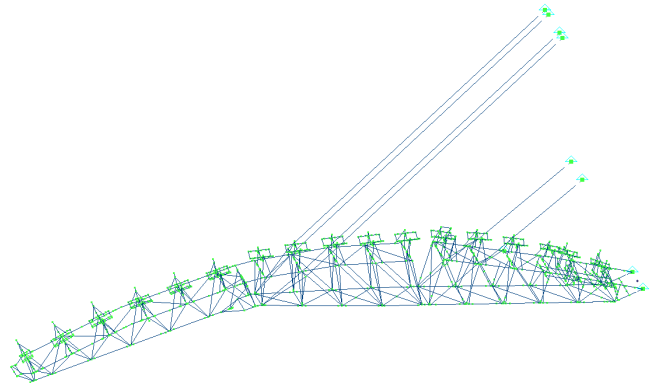


Fig. 2. Beam model of the Solitaire stinger

The stinger is subjected to multiple loads. The hydrodynamic loads make the stinger, especially the tubular joints sensitive for fatigue. Fatigue is defined as the weakening of a material through large amounts of cycles consisting of different stress levels. Due to the nature of the previously mentioned loads, fatigue assessment is important for the lifetime prediction of the stinger. Sub-load-cases are applied in a beam model, in order to calculate the member forces on the tubular joints. An example of a beam model of a stinger is shown in figure 2. The beam member forces are used to calculate the accumulated fatigue damage in the brace and thereby the predicted fatigue life. A beam model is a simplified method of modelling structures. The results of a beam model are not as accurate as the results of a shell model. However, for complex geometries subjected to a high number of load-case ( $\approx 10000$ ) a beam model is a

more efficient method of modelling and computational times are strongly reduced.

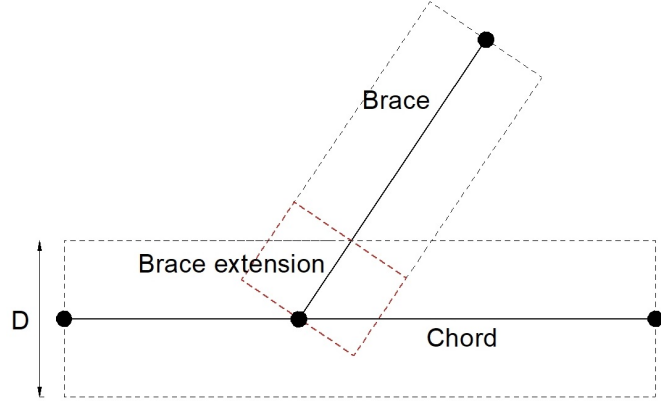


Fig. 3. Schematic presentation of the simplification made when modelling tubular joints with beam elements.

In a standard beam model, no attention is paid to modelling the joint itself. In the model, the beam elements of the brace is extended from the surface of the chord to the centerline of the chord. This simplification is schematically shown in figure 3 and also referred to as 'brace extension element'. This connection is also referred to as rigid [11] [34] [21]. In reality, tubular joints possess considerable elastic flexibility through local deformation of the chord wall (figure 4). In literature, this is also described as Local Joint Flexibility (LJF). MSL Engineering Ltd. [29]: "Structural engineering mechanics suggests that, in essence, representing the joints with finite linear elastic flexibility instead of no flexibility, would result in a reduction of acting loads at the joints, with a commensurate increase in member loads to maintain equilibrium". A more accurate beam model taking LJF into account, leads to a redistribution of the loads which can possibly lead to a reduction of the stresses in the joints [8]. For the determination of the ultimate strength of a joint the influence of LJF is negligible, but for fatigue assessment the influence can lead to considerable differences in predicted fatigue life.

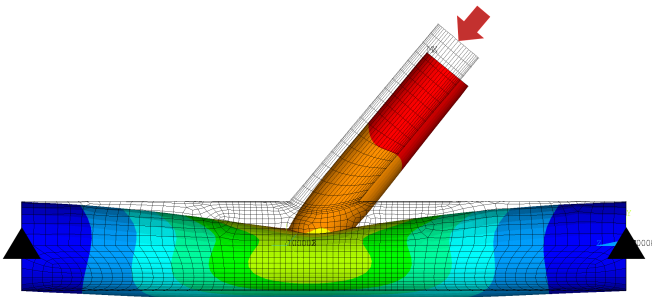


Fig. 4. Chord wall deformation as effect of an axial force

In this research a new state of the art method to model LJF is developed and the influence on the fatigue assessment of a stinger is investigated. In section 2, the presented literature is discussed. In section 3, the flexibilities of tubular joints are discussed. In section 4, the methodology applied in this research is discussed. In section 5, the test-case is described. In section 6, the results of implementation are discussed. In section 7, the obtained results are compared with the results presented in literature. In section 8, the conclusion is presented.

## 2. LITERATURE

In this section, literature considering LJF is discussed.

In a case study, MSL Engineering Ltd.[29], investigated the influence of modelling LJF in an offshore steel jacket structure and found an increase in predicted fatigue life of factor 19.3, 9.2 and 8.0 for transverse-, longitudinal- and horizontal- frames. Golafshani et al. [25], investigated the influence of modelling LJF on the member forces of joint in a jacket structure and found alterations in member loads of factor 0.64 up to 1.18.

Several methods are presented in literature to determine the LJF of a tubular joint. Fessler et al. [19], Tebbett [33], McDermott [16] according to [21] and Fessler et al. [21][18] determined the flexibilities of tubular joints with physical experiments. Romeijn [31] investigated modelling tubular joints for joint flexibility and stress and strain concentration factors in FEA. Ahmadi and Nejad [3][1][2], Asgarian et al. [7], Buitrago et al. [9], Chen and Zhang [10], DNV [12] as cited in [10], Efthymiou [15] as cited in [21], Fessler et al. [19][21][20], Hoshyari [26], Khan et al. [28], Nassiraei [30][27], Gao et al. [22][24][23] and Ueda et al. [34] developed parametric equations for tubular joints. However, the equations are not suitable for the geometries of the joints in a stinger.

Several methods are presented in literature to model LJF in a beam model. MSL [29], Buitrago et al. [9], Ueda et al. [34] and DNV-GL [13] propose to model LJF with an adapted version of a beam element or a spring element. However the method is not able to model off-diagonal flexibilities and interaction among braces. Alanjari et al. [4][5], Alanjari and Asgarian [4], Golafshani et al. [25], Asgarian et al. [6] and Chen and Zhang [11] propose modelling LJF via a global stiffness matrix. This method is able to model all flexibilities, but is only presented for a limited number of flexibilities.

## 3. LOCAL JOINT FLEXIBILITY

The geometry of tubular joints is defined with dimensionless geometric parameters. The dimensions of a tubular joint are presented in figure 5.

$$\alpha = \frac{2L}{D}, \alpha_b = \frac{2l}{d}, \beta = \frac{d}{D}, \gamma = \frac{D}{2T}, \epsilon = \frac{e}{D}, \zeta = \frac{g}{D}, \tau = \frac{t}{T} \quad (1)$$

Flexibility  $f$  is defined as the deformation per unit-load. Also noted as:

$$f = \frac{\delta}{P} \quad (2)$$

The deformation  $\delta$  can be a translation as well as a rotation and unit-load  $P$  can be a unit-force as well as a unit-bending moment. Local Joint Flexibility is defined as the local chord wall deformation as effect of an external load. The deformations appear due to bending of the chord wall, in the direction perpendicular to the chord axis. In the direction parallel to the chord axis, the joint is loaded fully on shear and therefore the flexibility in this direction assumed to be small/zero [4] [5] [25] [11] [9]. Three flexibilities are described: Axial flexibility, out-of-plane bending flexibility and in-plane bending flexibility. The flexibilities are a combination of a unit-load and a deformation and are defined following:

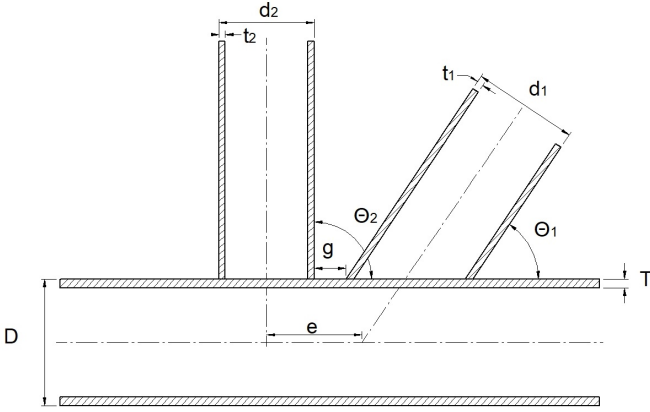


Fig. 5. Dimensions of a tubular joint

$$LJF_{ax} = \frac{\delta_1}{P_1}, LJF_{opb} = \frac{\delta_2}{P_2}, LJF_{ipb} = \frac{\delta_3}{P_3} \quad (3)$$

Deformations and unit-loads are indexed under  $i$  and  $j$  (this notation becomes convenient for the application in multi-brace joints). Deformations are defined with  $\delta_i$  following:

- $\delta_1$  = axial deformation [m]
- $\delta_2$  = out-of-plane bending deformation [rad]
- $\delta_3$  = in-plane bending deformation [rad]

Unit-loads are defined with  $P_j$  following:

- $P_1$  = axial force [N]
- $P_2$  = out-of-plane bending moment [Nm]
- $P_3$  = in-plane bending moment [Nm]

The flexibilities of a joint are defined in the local coordinate system of the brace and visualised in figure 8. A physical impression of the deformations is shown in figure 7.

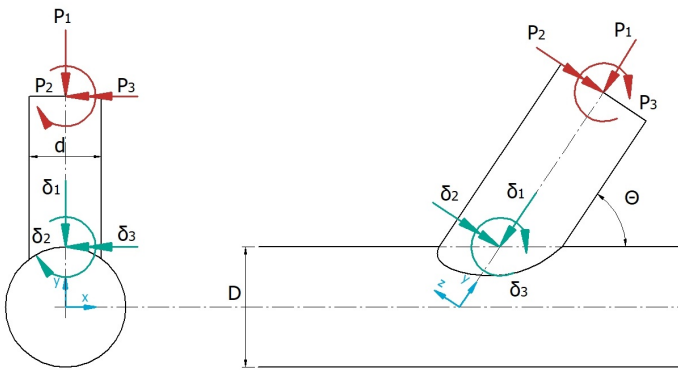


Fig. 6. The flexibilities of a single-brace joint defined in the local brace coordinate system

The previously defined flexibilities define the relation between a deformation and an unit-load in equal DOF. Additionally, there can be coupling between the unit-load in one DOF and the deformation in another DOF. E.g. axial deformations can appear as effect of an in-plane bending moment. The relation

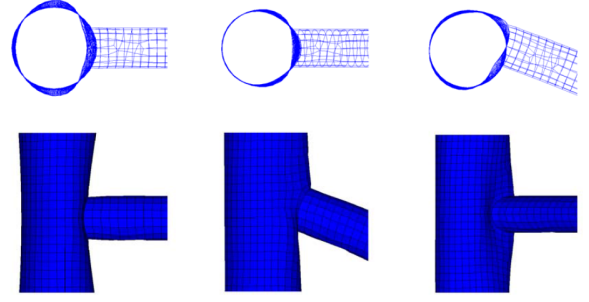


Fig. 7. Deformations of a T-joint. From left to right: axial, in-plane bending and out-of-plane bending [4].

between deformations in the three DOF as effect of the three possible DOF unit-loads, are defined in the LJF matrix  $[LJF]$ . Because there are three DOF the dimension of this matrix is  $3 \times 3$ .

$$\underline{\Delta} = [LJF] \underline{P} \quad (4)$$

Written out:

$$\begin{bmatrix} \delta_1 \\ \delta_2 \\ \delta_3 \end{bmatrix} = \begin{bmatrix} f_{11} & f_{12} & f_{13} \\ f_{21} & f_{22} & f_{23} \\ f_{31} & f_{32} & f_{33} \end{bmatrix} \begin{bmatrix} P_1 \\ P_2 \\ P_3 \end{bmatrix} \quad (5)$$

Here,  $f_{ij}$  represents the flexibility defined by a deformation in DOF  $i$  as effect of the unit-load in DOF  $j$ . Because of the Maxwell-Betti reciprocal work theorem, the flexibility matrix shall be symmetrical.

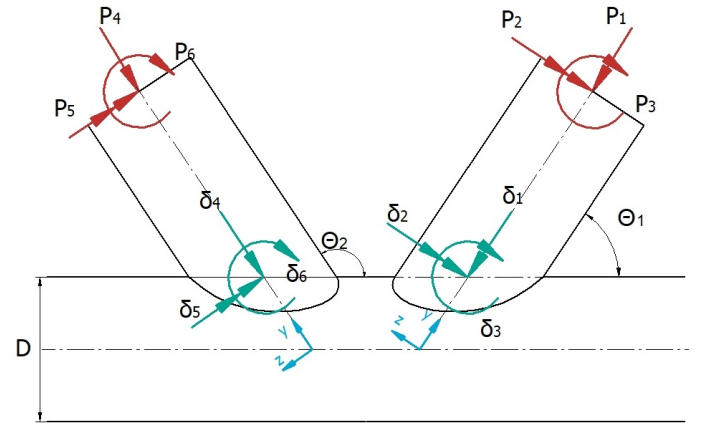


Fig. 8. The flexibilities of a multi-brace joint defined in the local brace coordinate system

When braces in multi-brace joints are located close to each other, a brace can deform as effect of a load on an adjacent brace. The single-brace theorem for flexibilities is expanded for multi-brace joints. With every additional brace, three DOF deformations and three possible unit-loads are added to the joint. The deformations and loads are schematically shown in figure 8. The index for deformation  $\delta_i$  and unit-load  $P_j$  is expanded:

- $\delta_1$  = axial deformation of brace 1
- $\delta_2$  = out-of-plane bending deformation of brace 1



## 6. RESULTS

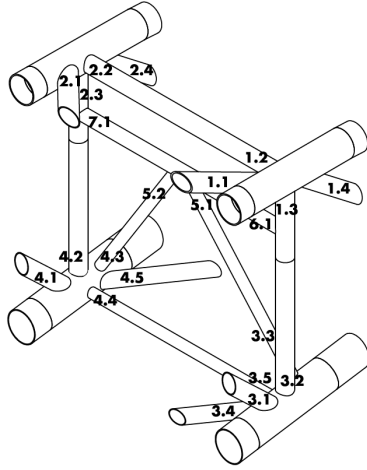


Fig. 9. Overview of braces/joints of interest.

the fatigue damage is strongly load-case dependent. To retrieve reliable and representative results, the stinger is assessed to a total of sixteen different load-cases of three hours each. The load-cases concern loads as effect of waves from varying headings, but with identical wave height and period. An overview of the load-cases is presented in table 1. The definition of the wave heading is shown in figure 10. The hydrodynamic loads on the stinger are calculated in AQWA simulations.

Table 1. Overview of load-cases

load-case	wave height [m]	wave heading [°]	wave period [s]
1	2.5	0	8.5
2	2.5	22.5	8.5
3	2.5	45	8.5
4	2.5	67.5	8.5
5	2.5	90	8.5
6	2.5	112.5	8.5
7	2.5	135	8.5
8	2.5	157.5	8.5
9	2.5	180	8.5
10	2.5	202.5	8.5
11	2.5	225	8.5
12	2.5	247.5	8.5
13	2.5	270	8.5
14	2.5	292.5	8.5
15	2.5	315	8.5
16	2.5	337.5	8.5

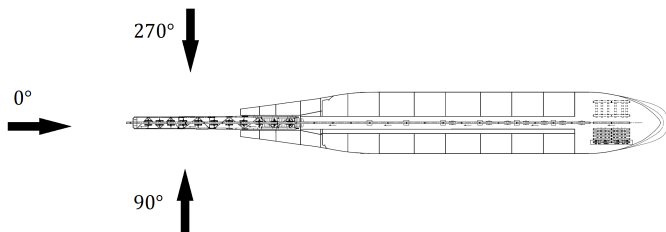


Fig. 10. Definition of heading.

The fatigue assessment is performed following the procedure applied by Allseas [17]. The procedure follows DNV-RP-C203 [14].

In this section, the results of modelling LJF in the stinger are discussed. The predicted fatigue life of the braces in the stinger is dependent on the accumulated fatigue damage in the most affected hot spot. The damage in the most affected hot spots of the 22 braces after exposure to the sixteen different load-cases for three hours each, is shown in table 2. The accumulated fatigue damage in the most affected hot spots of the braces has changed with factor 0.29 up to factor 2.88 as effect of LJF. An increase of fatigue damage with factor 3 may seem large but due to the nature of fatigue, it is only the results of an increase in stress range of  $\sqrt[3]{3} = 1.25$  (where 5 is equal to the inverse slope of the SN curve for tubular joints [14]). The change in predicted fatigue life as effect of modelling LJF, is equal to factor 0.35 up to 3.45. These values are not expected to be the maximum and minimum values, in exceptional cases these values can be exceeded. However, the values are considered as a reliable impression of the influence of modelling LJF in the joints of the stinger. No large alterations in critical braces or most affected hot spot within the brace, as effect of modelling LJF are observed.

Table 2. Comparison of critical fatigue damage according to a model with and without LJF

Joint no.	Brace no.	Model without LJF		Model with LJF		Ratio with/without
		Most affected hot spot	Calculated fatigue damage	Most affected hot spot	Calculated fatigue damage	
1	1	2 <sub>c</sub>	1.24 e-06	2 <sub>c</sub>	2.15 e-06	1.74
	2	6 <sub>c</sub>	4.59 e-07	6 <sub>c</sub>	1.27 e-06	2.78
	3	7 <sub>c</sub>	1.62 e-05	8 <sub>c</sub>	1.94 e-05	1.20
	4	4 <sub>c</sub>	3.38 e-05	4 <sub>c</sub>	5.40 e-05	1.60
2	1	3 <sub>c</sub>	1.59 e-08	3 <sub>c</sub>	4.59 e-08	2.88
	2	3 <sub>c</sub>	1.11 e-05	3 <sub>c</sub>	3.25 e-06	0.29
	3	3 <sub>c</sub>	3.07 e-05	2 <sub>c</sub>	1.22 e-05	0.40
3	4	6 <sub>c</sub>	4.34 e-05	6 <sub>c</sub>	7.12 e-05	1.64
	1	3 <sub>c</sub>	5.93 e-07	2 <sub>c</sub>	6.74 e-07	1.14
	2	5 <sub>b</sub>	2.27 e-05	5 <sub>b</sub>	3.39 e-05	1.49
	3	1 <sub>b</sub>	4.45 e-07	1 <sub>b</sub>	5.43 e-07	1.22
4	4	1 <sub>b</sub>	1.12 e-05	1 <sub>b</sub>	2.27 e-05	2.03
	5	6 <sub>b</sub>	5.88 e-05	5 <sub>b</sub>	8.54 e-05	1.45
	1	7 <sub>c</sub>	9.36 e-07	7 <sub>c</sub>	1.47 e-06	1.57
	2	4 <sub>b</sub>	2.76 e-05	5 <sub>b</sub>	2.77 e-05	1.00
	3	8 <sub>b</sub>	8.10 e-07	8 <sub>b</sub>	7.02 e-07	0.87
5	4	8 <sub>b</sub>	5.56 e-05	1 <sub>b</sub>	8.77 e-05	1.58
	5	5 <sub>b</sub>	2.90 e-06	5 <sub>b</sub>	6.96 e-06	2.40
	1	3 <sub>c</sub>	5.00 e-04	3 <sub>c</sub>	4.26 e-04	0.85
6	2	3 <sub>c</sub>	5.17 e-04	3 <sub>c</sub>	4.32 e-04	0.84
	1	3 <sub>c</sub>	5.54 e-04	3 <sub>c</sub>	2.78 e-04	0.50
7	1	7 <sub>c</sub>	4.49 e-04	7 <sub>c</sub>	2.29 e-04	0.51

## 7. DISCUSSION

The obtained results do not correspond with the results obtained by MSL Engineering Ltd.[29]. No considerable overall benefit as found by MSL Engineering Ltd.[29] in predicted fatigue life of the joints in the stinger as effect of modelling LJF is observed. Furthermore, the magnitude of the influence of modelling LJF on the predicted fatigue life is larger in the publication of MSL Engineering Ltd.[29]. The difference in results can be caused by the following reasons: Firstly, MSL Engineering Ltd.[29] only modelled LJF to a selection of braces throughout the jacket. It is observed that by modelling LJF in one brace, its predicted fatigue life increases, but as effect

the predicted fatigue life of adjacent and surrounding braces decreases. The fatigue life of the adjacent braces is not mentioned in the research of MSL Engineering Ltd. Furthermore, modelling LJF in adjacent and surrounding braces, would have led to a decrease in predicted fatigue life of the braces of consideration. Secondly, MSL Engineering Ltd.[29] models LJF via a 'custom beam element'. This element possess flexibility in the direction parallel to the chord wall. Third, in the publication of MSL Engineering Ltd.[29] it is suggested that the joints have a relative high  $\gamma$  value ( $\gamma > 15$ ). Joints with this geometry possess more flexibility, leading to larger differences. Fourth, MSL Engineering Ltd. determines the LJF with the parametric equations of Buitrago et al. [9] which tend to overestimate the LJF.

The observations of this research correspond partially with the observations in the research of Golafshani et al. [25]. Golafshani et al.[25] did not calculate the predicted fatigue life, but provides the member forces as result of modelling LJF. Golafshani et al.[25] does observe the increase of member loads as effect of modelling LJF which would potentially lead to a decreased predicted fatigue life of the brace.

For both researches it is though to take a conclusion about the reason of the different results, due to the limited available data.

## 8. CONCLUSION

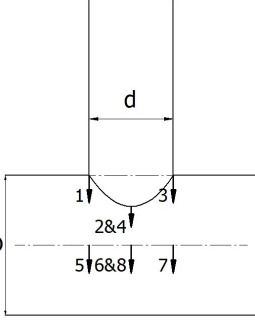
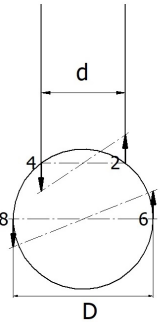
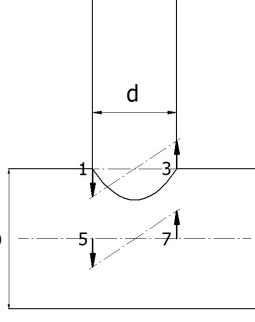
LJF is defined as the flexibility through local chord wall deformation caused by an external load. A new method is developed to determine the LJF of any non-overlapping joint. The flexibilities are inserted directly in the global stiffness matrix via FEMAP general elements. In a test-case on the stinger, the total accumulated fatigue damage as effect of exposure to 16 load-cases changed with factor 0.29 up to factor 2.88 as effect of modelling LJF. Thereby the predicted fatigue life of the braces would change with factor 0.35 up to 3.45 as effect of modelling LJF. The observed changes in predicted fatigue life as effect of modeling LJF are considered as reliable, because they are based on the total accumulated fatigue damage of sixteen different load-cases. However, they not expected to be the maximum and minimum values, in exceptional cases these values can be exceeded.

## REFERENCES

- [1] H. Ahmadi and A. Ziaei Nejad. Geometrical effects on the local joint flexibility of two-planar tubular DK-joints in jacket substructure of offshore wind turbines under OPB loading. *Thin-Walled Structures*, 114:122–133, 2017.
- [2] H. Ahmadi and A. Ziaei Nejad. Local joint flexibility of two-planar tubular DK-joints in OWTs subjected to axial loading: parametric study of geometrical effects and design formulation. *Ocean Engineering*, 136:1–10, 2017.
- [3] H. Ahmadi and A. Ziaei Nejad. A study on the local joint flexibility (LJF) of two-planar tubular DK-joints in jacket structures under in-plane bending loads. *Applied Ocean Research*, 64:1–14, 2017.
- [4] P. Alanjari, B. Asgarian, and M. Kia. Nonlinear joint flexibility element for the modeling of jacket-type offshore platforms. *Applied Ocean Research*, 33(2):147–157, 2011.
- [5] P. Alanjari, B. Asgarian, and N. Salari. Elastic tubular joint element for modelling of multi-brace, uni-planar tubular connections. *Ships and Offshore Structures*, 10(4):404–415, 2015.
- [6] B. Asgarian, P. Alanjari, and V. Aghaeidoost. Three-dimensional joint flexibility element for modeling of tubular offshore connections. *Schmerz*, 29(6):629–639, 2015.
- [7] B. Asgarian, V. Mokarram, and P. Alanjari. Local joint flexibility equations for y-t and k-type tubular joints. *Ocean Systems Engineering*, 4(2):151–167, 2014.
- [8] J.G. Bouwkamp, J.P. Hollings, B.F. Maison, and D.G. Row. Effects of joint flexibility on the response of offshore towers. volume 1980-May, pages 455–464, 1980.
- [9] J. Buitrago, B.E. Healy, and T.Y. Chang. Local joint flexibility of tubular joints. volume 1, pages 405–411, 1993.
- [10] B. Chen, Y. Hu, and M. Tan. Local joint flexibility of tubular joints of offshore structures. *Marine Structures*, 3(3):177–197, 1990.
- [11] T.-Y. Chen and H.-Y. Zhang. Stress analysis of spatial frames with consideration of local flexibility of multiplanar tubular joint. *Engineering Structures*, 18(6):465–471, 1996.
- [12] DNV. Rules for the design, construction and inspection of offshore structures, 1977.
- [13] DNV. Dnv-os-j101 design of offshore wind turbine structures, 2014.
- [14] DNV GL. Dnvgl-rp-c203 fatigue design of offshore steel structures, 2019.
- [15] M. Efthymiou. Local rotational stiffness of unstiffened tubular joints. Report no. rker.85.199, Koninklijke/Shell exploratie en produktie laboratorium, Rijswijk, 1985.
- [16] McDermott Engineering. Occidental of Britain inc. piper a jacket, static load tests on model of 12 3/4 / 24 inch tubular joint. 1979.
- [17] N. Ermolaeva, Y. Yu, and L. Zhao. Design and fatigue assessment of a stinger. pages 547–555, 2010.
- [18] H. Fessler, P.B. Mockford, and J.J. Webster. An experimental technique for determining the flexibility of tubular joints in offshore structures. *The Journal of Strain Analysis for Engineering Design*, 22(1):7–15, 1987.
- [19] H. Fessler and H. Spooner. Experimental determination of stiffness of tubular joints. pages 493–511, 1981.
- [20] H. Fessler, J.J. Webster, and P.B. Mockford. Parametric equations for the flexibility matrices of multi-brace tubular joints in offshore structures. *INST. CIV. ENGRS. PROC. PART 2.*, 81, Dec. 1986:675–696, 1986.
- [21] H. Fessler, J.J. Webster, and P.B. Mockford. Parametric equations for the flexibility matrices of single brace tubular joints in offshore structures. *INST. CIV. ENGRS. PROC. PART 2.*, 81, Dec. 1986:659–673, 1986.
- [22] F. Gao and B. Hu. Local joint flexibility of completely overlapped tubular joints under out-of-plane bending. *Journal of Constructional Steel Research*, 115:121–130, 2015.
- [23] F. Gao, B. Hu, and H.P. Zhu. Parametric equations to predict LJF of completely overlapped tubular joints under lap brace axial loading. *Journal of Constructional Steel Research*, 89:284–292, 2013.
- [24] F. Gao, B. Hu, and H.P. Zhu. Local joint flexibility of completely overlapped tubular joints under in-plane bending. *Journal of Constructional Steel Research*, 99:1–9, 2014.
- [25] A.A. Golafshani, M. Kia, and P. Alanjari. Local joint flexibility element for offshore platforms structures. *Marine*

- Structures*, 33:56–70, 2013.
- [26] I. Hoshyari and R. Kohoutek. Rotational and axial flexibility of tubular T-joints. pages 192–198, 1993.
  - [27] H. Hossein. Local joint flexibility of CHS T/Y-connections strengthened with collar plate under in-plane bending load: parametric study of geometrical effects and design formulation. *Ocean Engineering*, 202:107054, apr 2020.
  - [28] R. Khan, K. Smith, and I. Kraincanic. Improved LJF equations for the uni-planar gapped K-type tubular joints of ageing fixed steel offshore platforms. *Journal of Marine Engineering and Technology*, 17(3):121–136, 2018.
  - [29] MSL Engineering Ltd. The effect of local joint flexibility on the reliability of fatigue life estimates and inspection planning. Technical Report 2001/056, Health and Safety Executive, 2001.
  - [30] H. Nassiraei. Local joint flexibility of chs x-joints reinforced with collar plates in jacket structures subjected to axial load. *Applied Ocean Research*, 93, 2019.
  - [31] A. Romeijn. *Stress and strain concentration factors of welded multiplanar tubular joints*. PhD thesis, Delft University of Technology, 1994.
  - [32] Siemens. *Simcenter nastran element library reference*. Siemens, 2020.
  - [33] I.E. Tebbett. The reappraisal of steel jacket structures allowing for the composite action of grouted piles. volume 1982-May, pages 329–333, 1982.
  - [34] Y. Ueda, S.M.H. Bashed, and K. Nakacho. An improved joint model and equations for flexibility of tubular joints. *Journal of Offshore Mechanics and Arctic Engineering*, 112(2):157–168, 1990.
  - [35] E. Wierenga. Local joint flexibility: A study to modelling LJF into a beam model for fatigue design of a stinger. Master’s thesis, Delft University of Technology, 2021.

Table A.1. Overview of equations to calculate the chord wall deformations of a multi-brace joint

<p><b>Axial deformation as effect of axial force</b></p> $\delta_{ij} = \frac{\kappa_{1,1} - \kappa_{5,jb} + \kappa_{2,jb} - \kappa_{6,jb} + \kappa_{3,jb} - \kappa_{7,jb} + \kappa_{4,jb} - \kappa_{8,jb}}{4} \sin \theta_b \quad (\text{A.1})$	
<p><b>Axial deformation as effect of out-of-plane bending moment</b></p> $\delta_{ij} = \frac{\kappa_{1,jb} + \kappa_{2,jb} + \kappa_{3,jb} + \kappa_{4,jb}}{4} \sin \theta_b \quad (\text{A.2})$	
<p><b>Axial deformation as effect of in-plane bending moment</b></p> $\delta_{ij} = \frac{\kappa_{1,jb} - \kappa_{5,jb} + \kappa_{2,jb} - \kappa_{6,jb} + \kappa_{3,jb} - \kappa_{7,jb} + \kappa_{4,jb} - \kappa_{8,jb}}{4} \sin \theta_b \quad (\text{A.3})$	
<p><b>Out-of-plane bending as effect of axial force</b></p> $\delta_{ij} = \left( \frac{\kappa_{2,jb} - \kappa_{4,jb}}{d_b} - \frac{\kappa_{6,jb} - \kappa_{8,jb}}{D} \right) \sin \theta_b \quad (\text{A.4})$	
<p><b>Out-of-plane bending as effect of out-of-plane bending moment</b></p> $\delta_{ij} = \left( \frac{\kappa_{2,jb} - \kappa_{4,jb}}{d_b} - \frac{\kappa_{6,jb} - \kappa_{8,jb}}{D} \right) \sin \theta_b \quad (\text{A.5})$	
<p><b>Out-of-plane bending as effect of in-plane bending moment</b></p> $\delta_{ij} = \left( \frac{\kappa_{2,jb} - \kappa_{4,jb}}{d_b} - \frac{\kappa_{6,jb} - \kappa_{8,jb}}{D} \right) \sin \theta_b \quad (\text{A.6})$	
<p><b>In-plane bending as effect of axial force</b></p> $\delta_{ij} = \frac{\kappa_{3,jb} - \kappa_{7,jb} - \kappa_{1,jb} + \kappa_{5,jb}}{d_b} \sin \theta_b \quad (\text{A.7})$	
<p><b>In-plane bending as effect of out-of-plane bending moment</b></p> $\delta_{ij} = \frac{\kappa_{3,jb} - \kappa_{1,jb}}{d_b} \sin \theta_b \quad (\text{A.8})$	
<p><b>In-plane bending as effect of in-plane bending moment</b></p> $\delta_{ij} = \frac{\kappa_{3,jb} - \kappa_{7,jb} - \kappa_{1,jb} + \kappa_{5,jb}}{d_b} \sin \theta_b \quad (\text{A.9})$	



# B

## Mesh contours

### B.1. Single-brace model numerical model

To mesh the joints, an approach from Cao et al. [15] [16] is used. In this appendix the approach is explained further.

A Cartesian  $XYZ$  coordinate system is defined in the center of the chord with the  $Z$ -axis along the length of the chord and the  $X$ -axis in the plane of the brace (Figure B.1). Cylindrical coordinates in the same system are defined by  $R\phi Z$ :

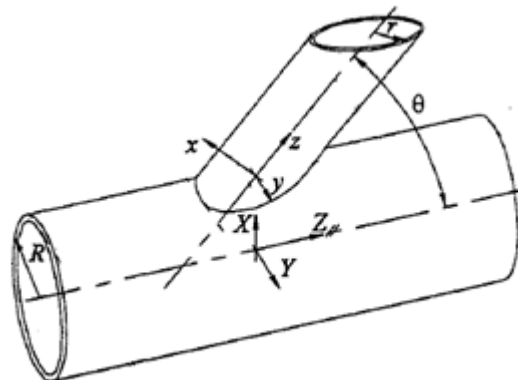


Figure B.1: The coordinate systems of the chord and brace [15]

$$x = r \cos(\phi) \tag{B.1}$$

$$y = r \sin(\phi) \tag{B.2}$$

$$r^2 = x^2 + y^2 \tag{B.3}$$

System  $xyz$  is located at  $X = R$ ,  $Y = 0$  and  $Z = 0$ . The difference in orientation between the  $XYZ$  and  $xyz$  coordinate system is a rotation around the  $Y/y$  axis equal to the in-plane angle of the brace described by  $\theta$ . The relationship between coordinates in the  $XYZ$  and  $xyz$  system is described with:

$$X = x \cos(\theta) + z \sin(\theta) + R \quad (\text{B.4})$$

$$Y = y \quad (\text{B.5})$$

$$Z = z \cos(\theta) - z \sin(\theta) + R \quad (\text{B.6})$$

The coordinates of the intersection between brace and chord are given by:

$$X_i = \sqrt{R^2 - Y_i^2} \quad (\text{B.7})$$

$$Y_i = y \quad (\text{B.8})$$

$$Z_i = \frac{y}{\sin(\theta)} - (R - X) \frac{\cos(\theta)}{\sin(\theta)} \quad (\text{B.9})$$

The chord wall is unfolded into a flat surface with coordinate system  $Y' Z'$  which is located on  $X = R$  (Figure B.2).  $Z'$  is equal to the chord length and  $Y'$  has dimensions  $[-\pi R, \pi R]$  representing the chord circumference. The relation between  $XYZ$  and  $Y'Z'$  system is given by:

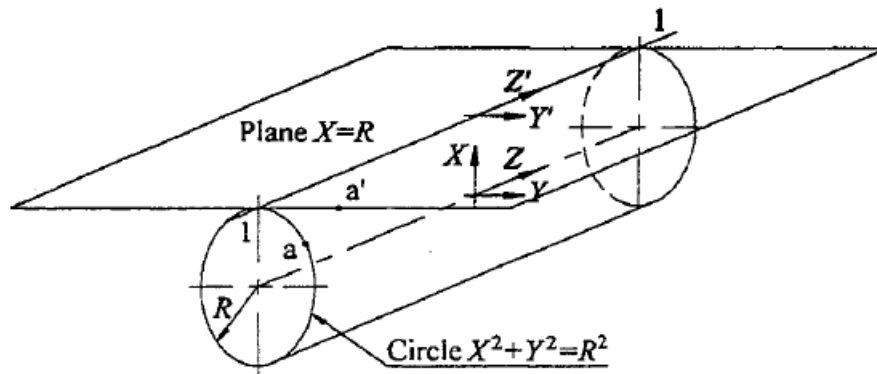


Figure B.2: Unfolding of the chord surface [15]

$$X = R \cos\left(\frac{Y'}{R}\right) \quad (\text{B.10})$$

$$Y = R \sin\left(\frac{Y'}{R}\right) \quad (\text{B.11})$$

$$Z = Z' \quad (\text{B.12})$$

The intersection on the unfolded surface  $Y'Z'$  is described by:

$$Y'_i = R \sin^{-1} \left( \frac{Y_i}{R} \right) \quad (\text{B.13})$$

$$Z'_i = Z_i \quad (\text{B.14})$$

To generate squared elements around the chord/brace intersection, contours maintaining a constant width  $w$  are drawn around the intersection over the unfolded chord surface, following an approach from Ermolaeva et al. [27].

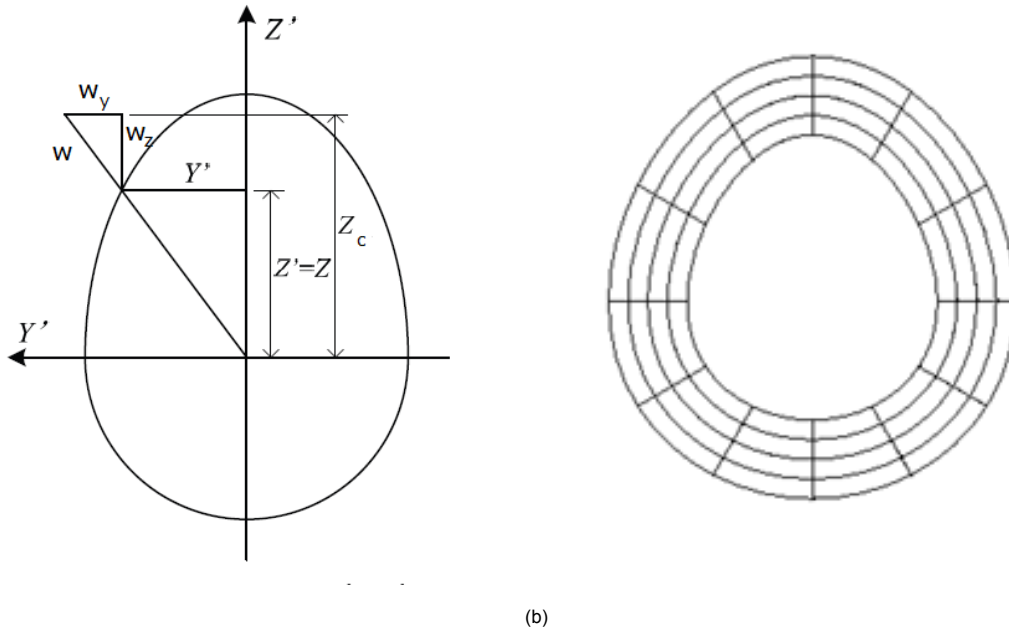


Figure B.3: The chord intersection in the  $Y'Z'$  plane [27] (a) and the mesh contours on the flattened chord surface, on the in- and outside of the intersection line (b).

$$W_{Y'} = w \sin \left( \arctan \left( \frac{Y'_i}{Z'_i} \right) \right) \quad (\text{B.15})$$

$$W_{Z'} = w \cos \left( \arctan \left( \frac{Y'_i}{Z'_i} \right) \right) \quad (\text{B.16})$$

On the in- and outside of the intersection line, two contours with width  $w$ , equal to the chord wall thickness  $t$ , are generated (Figure B.3). The coordinates of the contours in the  $XYZ$  system are obtained by:

$$X_C = R \cos \left( \frac{Y'_i + W_{Y'}}{R} \right) \quad (\text{B.17})$$

$$Y_C = R \sin \left( \frac{Y'_i + W_{Y'}}{R} \right) \quad (\text{B.18})$$

$$Z_C = Z'_i + W_{Z'} \quad (\text{B.19})$$

An example of the mesh contours on the chord wall is shown in Figure B.4.

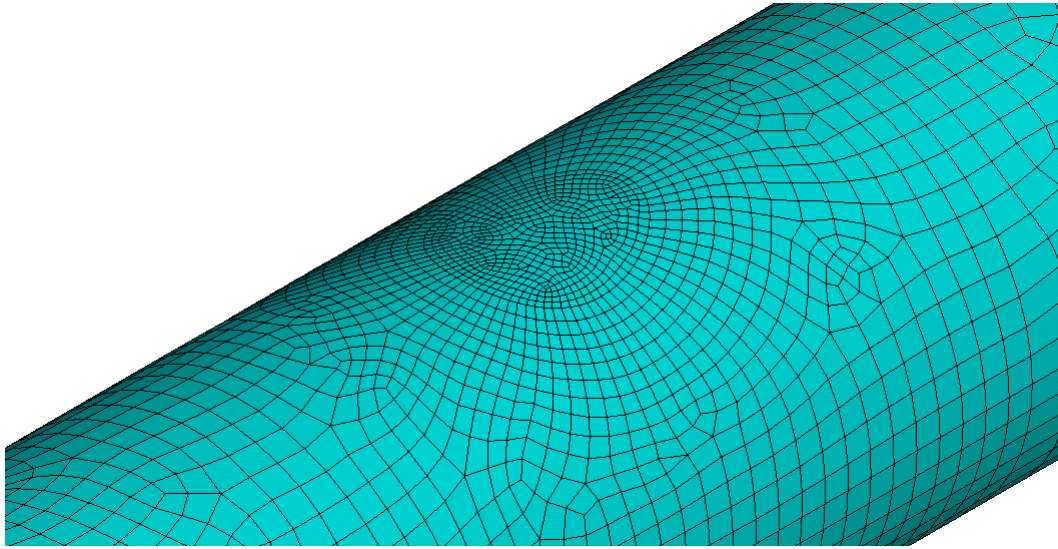


Figure B.4: An example of the mesh contours on the chord wall

## B.2. Multi-brace numerical model expansion

In this appendix the mathematics behind the algorithm used to generate a mesh for the multi-brace model is explained further. The approach is an adaption of the approach from Cao et al.[15] used for the single-brace model.

The mesh contour reduction for in-plane intersections is calculated with:

$$w_r = \frac{(Z' - Z'_{mid})^2}{(Z'_{max} - Z'_{mid})^2} * \left( w - \frac{g}{2.5} \right) \quad (\text{B.20})$$

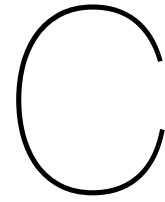
The mesh contour reduction for out-of-plane intersections is calculated with:

$$w_r = \frac{(Y' - Y'_{mid})^2}{(Y'_{max} - Y'_{mid})^2} * \left( w - \frac{g}{2.5} \right) \quad (\text{B.21})$$

Reduction  $w_r$  is inserted in equations B.15 and B.16:

$$W_{Y'} = (w - w_r) \sin \left( \arctan \left( \frac{Y'_i}{Z'_i} \right) \right) \quad (\text{B.22})$$

$$W_{Z'} = (w - w_r) \cos \left( \arctan \left( \frac{Y'_i}{Z'_i} \right) \right) \quad (\text{B.23})$$



## Coordinate systems

Within the report four different coordinate systems are referred to. The global coordinate system, the local joint coordinate system, the local chord coordinate system and the local brace coordinate system. In this appendix the orientation of the coordinate systems is explained. The coordinate systems are schematically presented in figure C.1

### C.1. Global coordinate system

The global coordinate system, is the coordinate system of the environment in which the joint is located. The other coordinate systems are defined within the global coordinate system.

### C.2. Local joint coordinate system

The local joint coordinate system is aligned with the joint of consideration. The z-axis points in the direction of the chord. The y-axis points in the direction of  $\psi = 0^\circ$  and  $\theta = 90^\circ$ .

The coordinate system of the joint can have any orientation within the global coordinate system.

### C.3. Local chord coordinate system

The local chord coordinate system, is aligned with the plane, defined by the centerline of the brace of consideration and the centerline of the chord. The z-axis points in the direction of the chord. The y-axis is oriented perpendicular to the chord wall, in the direction of out-of-plane angle  $\psi$  of the brace of consideration. The x-axis is oriented perpendicular to the plane defined by the y- and z-axis.

Rotation from local joint coordinate system to local chord coordinate system, is performed through rotation around the z-axis, equal to out-of-plane angle  $\psi$ . When  $\psi = 0$ , the local chord coordinate system is equal to the local joint coordinate system.

### C.4. Local brace coordinate system

The local brace coordinate system is aligned with the brace of consideration. The y-axis points in the direction of the centerline of the brace. The x-axis point perpendicular to the surface created by the centerline of the chord and the center line of the brace. The z-axis is oriented perpendicular to the surface created by the x- and y- axis.

Rotation from local chord coordinate system to local brace coordinate system, is performed through rotation around the x-axis, equal to in-plane angle  $90 - \theta$ . When  $\theta = 90$ , the local brace coordinate system is equal to the local chord coordinate system.

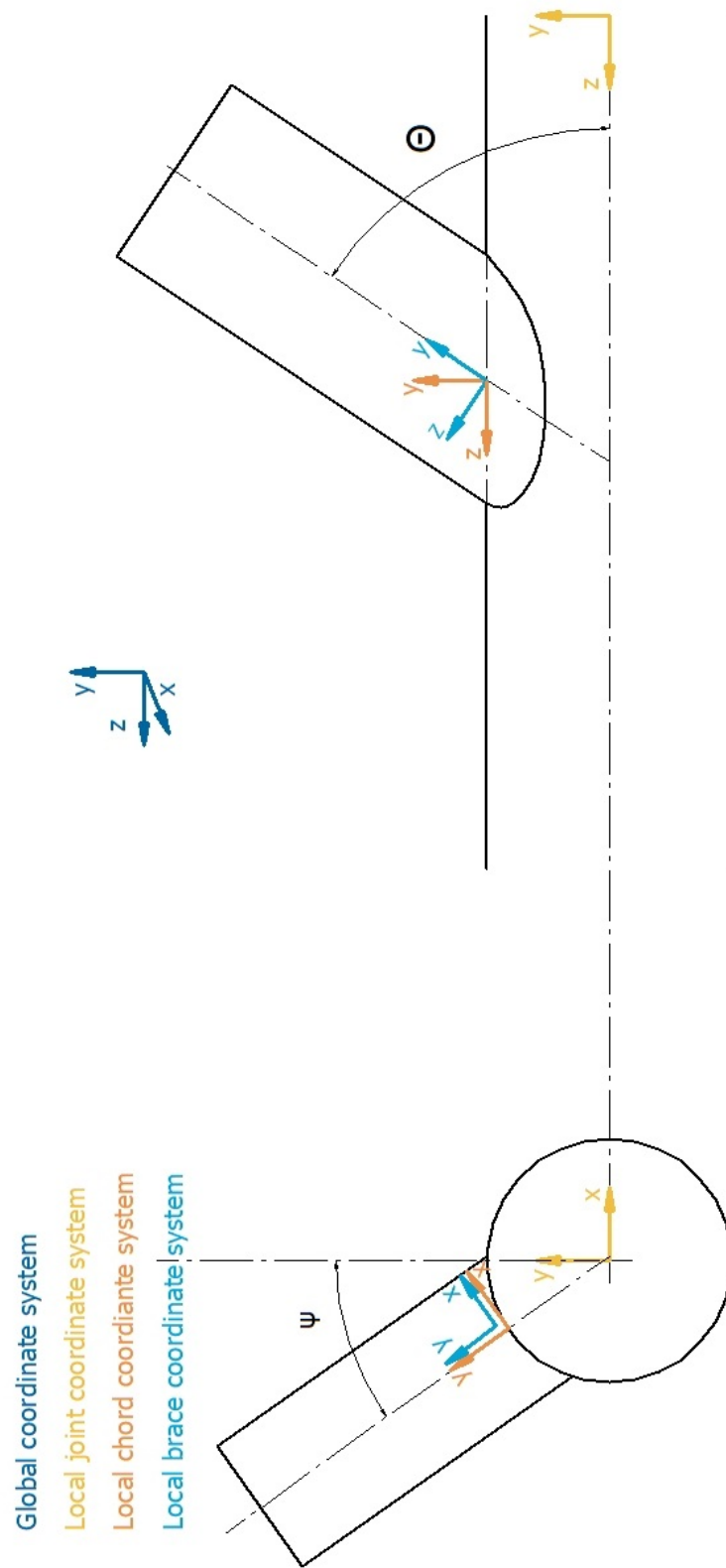
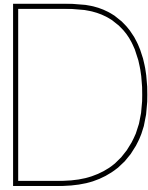


Figure C.1: Schematic presentation of the coordinate systems



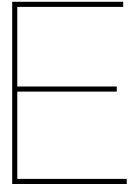
## Results verification single-brace numerical model

In this appendix the results from the verification from the single-brace model are shown. The results are shown in Table D.1.

The constraints are appointed as:

- F= Fixed support
- P= Pinned support
- R= Roller support





## Results of validations of single-brace joint

This appendix contains the results of the validation, discussed in section 4.4.

Table E.1: Comparison of results from 31 measurements for axial flexibility.

Specifications		Axial flexibility $f_{11}^*$ [-]											
No.	Author	$\gamma$	$\beta$	$\tau$	$\theta$	Experiment	Numerical Model (mid-plane)	Numerical Model	Brace extended element	Fessler et al. [31]	Buitrago et al. [13]	Chen et al. [17]	Ueda et al. [54]
1	Fessler	10.0	0.333	0.394	35	52	52 +1%	49 +7%	45 -14%	48 -7%	88 +70%	77 +48%	77 +48%
2	Fessler	10.0	0.333	0.394	50	85	98 +15%	90 +6%	34 -60%	91 +7%	147 +73%	138 +62%	137 +61%
3	Fessler	10.0	0.333	0.394	90	152	171 +12%	157 +3%	26 -83%	163 +7%	236 +55%	236 +55%	234 +54%
4	Fessler	10.0	0.525	0.379	35	41	31 -25%	29 -30%	29 -29%	31 -24%	57 +40%	41 +0%	45 +9%
5	Fessler	10.0	0.525	0.379	50	55	57 +4%	53 -3%	22 -61%	58 +6%	96 +74%	74 +34%	79 +44%
6	Fessler	10.0	0.525	0.379	90	105	98 -7%	91 -13%	17 -84%	105 -0%	154 +46%	126 +20%	135 +29%
7	Fessler	10.0	0.756	0.485	35	24	14 -41%	13 -45%	16 -35%	13 -46%	33 +39%	19 -19%	29 +20%
8	Fessler	10.0	0.756	0.485	50	34	25 -27%	23 -31%	12 -66%	25 -28%	55 +63%	35 +2%	51 +51%
9	Fessler	10.0	0.756	0.485	90	57	41 -28%	39 -32%	9 -84%	44 -23%	89 +56%	60 +5%	87 +53%
10	Fessler	14.8	0.333	0.590	35	121	142 +18%	133 +10%	44 -63%	112 -8%	177 +47%	180 +49%	189 +57%
11	Fessler	14.8	0.333	0.590	50	223	260 +17%	243 +9%	33 -85%	211 -5%	296 +33%	323 +45%	338 +52%
12	Fessler	14.8	0.333	0.590	90	390	447 +15%	418 +7%	26 -93%	378 -3%	474 +22%	553 +42%	576 +48%
13	Fessler	14.8	0.525	0.568	35	80	84 +4%	79 -1%	29 -64%	72 -10%	116 +45%	96 +20%	110 +37%
14	Fessler	14.8	0.525	0.568	50	120	150 +25%	142 +18%	21 -82%	136 +13%	193 +61%	173 +44%	196 +63%
15	Fessler	14.8	0.525	0.568	90	267	254 -5%	240 -10%	16 -94%	243 -9%	309 +16%	296 +11%	333 +25%
16	Fessler	14.8	0.756	0.727	35	31	36 +16%	34 +11%	15 -50%	30 -2%	67 +116%	45 +47%	71 +128%
17	Fessler	14.8	0.756	0.727	50	52	62 +19%	59 +13%	12 -78%	57 +10%	112 +115%	82 +57%	126 +143%
18	Fessler	14.8	0.756	0.727	90	65	102 +57%	97 +50%	9 -86%	102 +57%	179 +175%	140 +115%	215 +231%
19	Fessler	19.6	0.333	0.788	35	221	282 +28%	266 +21%	44 -80%	204 -8%	291 +32%	329 +49%	359 +63%
20	Fessler	19.6	0.333	0.788	50	385	512 +33%	484 +26%	33 -91%	384 -0%	486 +26%	590 +53%	641 +66%
21	Fessler	19.6	0.333	0.788	90	737	882 +20%	833 +13%	25 -97%	688 -7%	779 +6%	1011 +37%	1092 +48%
22	Fessler	19.6	0.525	0.746	35	149	164 +10%	157 +5%	29 -81%	131 -12%	190 +28%	176 +18%	208 +40%
23	Fessler	19.6	0.525	0.746	50	239	293 +23%	280 +17%	22 -91%	247 +3%	318 +33%	316 +32%	371 +55%

24	Fessler	19.6	0.525	0.746	90	430	503	+17%	479	+11%	16	-96%	442	+3%	509	+18%	542	+26%	632	+47%
25	Fessler	19.6	0.756	0.970	35	56	67	+20%	65	+16%	15	-73%	55	-2%	110	+96%	83	+49%	134	+140%
26	Fessler	19.6	0.756	0.970	50	118	117	-1%	112	-5%	11	-90%	104	-12%	183	+55%	149	+26%	240	+103%
27	Fessler	19.6	0.756	0.970	90	219	197	-10%	189	-14%	9	-96%	186	-15%	294	+34%	256	+17%	408	+86%
28	Tebbett	32.0	0.589	0.500	90	-	-	-	-	-	-	-	-	-	-	-	-	-	-	-
29	Tebbett	20.0	0.331	0.500	90	863	994	+15%	956	+11%	10	-99%	722	-16%	859	-0%	1069	+24%	1159	+34%
30	Tebbett	20.0	0.537	0.500	90	454	547	+20%	529	+17%	6	-99%	400	-12%	541	+19%	547	+20%	648	+43%
31	Tebbett	20.0	0.924	0.500	90	148	83	-44%	86	-42%	3	-98%	132	-11%	226	+53%	156	+5%	338	+128%

Table E.2: Comparison of results from 31 measurements for out-of-plane bending flexibility.

Specifications		Out-of-plane bending flexibility $f_{22}^*$ [-]										
No.	Author	$\gamma$	$\beta$	$\tau$	$\theta$	Experiment	Numerical Model (mid-plane)	Numerical Model	Brace extended element	Fessler et al. [31]	Buitrago et al. [13]	Efthymiou [24]
1	Fessler	10.0	0.333	0.394	35	1382	1108 -20%	1082 -22%	3650 +164%	1132 -18%	1593 +15%	2122 +54%
2	Fessler	10.0	0.333	0.394	50	1665	2130 +28%	2040 +23%	2733 +64%	2114 +27%	2747 +65%	3404 +104%
3	Fessler	10.0	0.333	0.394	90	4153	3867 -7%	3647 -12%	2093 -50%	3760 -9%	4538 +9%	5261 +27%
4	Fessler	10.0	0.525	0.379	35	405	453 +12%	455 +12%	903 +123%	540 +33%	735 +81%	783 +93%
5	Fessler	10.0	0.525	0.379	50	700	878 +25%	865 +24%	676 -3%	1010 +44%	1267 +81%	1328 +90%
6	Fessler	10.0	0.525	0.379	90	1455	1597 +10%	1552 +7%	518 -64%	1795 +23%	2093 +44%	2160 +48%
7	Fessler	10.0	0.756	0.485	35	157	125 -21%	133 -15%	233 +49%	222 +41%	271 +73%	297 +89%
8	Fessler	10.0	0.756	0.485	50	260	244 -6%	255 -2%	175 -33%	415 +60%	468 +80%	539 +107%
9	Fessler	10.0	0.756	0.485	90	664	442 -33%	458 -31%	134 -80%	738 +11%	773 +16%	932 +40%
10	Fessler	14.8	0.333	0.590	35	2358	3054 +30%	2889 +23%	3615 +53%	2681 +14%	3761 +59%	4963 +110%
11	Fessler	14.8	0.333	0.590	50	5719	5831 +2%	5451 -5%	2707 -53%	5009 -12%	6485 +13%	7961 +39%
12	Fessler	14.8	0.333	0.590	90	9503	10512 +11%	9746 +3%	2073 -78%	8907 -6%	10711 +13%	12303 +29%
13	Fessler	14.8	0.525	0.568	35	1399	1258 -10%	1217 -13%	893 -36%	1280 -8%	1734 +24%	1855 +33%
14	Fessler	14.8	0.525	0.568	50	2361	2400 +2%	2298 -3%	668 -72%	2392 +1%	2990 +27%	3145 +33%
15	Fessler	14.8	0.525	0.568	90	3489	4295 +23%	4088 +17%	512 -85%	4253 +22%	4938 +42%	5116 +47%
16	Fessler	14.8	0.756	0.727	35	491	347 -29%	347 -29%	231 -53%	526 +7%	640 +30%	696 +42%
17	Fessler	14.8	0.756	0.727	50	1056	662 -37%	657 -38%	173 -84%	983 -7%	1104 +5%	1262 +19%
18	Fessler	14.8	0.756	0.727	90	1626	1181 -27%	1170 -28%	132 -92%	1748 +7%	1824 +12%	2182 +34%
19	Fessler	19.6	0.333	0.788	35	5463	6174 +13%	5751 +5%	3582 -34%	4946 -9%	6915 +27%	9073 +66%
20	Fessler	19.6	0.333	0.788	50	9465	11733 +24%	10866 +15%	2682 -72%	9240 -2%	11924 +26%	14553 +54%
21	Fessler	19.6	0.333	0.788	90	12640	21074 +67%	19446 +54%	2055 -84%	16432 +30%	19695 +56%	22489 +78%
22	Fessler	19.6	0.525	0.746	35	2429	2522 +4%	2410 -1%	897 -63%	2362 -3%	3200 +32%	3422 +41%
23	Fessler	19.6	0.525	0.746	50	4610	4774 +4%	4521 -2%	672 -85%	4412 -4%	5518 +20%	5802 +26%

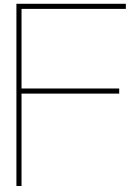
24	Fessler	19.6	0.525	0.746	90	7739	8502	+10%	8073	+4%	515	-93%	7846	+1%	9114	+18%	9436	+22%
25	Fessler	19.6	0.756	0.970	35	891	683	-23%	668	-25%	229	-74%	970	+9%	1178	+32%	1273	+43%
26	Fessler	19.6	0.756	0.970	50	1973	1300	-34%	1269	-36%	171	-91%	1813	-8%	2031	+3%	2308	+17%
27	Fessler	19.6	0.756	0.970	90	4232	2330	-45%	2272	-46%	131	-97%	3224	-24%	3355	-21%	3993	-6%
28	Tebbett	32.0	0.589	0.500	90	22060	22159	+0%	22317	+1%	830	-96%	21509	-2%	25229	+14%	21080	-4%
29	Tebbett	20.0	0.331	0.500	90	25870	24028	-7%	22769	-12%	3148	-88%	17656	-32%	23187	-10%	23885	-8%
30	Tebbett	20.0	0.537	0.500	90	-	-	-	-	-	-	-	-	-	-	-	-	-
31	Tebbett	20.0	0.924	0.500	90	0	-	-	-	-	-	-	-	-	-	-	-	-

Table E.3: Comparison of results from 31 measurements for in-plane bending flexibility.

In-plane bending flexibility $f_{33}^*$ [-]														
Specifications														
No.	Author	$\gamma$	$\beta$	$\tau$	$\theta$	Experiment	Numerical Model (mid-plane)	Numerical Model	Brace extended element	Fessler et al. [31]	Buitrago et al. [13]	Chen et al. [17]	Ueda et al. [54]	Efthymiou [24]
1	Fessler	10.0	0.333	0.394	35	805	1004 +25%	875 +9%	3649.7 +353%	811 +1%	848 +5%	879 +9%	1363 +69%	1463 +82%
2	Fessler	10.0	0.333	0.394	50	1232	1507 +22%	1329 +8%	2732.7 +122%	1154 -6%	1214 -1%	1261 +2%	1820 +48%	1809 +47%
3	Fessler	10.0	0.333	0.394	90	1761	2131 +21%	1913 +9%	2093.4 +19%	1597 -9%	1689 -4%	1760 -0%	2376 +35%	2199 +25%
4	Fessler	10.0	0.525	0.379	35	364	385 +6%	345 -5%	902.7 +148%	340 -6%	308 -15%	365 +0%	501 +38%	455 +25%
5	Fessler	10.0	0.525	0.379	50	450	574 +27%	521 +16%	675.9 +50%	485 +8%	442 -2%	524 +16%	669 +49%	595 +32%
6	Fessler	10.0	0.525	0.379	90	710	811 +14%	746 +5%	517.7 -27%	671 -6%	614 -13%	731 +3%	873 +23%	761 +7%
7	Fessler	10.0	0.756	0.485	35	179	157 -12%	143 -20%	233.4 +30%	120 -33%	127 -29%	127 -29%	224 +25%	171 -4%
8	Fessler	10.0	0.756	0.485	50	202	228 +13%	211 +4%	174.7 -13%	171 -16%	182 -10%	182 -10%	300 +48%	239 +18%
9	Fessler	10.0	0.756	0.485	90	254	313 +23%	293 +15%	133.9 -47%	236 -7%	253 -0%	254 -0%	391 +54%	326 +28%
10	Fessler	14.8	0.333	0.590	35	1694	2145 +27%	1866 +10%	3614.8 +113%	1598 -6%	1591 -6%	1697 +0%	2654 +57%	2684 +58%
11	Fessler	14.8	0.333	0.590	50	2486	3162 +27%	2776 +12%	2706.6 +9%	2274 -9%	2278 -8%	2437 -2%	3545 +43%	3319 +33%
12	Fessler	14.8	0.333	0.590	90	2936	4444 +51%	3960 +35%	2073.4 -29%	3148 +7%	3171 +8%	3401 +16%	4628 +58%	4035 +37%
13	Fessler	14.8	0.525	0.568	35	725	802 +11%	727 +0%	892.6 +23%	671 -7%	579 -20%	705 -3%	975 +34%	821 +13%
14	Fessler	14.8	0.525	0.568	50	977	1149 +18%	1053 +8%	668.4 -32%	955 -2%	829 -15%	1012 +4%	1302 +33%	1073 +10%
15	Fessler	14.8	0.525	0.568	90	1347	1581 +17%	1463 +9%	512.0 -62%	1322 -2%	1153 -14%	1411 +5%	1700 +26%	1373 +2%
16	Fessler	14.8	0.756	0.727	35	240	311 +30%	288 +20%	230.7 -4%	236 -2%	238 -1%	245 +2%	437 +82%	304 +27%
17	Fessler	14.8	0.756	0.727	50	296	436 +47%	408 +38%	172.7 -42%	336 +14%	341 +15%	351 +19%	584 +97%	425 +44%
18	Fessler	14.8	0.756	0.727	90	459	582 +27%	548 +19%	132.3 -71%	465 +1%	474 +3%	490 +7%	762 +66%	579 +26%
19	Fessler	19.6	0.333	0.788	35	2722	3562 +31%	3121 +15%	3582.4 +32%	2586 -5%	2487 -9%	2710 -0%	4261 +57%	4179 +54%
20	Fessler	19.6	0.333	0.788	50	3882	5173 +33%	4569 +18%	2682.3 -31%	3680 -5%	3560 -8%	3690 +0%	5690 +47%	5166 +33%
21	Fessler	19.6	0.333	0.788	90	5572	7228 +30%	6448 +16%	2054.8 -63%	5095 -9%	4955 -11%	5428 -3%	7428 +33%	6281 +13%
22	Fessler	19.6	0.525	0.746	35	1110	1307 +18%	1201 +8%	897.2 -19%	1086 -2%	909 -18%	1125 +1%	1565 +41%	1256 +13%
23	Fessler	19.6	0.525	0.746	50	1499	1834 +22%	1701 +13%	671.8 -55%	1545 +3%	1301 -13%	1615 +8%	2090 +39%	1641 +9%
24	Fessler	19.6	0.525	0.746	90	2124	2484 +17%	2303 +8%	514.6 -76%	2139 +1%	1811 -15%	2253 +6%	2728 +28%	2100 -1%
25	Fessler	19.6	0.756	0.970	35	413	493 +19%	462 +12%	228.6 -45%	382 -7%	372 -10%	390 -5%	702 +70%	459 +11%
26	Fessler	19.6	0.756	0.970	50	555	682 +23%	643 +16%	171.2 -69%	544 -2%	533 -4%	561 +1%	937 +69%	642 +16%
27	Fessler	19.6	0.756	0.970	90	869	901 +4%	853 -2%	131.1 -85%	753 -13%	741 -15%	782 -10%	1223 +41%	873 +0%
28	Tebbett	32.0	0.589	0.500	90	4280	4375 +2%	4343 +1%	830.0 -81%	3766 -12%	3991 -7%	3846 -10%	4896 +14%	3413 -20%

29	Tebbett	20.0	0.331	0.500	90	5320	7991	+50%	7394	+39%	3147.8	-41%	5289	-1%	2319	-56%	5692	+7%	7824	+47%	6611	+24%
30	Tebbett	20.0	0.537	0.500	90	3125	2556	-18%	2445	-22%	705.5	-77%	2159	-31%	2013	-36%	2185	-30%	2666	-15%	2032	-35%
31	Tebbett	20.0	0.924	0.500	90	0	-	-	-	-	-	-	-	-	-	-	-	-	-	-	-	-





## Plots of results of validations of single-brace joint

This appendix contains the plots of the results of the validation, discussed in section 4.7. The numerical values are shown in Appendix E

## Calculated axial LJF of 27 joint geometries

presented under variable  $\beta$

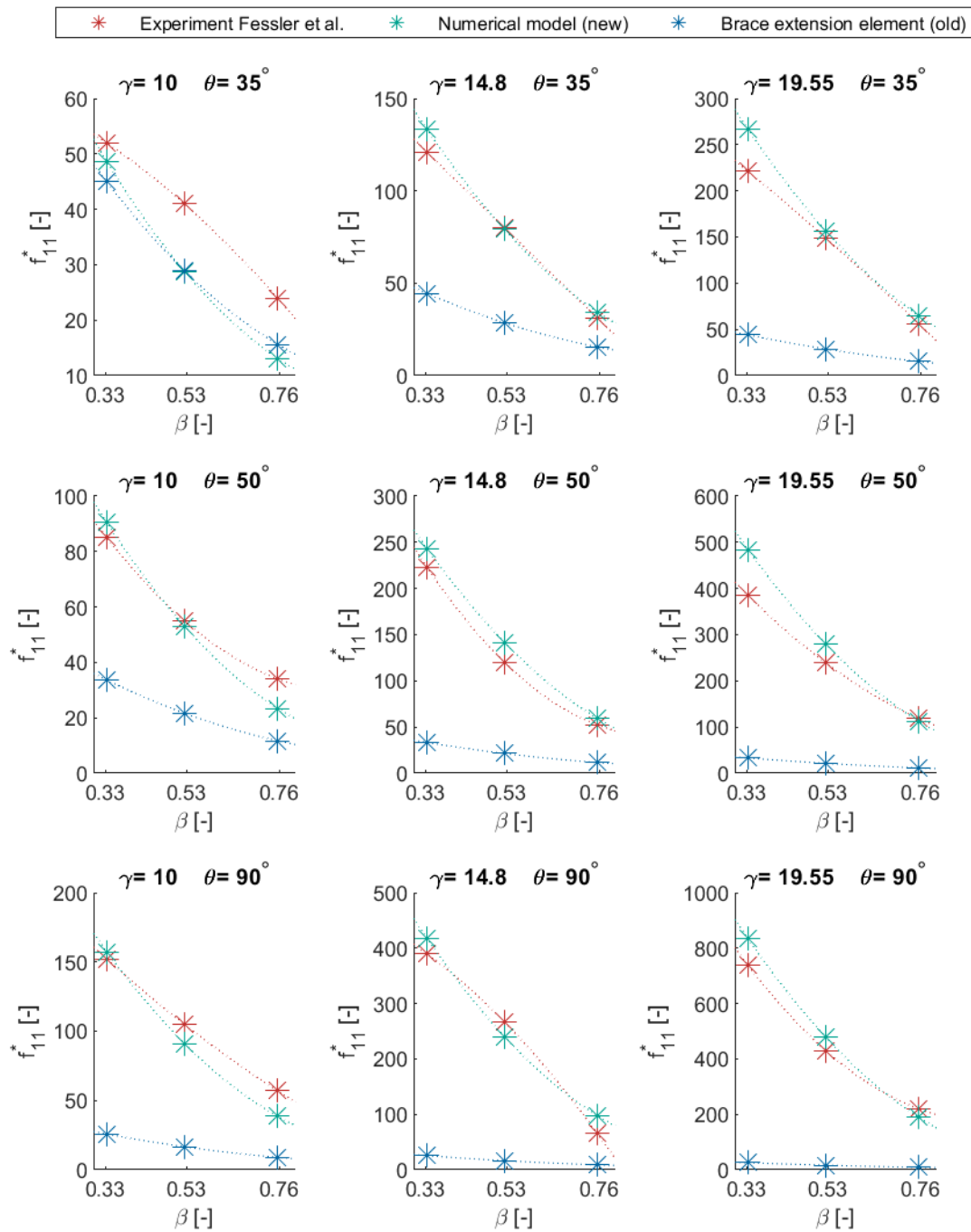


Figure F.1: The axial LJF of the 27 joint geometries investigated by Fessler et al., according to: the experiment of Fessler et al., the numerical model and the flexibility of the brace extension element, presented under a variable  $\beta$

## Calculated axial LJF of 27 joint geometries

presented under variable  $\gamma$

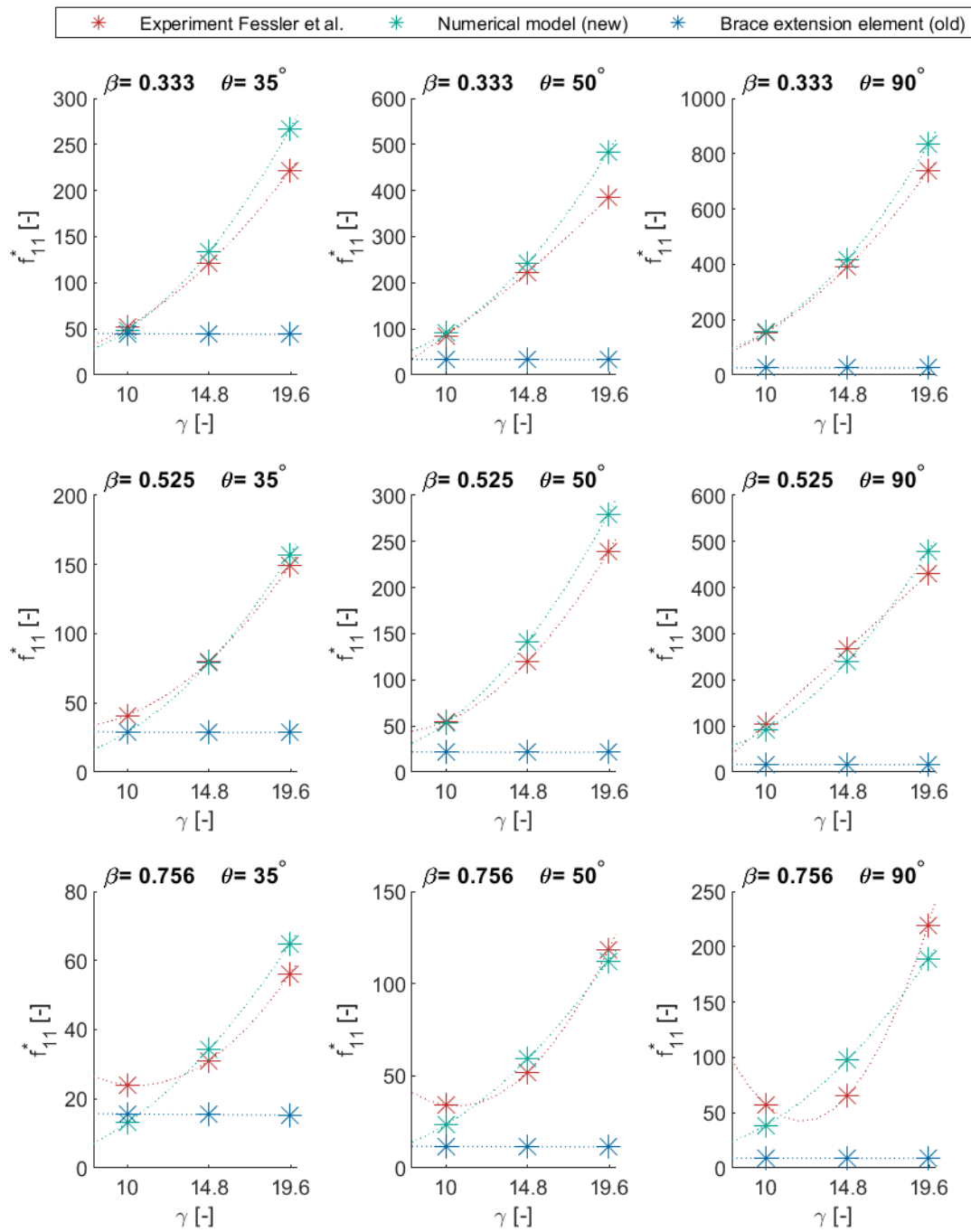


Figure F.2: The axial LjF of the 27 joint geometries investigated by Fessler et al., according to: the experiment of Fessler et al., the numerical model and the flexibility of the brace extension element, presented under a variable  $\gamma$

### Calculated axial LJF of 27 joint geometries

presented under variable  $\theta$

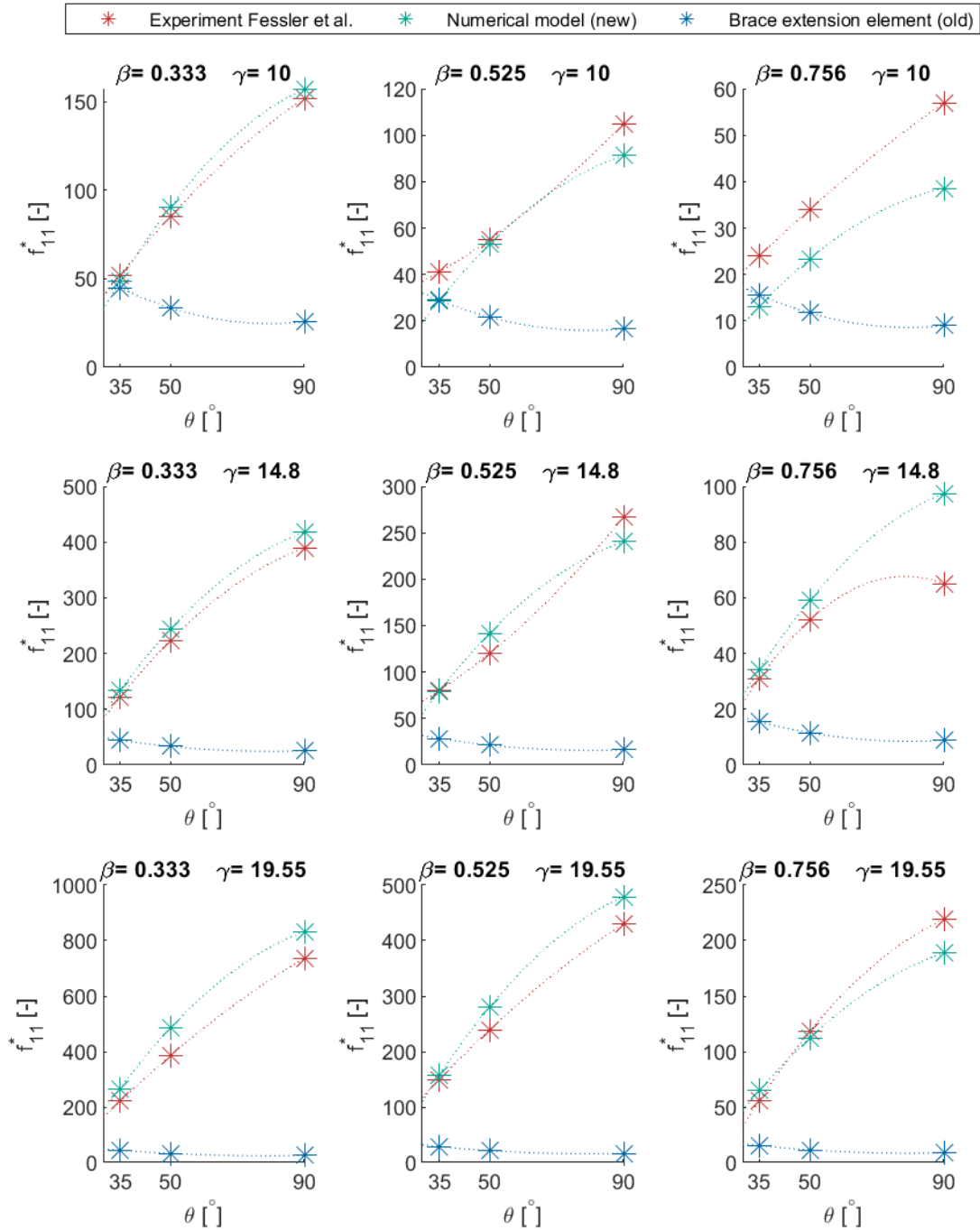


Figure F.3: The axial LJF of the 27 joint geometries investigated by Fessler et al., according to: the experiment of Fessler et al., the numerical model and the flexibility of the brace extension element, presented under a variable  $\theta$

## Calculated out-of-plane bending LJF of 27 joint geometries

presented under variable  $\beta$

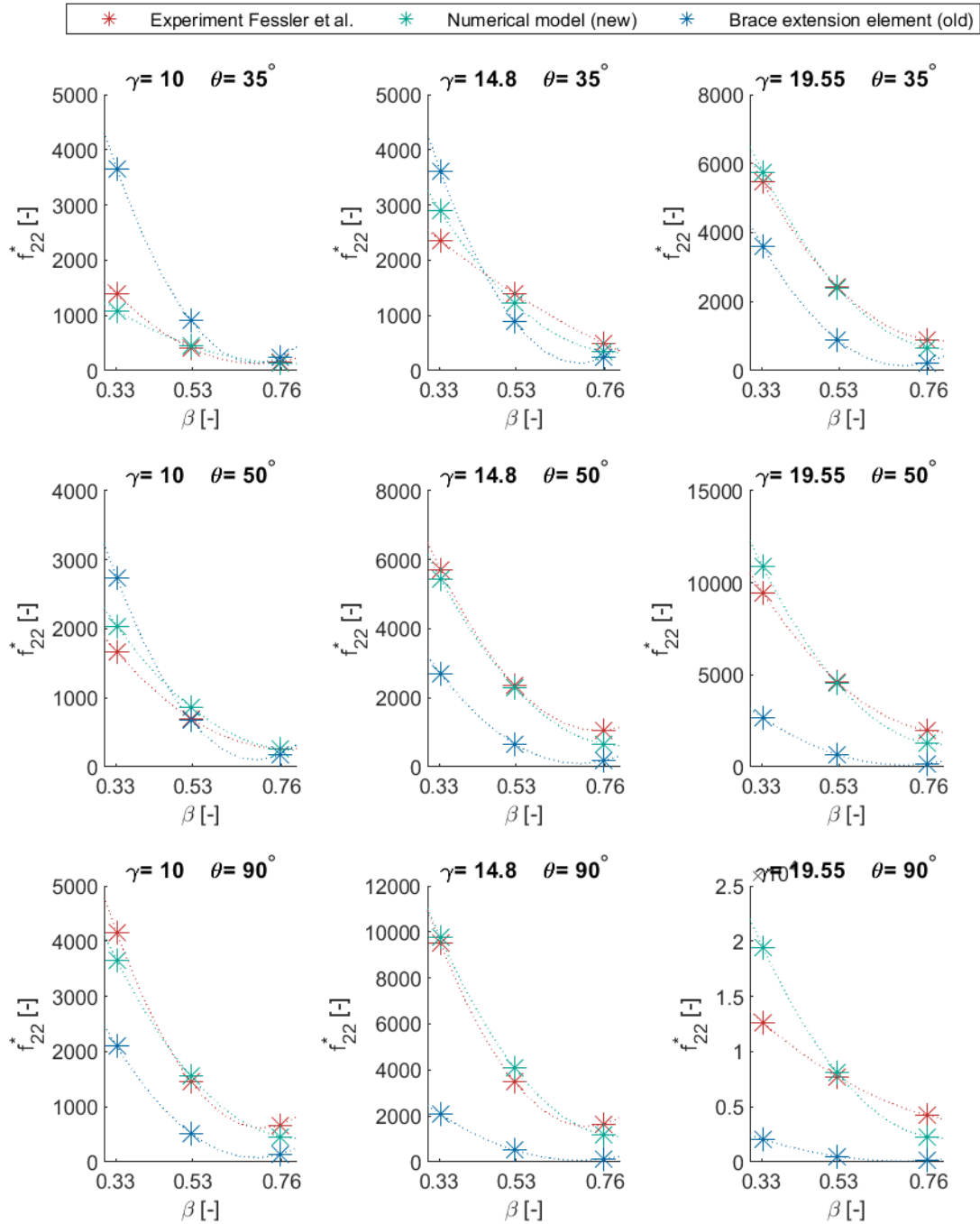


Figure F.4: The out-of-plane bending LjF of the 27 joint geometries investigated by Fessler et al., according to: the experiment of Fessler et al., the numerical model and the flexibility of the brace extension element, presented under a variable  $\beta$

### Calculated out-of-plane bending LJJ of 27 joint geometries

presented under variable  $\gamma$

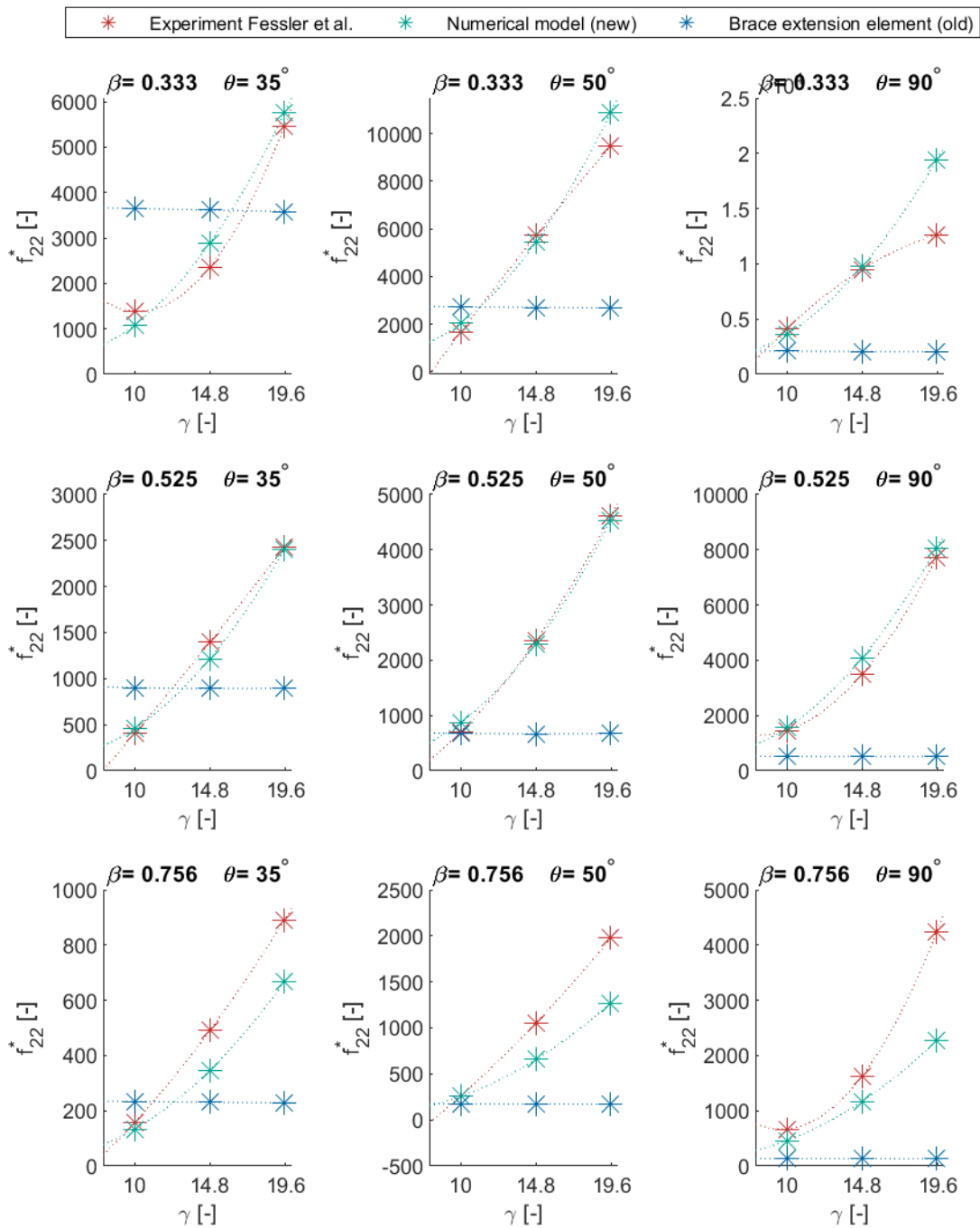


Figure F.5: The out-of-plane bending LJJ of the 27 joint geometries investigated by Fessler et al., according to: the experiment of Fessler et al., the numerical model and the flexibility of the brace extension element, presented under a variable  $\gamma$

## Calculated out-of-plane bending LJF of 27 joint geometries

presented under variable  $\theta$

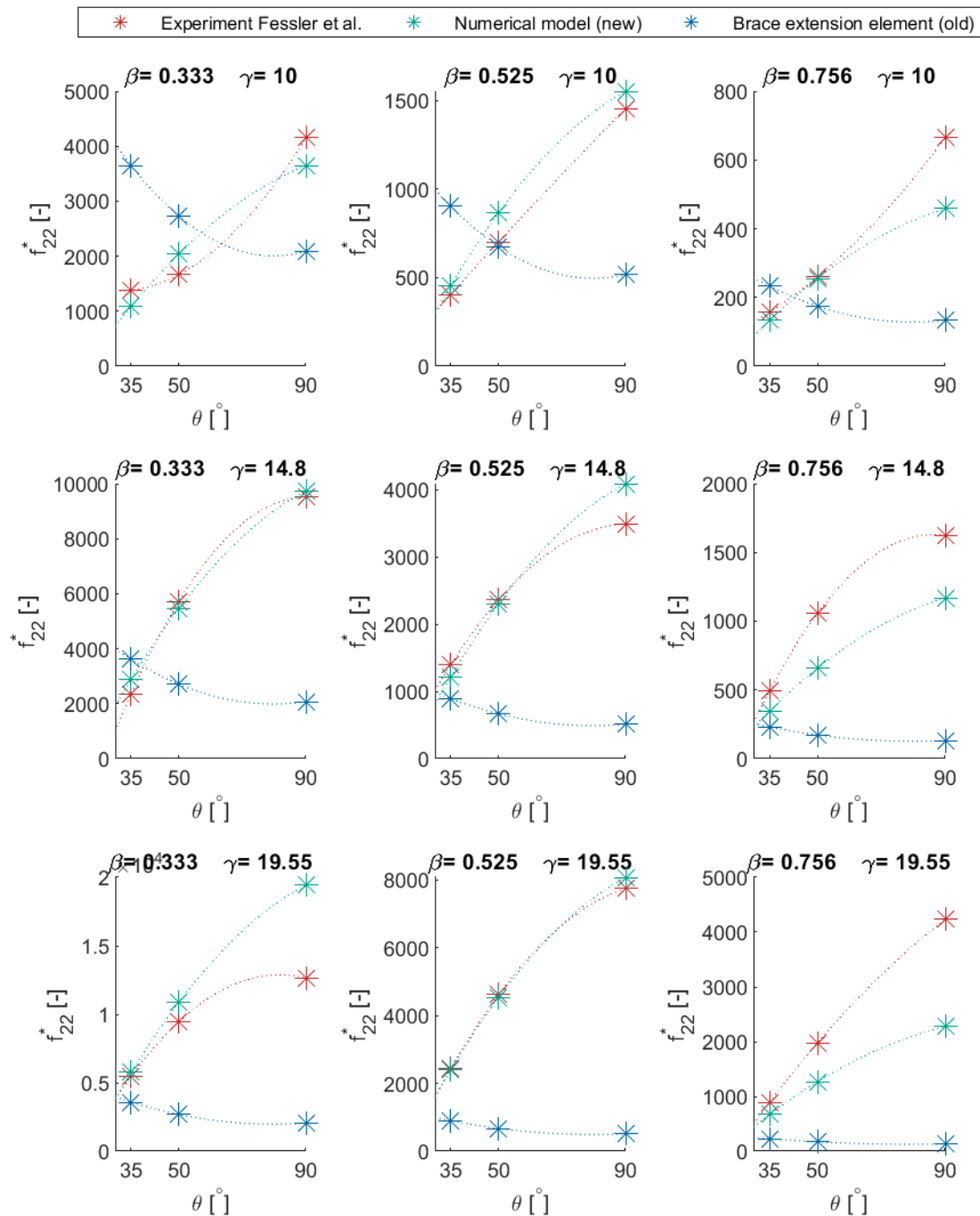


Figure F.6: The out-of-plane bending LjF of the 27 joint geometries investigated by Fessler et al., according to: the experiment of Fessler et al., the numerical model and the flexibility of the brace extension element, presented under a variable  $\theta$



# G

## Equations to calculate the non-dimensional flexibility of a joint

### G.1. Single-brace joint

This appendix contains the equations used to calculate the non-dimensional flexibilities of a single-brace joint, written out. In section 4.2.4 the calculation is explained and written in matrix notation.

$$f_{11}^* = \delta_{11} * \frac{ED}{P_1} \quad (\text{G.1})$$

$$f_{12}^* = \delta_{12} * \frac{ED^2}{P_2} \quad (\text{G.2})$$

$$f_{13}^* = \delta_{13} * \frac{ED^2}{P_3} \quad (\text{G.3})$$

$$f_{21}^* = \delta_{21} * \frac{ED^2}{P_1} \quad (\text{G.4})$$

$$f_{22}^* = \delta_{22} * \frac{ED^3}{P_2} \quad (\text{G.5})$$

$$f_{23}^* = \delta_{23} * \frac{ED^3}{P_3} \quad (\text{G.6})$$

$$f_{31}^* = \delta_{31} * \frac{ED^2}{P_1} \quad (\text{G.7})$$

$$f_{32}^* = \delta_{32} * \frac{ED^3}{P_2} \quad (\text{G.8})$$

$$f_{33}^* = \delta_{33} * \frac{ED^3}{P_3} \quad (\text{G.9})$$

## G.2. Multi-brace joint

This appendix contains the equations used to calculate the non-dimensional flexibilities of a multi-brace joint, written out. In section 4.5.4 the calculation is explained and written in matrix notation.

If  $i=1,4,7,\dots \cap j=1,4,7,\dots$

$$f_{ij}^* = \delta_{ij} * \frac{ED}{P_j} \quad (\text{G.10})$$

If  $i=1,4,7,\dots \cap j=2,5,8,\dots$

$$f_{ij}^* = \delta_{ij} * \frac{ED^2}{P_j} \quad (\text{G.11})$$

If  $i=1,4,7,\dots \cap j=3,6,9,\dots$

$$f_{ij}^* = \delta_{ij} * \frac{ED^2}{P_j} \quad (\text{G.12})$$

If  $i=2,5,8,\dots \cap j=1,4,7,\dots$

$$f_{ij}^* = \delta_{ij} * \frac{ED^2}{P_j} \quad (\text{G.13})$$

If  $i=2,5,8,\dots \cap j=2,5,8,\dots$

$$f_{ij}^* = \delta_{ij} * \frac{ED^3}{P_j} \quad (\text{G.14})$$

If  $i=2,5,8,\dots \cap j=3,6,9,\dots$

$$f_{ij}^* = \delta_{ij} * \frac{ED^3}{P_j} \quad (\text{G.15})$$

If  $i=3,6,9,\dots \cap j=1,4,7,\dots$

$$f_{ij}^* = \delta_{ij} * \frac{ED^2}{P_j} \quad (\text{G.16})$$

If  $i=3,6,9,\dots \cap j=2,5,8,\dots$

$$f_{ij}^* = \delta_{ij} * \frac{ED^3}{P_j} \quad (\text{G.17})$$

If  $i=3,6,9,\dots \cap j=3,6,9,\dots$

$$f_{ij}^* = \delta_{ij} * \frac{ED^3}{P_j} \quad (\text{G.18})$$



## Parametric equations

Author	Joint classification	Equation	Domain
DNV [21] as stated by Fessler et al. [31]	T-joint	$f_{22}^* = \frac{5000 * [\frac{1}{\gamma} - 0.22]^{1.6\beta - 2.45}}{215 - 135\beta}$ $f_{33}^* = 18.6 * [\frac{1}{\gamma} - 0.01]^{1.5\beta - 2.35}$	$10 \leq \gamma \leq 30$ $0.33 \leq \beta \leq 0.8$ $\theta = 90^\circ$
Fessler et. al [29] as stated by Chen and Zhang [17]	T-joint Y-joint	$f_{11}^* = 2.3 * \gamma^{2.3} * \sin^2 \theta * e^{-3.3\beta}$ $f_{33}^* = 171 * \gamma^{1.65} * \sin^{1.7} \theta * e^{-4.6\beta}$	unknown
Efthymiou [24] as stated by Fessler et al. [31]	T-joint Y-joint	$f_{22}^* = 3.48 * \gamma^{2.20 - 0.7(0.55 - \beta)^2} * \sin^{1.3 + \beta} \theta * \beta^{-2.12}$ $f_{33}^* = 6.16 * \gamma^{1.44} * \sin^{\beta + 0.4} \theta * \beta^{-(2.25 + \frac{\gamma}{125})}$	$10 \leq \gamma \leq 30$ $0.3 \leq \beta \leq 0.8$ $35^\circ \leq \theta \leq 90^\circ$
Fessler et. al [31]	T-joint Y-joint	$f_{11}^* = 1.95 * \gamma^{2.15} * \sin^{2.19} \theta * (1 - \beta)^{1.3}$ $f_{22}^* = 85.5 * \gamma^{2.20} * \sin^{2.16} \theta * e^{-3.85\beta}$ $f_{33}^* = 134 * \gamma^{1.73} * \sin^{1.22} \theta * e^{-4.52\beta}$	$10 \leq \gamma \leq 20$ $0.3 \leq \beta \leq 0.8$ $30^\circ \leq \theta \leq 90^\circ$
Fessler et. al [30]	DY-joint TY-joint K-joint $\psi_1 = \psi_2$	$f_{14}^* = 1.26 * \gamma^{2.30} * \sin^{1.58} \theta_1 * (1 - \beta_1)^{0.71} * \sin^{1.76} \theta_2 * (1 - \beta_2)^{0.48} * e^{-0.58 * \frac{e}{D}}$ $f_{16}^* = -16.5 * \gamma^{1.20} * \sin^{0.71} \theta_1 * (1 - \beta_1)^{1.62} * \sin^{-0.36} \theta_2 * (1 - \beta_2)^{0.08} * e^{0.42 * \frac{e}{D}}$ $f_{25}^* = 67.9 * \gamma^{2.04} * \sin^{1.61} \theta_1 * e^{-1.22 * \beta_1} * \sin^{2.34} \theta_2 * e^{-1.55 * \beta_2} * e^{-0.94 * \frac{e}{D}}$ $f_{34}^* = 9.42 * \gamma^{1.84} * \sin^{0.79} \theta_1 * e^{-1.67 * \beta_1} * \cos(0.52 * \theta_2) * e^{-0.81 * \beta_2} * e^{-0.52 * \frac{e}{D}}$ <p> <math>f_{15}^*, f_{24}^*, f_{26}^*, f_{35}^* = 0</math> on account of symmetry  <math>f_{36}^* = 0</math> no significant values were obtained </p>	$10 \leq \gamma \leq 20$ $0.3 \leq \beta \leq 0.8$ $30^\circ \leq \theta \leq 90^\circ$

Fessler et. al [30]	DY-joint TY-joint K-joint $\psi_1 - \psi_2 = 90^\circ$	$f_{14}^* = -0.77 * \gamma^{2.34} * \sin^{1.11} \theta_1 * (1 - \beta_1)^{0.58} * \sin^{1.35} \theta_2$ $* (1 - \beta_2)^{0.41} * e^{-0.22 * \frac{e}{D}}$ $f_{15}^* = -58.4 * \gamma^{1.23} * \sin^{1.18} \theta_1 * (1 - \beta_1)^{1.60} * \sin^{1.20} \theta_2$ $* (1 - \beta_2)^{1.22}$ $f_{16}^* = -5.83 * \gamma^{1.36} * \sin^{1.19} \theta_1 * (1 - \beta_1)^{0.29} * \cos(1.02 * \theta_2)$ $* (1 - \beta_2)^{0.10} * e^{0.60 * \frac{e}{D}}$ $f_{24}^* = 8.67 * \gamma^{2.06} * \sin \theta_1 * e^{-2.97 * \beta_1} * \sin^{1.36} \theta_2 * e^{-1.78 * \beta_2}$ $* e^{-0.24 * \frac{e}{D}}$ $f_{25}^* = -5.48 * \gamma^{2.29} * \sin^{1.13} \theta_1 * e^{-0.14 * \beta_1} * \sin^{1.28} \theta_2 * e^{-0.79 * \beta_2}$ $* e^{-0.22 * \frac{e}{D}}$ $f_{34}^* = 1.39 * \gamma^{1.49} * \sin^{0.15} \theta_1 * \cos(1.56 * \theta_2) * e^{0.14 * \frac{e}{D}}$ $f_{35}^* = 34.2 * \gamma * \sin \theta_1 * \cos \theta_2 * e^{0.66 * \frac{e}{D}}$ $f_{26}^* = 0 \text{ by the author assumed to be negligible}$ $f_{36}^* = 0 \text{ no significant values were obtained}$	$10 \leq \gamma \leq 20$ $0.3 \leq \beta \leq 0.8$ $30^\circ \leq \theta \leq 90^\circ$
Fessler et. al [30]	DY-joint TY-joint K-joint $\psi_1 - \psi_2 = 180^\circ$	$f_{14}^* = 0.85 * \gamma^{2.24} * \sin^{1.14} \theta_1 * (1 - \beta_1)^{0.49} * \sin^{1.41} \theta_2$ $* (1 - \beta_2)^{0.31} * e^{-0.28 * \frac{e}{D}}$ $f_{16}^* = 2.42 * \gamma^{1.61} * \sin^{1.07} \theta_1 * (1 - \beta_1)^{0.27} * \cos(1.03 * \theta_2)$ $* (1 - \beta_2)^{0.11} * e^{0.69 * \frac{e}{D}}$ $f_{25}^* = 3.06 * \gamma^{2.32} * \sin^{1.21} \theta_1 * e^{-0.73 * \beta_1} * \sin^{1.15} \theta_2 * e^{-0.14 * \frac{e}{D}}$ $f_{15}^*, f_{24}^*, f_{26}^*, f_{35}^* = 0 \text{ on account of symmetry}$ $f_{34}^*, f_{36}^* = 0 \text{ no significant values were obtained}$	$10 \leq \gamma \leq 20$ $0.3 \leq \beta \leq 0.8$ $30^\circ \leq \theta \leq 90^\circ$
Ueda et al.[54] as stated by Chen and Zhang [17]	T-joint Y-joint TY-joint K-joint	$f_{11}^* = 0.313 * \gamma^{2.3} * \beta^{-1.2} * \sin^2 \theta$ $f_{33}^* = 4.22 * \gamma^{1.7} * \beta^{-2.2} * \sin \theta$	unknown
Chen and Zhang [17]	T-joint Y-joint K-joint	$f_{11}^* = 4.71 * \gamma^{2.17} * \sin^{2.02} \theta * e^{-3.25\beta}$ $f_{14}^* = 1.79 * \gamma^{2.39} * \sin^{3.07} \theta * e^{-2.49\beta}$ $f_{16}^* = 6.69 * \gamma^{1.68} * \sin^{1.2} \theta * e^{-2.62\beta}$ $f_{33}^* = 169 * \gamma^{1.68} * \sin^{1.25} \theta * e^{-4.58\beta}$ $f_{34}^* = -f_{16}^*$ $f_{36}^* = 19.1 * \gamma^{1.43} * \sin^{0.86} \theta * e^{-3.00\beta}$	$7.5 \leq \gamma \leq 35$ $0.3 \leq \beta \leq 0.8$ $30^\circ \leq \theta \leq 90^\circ$
Buitrago and Healy [13]	T-joint Y-joint	$f_{11}^* = 5.69 * \gamma^{1.898} * \sin^{1.769} \theta * \tau^{-0.111} * e^{-2.251\beta}$ $f_{22}^* = 55 * \gamma^{2.417} * \sin^{1.883} \theta * \tau^{-0.220} * e^{-4.076\beta}$ $f_{33}^* = 1.39 * \gamma^{1.898} * \sin^{1.240} \theta * \tau^{-0.283} * \beta^{-2.245}$	$10 \leq \gamma \leq 20$ $0.3 \leq \beta \leq 1.0$ $0.25 \leq \tau \leq 1.090$ $30^\circ \leq \theta \leq 90^\circ$ $0.02 \leq \zeta \leq 0.5$
Buitrago and Healy [13]	X-joint	$f_{11}^* = 8.94 * \gamma^{1.791} * \sin^{1.700} \theta * \tau^{-0.198} * e^{-2.759\beta}$ $f_{14}^* = \tau^{-0.1} (-353 + 1197\beta - 1108\beta * \sin \theta - 40\beta * \gamma$ $+ 50\gamma * \sin \theta)$ $f_{22}^* = 73.95 * \gamma^{2.376} * \sin^{1.926} \theta * \tau^{-0.300} * e^{-4.478\beta}$ $f_{25}^* = \tau^{-0.1} (2249 - 5879\beta + 5515\beta * \sin \theta + 221\beta * \gamma$ $- 358\gamma * \sin \theta)$ $f_{33}^* = 67.60 * \gamma^{1.892} * \sin^{1.255} \theta * \tau^{-0.063} * e^{-4.056\beta}$ $f_{36}^* = \tau^{-0.1} (26 - 75\beta^2 - 8.5\beta^2 * \sin \theta + 85\beta^2 * \gamma - 7.4\gamma$ $* \sin \theta)$	$10 \leq \gamma \leq 20$ $0.3 \leq \beta \leq 1.0$ $0.25 \leq \tau \leq 1.090$ $30^\circ \leq \theta \leq 90^\circ$ $0.02 \leq \zeta \leq 0.5$

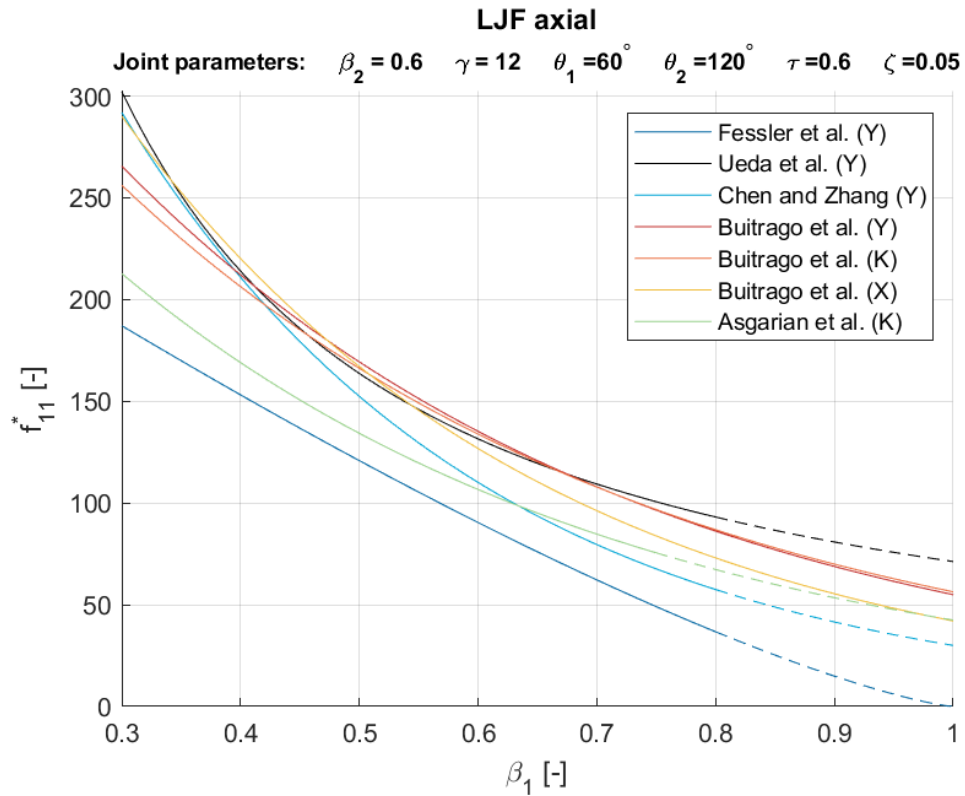
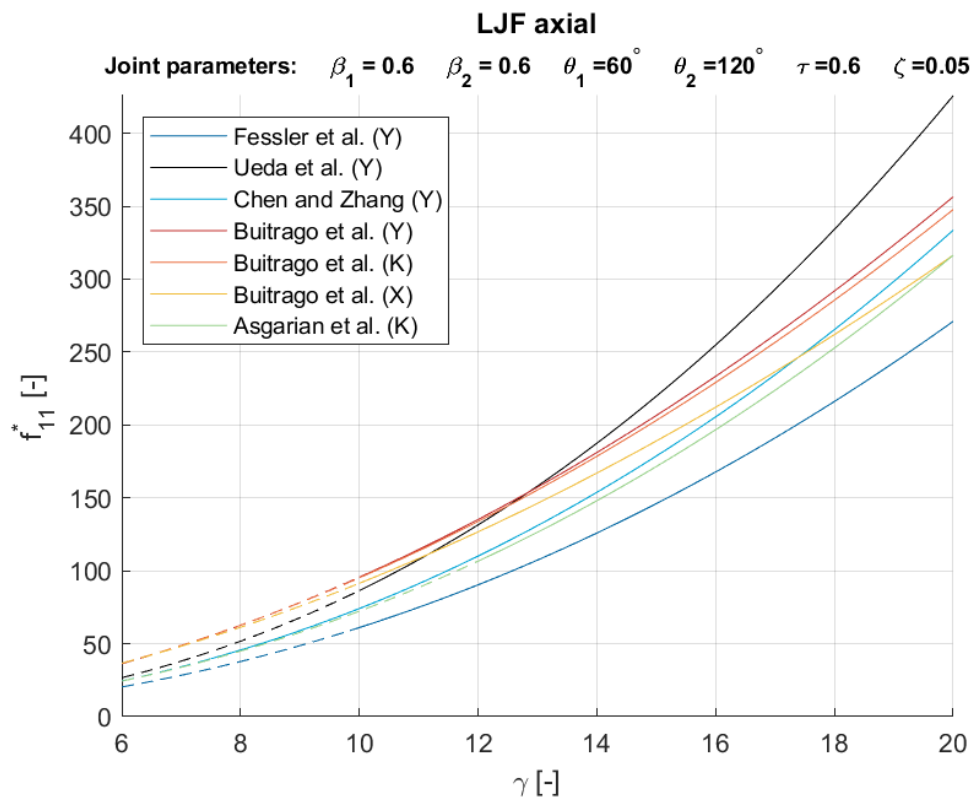
Buitrago and Healy [13]	K-joint	$f_{11}^* = 5.90\tau^{-0.114} * e^{-2.163\beta} * \gamma^{1.869} * \zeta^{0.009} * \sin^{1.869} \theta_1$ $* \sin^{-0.089} \theta_2$ $f_{14}^* = 3.93\tau^{-0.113} * e^{-2.198\beta} * \gamma^{1.847} * \zeta^{-0.056} * \sin^{0.837} \theta_1$ $* \sin^{-0.784} \theta_2$ $f_{22}^* = 49.7\tau^{-0.251} * e^{-4.165\beta} * \gamma^{2.449} * \zeta^{0.004} * \sin^{1.865} \theta_1$ $* \sin^{-0.054} \theta_2$ $f_{25}^* = 4.37\tau^{-0.295} * e^{-3.814\beta} * \gamma^{2.875} * \zeta^{-0.149} * \sin^{0.885} \theta_1$ $* \sin^{1.109} \theta_2$ $f_{33}^* = 52.2\tau^{-0.119} * e^{-3.835\beta} * \gamma^{1.934} * \zeta^{0.011} * \sin^{1.417} \theta_1$ $* \sin^{-0.108} \theta_2$ $f_{36}^* = f_{33} - 1.83\tau^{-0.212} * \beta^{-2.102} * \gamma^{1.872} * \zeta^{0.020} * \sin^{1.249} \theta_1$ $* \sin^{-0.060} \theta_2$	$10 \leq \gamma \leq 20$ $0.3 \leq \beta \leq 1.0$ $0.25 \leq \tau \leq 1.090$ $30^\circ \leq \theta \leq 90^\circ$ $0.02 \leq \zeta \leq 0.5$
Hoshyari [38]	K-joint	$f_{11}^* = \frac{1}{2.294} * \beta^{\frac{\gamma}{27.2}-0.31} * \gamma^{3-1.39\beta} * \tau^{-0.74}$ $f_{22}^* = \frac{1}{0.088} * \beta^{\frac{\gamma}{86.4}+0.31} * \gamma^{3.27-1.87\beta} * \tau^{-0.212}$ $f_{33}^* = \frac{1}{0.143} * \beta^{\frac{1.51\gamma}{109.8}} * \gamma^{1.75-\frac{\beta}{2.31}} * \tau^{-0.205}$	$13 \leq \gamma \leq 30$ $0.3 \leq \beta \leq 0.9$ $0.2 \leq \tau \leq 1.0$ $\theta = 90^\circ$
Asgarian [11]	Y-joint T-joint K-joint	$f_{11}^* = 3.501(\sin \theta_1)^{1.898}(\sin \theta_2)^{-0.114} * \gamma^{2.129} * e^{-2.302\beta_1}$ $* e^{-0.412\beta_2} * e^{0.221\zeta}$ $f_{13}^* = -10.070 + 0.408[(\sin \theta_1)^{2.457}(\sin \theta_2)^{1.375} * \gamma^{2.458} * e^{-5.581\beta_1} * e^{2.761\beta_2} e^{2.492\zeta}]$ $f_{14}^* = 2.789(\sin \theta_1)^{0.949}(\sin \theta_2)^{0.949} * \gamma^{2.225} * e^{-1.636\beta_1}$ $* e^{1.636\beta_2} * e^{0.256\zeta}$ $f_{16}^* = 10.116(\sin \theta_1)^{0.716}(\sin \theta_2)^{1.033} * \gamma^{1.710} * e^{-3.064\beta_1}$ $* e^{-0.863\beta_2} * e^{-2.095\zeta}$ $f_{33}^* = 102.164(\sin \theta_1)^{2.411}(\sin \theta_2)^{0.042} * \gamma^{2.166} * e^{-6.255\beta_1}$ $* e^{0.003\beta_2} * e^{0.419\zeta}$ $f_{34}^* = -10.116(\sin \theta_1)^{1.033}(\sin \theta_2)^{0.716} * \gamma^{1.710} * e^{-0.863\beta_1}$ $* e^{-3.064\beta_2} * e^{-2.095\zeta}$ $f_{36}^* = -40.793 - 953.641[(\sin \theta_1)^{2.016}(\sin \theta_2)^{2.016} * \gamma^{1.500}$ $* e^{-6.317\beta_1} * e^{6.317\beta_2} e^{-3.955\zeta}]$	$12 \leq \gamma \leq 30$ $0.25 \leq \beta \leq 0.75$ $30^\circ \leq \theta \leq 90$ $0.1 \leq \zeta \leq 0.8$
Ahmadi et al. [4] [3] [5]	DK-joint load-case dependent	$f_{11}^* = 0.0190\theta^{1.71} * e^{\tau^{-0.153} + \gamma^{0.486} + \beta^{-1.015}}$ $f_{11}^* = 0.011\theta^{1.682} * e^{\tau^{-0.229} + \gamma^{0.499} + \beta^{-1.173}}$ $f_{22}^* = 0.190\tau^{-0.162} * \gamma^{2.539} * \beta^{-3.545} * \theta^{1.835}$ $f_{22}^* = 4.232\tau^{-0.063} * \gamma^{2.054} * \beta^{-2.011} * \theta^{2.141}$ $f_{22}^* = 1.189\tau^{-0.108} * \gamma^{1.931} * \beta^{-2.612} * \theta^{1.826}$ $f_{22}^* = 0.465\tau^{-0.165} * \gamma^{2.250} * \beta^{-3.091} * \theta^{1.583}$ $f_{33}^* = 18.661\tau^{-0.058} * \gamma^{1.293} * \beta^{-1.577} * \theta^{0.721}$ $f_{33}^* = 10.681\tau^{-0.083} * \gamma^{1.428} * \beta^{-1.797} * \theta^{0.851}$ $f_{33}^* = 0.341\tau^{-0.138} * \gamma^{1.967} * \beta^{-3.513} * \theta^{1.419}$ $f_{33}^* = 0.426\tau^{-0.144} * \gamma^{1.866} * \beta^{-3.328} * \theta^{1.425}$	$12 \leq \gamma \leq 24$ $0.4 \leq \beta \leq 0.6$ $30^\circ \leq \theta \leq 60^\circ$ $0.4 \leq \tau \leq 1.08$
Khan et al.[44]	K-joint	$f_{11}^* = 2.0275 * e^{-1.7232\beta} * \sin^{1.0098} \theta * \gamma^{1.619}$ $f_{22}^* = 0.8307 * e^{-4.5722\beta} * \sin^{1.8970} \theta * \gamma^{2.2862}$ $f_{25}^* = 0.08307 * e^{-3.9514\beta} * \sin^{2.1652} \theta * \gamma^{2.5093}$ $f_{33}^* = 0.0122 * e^{-2.3395\beta} * \sin^{1.1865} \theta * \gamma^{1.7334}$ $f_{36}^* = -0.04478 * e^{-1.3873\beta} * (\sin \theta - 1.1696) * \gamma^{1.4504}$	unknown





## Plots of parametric equations

In sub-section 2.3.3, plots for the in-plane flexibility according to parametric equations are presented. In this appendix the same plots for axial and out-of-plane flexibility are presented.

Figure I.1: The influence of  $\beta_1$  on the dimensionless axial flexibility.Figure I.2: The influence of  $\gamma$  on the dimensionless axial flexibility.

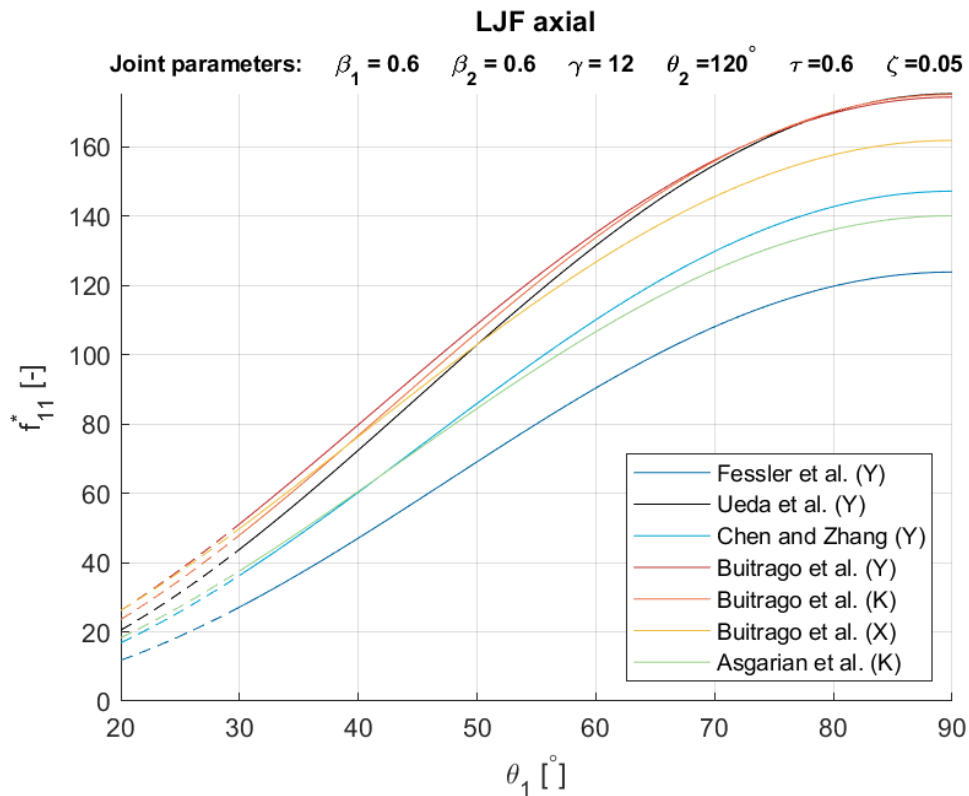


Figure I.3: The influence of  $\theta_1$  on the dimensionless axial flexibility.

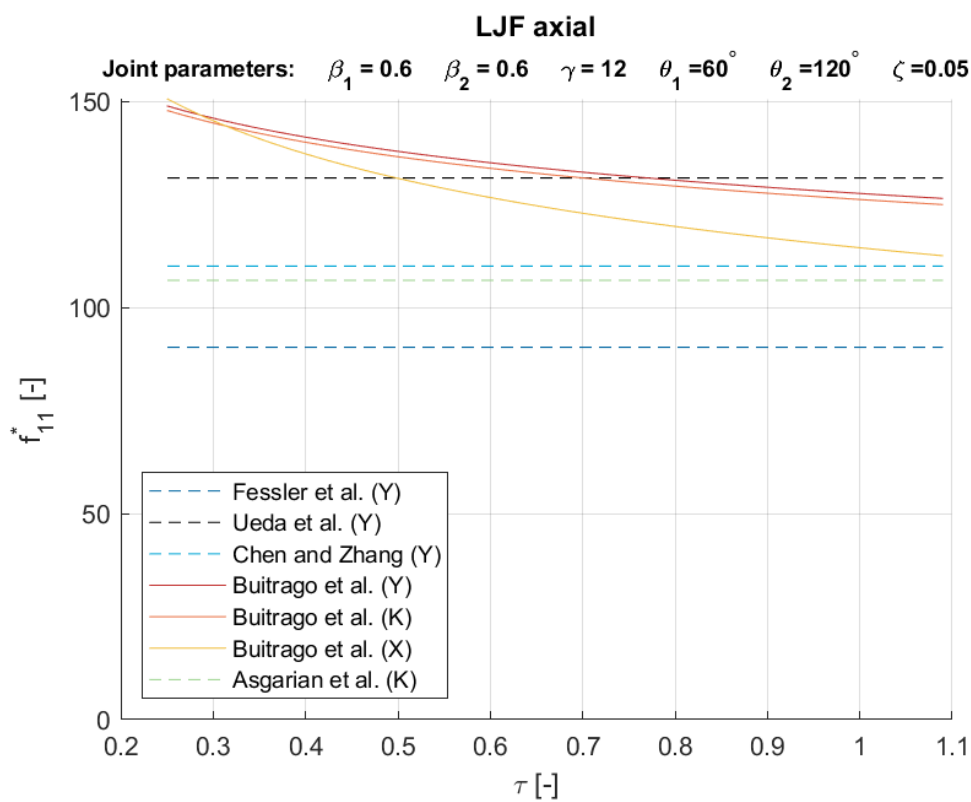


Figure I.4: The influence of  $\tau$  on the dimensionless axial flexibility.

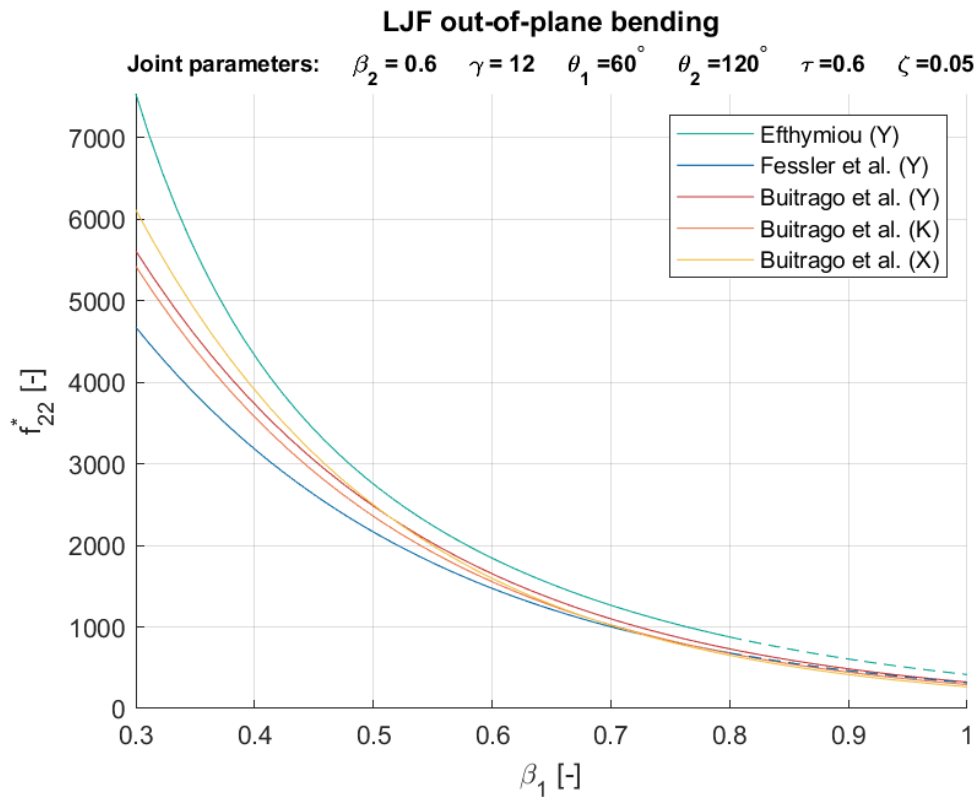


Figure I.5: The influence of  $\beta_1$  on the dimensionless out-of-plane bending flexibility.

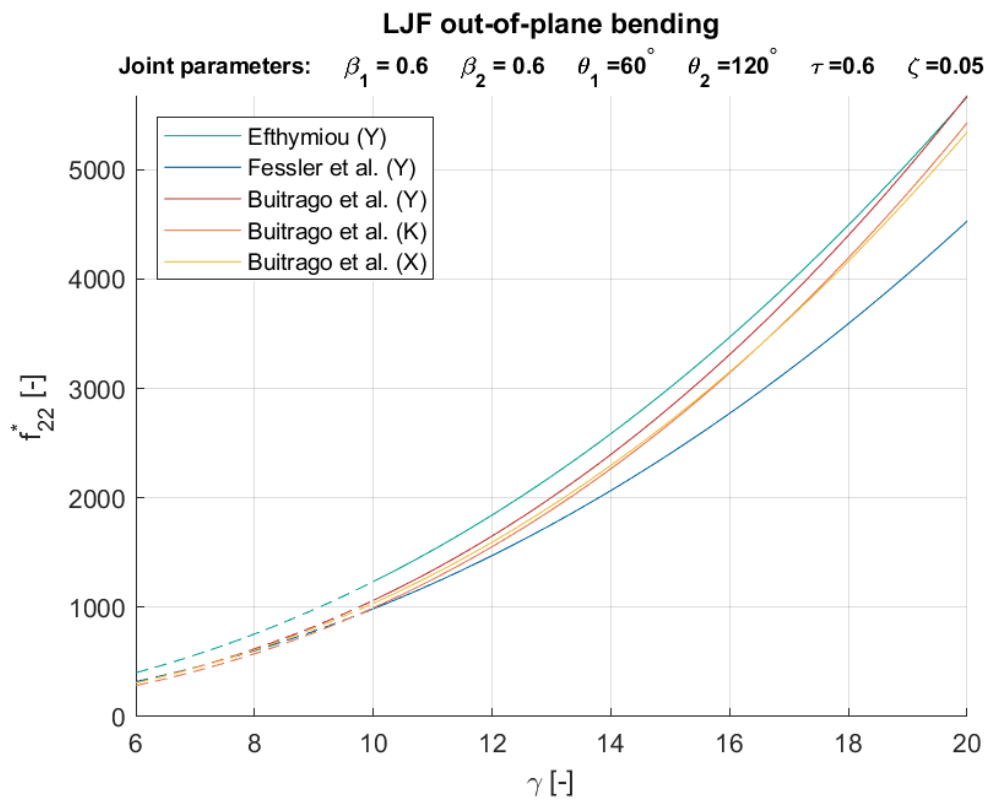


Figure I.6: The influence of  $\gamma$  on the dimensionless out-of-plane bending flexibility.

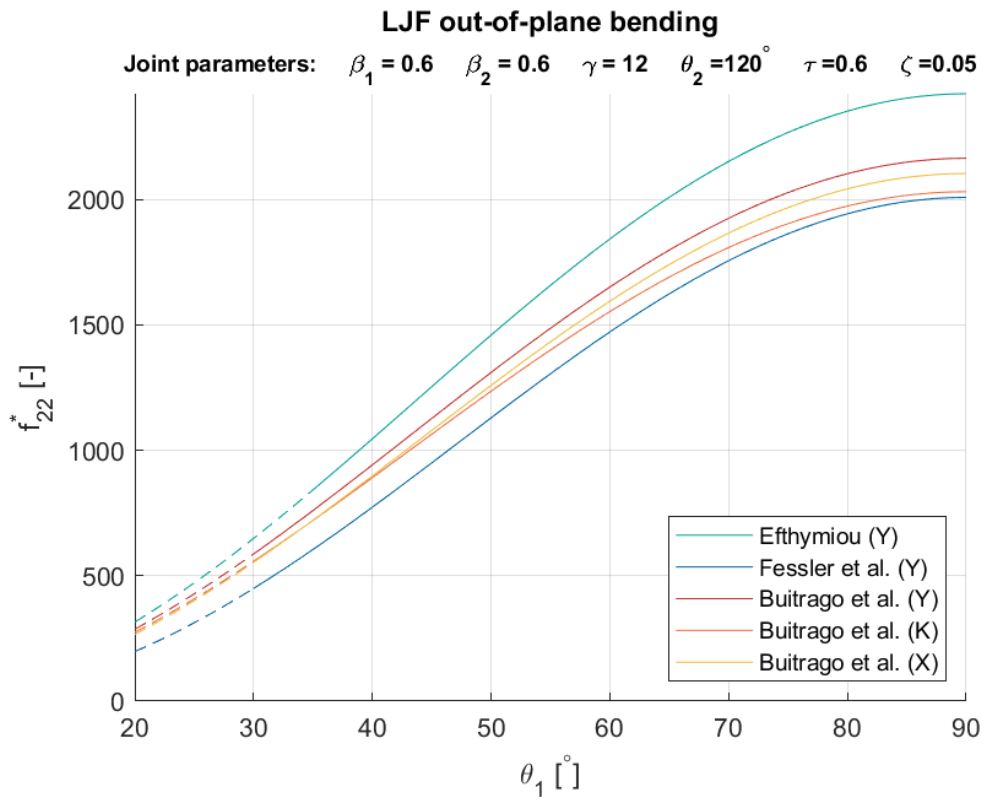


Figure I.7: The influence of  $\theta_1$  on the dimensionless out-of-plane bending flexibility.

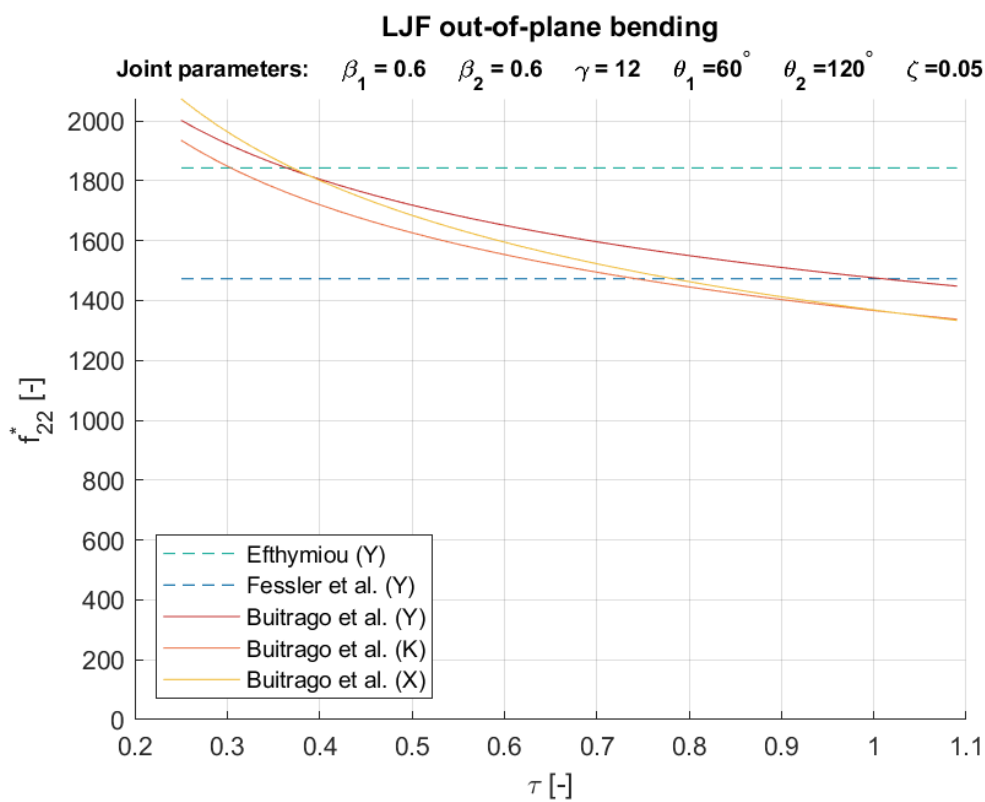


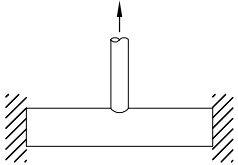
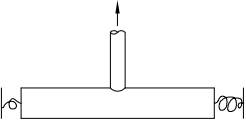
Figure I.8: The influence of  $\tau$  on the dimensionless out-of-plane bending flexibility.

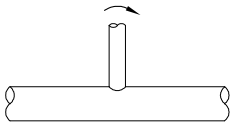
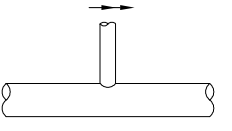




## Stress Concentration Factors

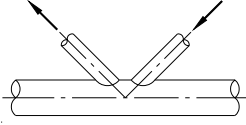
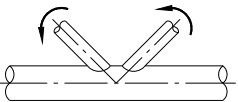
This appendix contains the SCF according to DNV [23].

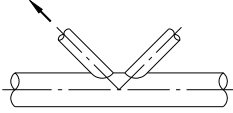
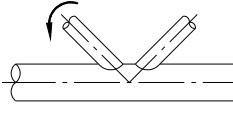
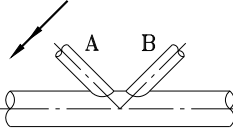
Load type and fixity conditions	SCF equations	Eqn. No.	Short chord correction
<p>Axial load- Chord ends fixed</p> 	<p>Chord saddle:  <math display="block">\gamma \tau^{1.1} (1.11 - 3(\beta - 0.52)^2) (\sin \theta)^{1.6}</math></p> <p>Chord crown:  <math display="block">\gamma^{0.2} \tau (2.65 + 5(\beta - 0.65)^2) + \tau \beta (0.25\alpha - 3) \sin \theta</math></p> <p>Brace saddle:  <math display="block">1.3 + \gamma \tau^{0.52} \alpha^{0.1} (0.187 - 1.25\beta^{1.1}(\beta - 0.96)) (\sin \theta)^{(2.7-0.01\alpha)}</math></p> <p>Brace crown:  <math display="block">3 + \gamma^{1.2} (0.12 \exp(-4\beta) + 0.011\beta^2 - 0.045) + \beta \tau (0.1\alpha - 1.2)</math></p>	<p>(1)</p> <p>(2)</p> <p>(3)</p> <p>(4)</p>	<p>F1</p> <p>None</p> <p>F1</p> <p>None</p>
<p>Axial load- General fixity conditions</p> 	<p>Chord saddle:  (Eqn.(1)) + <math>C_1(0.8\alpha - 6)\tau\beta^2(1 - \beta^2)^{0.5}(\sin 2\theta)^2</math></p> <p>Chord crown:  <math display="block">\gamma^{0.2} \tau (2.65 + 5(\beta - 0.65)^2) + \tau \beta (C_2\alpha - 3) \sin \theta</math></p> <p>Alternatively</p> $SCF_{Cc} = \gamma^{0.2} \tau (2.65 + 5(\beta - 0.65)^2) - 3\tau \beta \sin \theta + \frac{\sigma_{BendingChord}}{\sigma_{Axial brace}} SCF_{att}$ <p>where</p> <p><math>\sigma_{Bending Chord}</math> = nominal bending stress in the chord  <math>\sigma_{Axial brace}</math> = nominal axial stress in the brace.  <math>SCF_{att}</math> = stress concentration factor for an attachment = 1.27</p> <p>Brace saddle:  (Eqn. (3))</p> <p>Brace crown:  <math display="block">3 + \gamma^{1.2} (0.12 \exp(-4\beta) + 0.011\beta^2 - 0.045) + \beta \tau (C_3\alpha - 1.2)</math></p> <p>Alternatively</p> $SCF_{Bc} = 3 + \gamma^{1.2} (0.12 \exp(-4\beta) + 0.011\beta^2 - 0.045) - 1.2\beta\tau + \frac{0.4 \sigma_{Bending Chord}}{\sigma_{Axial brace}} SCF_{att}$	<p>(5)</p> <p>(6a)</p> <p>(6b)</p> <p>(7a)</p> <p>(7b)</p>	<p>F2</p> <p>None</p> <p>F2</p> <p>None</p>

<p>In-plane bending</p> 	<p>Chord crown:</p> $1.45\beta \tau^{0.85} \gamma^{(1-0.68\beta)} (\sin \theta)^{0.7}$ <p>Brace crown:</p> $1 + 0.65\beta \tau^{0.4} \gamma^{(1.09-0.77\beta)} (\sin \theta)^{(0.06\gamma-1.16)}$	<p>(8)</p> <p>(9)</p>	<p>None</p> <p>None</p>
<p>Out-of-plane bending</p> 	<p>Chord saddle:</p> $\gamma \tau \beta (1.7 - 1.05\beta^3) (\sin \theta)^{1.6}$ <p>Brace saddle:</p> $\tau^{-0.54} \gamma^{-0.05} (0.99 - 0.47\beta + 0.08\beta^4) \cdot (\text{Eqn.10})$	<p>(10)</p> <p>(11)</p>	<p>F3</p> <p>F3</p>
<p>Short chord correction factors (<math>\alpha &lt; 12</math>)</p> $F1 = 1 - (0.83\beta - 0.56\beta^2 - 0.02) \gamma^{0.23} \exp(-0.21 \gamma^{-1.16} \alpha^{2.5})$ $F2 = 1 - (1.43\beta - 0.97\beta^2 - 0.03) \gamma^{0.04} \exp(-0.71 \gamma^{-1.38} \alpha^{2.5})$ $F3 = 1 - 0.55 \beta^{1.8} \gamma^{0.16} \exp(-0.49 \gamma^{-0.89} \alpha^{1.8})$ <p>where <math>\exp(x) = e^x</math></p>		<p>Chord-end fixity parameter</p> <p><math>C1 = 2(C-0.5)</math></p> <p><math>C2 = C/2</math></p> <p><math>C3 = C/5</math></p> <p><math>C =</math> chord end fixity parameter</p> <p><math>0.5 \leq C \leq 1.0</math>, Typically <math>C = 0.7</math></p>	

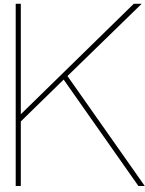
It should be noted that equations (6b) and (7b) will for general load conditions and moments in the chord member provide correct hot spot stresses at the crown points while equations (6a) and (7a) only provides correct hot spot stress due to a single action load in the considered brace. Equations (6b) and (7b) are also more general in that a chord-fixation parameter need not be defined. In principle it can account for joint flexibility at the joints when these are included in the structural analysis. Also the upper limit for the  $\alpha$ -parameter is removed with respect to validity of the SCF equations. Thus, these equations are in general recommended used.

Equation (6a) and (6b) will provide the same result only for the special case with a single action load in the considered brace and  $SCF_{att} = 1.0$ . For long chords the brace can be considered as an attachment to the chord with respect to axial stress at the crown points. This would give detail category F from [Table A-7](#) (for thick braces and E-curve for thinner) which corresponds to  $SCF_{att} = 1.27$  from [Table 2-1](#).

Load type and fixity conditions	SCF equation	Eqn. no.	Short chord correction
<p>Balanced axial load</p> 	<p>Chord:</p> $\tau^{0.9} \gamma^{0.5} (0.67 - \beta^2 + 1.16 \beta) \sin \theta \left( \frac{\sin \theta_{\max}}{\sin \theta_{\min}} \right)^{0.30}$ $\left( \frac{\beta_{\max}}{\beta_{\min}} \right)^{0.30} (1.64 + 0.29 \beta^{-0.38} \text{ATAN} (8 \zeta))$ <p>Brace:</p> $1 + (1.97 - 1.57 \beta^{0.25}) \tau^{-0.14} (\sin \theta)^{0.7} \cdot (\text{Eqn. (20)}) +$ $\sin^{1.8} (\theta_{\max} + \theta_{\min}) \cdot (0.131 - 0.084 \text{ATAN} (14 \zeta + 4.2 \beta)) \cdot$ $C \beta^{1.5} \gamma^{0.5} \tau^{-1.22}$ <p>Where:  C = 0 for gap joints  C = 1 for the through brace  C = 0.5 for the overlapping brace  Note that <math>\tau</math>, <math>\beta</math>, <math>\theta</math> and the nominal stress relate to the brace under consideration  ATAN is arctangent evaluated in radians</p>	(20)	None
<p>Unbalanced in plane bending</p> 	<p>Chord crown:  (Eqn. (8))  (for overlaps exceeding 30% of contact length use <math>1.2 \cdot (\text{Eqn. (8)})</math>)</p> <p>Gap joint brace crown:  (Eqn. (9))</p> <p>Overlap joint brace crown:  (Eqn. (9)) <math>\cdot (0.9 + 0.4\beta)</math></p>	(22)	
<p>Unbalanced out-of-plane bending</p> 	<p>Chord saddle SCF adjacent to brace A:  (Eqn. (10))<math>A \cdot (1 - 0.08 (\beta_B \gamma)^{0.5} \exp(-0.8 x)) + (\text{Eqn. (10)})B</math></p> $(1 - 0.08 (\beta_A \gamma)^{0.5} \exp(-0.8 x)) (2.05 \beta_{\max}^{0.5} \exp(-1.3 x))$ <p>where</p> $x = 1 + \frac{\zeta \sin \theta_A}{\beta_A}$ <p>Brace A saddle SCF</p> $\tau^{-0.54} \gamma^{-0.05} (0.99 - 0.47 \beta + 0.08 \beta^4) \cdot (\text{Eqn. (23)})$	(23)	F4
$F4 = 1 - 1.07 \beta^{1.88} \exp(-0.16 \gamma^{-1.06} \alpha^{2.4})$			
<p>(Eqn. (10))<sub>A</sub> is the chord SCF adjacent to brace A as estimated from Eqn. (10).</p>			
<p>Note that the designation of braces A and B is not geometry dependent. It is nominated by the user.</p>			

Load type and fixity conditions	SCF equations	Eqn. No.	Short chord correction
<p>Axial load on one brace only</p> 	<p>Chord saddle: (Eqn. (5))</p> <p>Chord crown: (Eqn. (6))</p> <p>Brace saddle: (Eqn.(3))</p> <p>Brace crown: (Eqn. (7))</p> <p>Note that all geometric parameters and the resulting SCFs relate to the loaded brace.</p>		<p>F1</p> <p>-</p> <p>F1</p> <p>-</p>
<p>In-plane-bending on one brace only</p> 	<p>Chord crown: (Eqn. (8))</p> <p>Brace crown: (Eqn. (9))</p> <p>Note that all geometric parameters and the resulting SCFs relate to the loaded brace.</p>		
<p>Out-of-plane bending on one brace only</p> 	<p>Chord saddle: (Eqn.(10))<math>A \cdot (1 - 0.08(\beta_B \gamma)^{0.5} \exp(-0.8x))</math></p> <p>where</p> $x = 1 + \frac{\zeta \sin \theta_A}{\beta_A}$ <p>Brace saddle: <math>\tau^{-0.54} \gamma^{-0.05} (0.99 - 0.47\beta + 0.08\beta^4) \cdot</math> (Eqn. (25))</p>	<p>(25)</p> <p>(26)</p>	<p>F3</p> <p>F3</p>
<p>Short chord correction factors:</p> $F1 = 1 - (0.83\beta - 0.56\beta^2 - 0.02)\gamma^{0.23} \exp(-0.21\gamma^{-1.16}\alpha^{2.5})$ $F3 = 1 - 0.55\beta^{1.8}\gamma^{0.16} \exp(-0.49\gamma^{-0.89}\alpha^{1.8})$			





## Joint classification

### K.1. Examples of joint classifications 1

Examples of different joint classifications are shown in figure K.1.

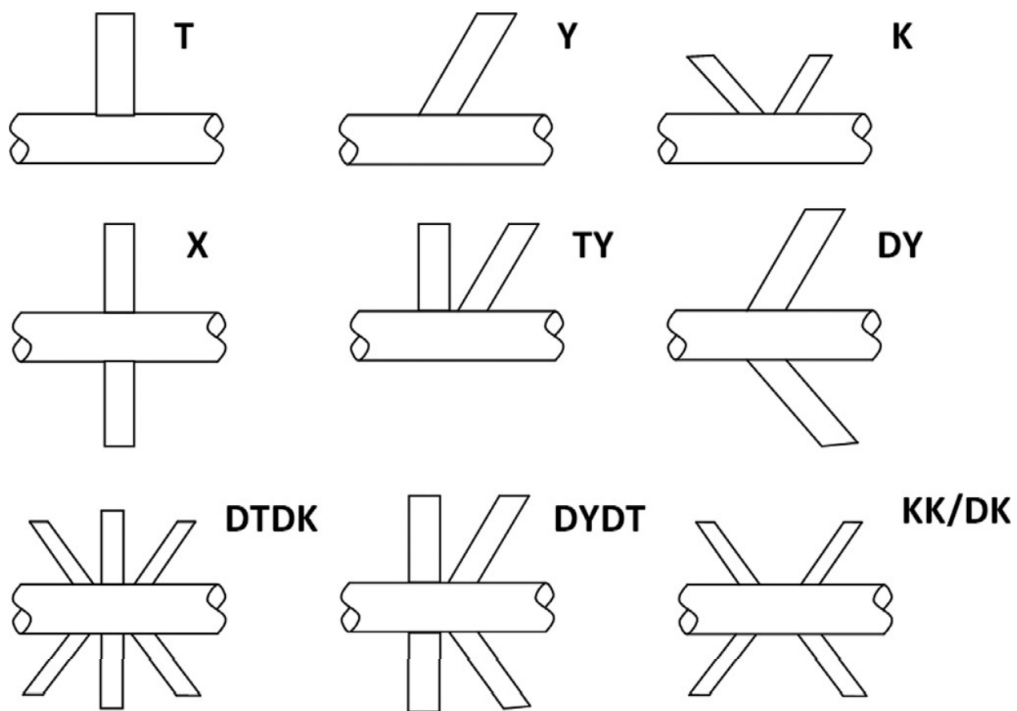


Figure K.1: Different classifications of a tubular joint [51]

## K.2. Examples of joint classifications 2

Examples of the different joint classifications for joint combinations are shown in figure K.2.

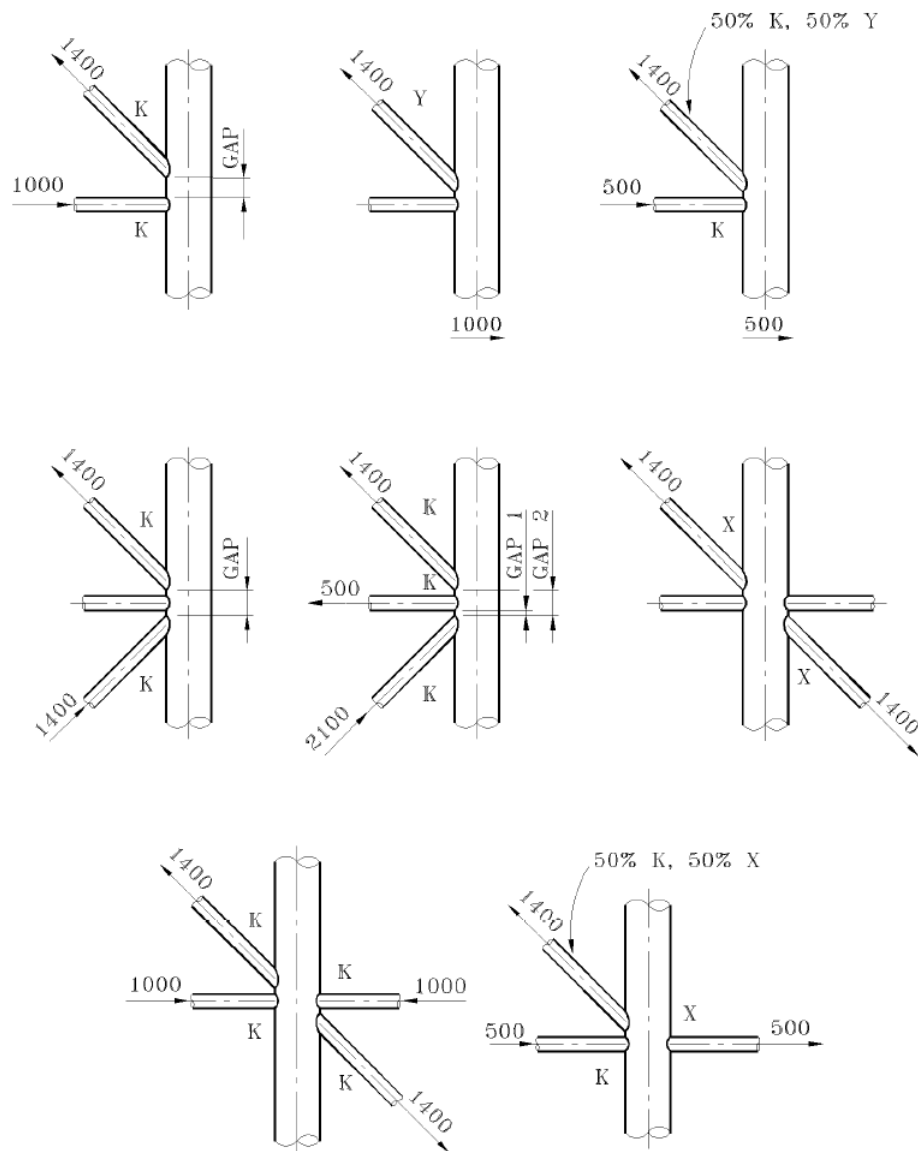


Figure K.2: Examples of combinations of different joint classifications [23]



# Results of implementation

This appendix contains the details of the fatigue assessment of the test-case, in order to support the results of chapter 6.

## **L.1. Member-loads**

Member-loads on brace 1.1 as effect of sub-load-cases

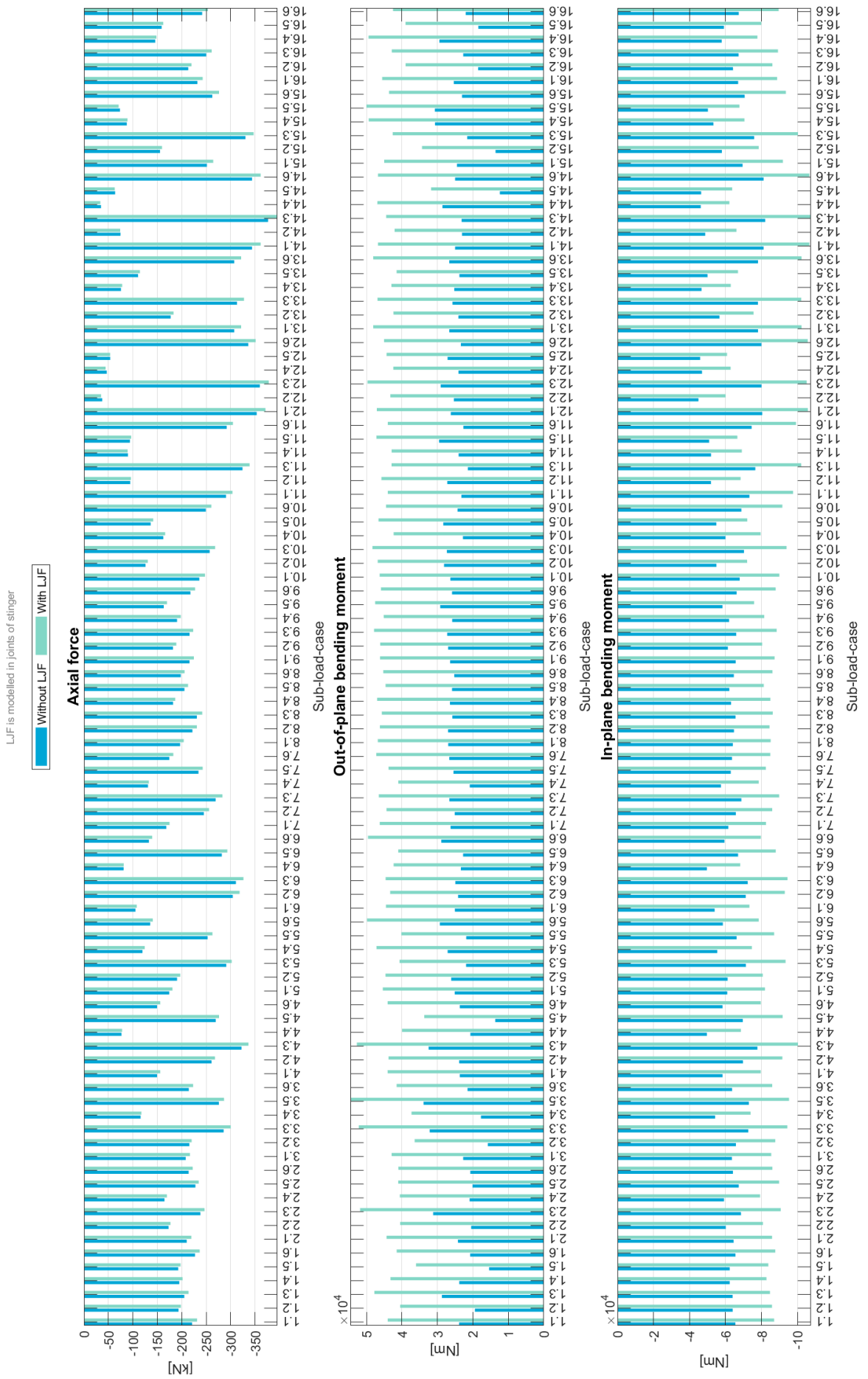


Figure L.1: Member loads on brace 1.1

**Member-loads on brace 1.2 as effect of sub-load-cases**

LjF is modelled in joints of slinger

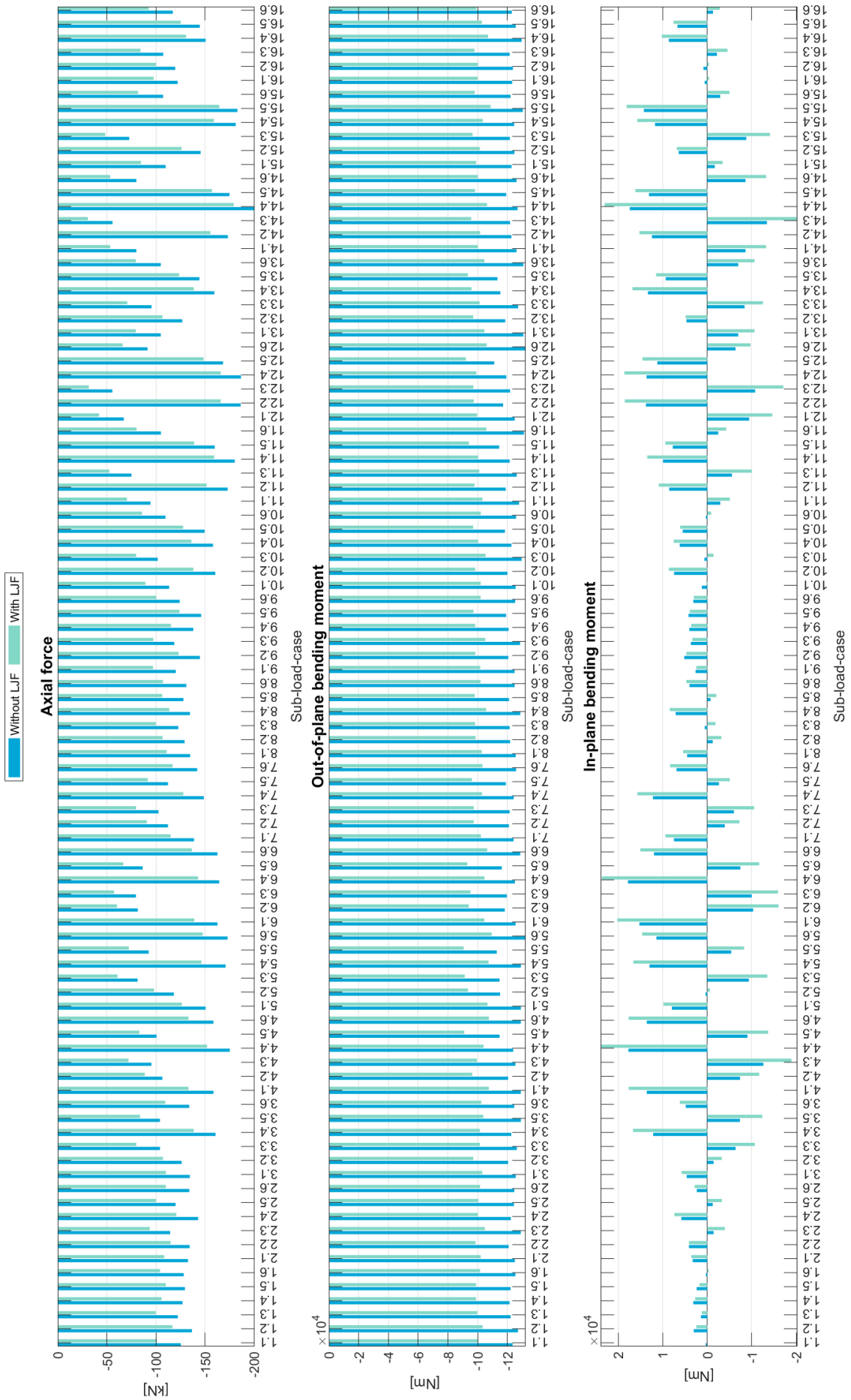


Figure L.2: Member loads on brace 1.2

Member-loads on brace 1.3 as effect of sub-load-cases

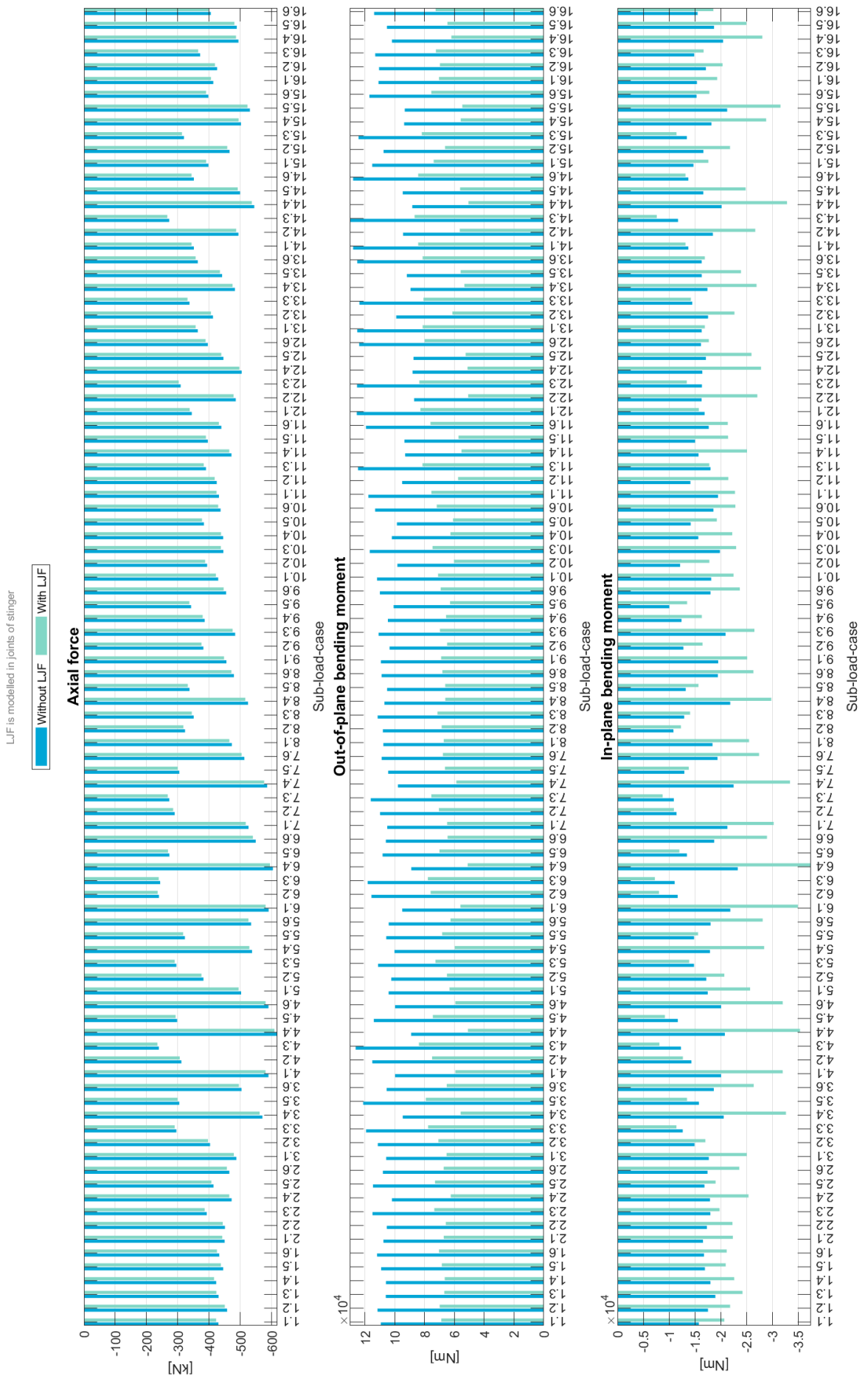


Figure L.3: Member loads on brace 1.3

Member-loads on brace 1.4 as effect of sub-load-cases

LJF is modelled in joints of stinger

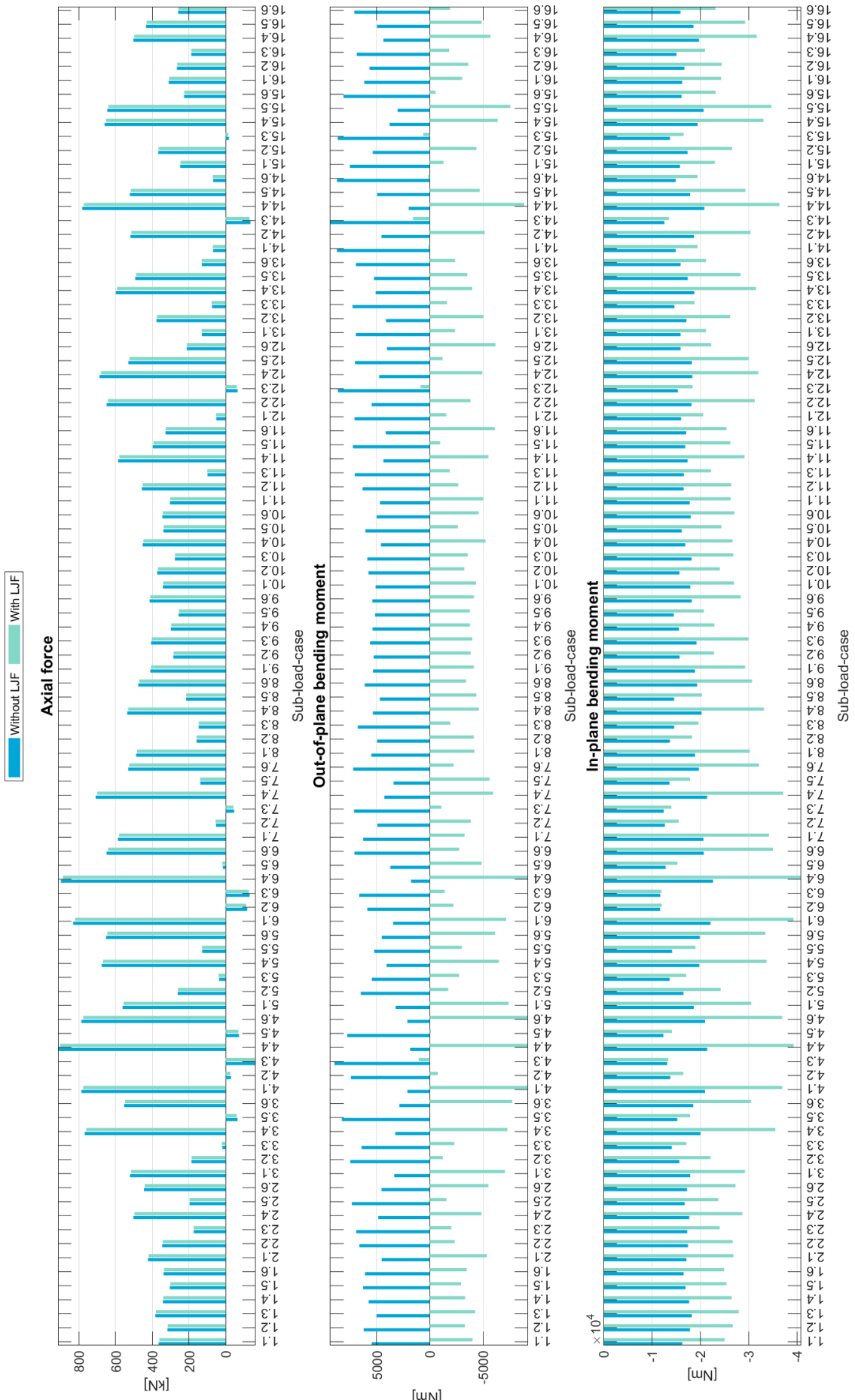


Figure L.4: Member loads on brace 1.4

Member-loads on brace 2.1 as effect of sub-load-cases

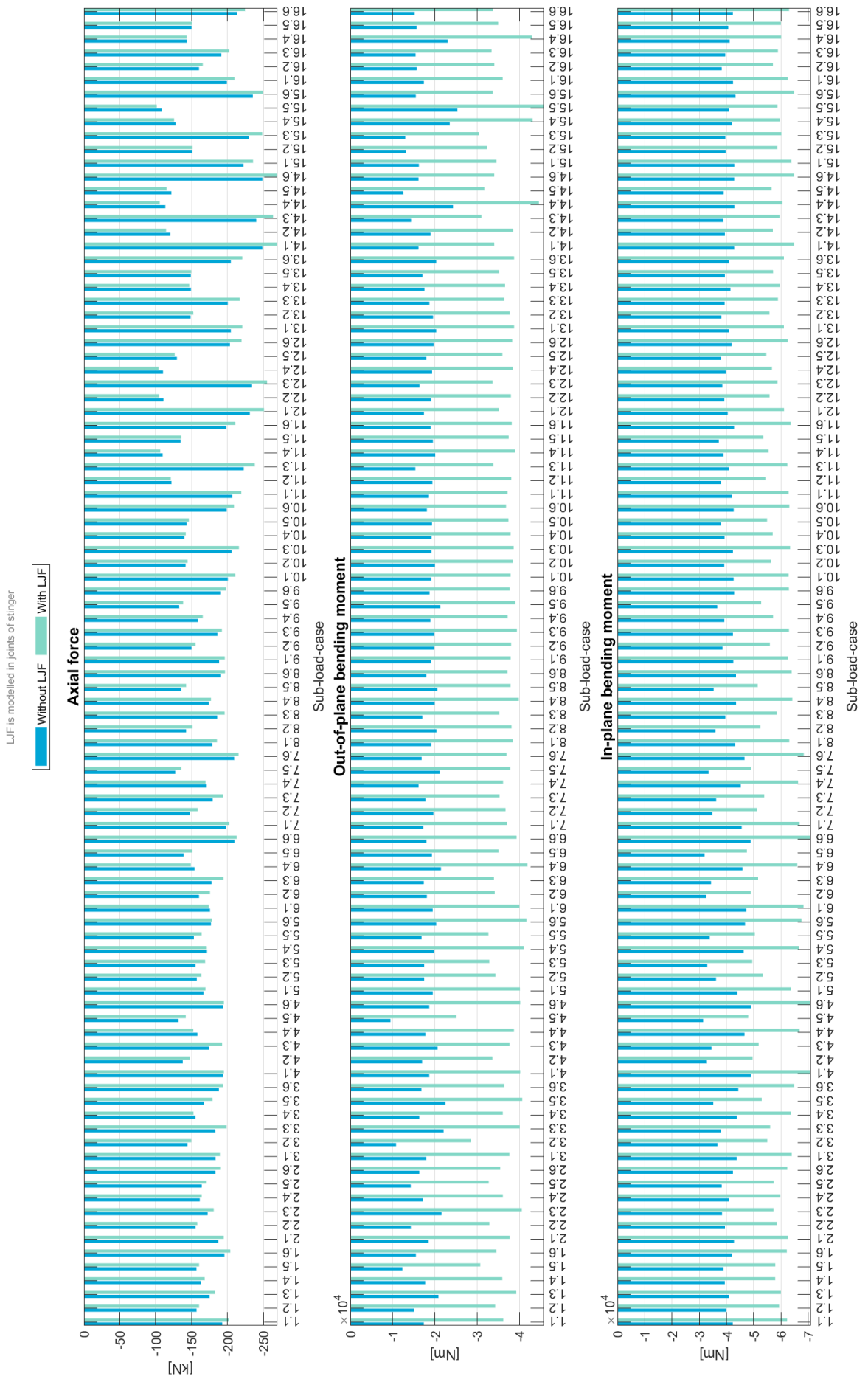


Figure L.5: Member loads on brace 2.1

Member-loads on brace 2.2 as effect of sub-load-cases

LjF is modelled in joints of slinger

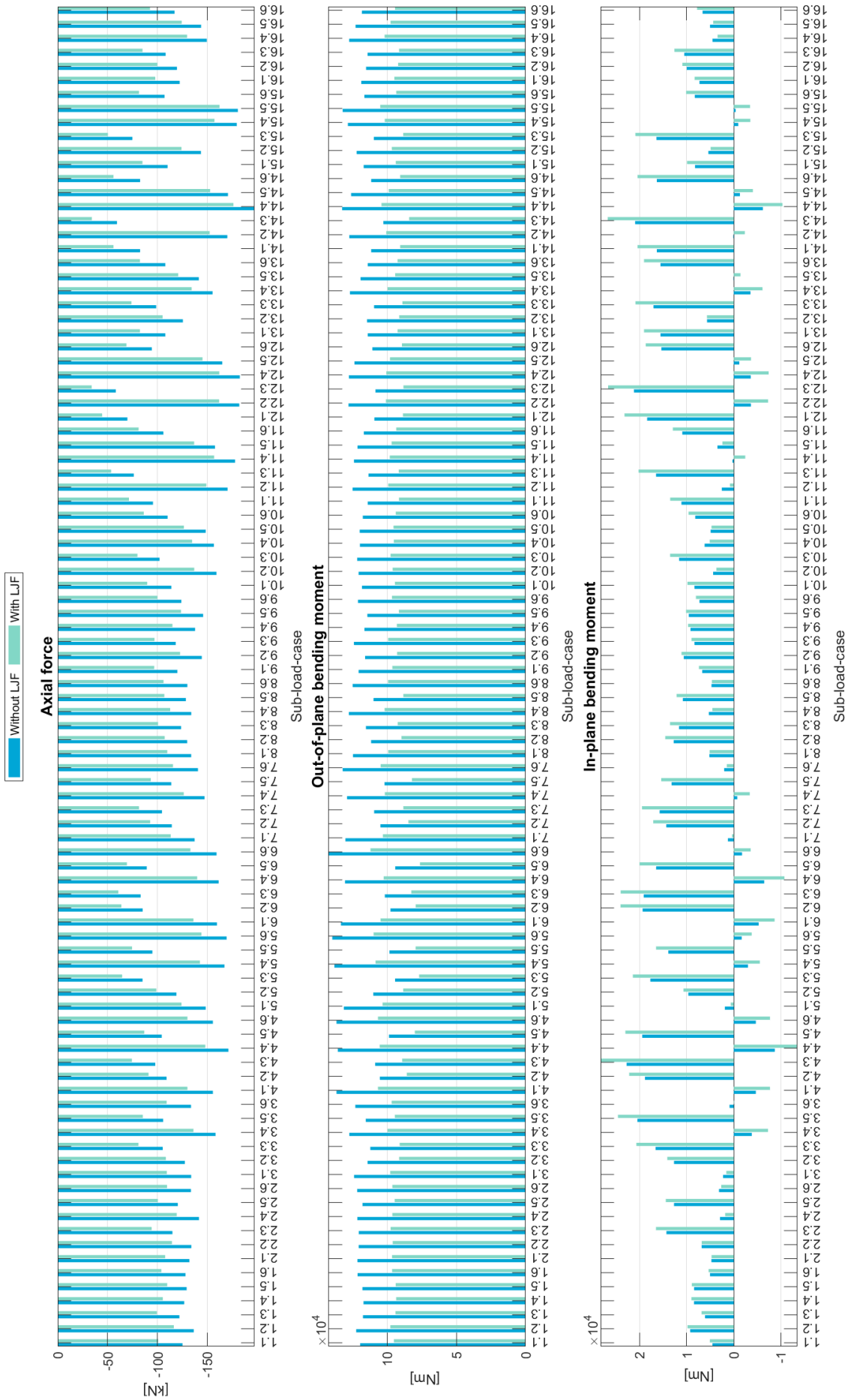


Figure L.6: Member loads on brace 2.2

Member-loads on brace 2.3 as effect of sub-load-cases

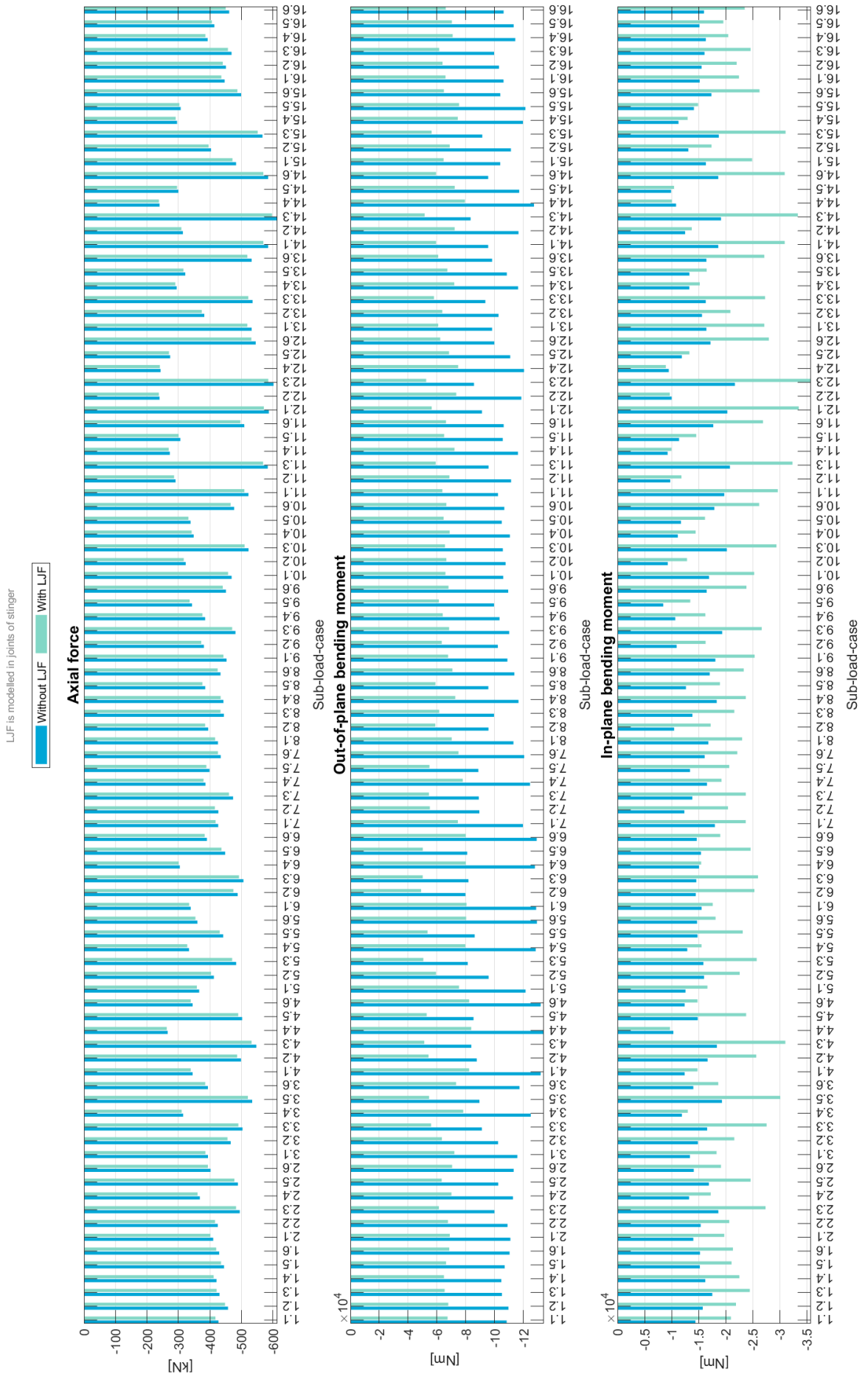


Figure L.7: Member loads on brace 2.3

Member-loads on brace 2.4 as effect of sub-load-cases

LjF is modelled in joints of slinger

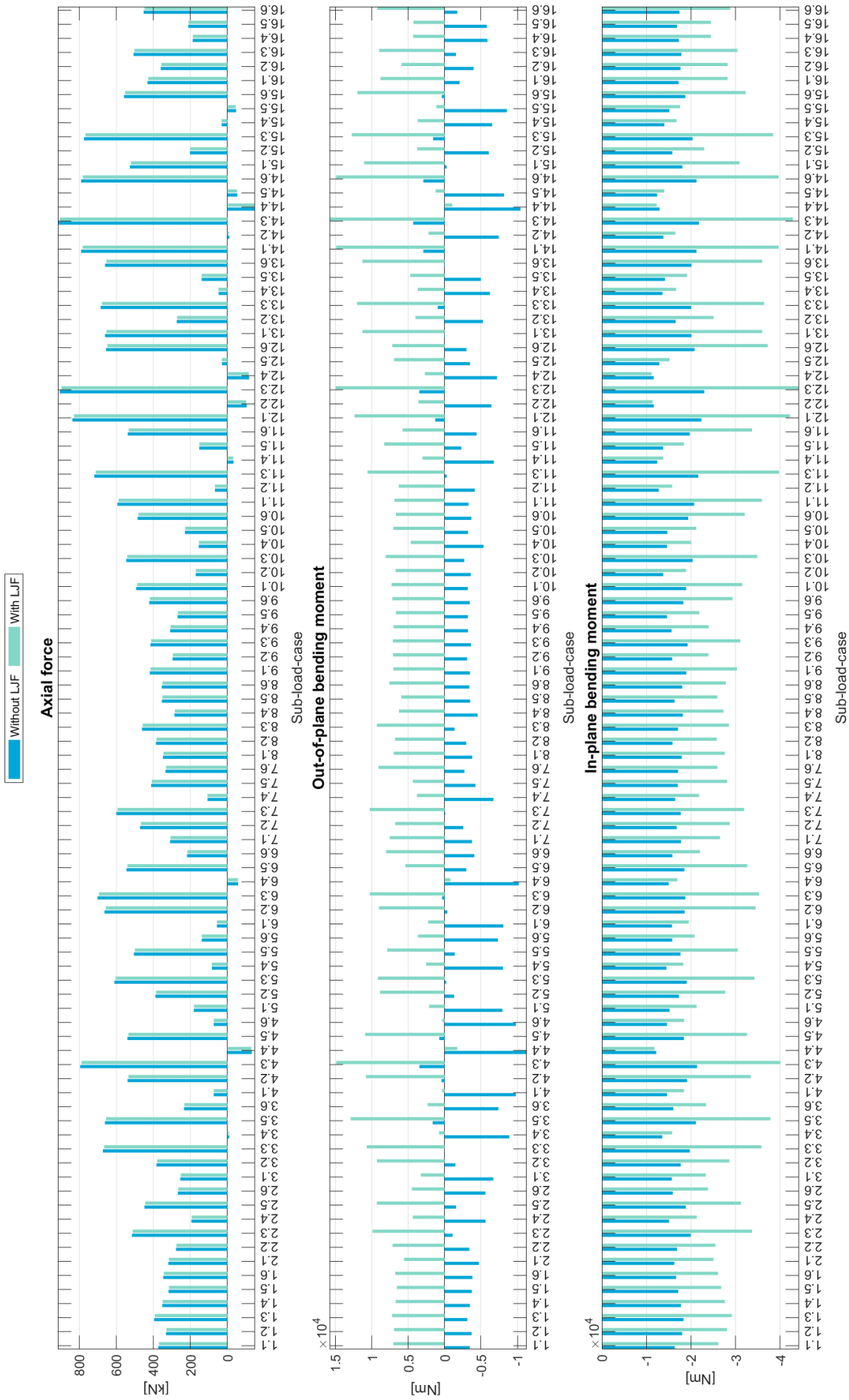


Figure L.8: Member loads on brace 2.4

**Member-loads on brace 3.1 as effect of sub-load-cases**

LJF is modelled in joints of stinger

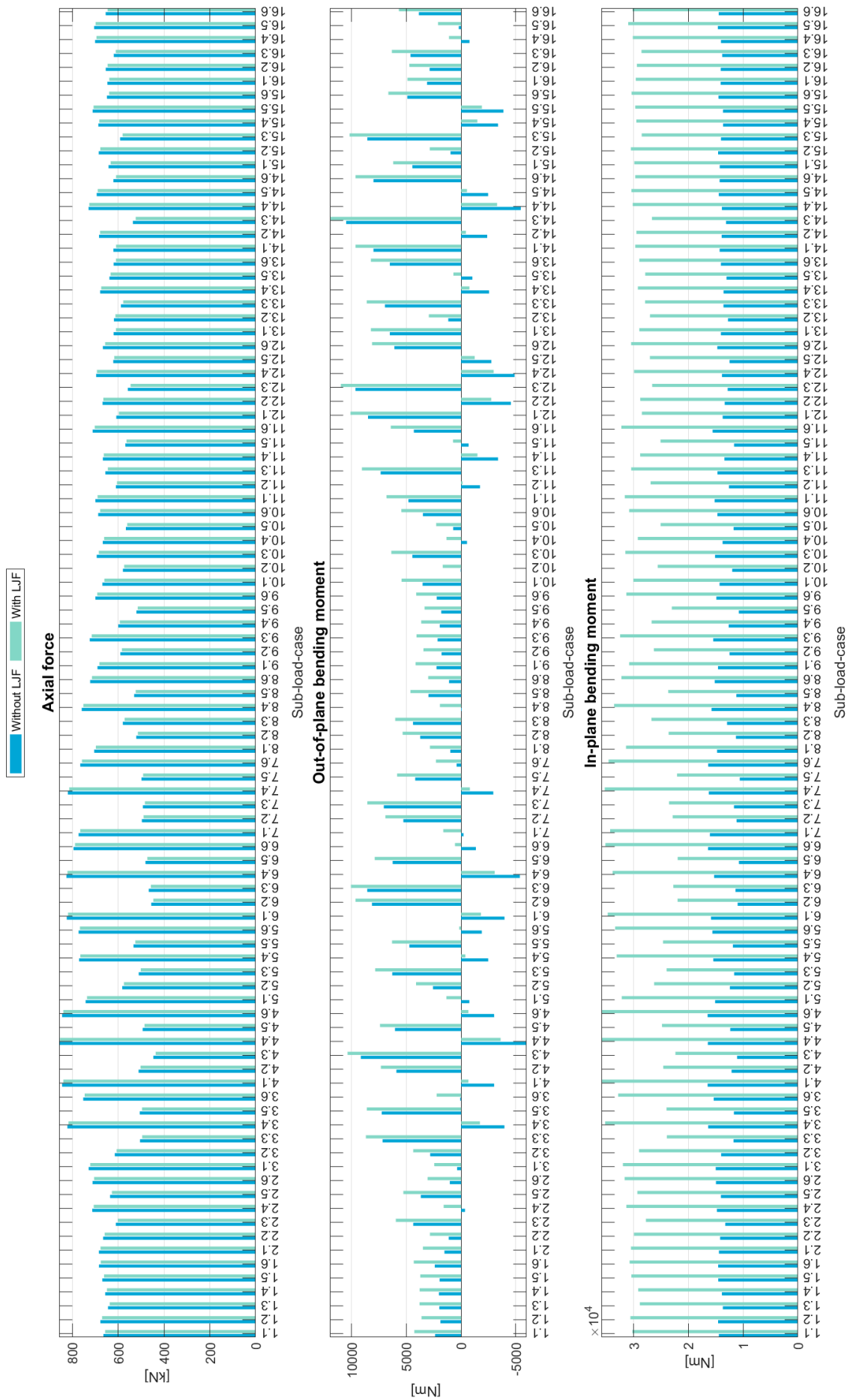


Figure L.9: Member loads on brace 3.1

Member-loads on brace 3.2 as effect of sub-load-cases

LJF is modelled in joints of stinger

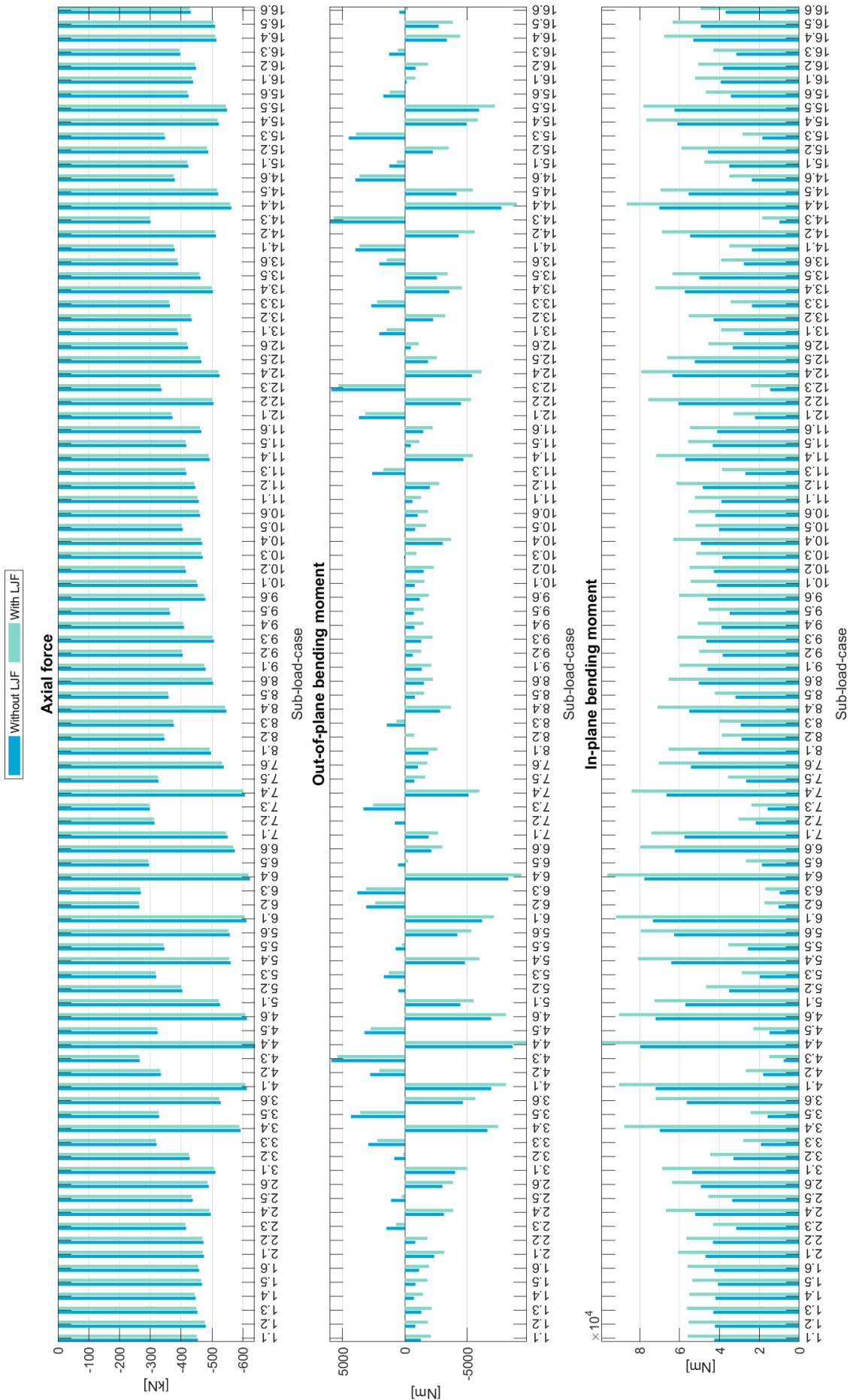


Figure L.10: Member loads on brace 3.2

Member-loads on brace 3.3 as effect of sub-load-cases

LJF is modelled in joints of stinger

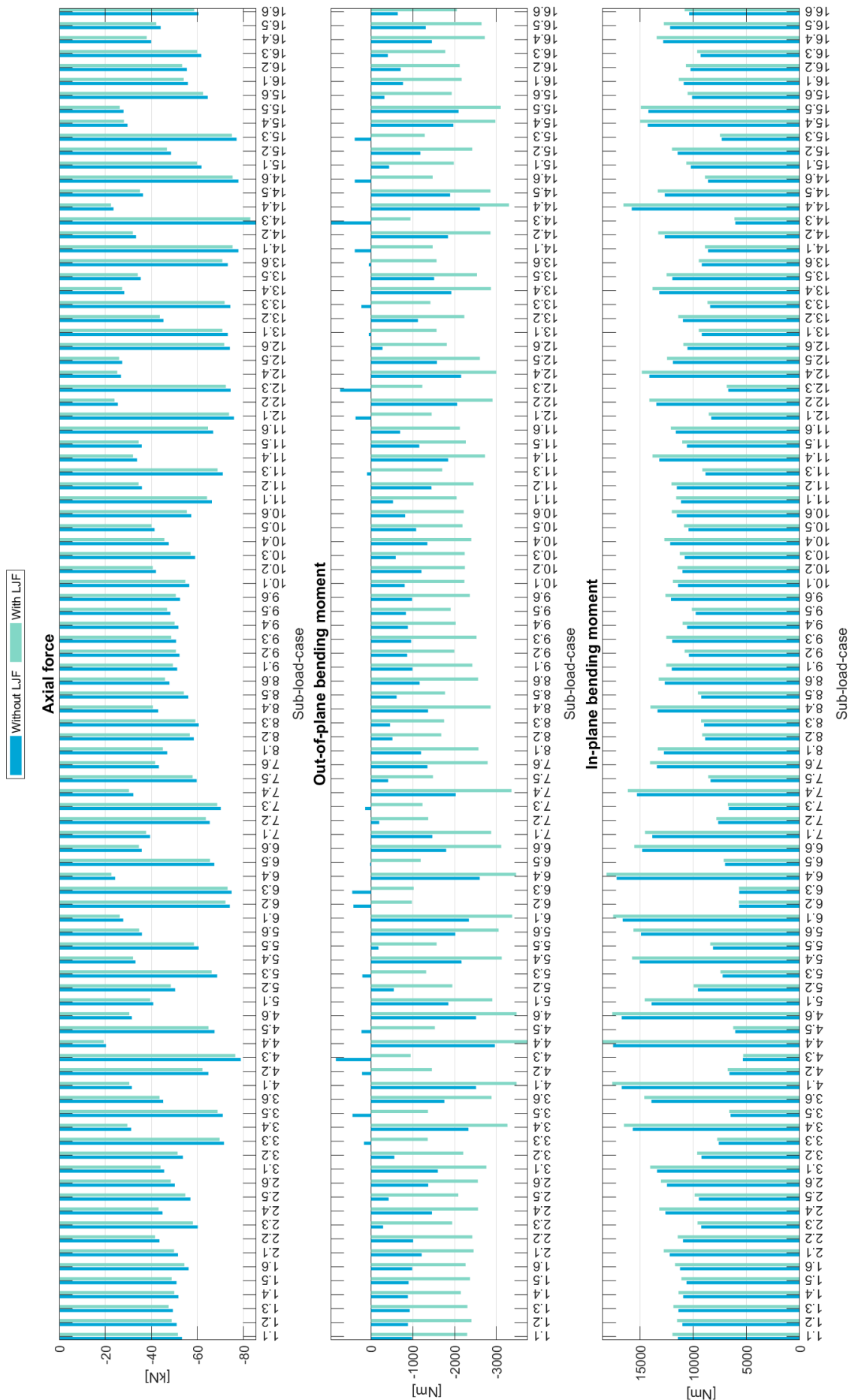


Figure L.11: Member loads on brace 3.3

Member-loads on brace 3.4 as effect of sub-load-cases

LJF is modelled in joints of stinger

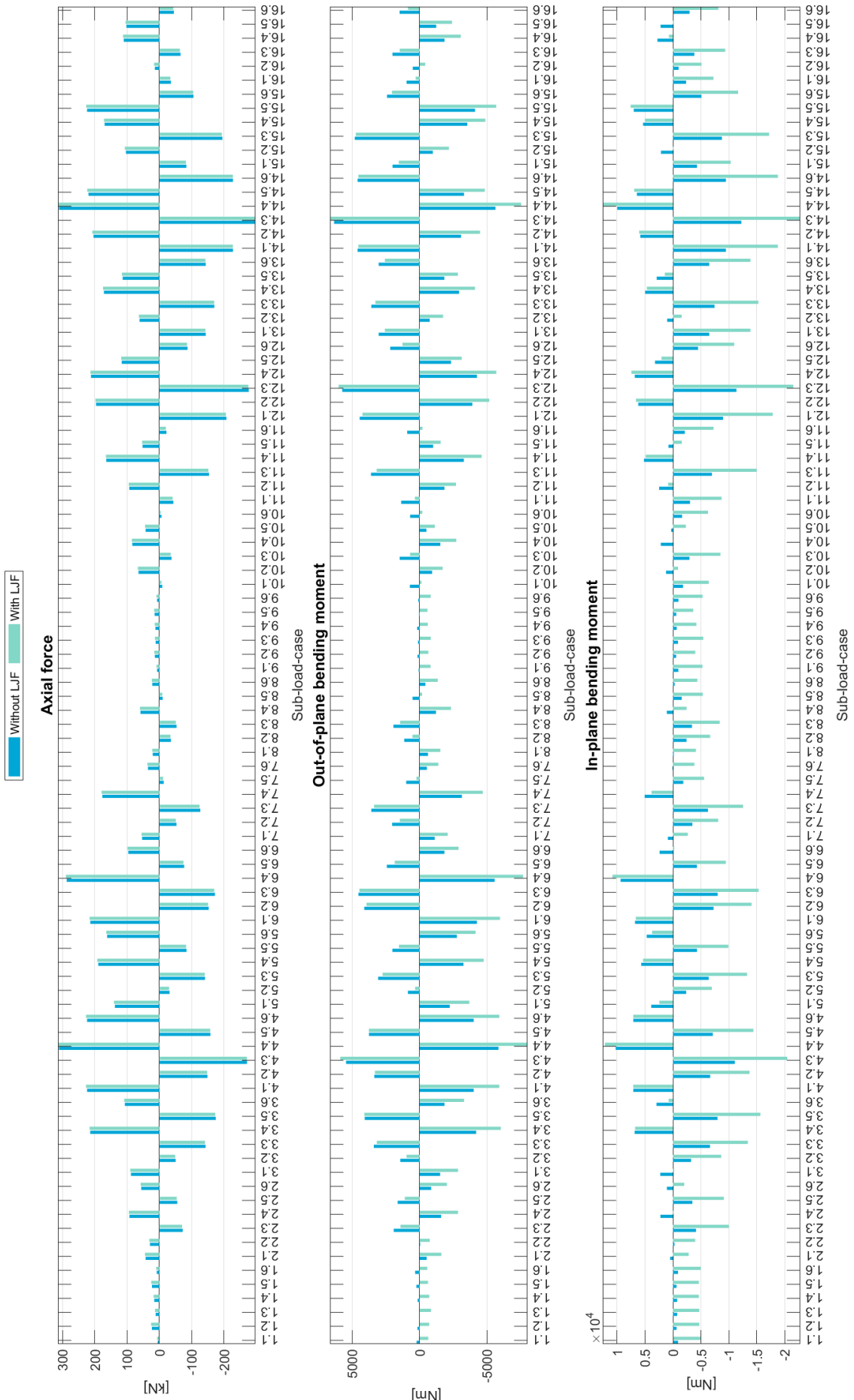


Figure L.12: Member loads on brace 3.4

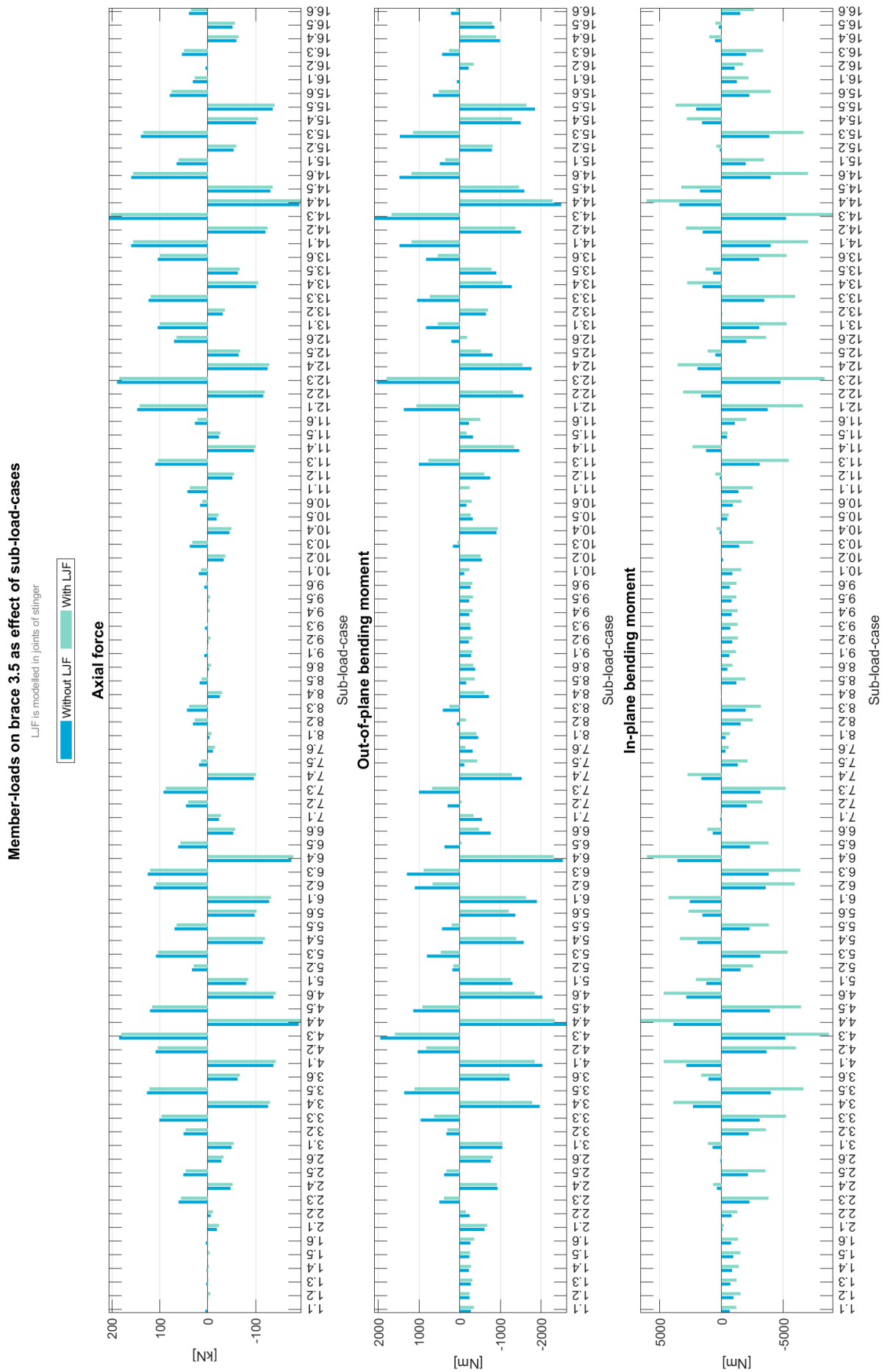


Figure L.13: Member loads on brace 3.5

**Member-loads on brace 4.1 as effect of sub-load-cases**

LJF is modelled in joints of slinger

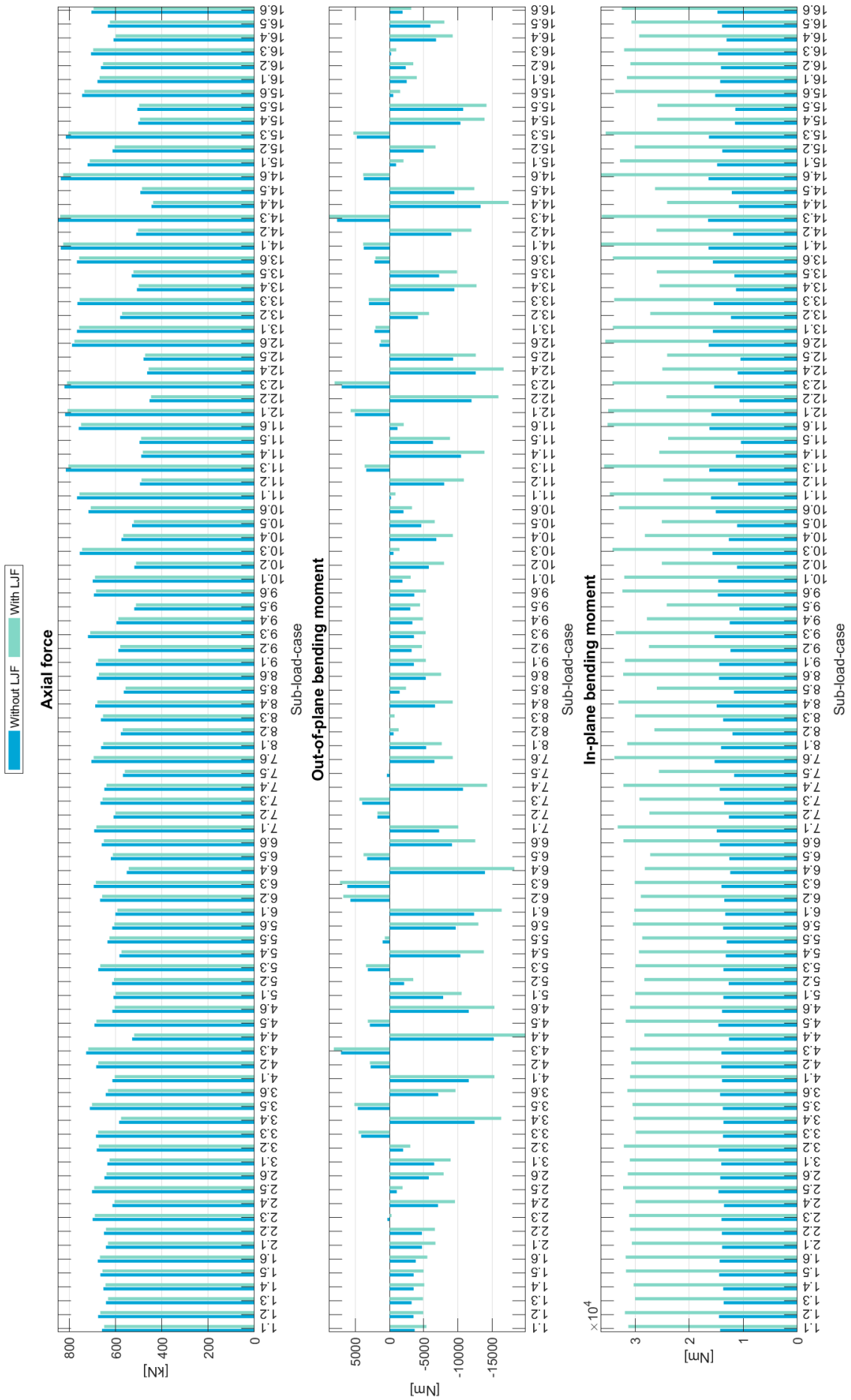


Figure L.14: Member loads on brace 4.1

Member-loads on brace 4.2 as effect of sub-load-cases

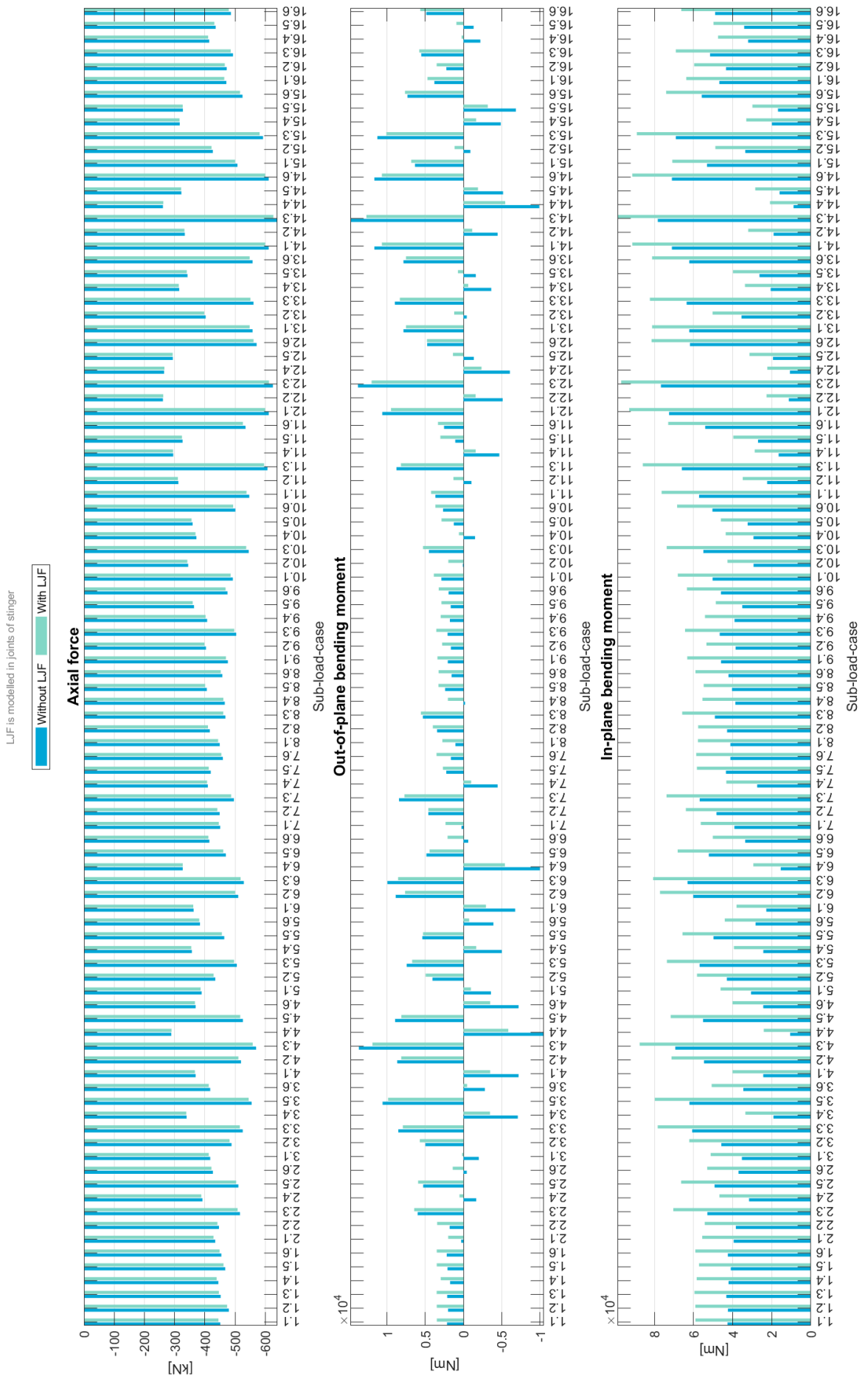


Figure L.15: Member loads on brace 4.2

Member-loads on brace 4.3 as effect of sub-load-cases

LJF is modelled in joints of stinger

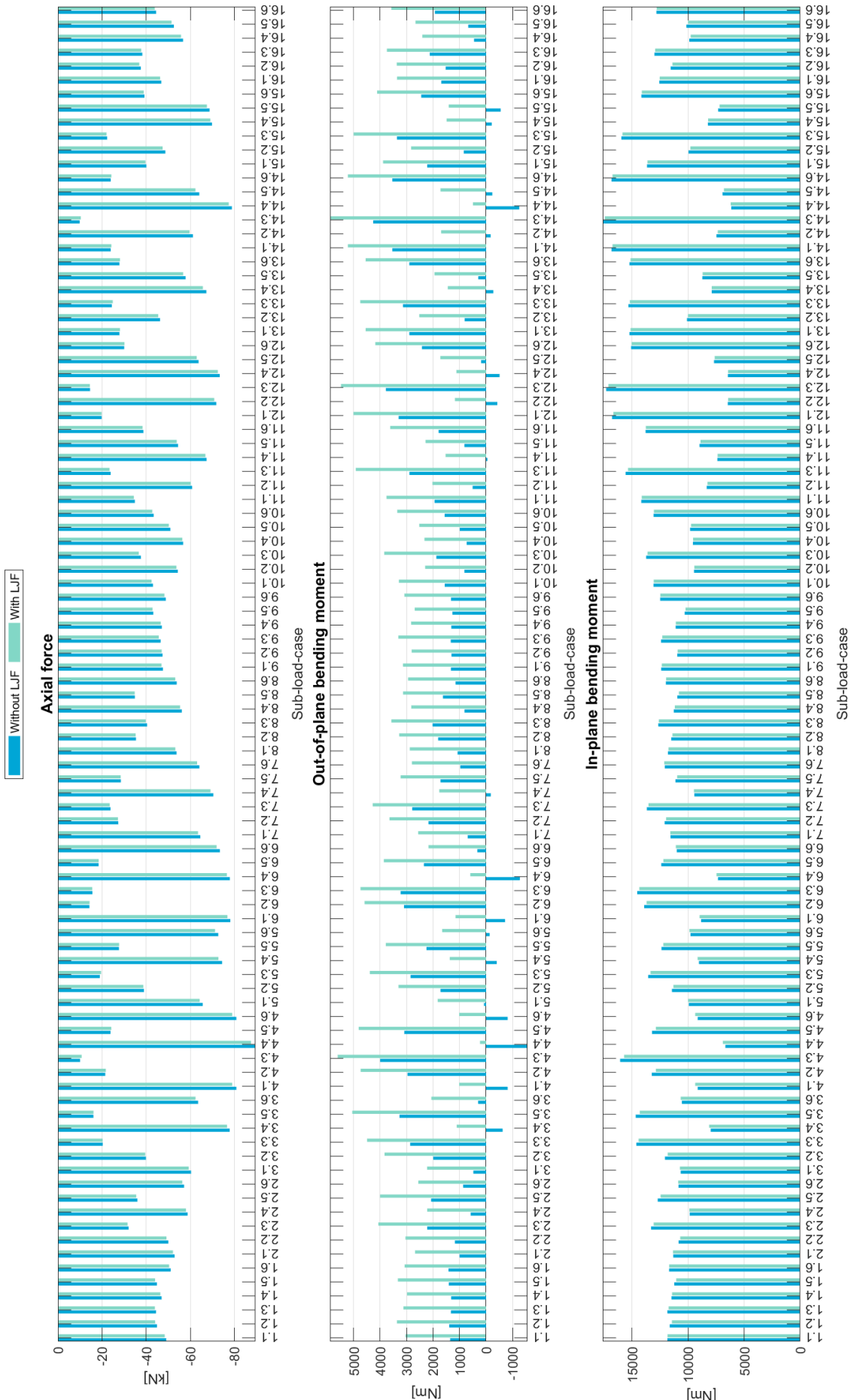


Figure L.16: Member loads on brace 4.3

**Member-loads on brace 4.4 as effect of sub-load-cases**

LJF is modelled in joints of stinger

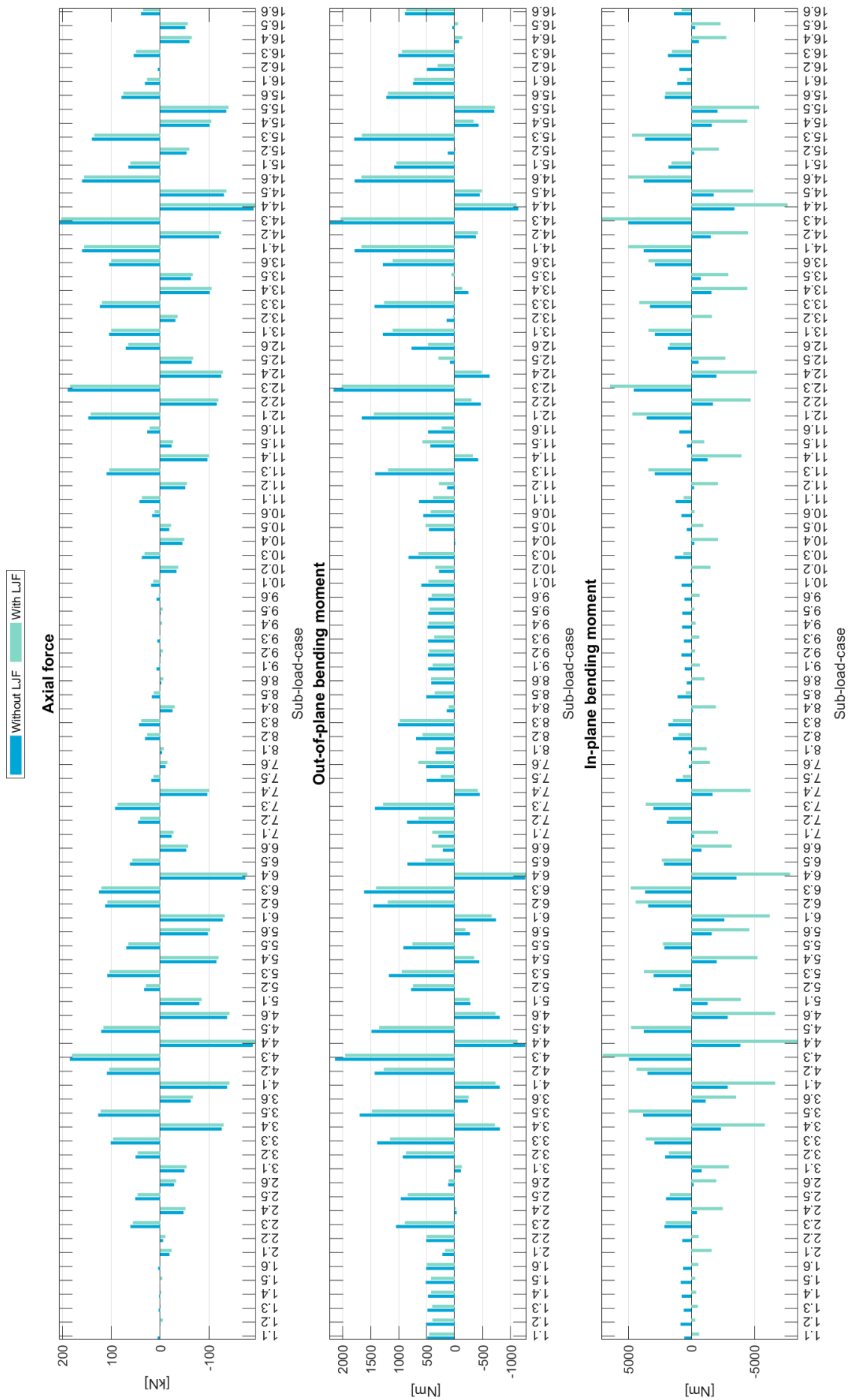


Figure L.17: Member loads on brace 4.4

Member-loads on brace 4.5 as effect of sub-load-cases

LJF is modelled in joints of stinger

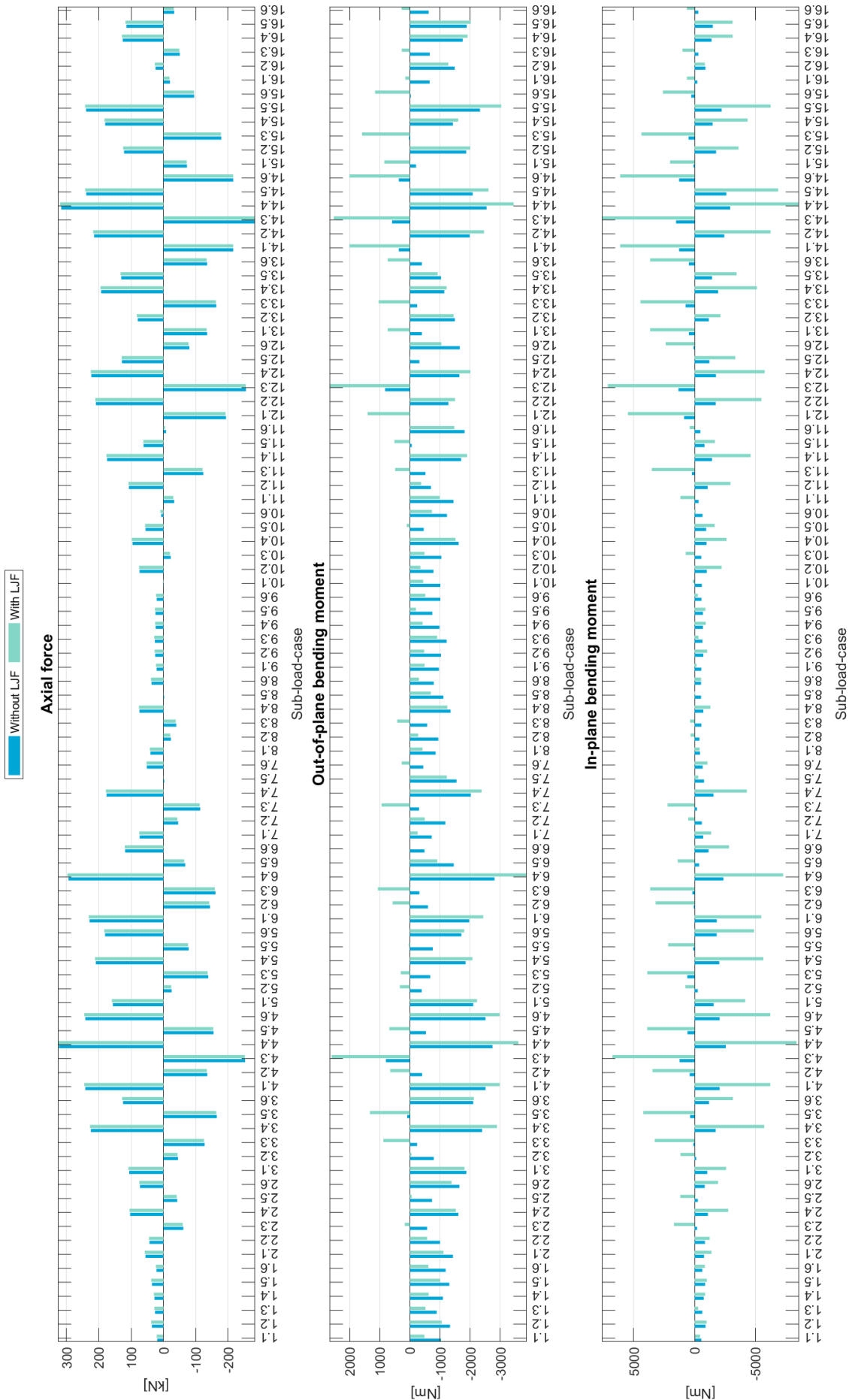


Figure L.18: Member loads on brace 4.5

Member-loads on brace 5.1 as effect of sub-load-cases

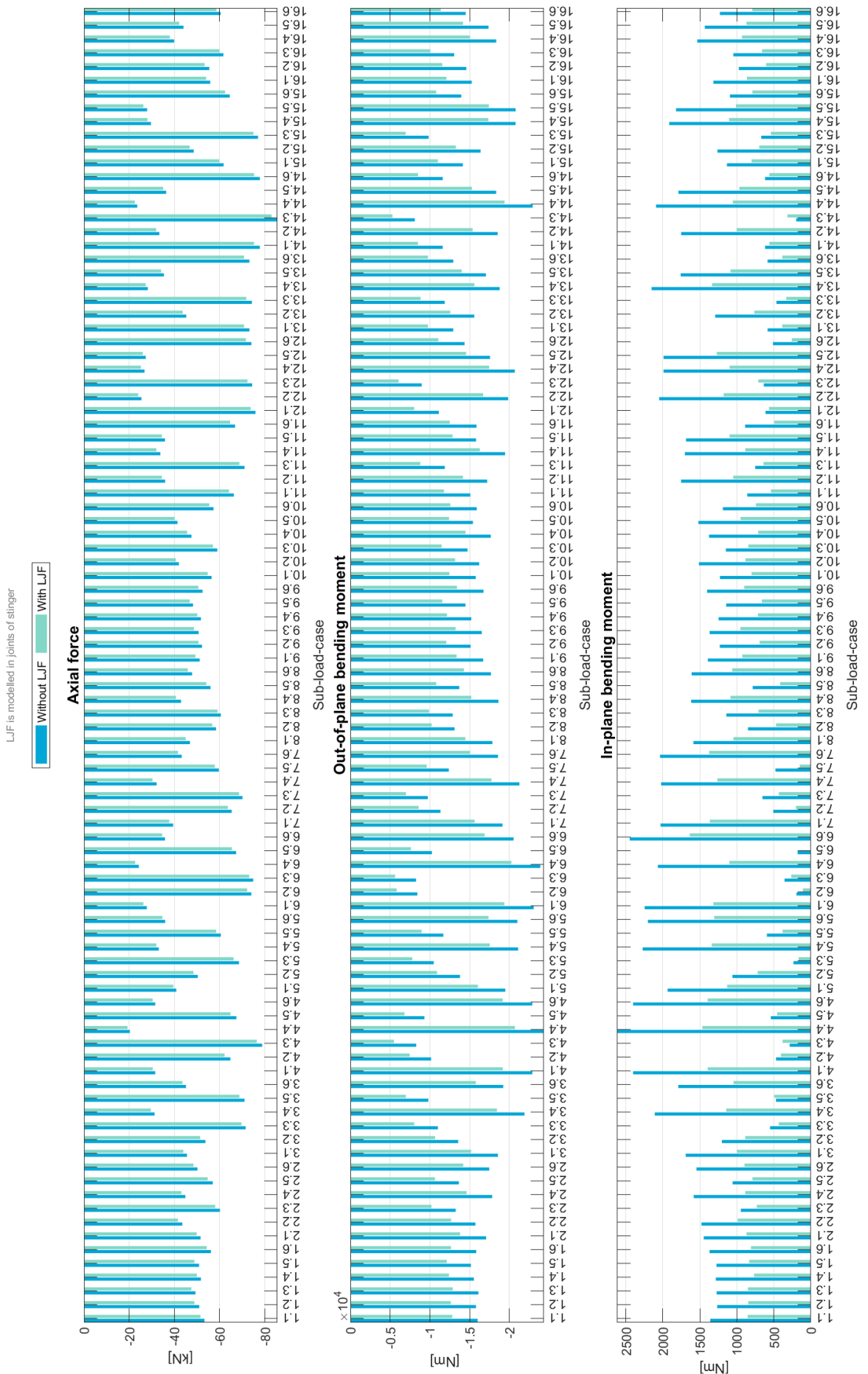


Figure L.19: Member loads on brace 5.1

Member-loads on brace 5.2 as effect of sub-load-cases

LJF is modelled in joints of stinger

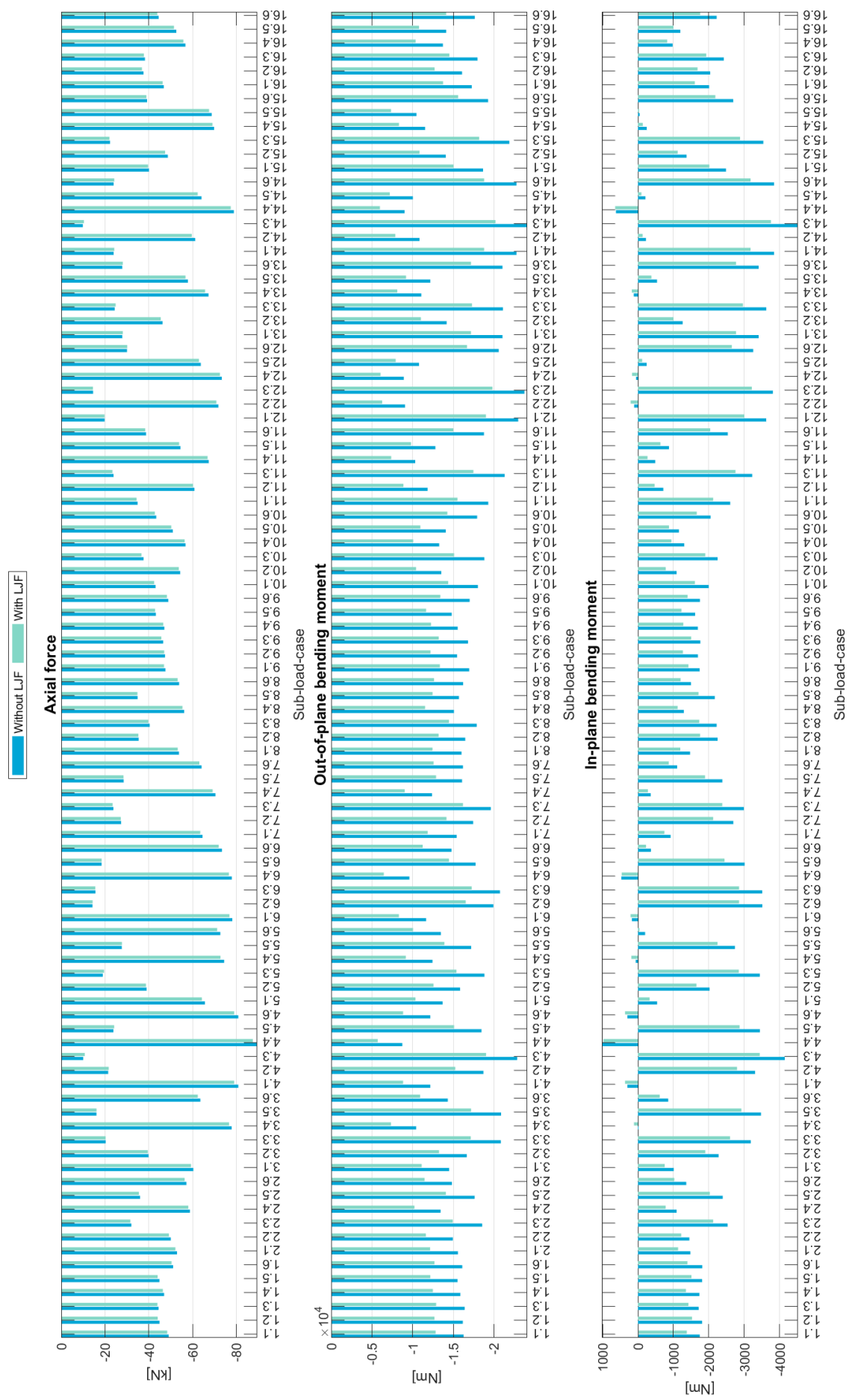


Figure L.20: Member loads on brace 5.2

**Member-loads on brace 6.1 as effect of sub-load-cases**

LJF is modelled in joints of stinger

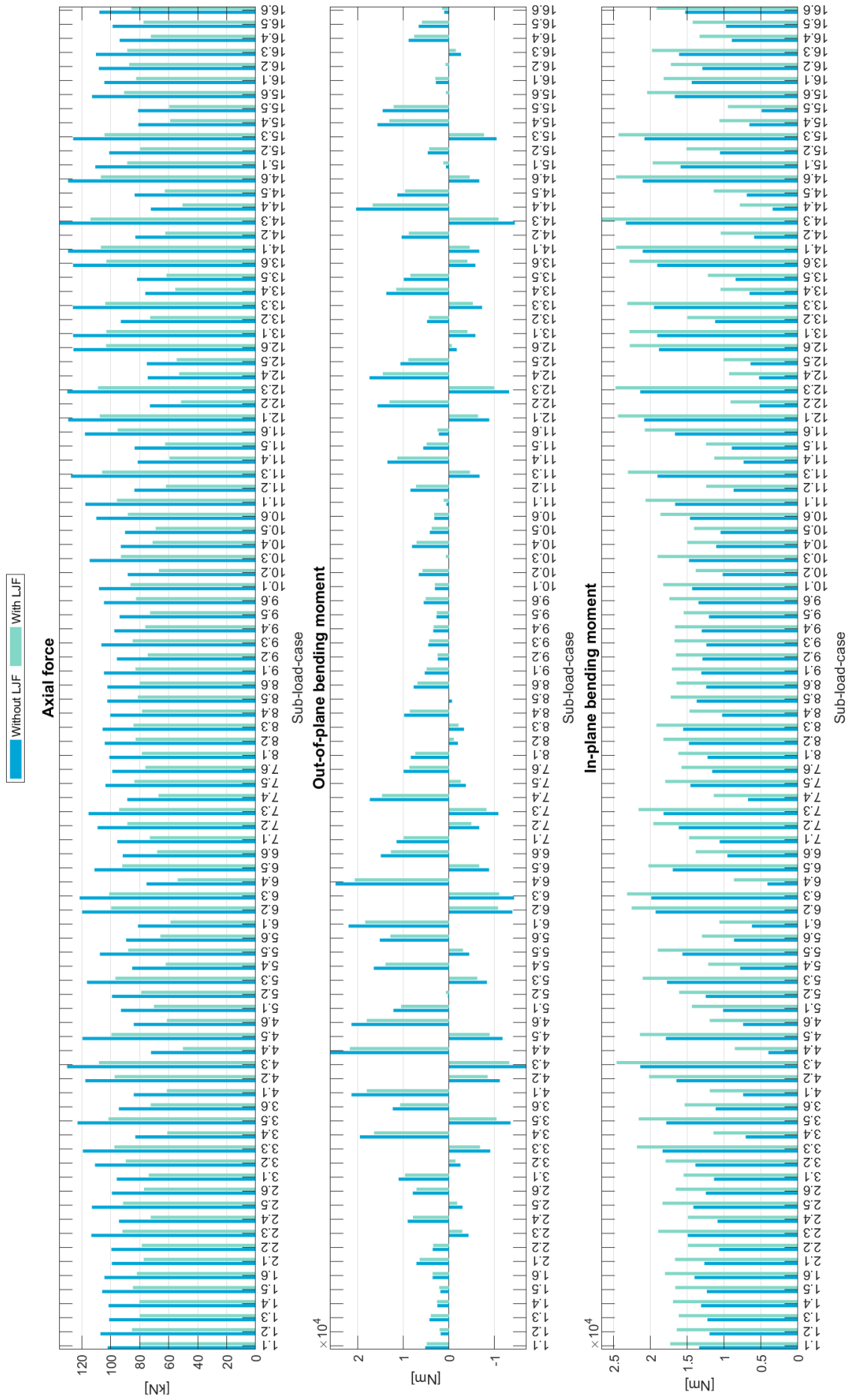


Figure L.21: Member loads on brace 6.1

Member-loads on brace 7.1 as effect of sub-load-cases

LJF is modelled in joints of stinger

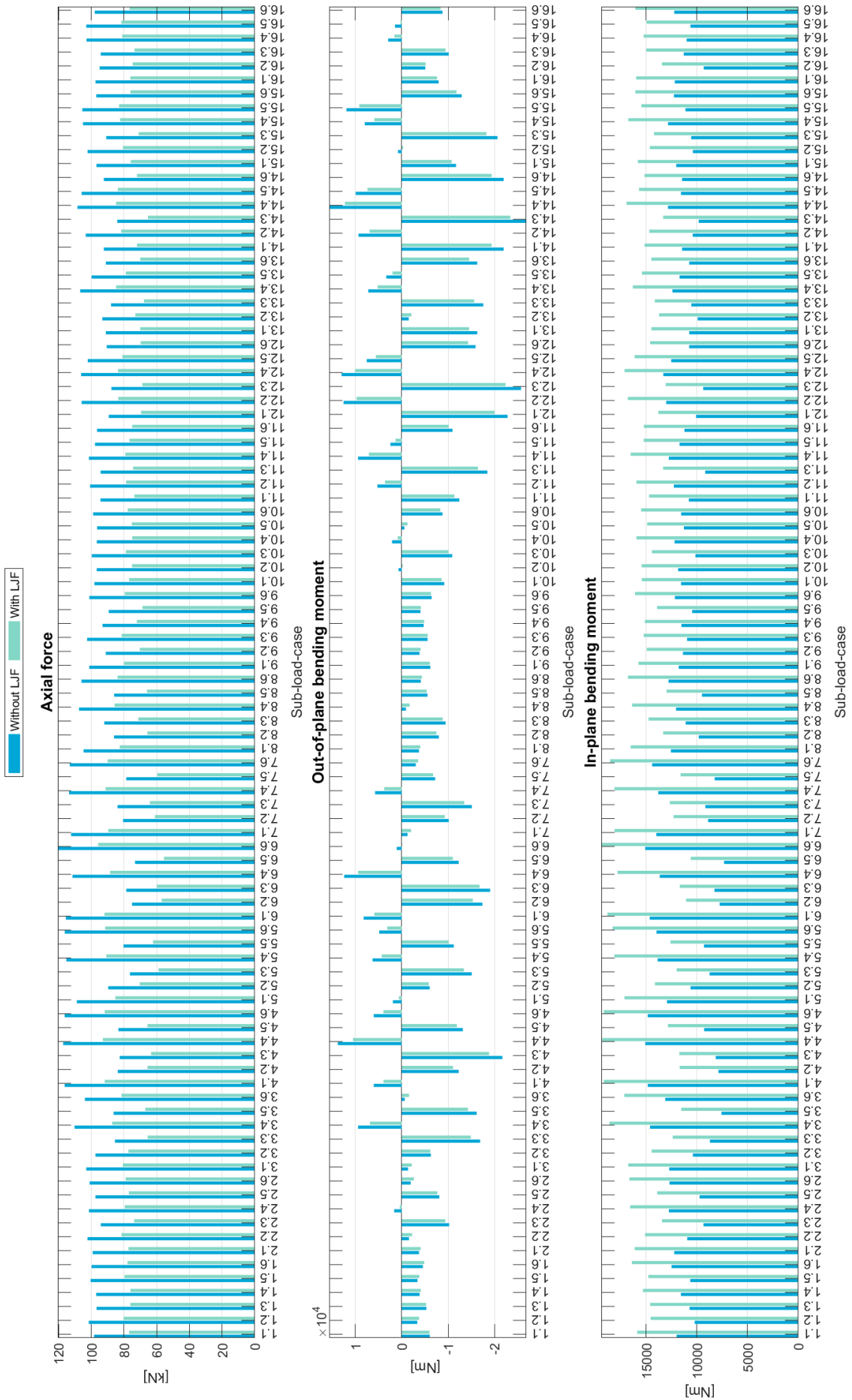


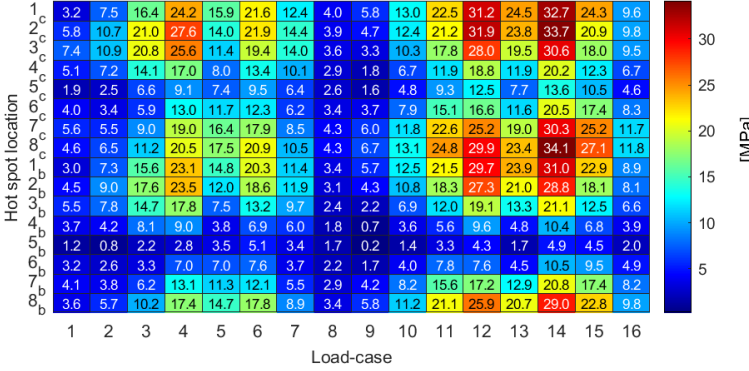
Figure L.22: Member loads on brace 7.1

## **L.2. Stress range and accumulated fatigue damage**

Details of fatigue assesment brace 1.1

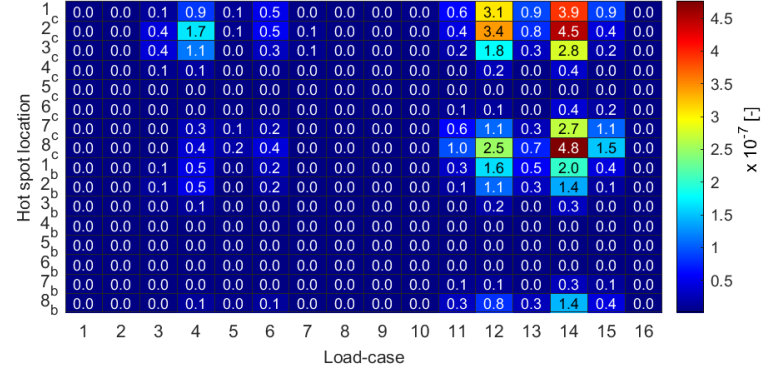
Stress range in hot spots

According to a model without LJF



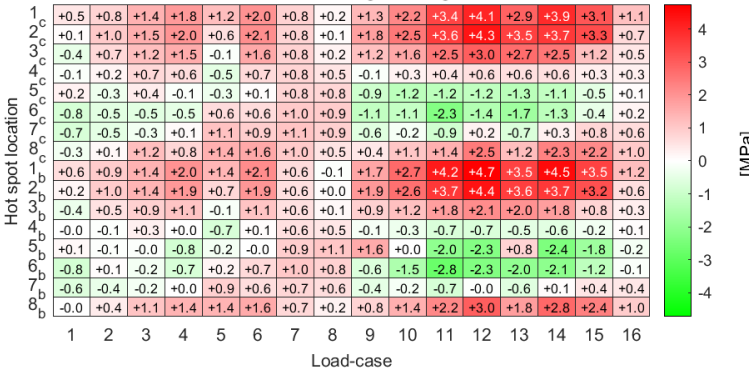
Accumulated fatigue damage in hot spots

According to a model without LJF



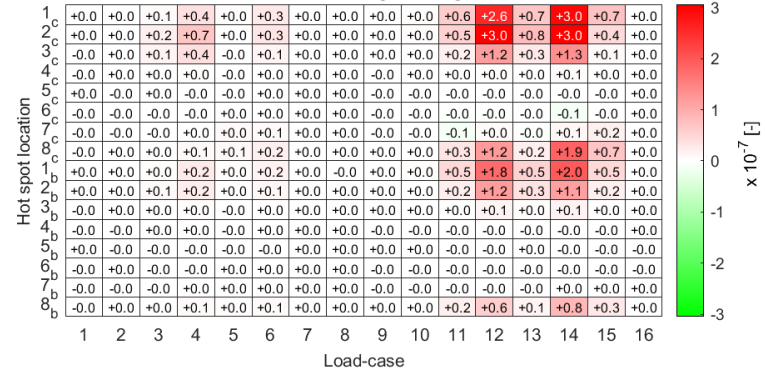
Absolute difference in hot spot stress range

As effect of modelling LJF in stinger



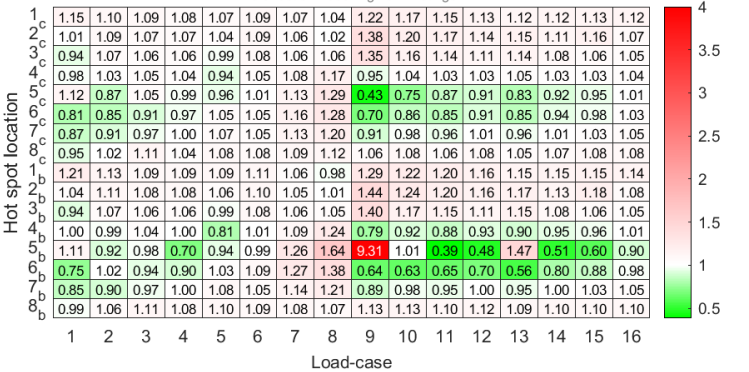
Absolute difference in accumulated fatigue damage

As effect of modelling LJF in stinger



Ratio with/without LJF of hot spot stress range

As effect of modelling LJF in stinger

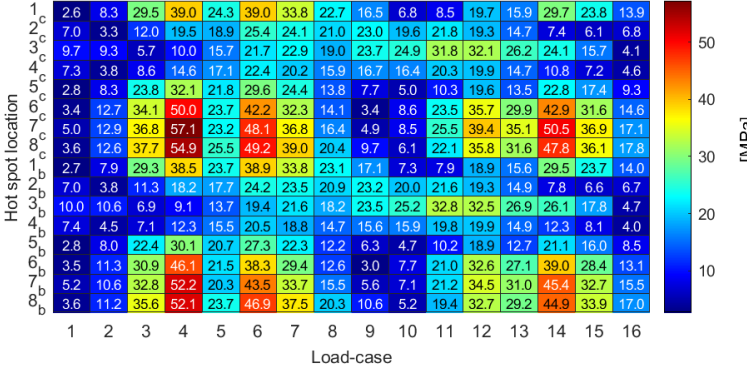




Details of fatigue assesment brace 1.3

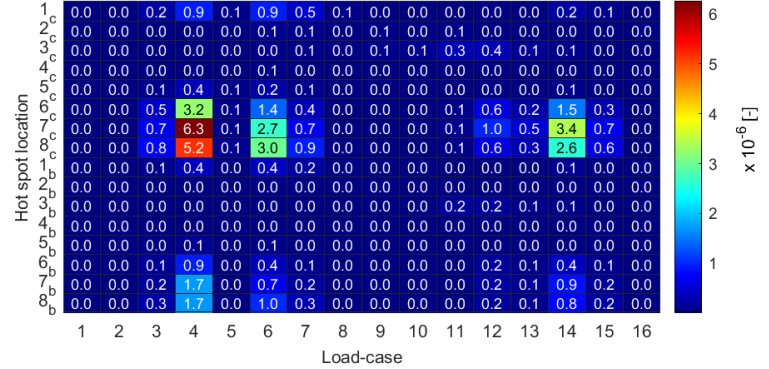
Stress range in hot spots

According to a model without LJF



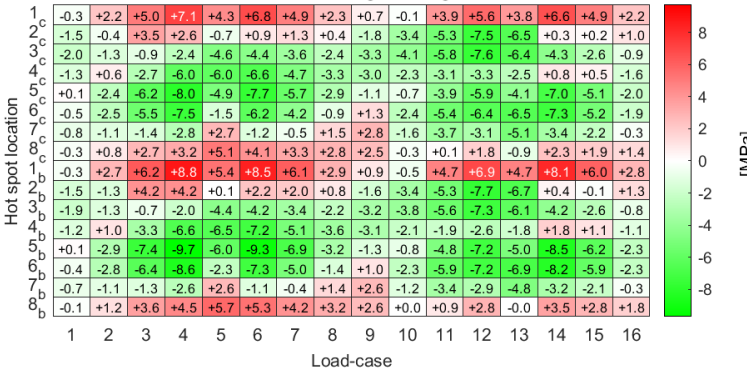
Accumulated fatigue damage in hot spots

According to a model without LJF



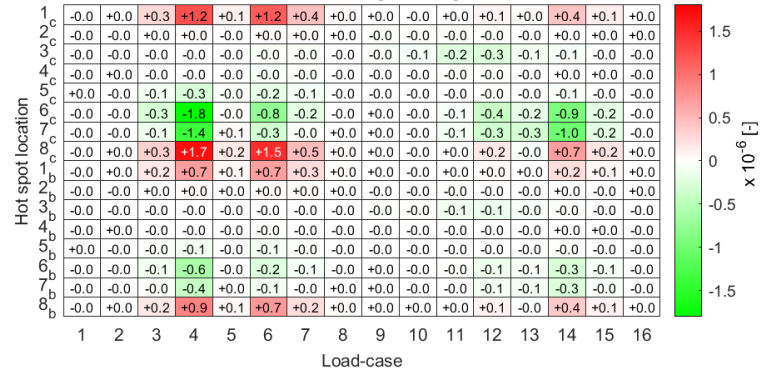
Absolute difference in hot spot stress range

As effect of modelling LJF in stinger



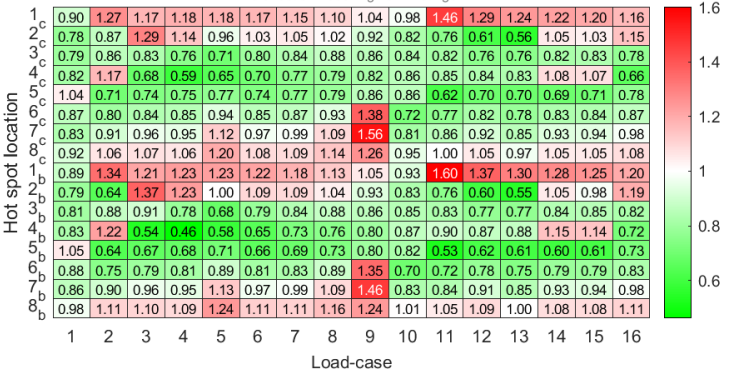
Absolute difference in accumulated fatigue damage

As effect of modelling LJF in stinger



Ratio with/without LJF of hot spot stress range

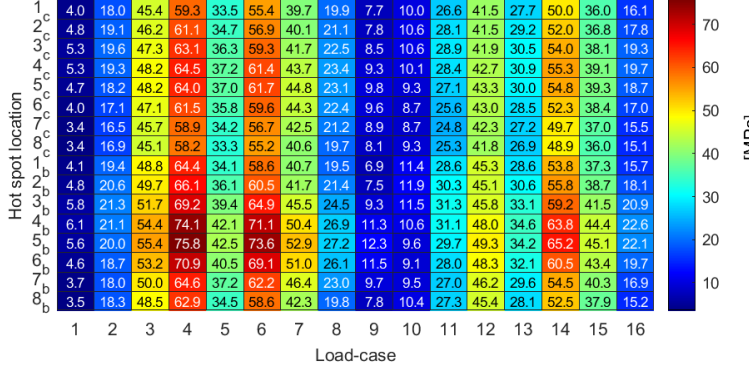
As effect of modelling LJF in stinger



Details of fatigue assessment brace 1.4

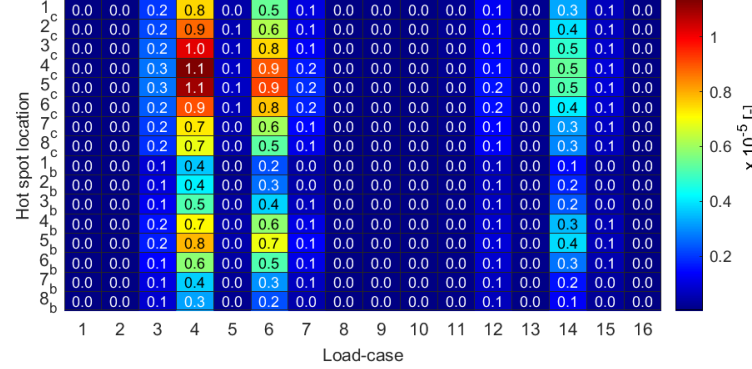
Stress range in hot spots

According to a model without LJF



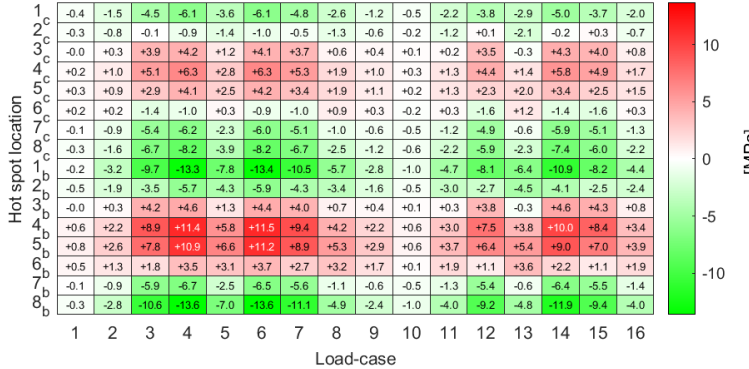
Accumulated fatigue damage in hot spots

According to a model without LJF



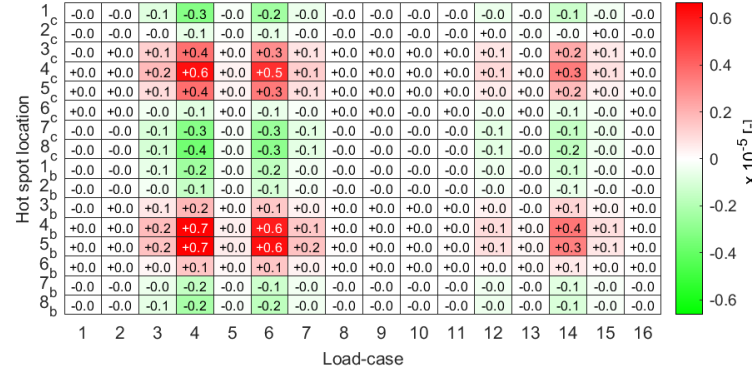
Absolute difference in hot spot stress range

As effect of modelling LJF in stinger



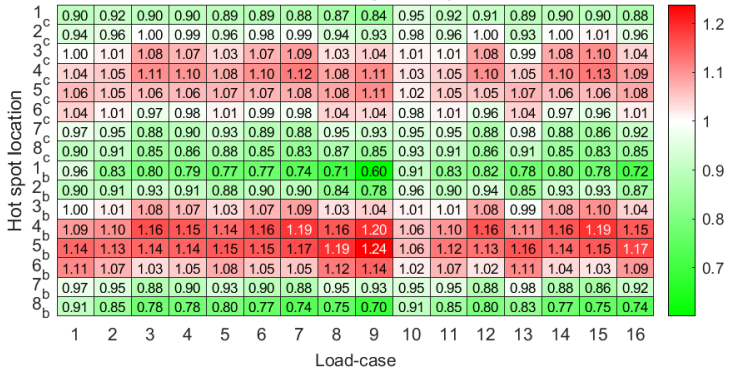
Absolute difference in accumulated fatigue damage

As effect of modelling LJF in stinger



Ratio with/without LJF of hot spot stress range

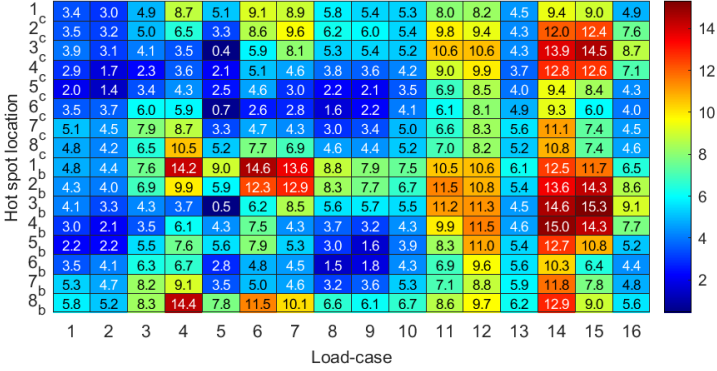
As effect of modelling LJF in stinger



Details of fatigue assesment brace 2.1

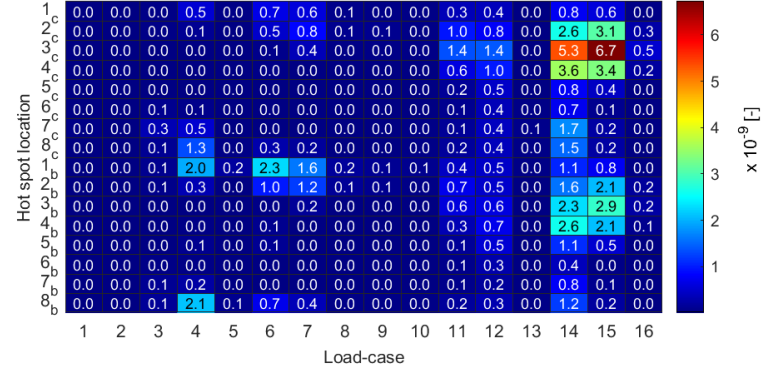
Stress range in hot spots

According to a model without LJF



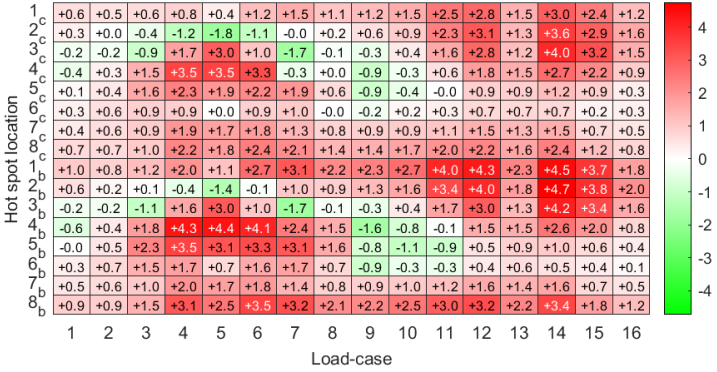
Accumulated fatigue damage in hot spots

According to a model without LJF



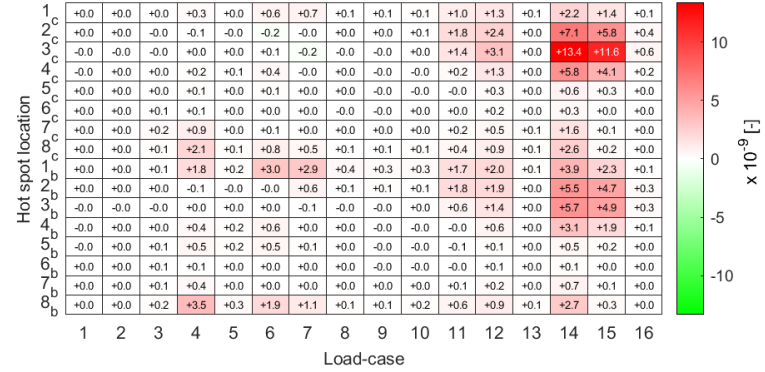
Absolute difference in hot spot stress range

As effect of modelling LJF in stinger



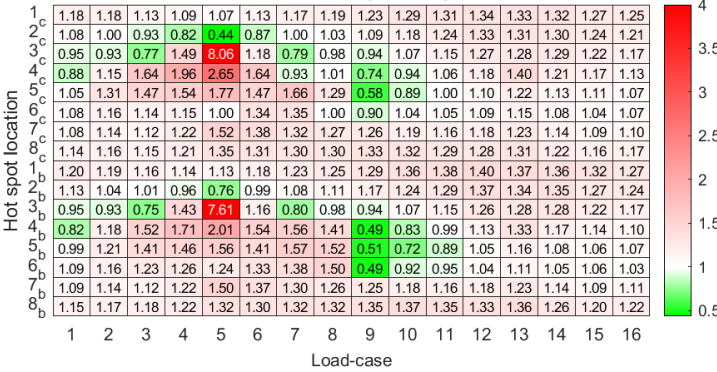
Absolute difference in accumulated fatigue damage

As effect of modelling LJF in stinger



Ratio with/without LJF of hot spot stress range

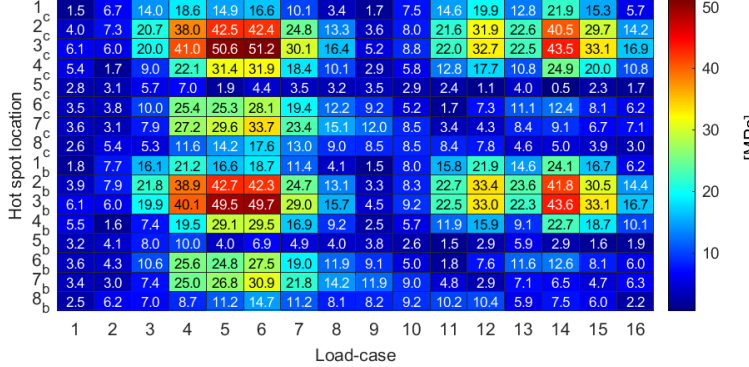
As effect of modelling LJF in stinger



Details of fatigue assessment brace 2.2

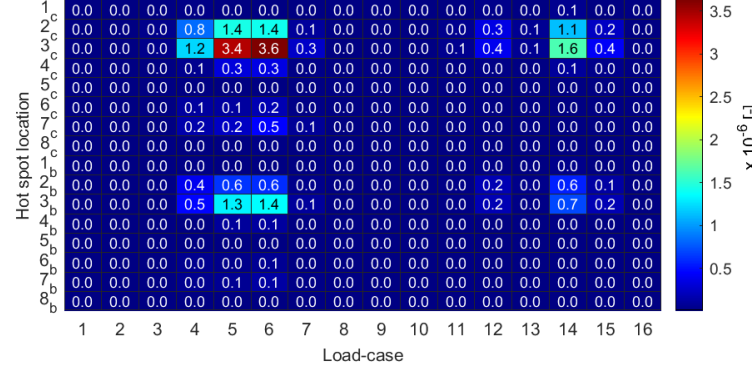
Stress range in hot spots

According to a model without LJF



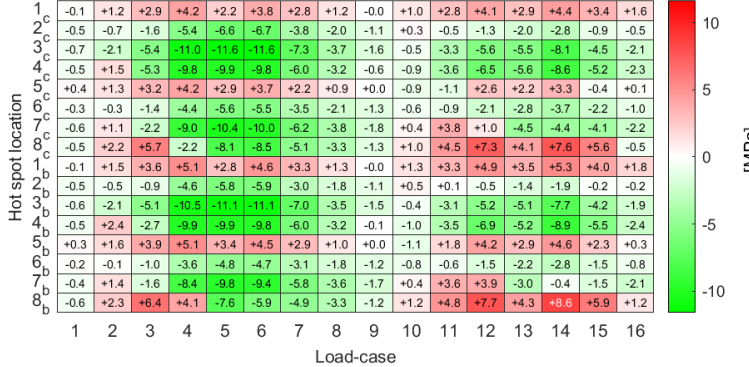
Accumulated fatigue damage in hot spots

According to a model without LJF



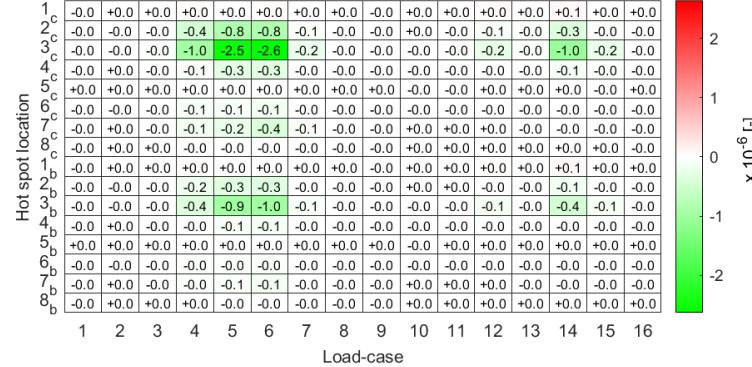
Absolute difference in hot spot stress range

As effect of modelling LJF in stinger



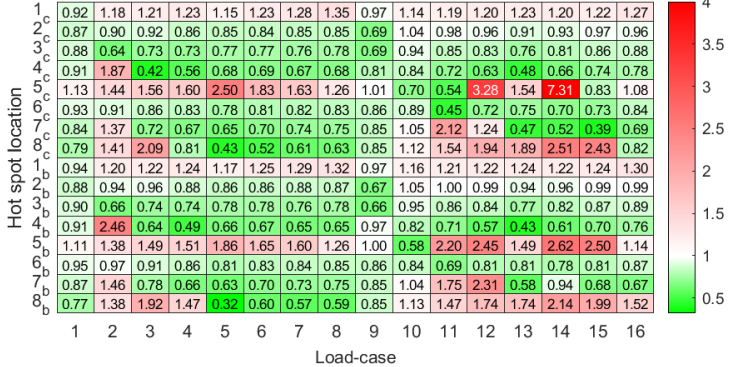
Absolute difference in accumulated fatigue damage

As effect of modelling LJF in stinger



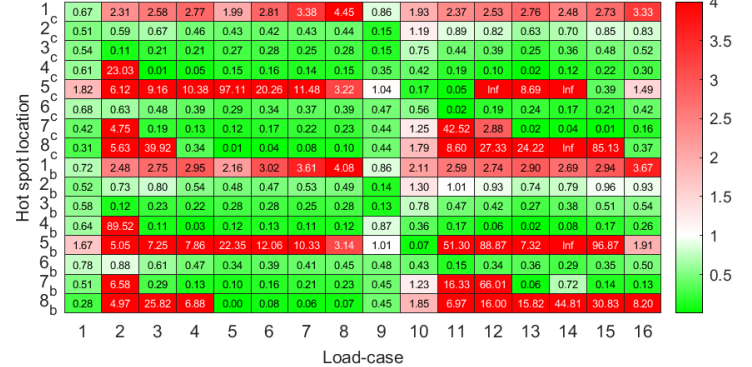
Ratio with/without LJF of hot spot stress range

As effect of modelling LJF in stinger



Ratio with/without LJF of accumulated fatigue damage

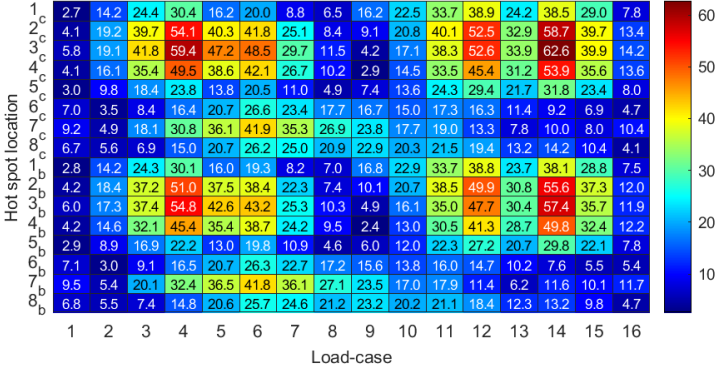
As effect of modelling LJF in stinger



Details of fatigue assessment brace 2.3

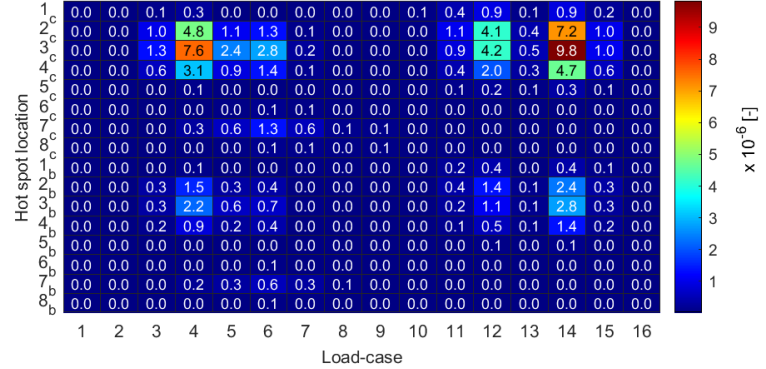
Stress range in hot spots

According to a model without LJF



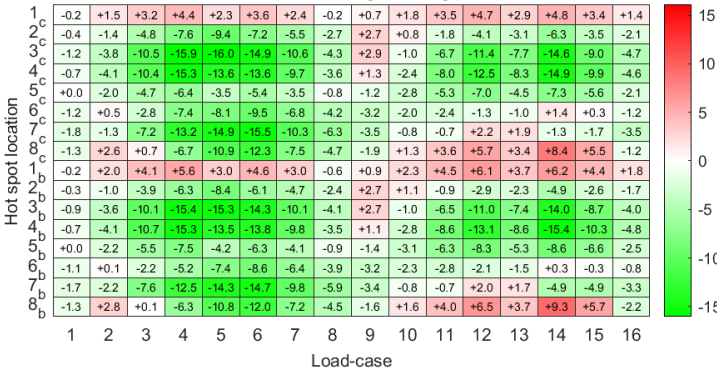
Accumulated fatigue damage in hot spots

According to a model without LJF



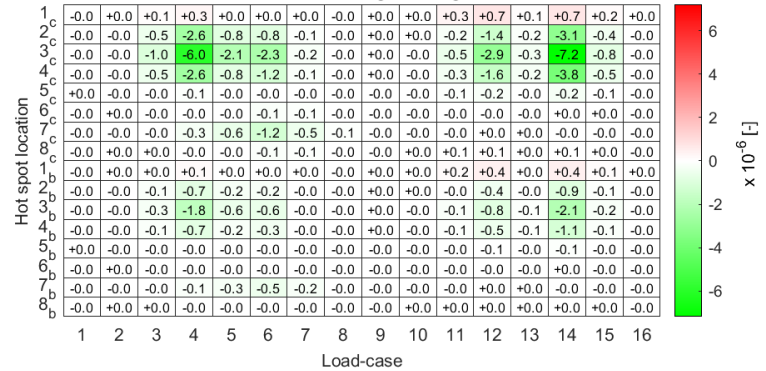
Absolute difference in hot spot stress range

As effect of modelling LJF in stinger



Absolute difference in accumulated fatigue damage

As effect of modelling LJF in stinger



Ratio with/without LMF of hot spot stress range

As effect of modelling LJF in stinger



Ratio with/without LMF of accumulated fatigue damage

As effect of modelling LJF in stinger

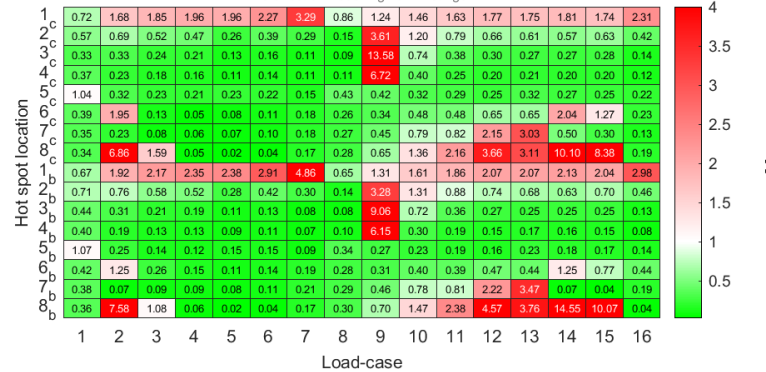
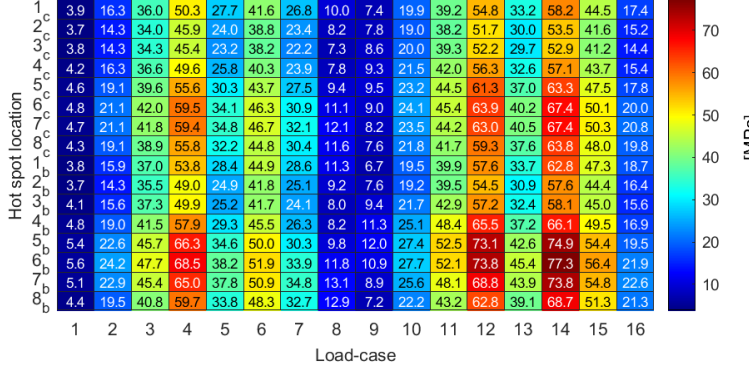


Figure L.29: Details of fatigue assessment brace 2.3

Details of fatigue assessment brace 2.4

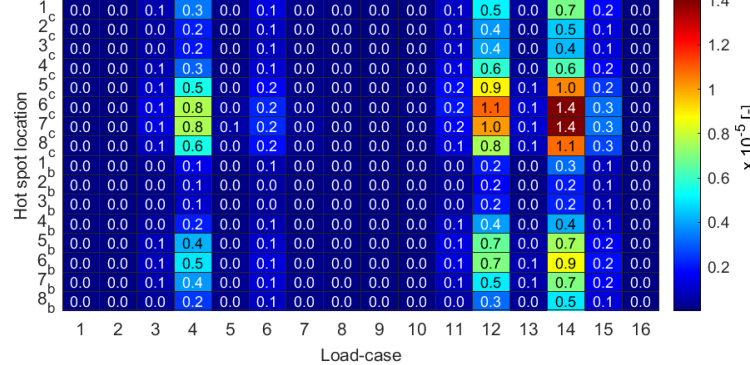
Stress range in hot spots

According to a model without LJJ



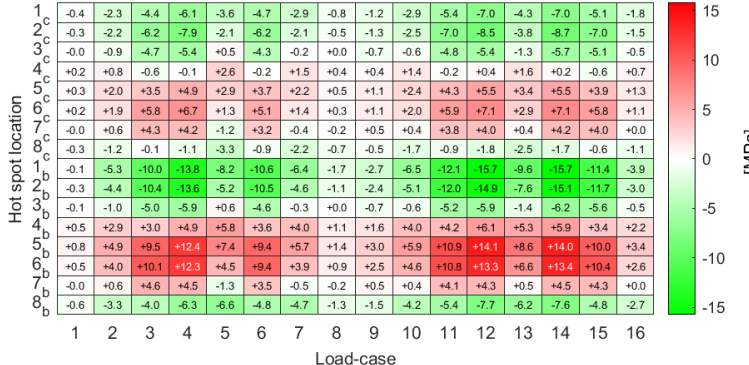
Accumulated fatigue damage in hot spots

According to a model without LJJ



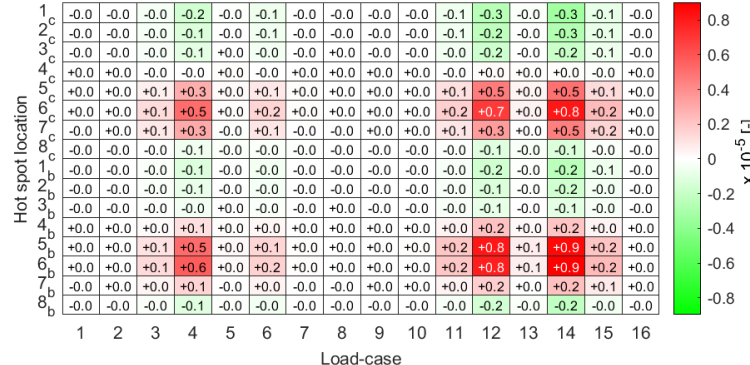
Absolute difference in hot spot stress range

As effect of modelling LJJ in stinger



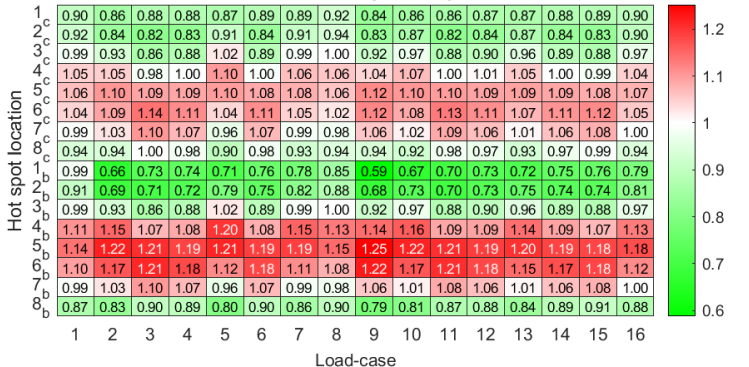
Absolute difference in accumulated fatigue damage

As effect of modelling LJJ in stinger



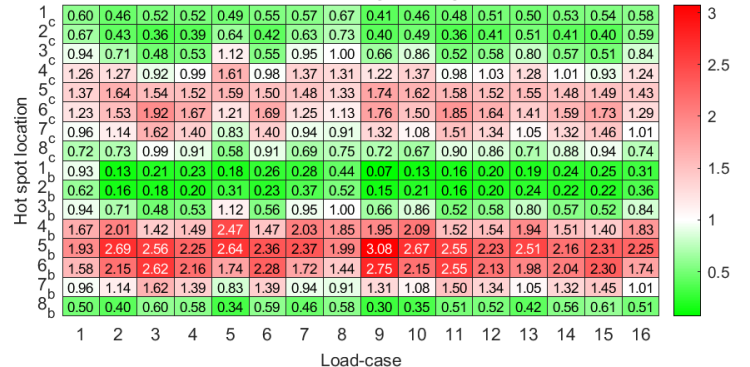
Ratio with/without LJJ of hot spot stress range

As effect of modelling LJJ in stinger



Ratio with/without LJJ of accumulated fatigue damage

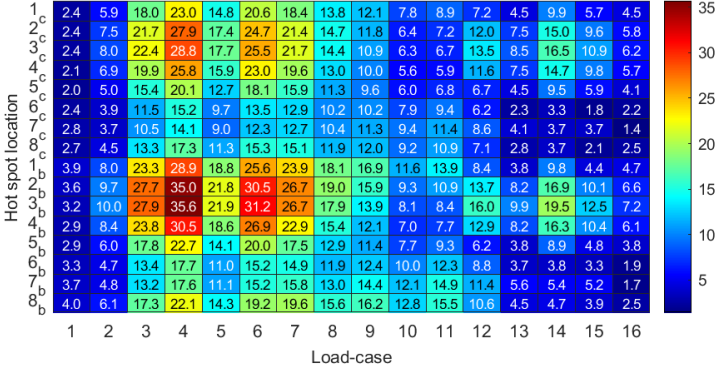
As effect of modelling LJJ in stinger



Details of fatigue assesment brace 3.1

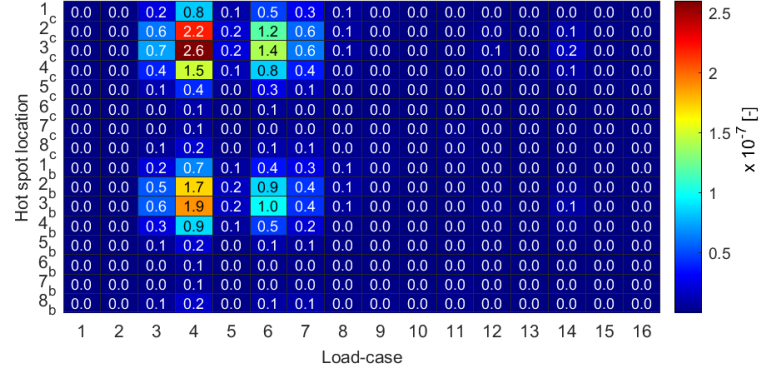
Stress range in hot spots

According to a model without LJF



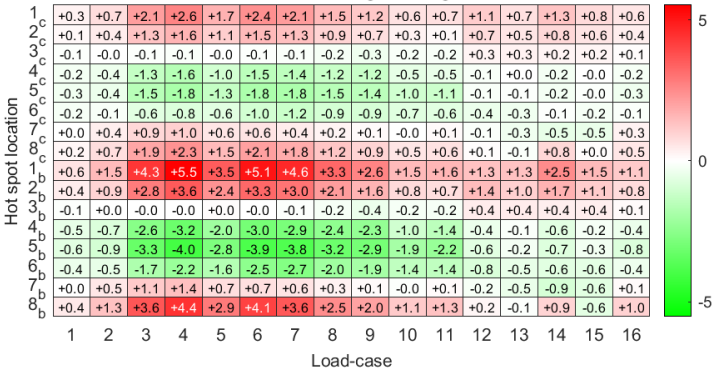
Accumulated fatigue damage in hot spots

According to a model without LJF



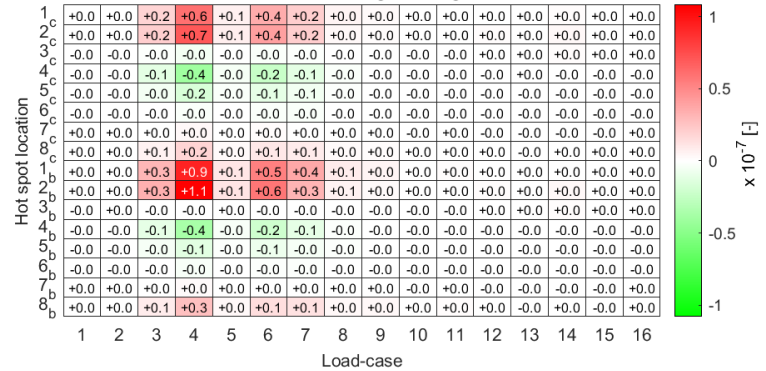
Absolute difference in hot spot stress range

As effect of modelling LJF in stinger



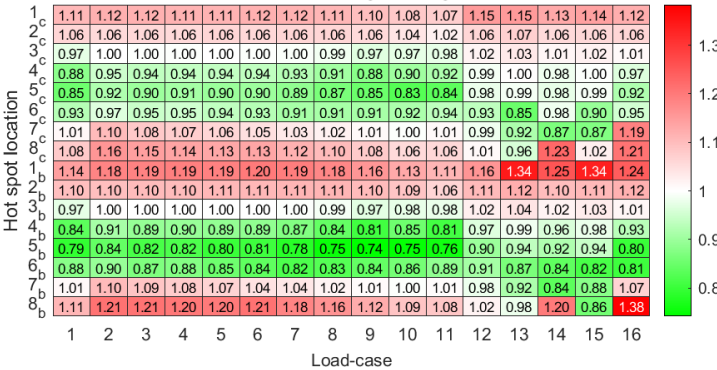
Absolute difference in accumulated fatigue damage

As effect of modelling LJF in stinger



Ratio with/without LJJF of hot spot stress range

As effect of modelling LJF in stinger



Ratio with/without LJJF of accumulated fatigue damage

As effect of modelling LJF in stinger

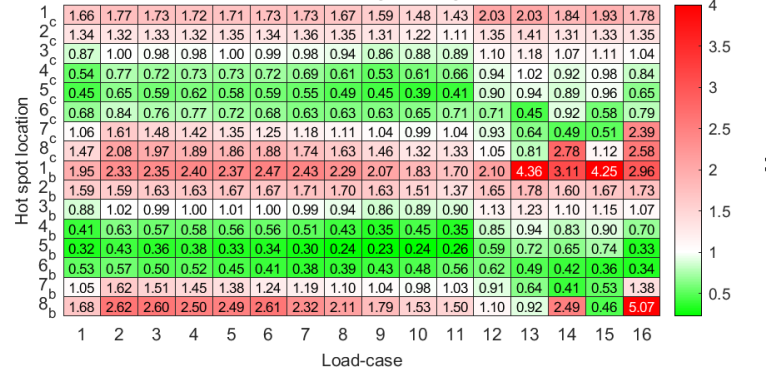
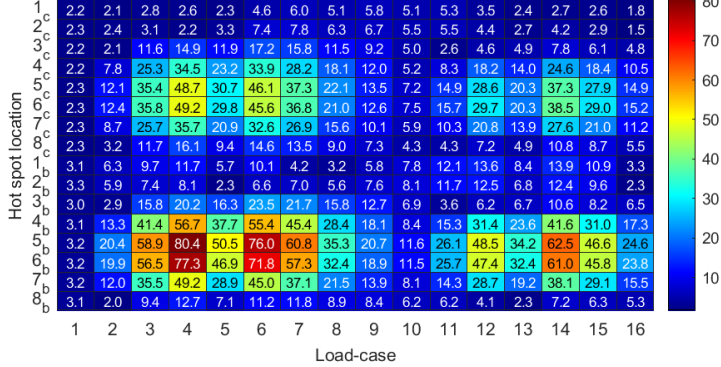


Figure L.31: Details of fatigue assesment brace 3.1

Details of fatigue assessment brace 3.2

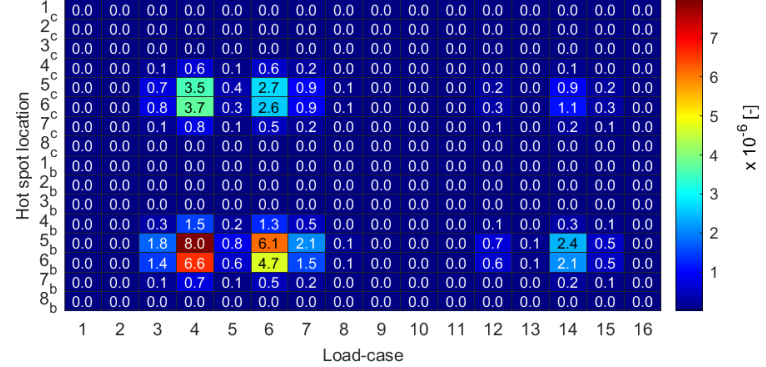
Stress range in hot spots

According to a model without LJF



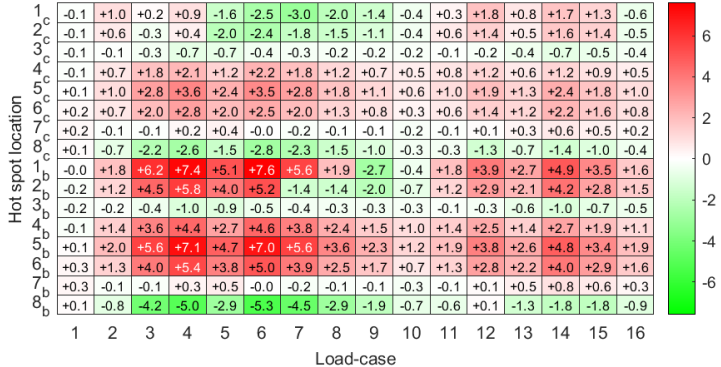
Accumulated fatigue damage in hot spots

According to a model without LJF



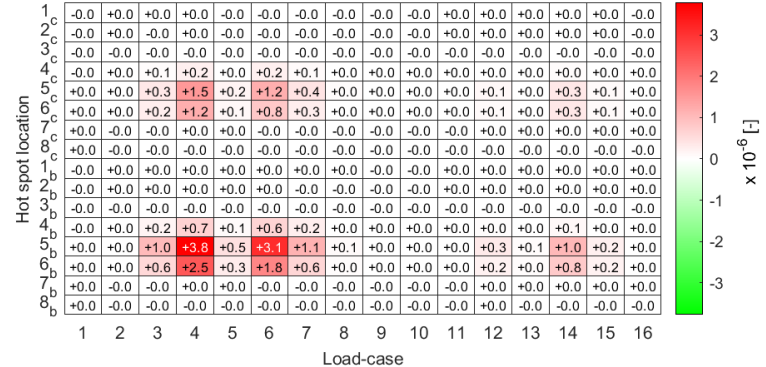
Absolute difference in hot spot stress range

As effect of modelling LJF in stinger



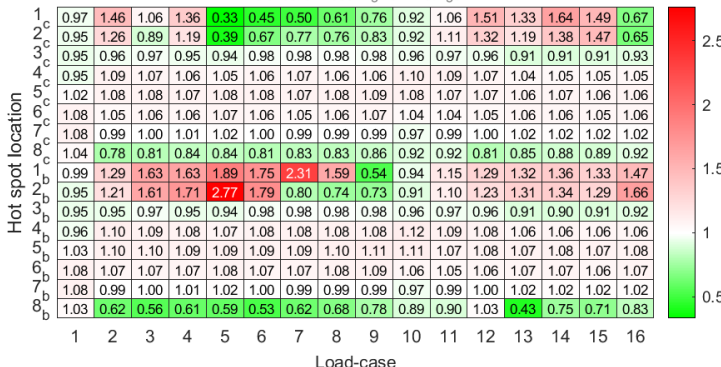
Absolute difference in accumulated fatigue damage

As effect of modelling LJF in stinger



Ratio with/without LJF of hot spot stress range

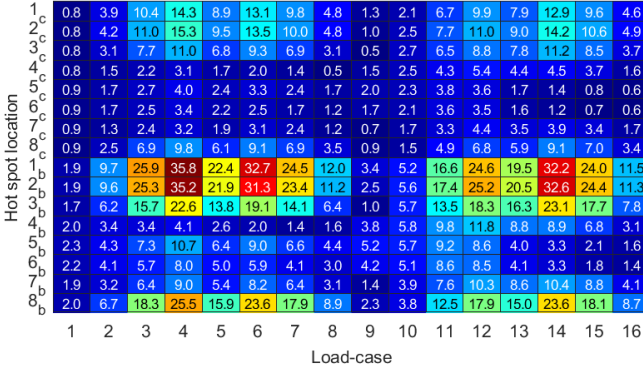
As effect of modelling LJF in stinger



Details of fatigue assesment brace 3.3

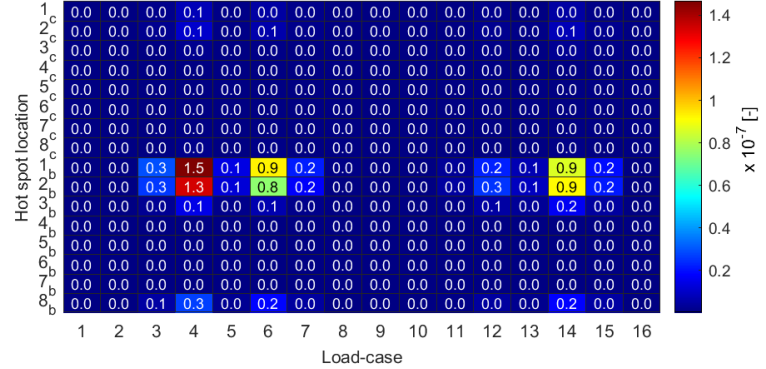
Stress range in hot spots

According to a model without LJF



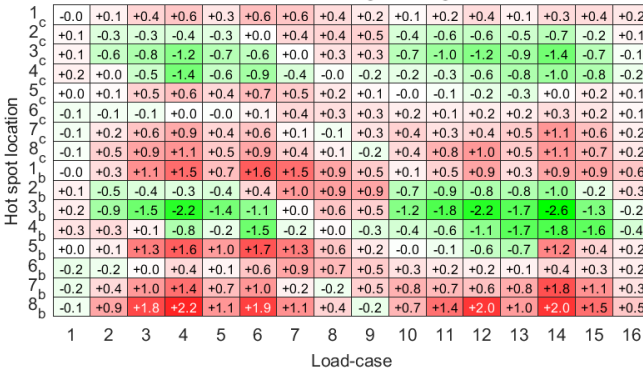
Accumulated fatigue damage in hot spots

According to a model without LJF



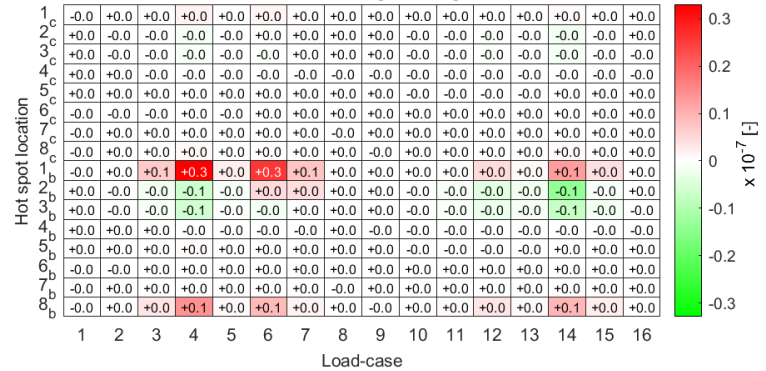
Absolute difference in hot spot stress range

As effect of modelling LJF in stinger



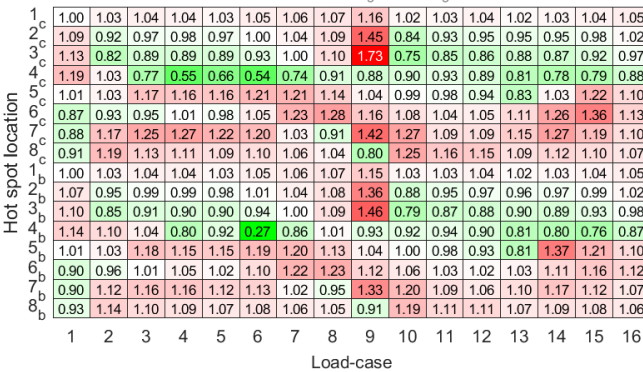
Absolute difference in accumulated fatigue damage

As effect of modelling LJF in stinger



Ratio with/without LJF of hot spot stress range

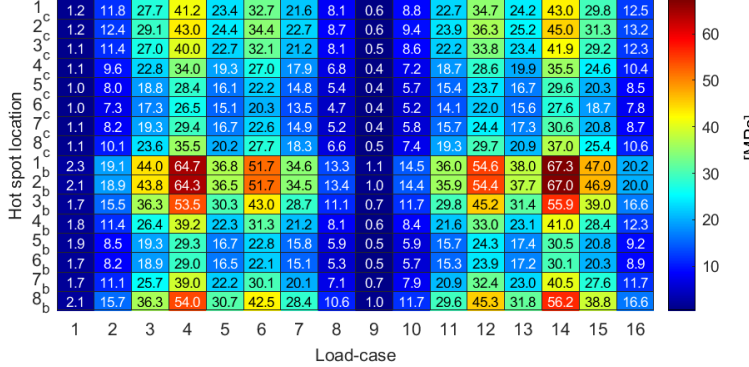
As effect of modelling LJF in stinger



Details of fatigue assesment brace 3.4

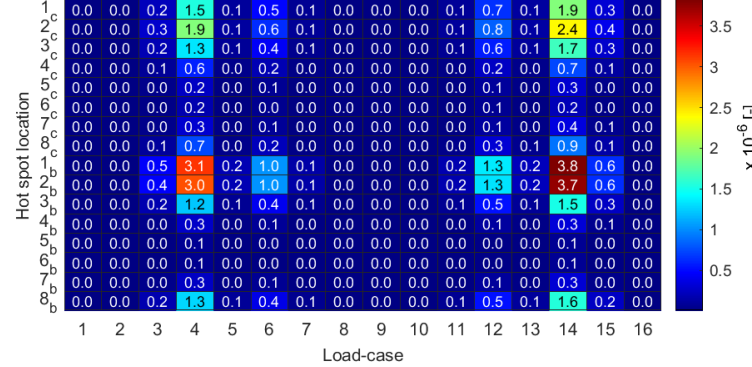
Stress range in hot spots

According to a model without LJF



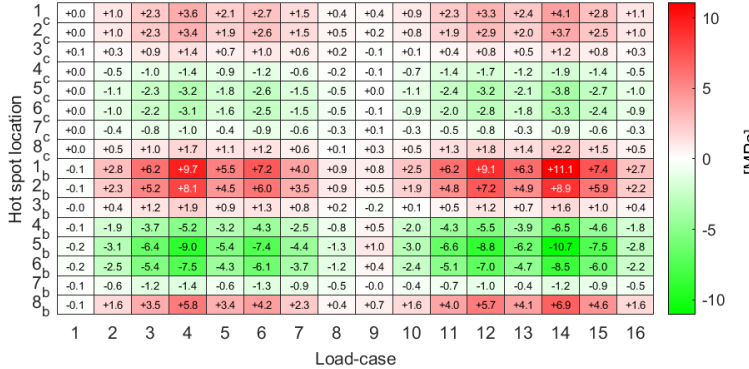
Accumulated fatigue damage in hot spots

According to a model without LJF



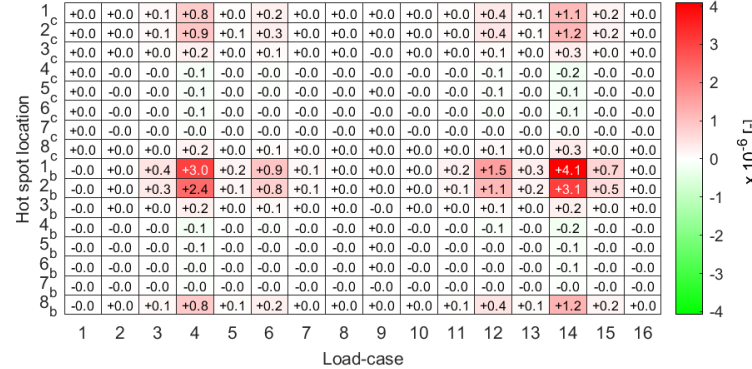
Absolute difference in hot spot stress range

As effect of modelling LJF in stinger



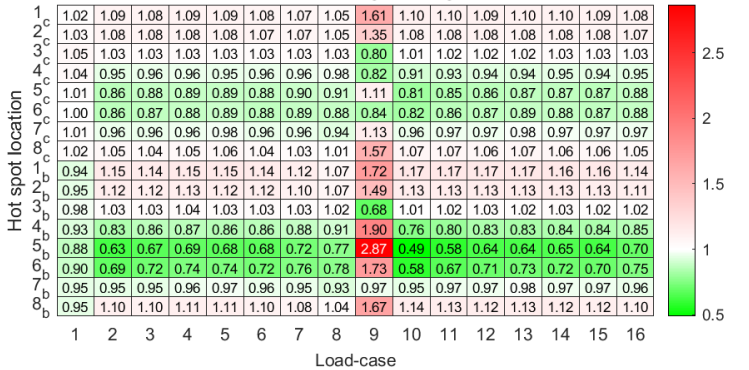
Absolute difference in accumulated fatigue damage

As effect of modelling LJF in stinger



Ratio with/without LJF of hot spot stress range

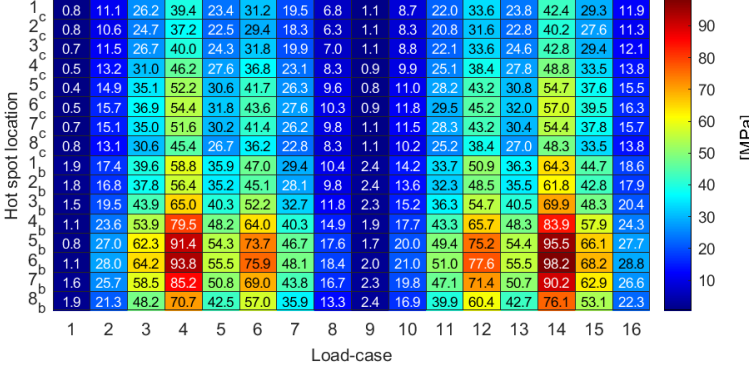
As effect of modelling LJF in stinger



Details of fatigue assesment brace 3.5

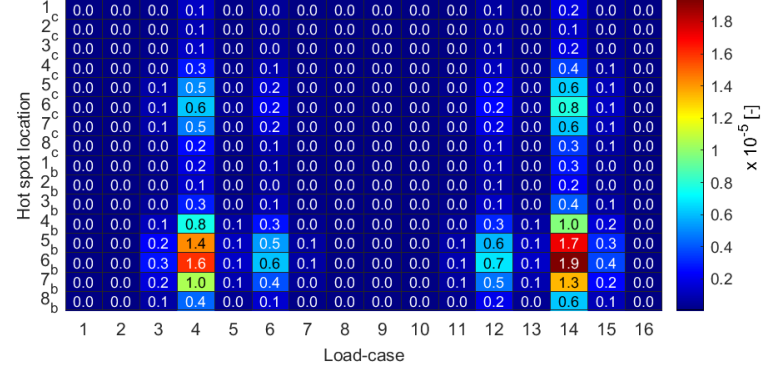
Stress range in hot spots

According to a model without LJF



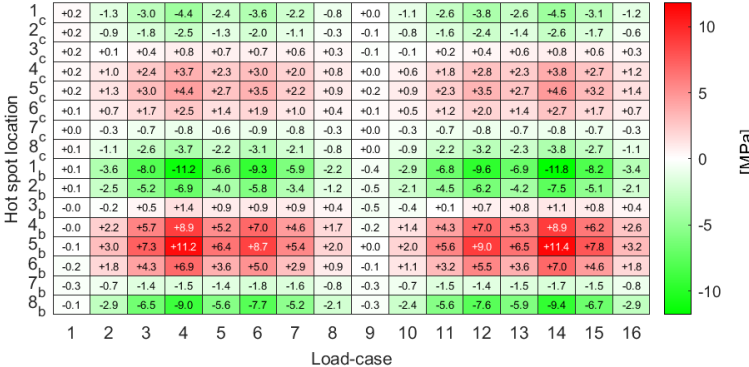
Accumulated fatigue damage in hot spots

According to a model without LJF



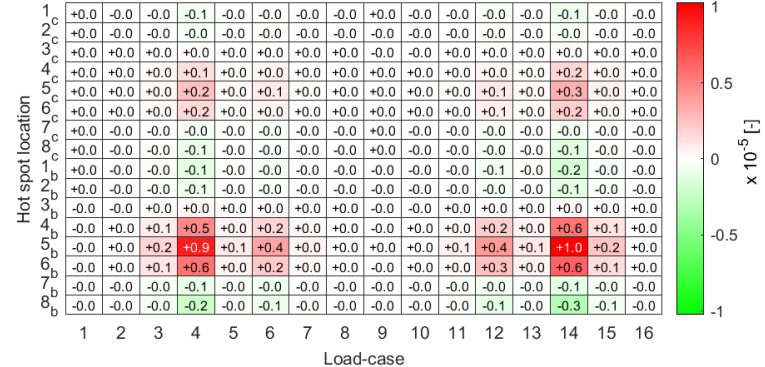
Absolute difference in hot spot stress range

As effect of modelling LJF in stinger



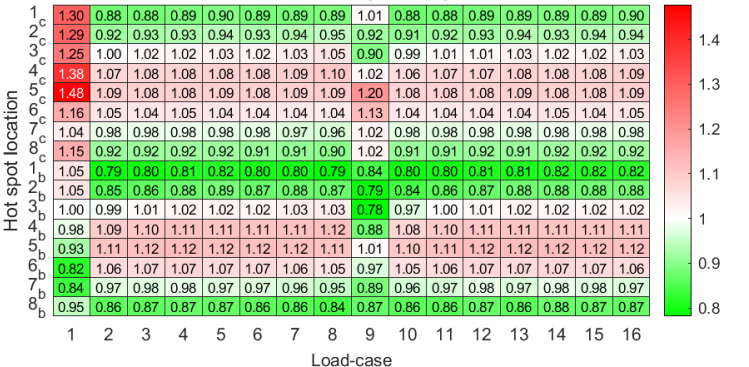
Absolute difference in accumulated fatigue damage

As effect of modelling LJF in stinger



Ratio with/without LJF of hot spot stress range

As effect of modelling LJF in stinger

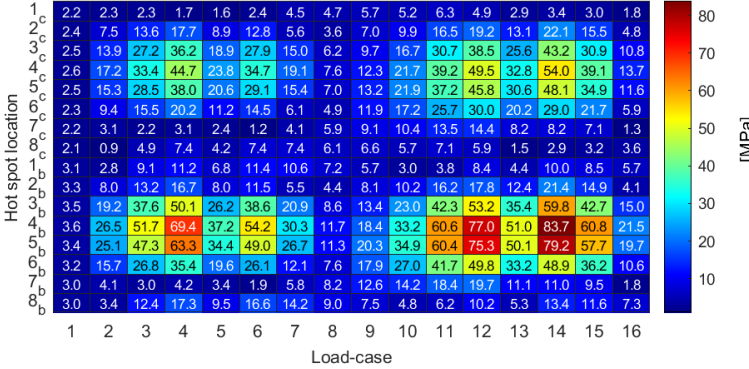




Details of fatigue assessment brace 4.2

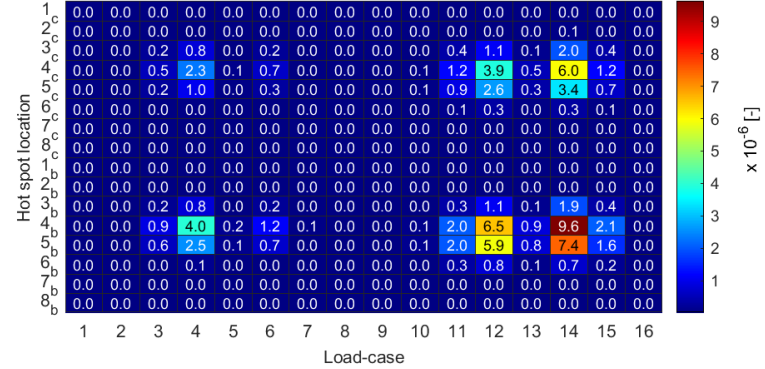
Stress range in hot spots

According to a model without LJF



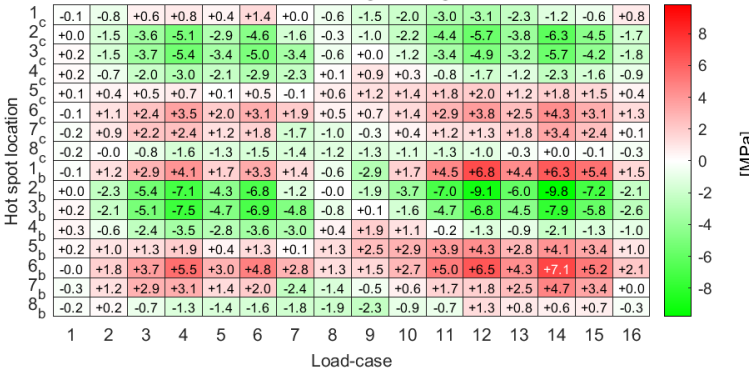
Accumulated fatigue damage in hot spots

According to a model without LJF



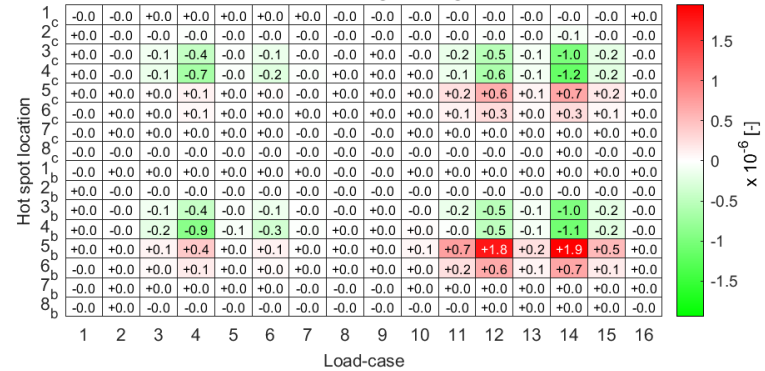
Absolute difference in hot spot stress range

As effect of modelling LJF in stinger



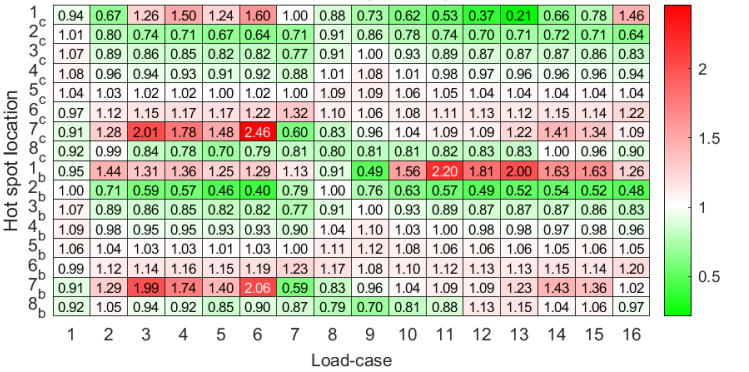
Absolute difference in accumulated fatigue damage

As effect of modelling LJF in stinger



Ratio with/without LJF of hot spot stress range

As effect of modelling LJF in stinger



Ratio with/without LJF of accumulated fatigue damage

As effect of modelling LJF in stinger

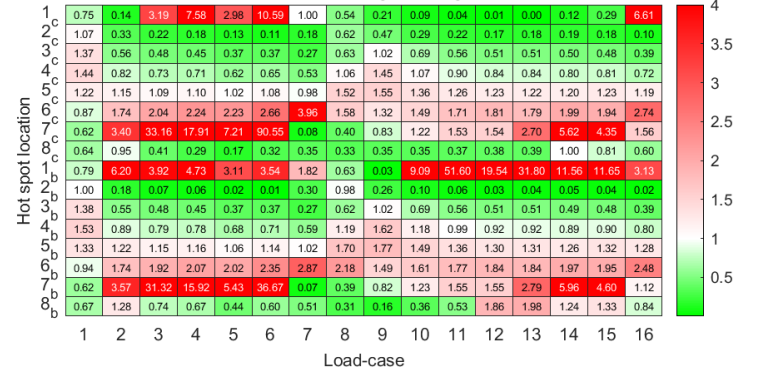
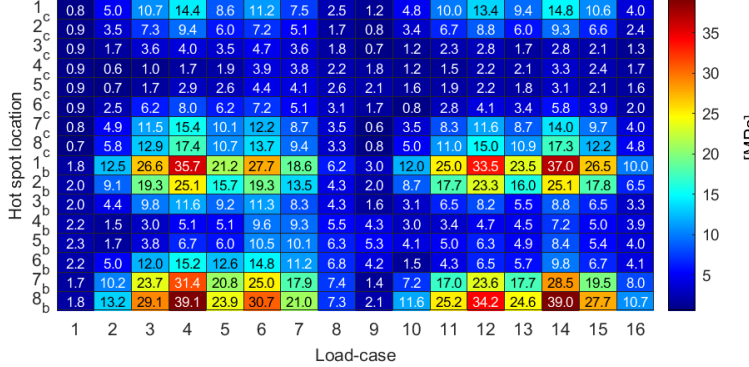


Figure L.37: Details of fatigue assessment brace 4.2

Details of fatigue assesment brace 4.3

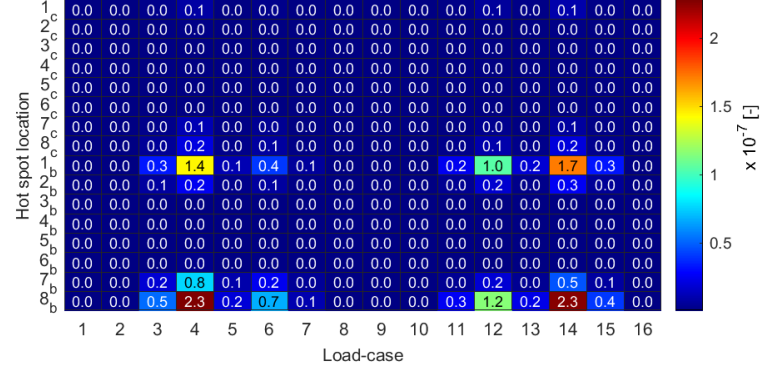
Stress range in hot spots

According to a model without LJF



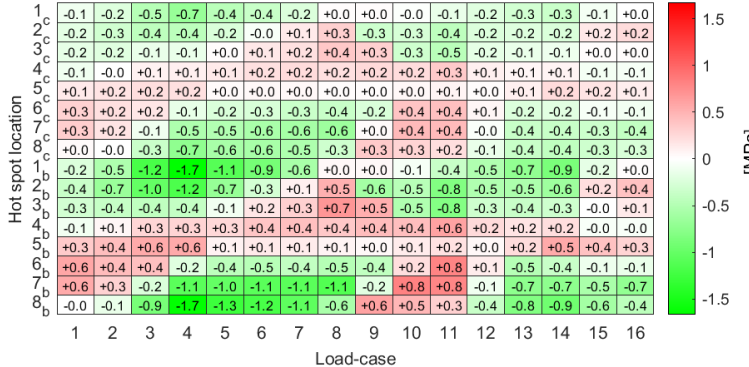
Accumulated fatigue damage in hot spots

According to a model without LJF



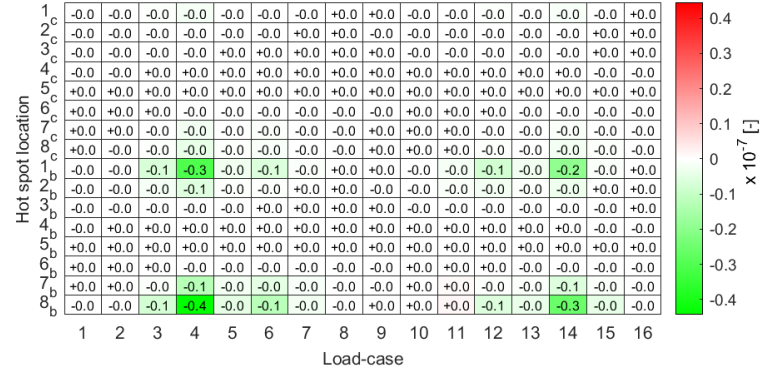
Absolute difference in hot spot stress range

As effect of modelling LJF in stinger



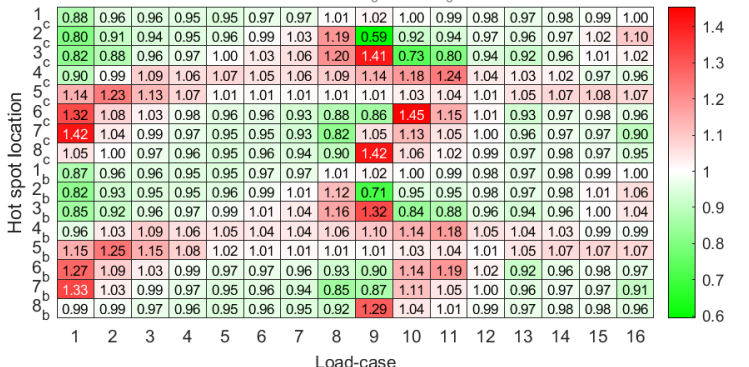
Absolute difference in accumulated fatigue damage

As effect of modelling LJF in stinger



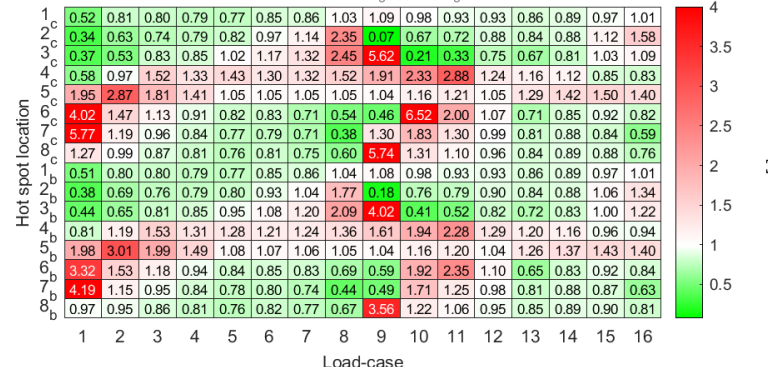
Ratio with/without LJF of hot spot stress range

As effect of modelling LJF in stinger



Ratio with/without LJF of accumulated fatigue damage

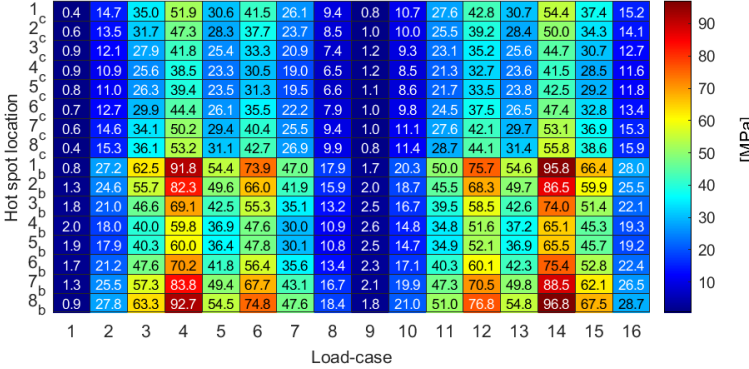
As effect of modelling LJF in stinger



Details of fatigue assesment brace 4.4

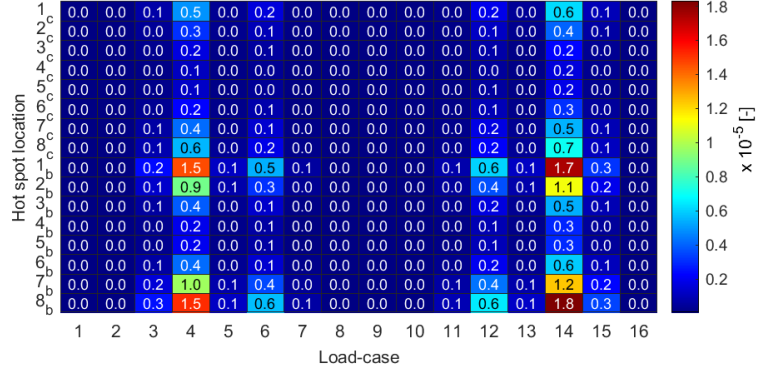
Stress range in hot spots

According to a model without LJF



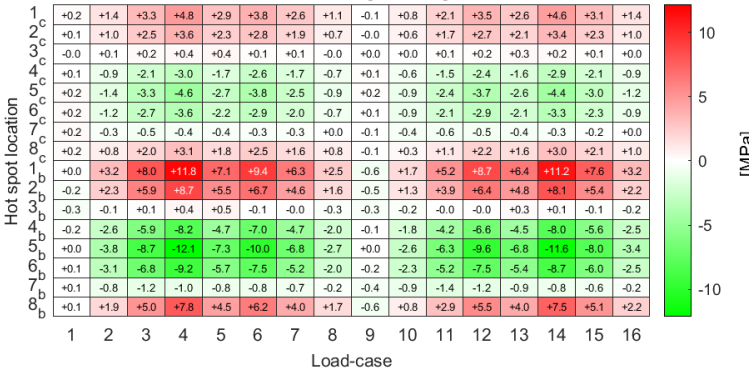
Accumulated fatigue damage in hot spots

According to a model without LJF



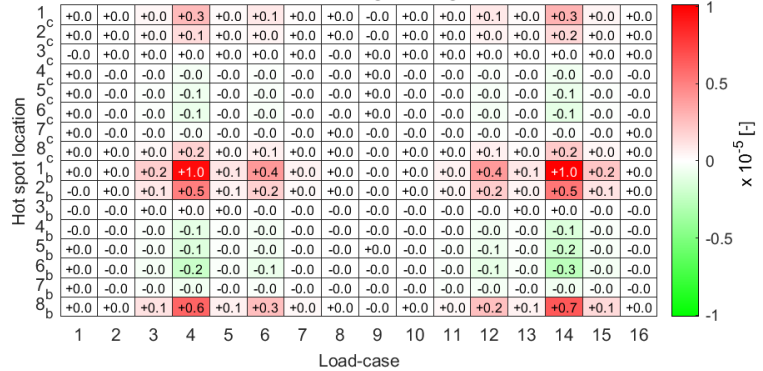
Absolute difference in hot spot stress range

As effect of modelling LJF in stinger



Absolute difference in accumulated fatigue damage

As effect of modelling LJF in stinger



Ratio with/without LJF of hot spot stress range

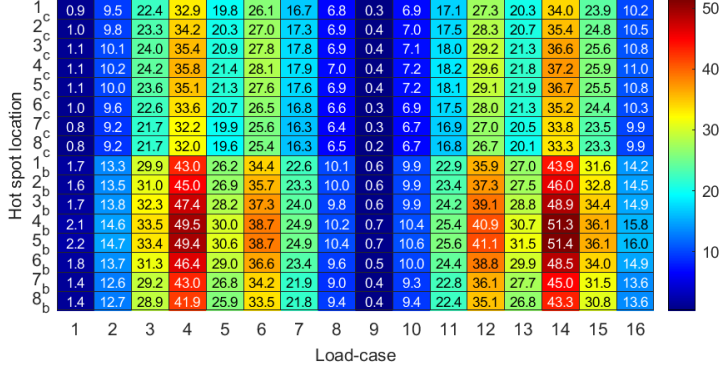
As effect of modelling LJF in stinger



Details of fatigue assessment brace 4.5

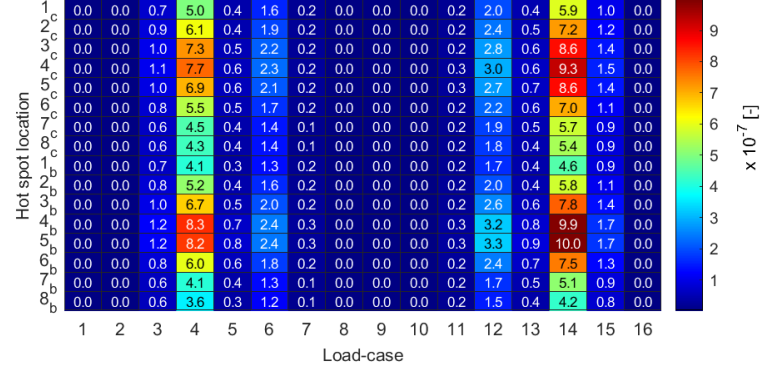
Stress range in hot spots

According to a model without LJF



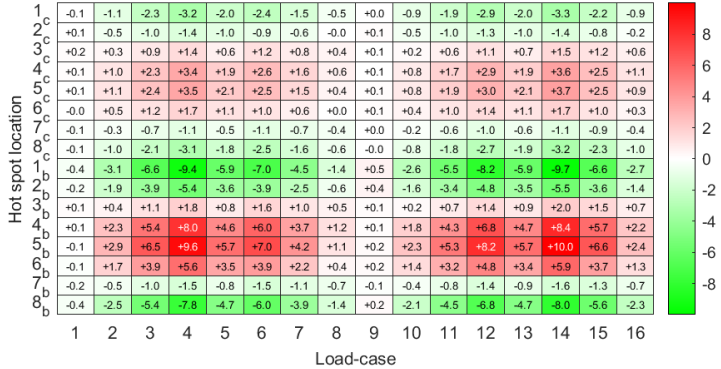
Accumulated fatigue damage in hot spots

According to a model without LJF



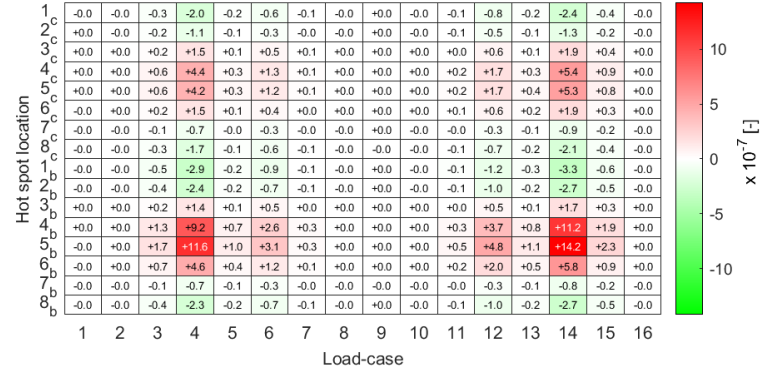
Absolute difference in hot spot stress range

As effect of modelling LJF in stinger



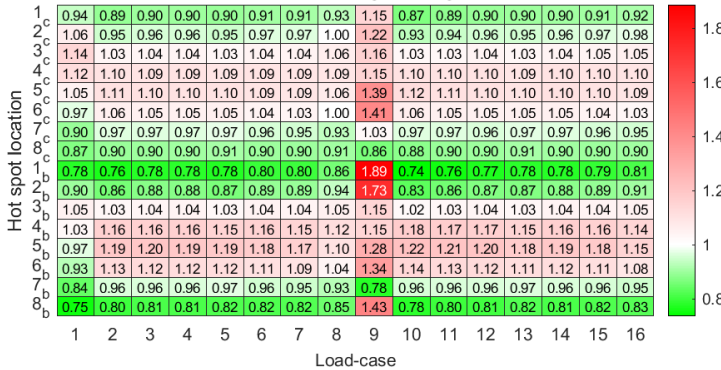
Absolute difference in accumulated fatigue damage

As effect of modelling LJF in stinger



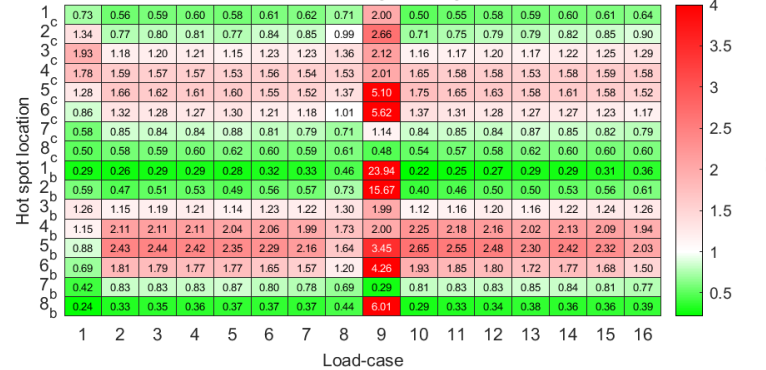
Ratio with/without LJF of hot spot stress range

As effect of modelling LJF in stinger



Ratio with/without LJF of accumulated fatigue damage

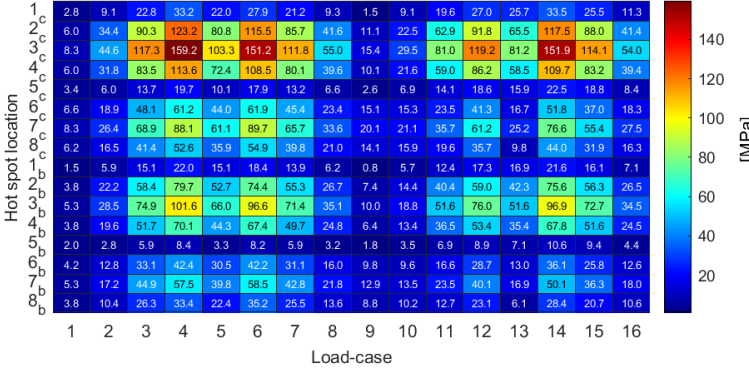
As effect of modelling LJF in stinger



Details of fatigue assesment brace 5.1

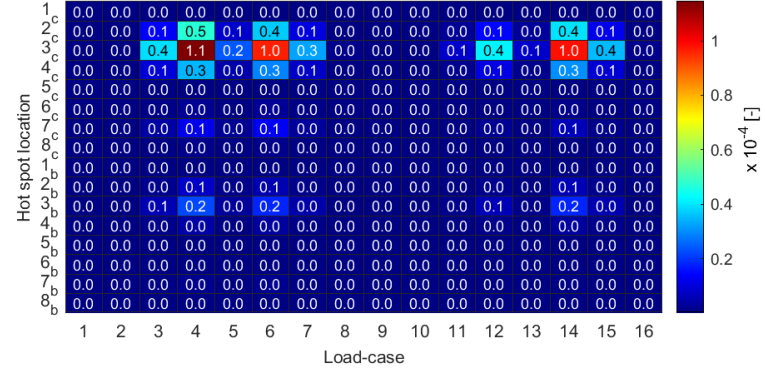
Stress range in hot spots

According to a model without LJF



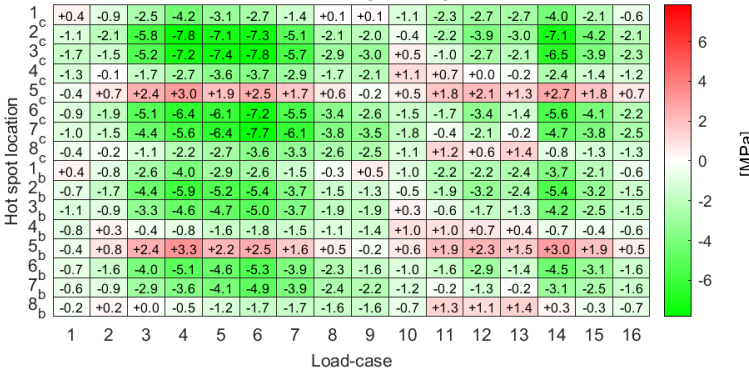
Accumulated fatigue damage in hot spots

According to a model without LJF



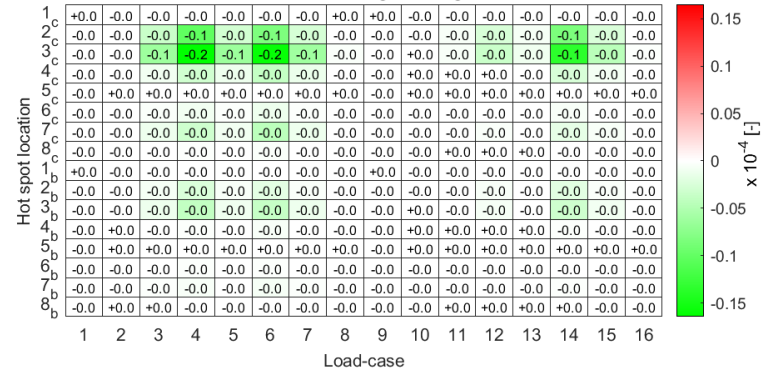
Absolute difference in hot spot stress range

As effect of modelling LJF in stinger



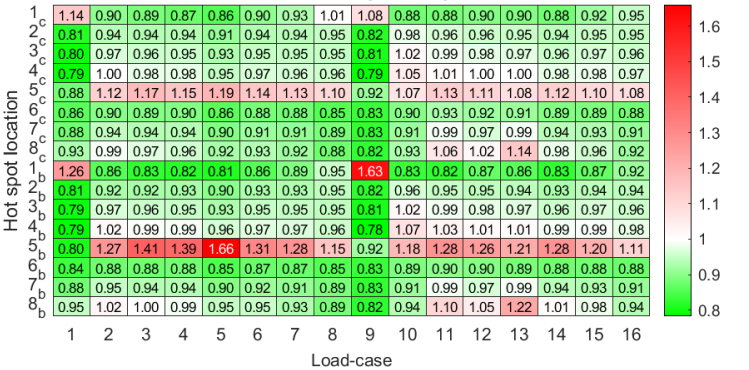
Absolute difference in accumulated fatigue damage

As effect of modelling LJF in stinger



Ratio with/without LJF of hot spot stress range

As effect of modelling LJF in stinger



Ratio with/without LJF of accumulated fatigue damage

As effect of modelling LJF in stinger

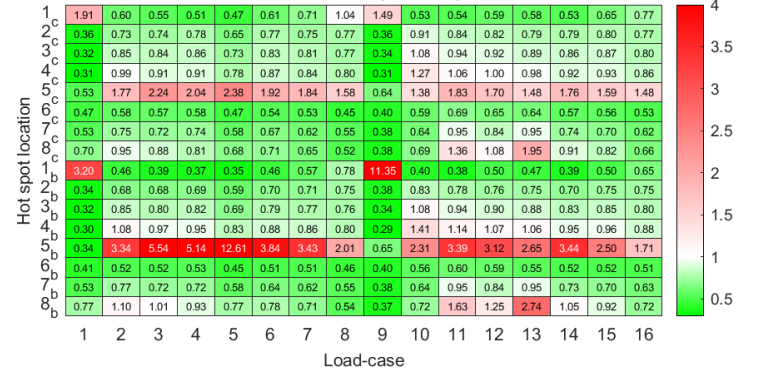


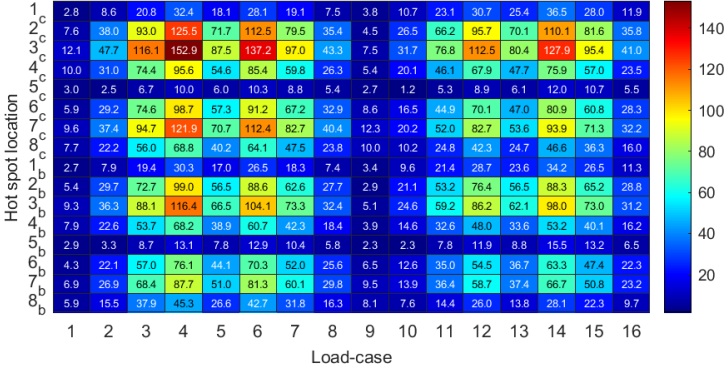
Figure L.41: Details of fatigue assesment brace 5.1



Details of fatigue assesment brace 6.1

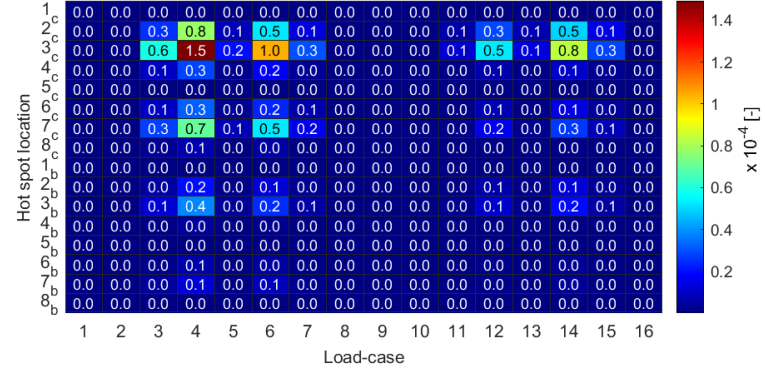
Stress range in hot spots

According to a model without LJF



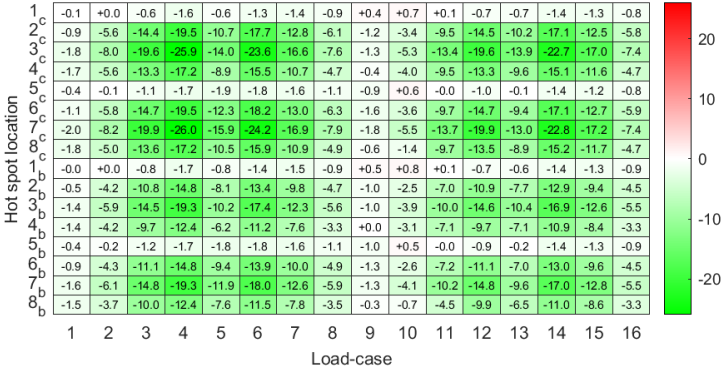
Accumulated fatigue damage in hot spots

According to a model without LJF



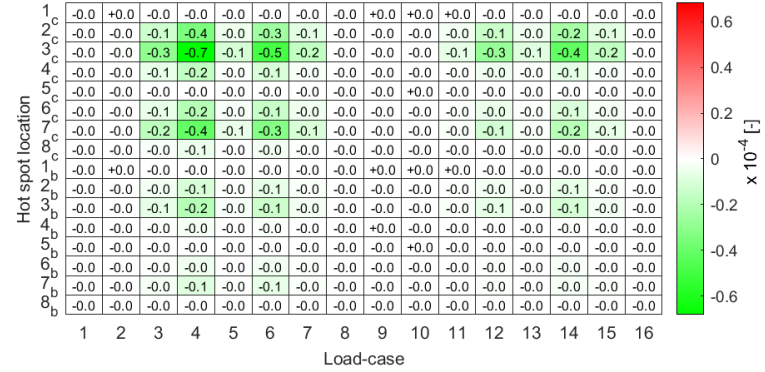
Absolute difference in hot spot stress range

As effect of modelling LJF in stinger



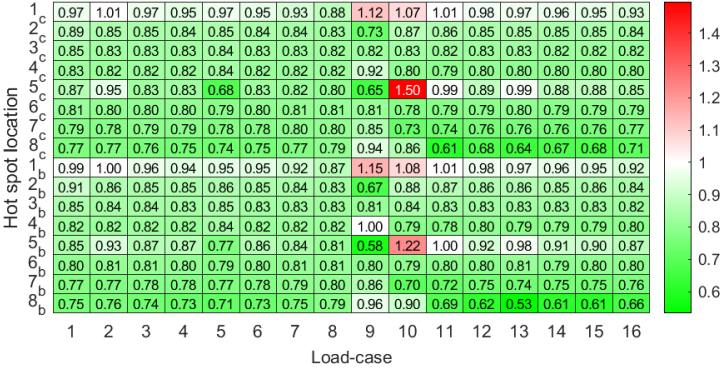
Absolute difference in accumulated fatigue damage

As effect of modelling LJF in stinger



Ratio with/without LJF of hot spot stress range

As effect of modelling LJF in stinger







# Chord wall displacements for single-brace model verification

## M.1. Chord wall displacements of joint 1

In this section the chord wall displacements of joint 1, discussed in section 4.3.1 are presented.

Table M.1: Joint 1: Chord wall displacements  $\kappa_{p,j}$  of point  $p$  as effect of unit-load  $P_j$

Unit-load $P_j$	Displacement $\kappa_{p,j}$ of point $p$ [mm]							
	1	2	3	4	5	6	7	8
1	-7.90e-01	-7.13e-01	-7.90e-01	-7.13e-01	-4.79e-01	-4.94e-01	-4.79e-01	-4.94e-01
2	4.06e-08	-1.27e-01	2.73e-06	1.27e-01	-5.51e-02	-5.92e-02	5.51e-02	5.92e-02
3	4.68e-02	4.23e-07	-4.68e-02	-4.18e-07	2.75e-03	-2.04e-07	-2.75e-03	-4.02e-07

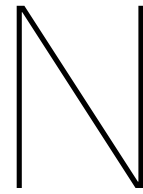
## M.2. Chord wall displacements of joint 2

In this section the chord wall displacements of joint 2, discussed in section 4.3.1 are presented.

Table M.2: Joint 2: Chord wall displacements  $\kappa_{p,j}$  of point  $p$  as effect of unit-load  $P_j$

Unit-load $P_j$	Displacement $\kappa_{p,j}$ of point $p$ [mm]							
	1	2	3	4	5	6	7	8
1	-6.52e-01	-5.55e-01	-6.08e-01	-5.55e-01	-3.91e-01	-3.98e-01	-3.68e-01	-3.98e-01
2	3.00e-06	-9.43e-02	9.32e-07	9.43e-02	-4.33e-02	-4.59e-02	3.85e-02	4.59e-02
3	3.15e-02	-6.79e-04	-5.65e-02	-6.76e-04	2.57e-04	-2.71e-03	-6.77e-03	-2.71e-03





## Flexibilities of braces in numerical test case

This appendix contains the 'main' flexibilities of the 7 joints / 22 braces of interest, discussed in the numerical test case of chapter 6. The flexibilities are presented in table N.1. The geometric properties are presented in confidential appendix P

Table N.1: The flexibilities of the 7 joints / 22 braces of interest, discussed in the numerical test case of chapter 6.

Joint	Brace	$f_{11}^* [-]$			$f_{22}^* [-]$			$f_{33}^* [-]$		
		Brace extension element	LJF	Ratio LJF/Brace extension element	Brace extension element	LJF	Ratio LJF/Brace extension element	Brace extension element	LJF	Ratio LJF/Brace extension element
1	1	9.7	23.7	2.44	238.1	359.1	1.51	238.1	246.6	1.04
	2	10.7	53.5	4.99	302.1	947.2	3.14	302.1	496.1	1.64
	3	10.7	53.6	5.00	302.1	953.5	3.16	302.1	495.9	1.64
	4	22.0	20.1	0.92	605.5	332.6	0.55	605.5	251.7	0.42
2	1	16.8	25.5	1.52	388.5	382.7	0.99	388.5	269.2	0.69
	2	10.7	54.1	5.05	302.1	959.8	3.18	302.1	502.4	1.66
	3	10.7	54.3	5.06	302.1	957.5	3.17	302.1	501.6	1.66
	4	22.0	20.2	0.92	605.5	333.1	0.55	605.5	253.3	0.42
3	1	21.6	37.3	1.73	746.3	652.7	0.87	746.3	420.7	0.56
	2	20.9	61.6	2.95	712.3	1079.8	1.52	712.3	593.4	0.83
	3	41.8	106.9	2.56	3527.9	2465.6	0.70	3527.9	1495.0	0.42
	4	31.5	31.5	1.00	1342.3	599.9	0.45	1342.3	431.5	0.32
	5	41.7	101.7	2.44	3523.1	2445.4	0.69	3523.1	1448.4	0.41
4	1	21.6	37.6	1.74	746.3	655.3	0.88	746.3	423.9	0.57
	2	20.9	61.5	2.94	712.3	1079.6	1.52	712.3	594.4	0.83
	3	41.8	105.0	2.51	3527.9	2423.9	0.69	3527.9	1495.6	0.42
	4	41.7	102.1	2.45	3523.1	2455.8	0.70	3523.1	1452.6	0.41
	5	32.1	30.2	0.94	1368.1	575.8	0.42	1368.1	423.1	0.31
5	1	7.9	37.5	4.77	106.5	380.0	3.57	106.5	276.2	2.59
	2	7.9	37.5	4.77	106.5	379.9	3.57	106.5	276.3	2.59
6	1	6.6	31.3	4.76	88.9	334.0	3.76	88.9	240.6	2.71
	1	6.6	31.3	4.76	88.9	334.0	3.76	88.9	240.6	2.71